NASA/TM-2000-210541

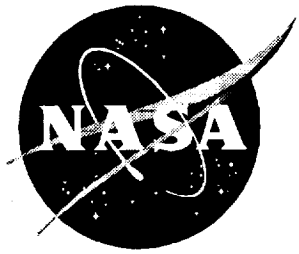

Reynolds Number Effects on the Performance of Lateral Control Devices

Raymond E. Mineck
Langley Research Center, Hampton, Virginia

October 2000

The NASA STI Program Office . . . in Profile

Since its founding, NASA has been dedicated to the advancement of aeronautics and space science. The NASA Scientific and Technical Information (STI) Program Office plays a key part in helping NASA maintain this important role.

The NASA STI Program Office is operated by Langley Research Center, the lead center for NASA's scientific and technical information. The NASA STI Program Office provides access to the NASA STI Database, the largest collection of aeronautical and space science STI in the world. The Program Office is also NASA's institutional mechanism for disseminating the results of its research and development activities. These results are published by NASA in the NASA STI Report Series, which includes the following report types:

- TECHNICAL PUBLICATION. Reports of completed research or a major significant phase of research that present the results of NASA programs and include extensive data or theoretical analysis. Includes compilations of significant scientific and technical data and information deemed to be of continuing reference value. NASA counterpart of peer-reviewed formal professional papers, but having less stringent limitations on manuscript length and extent of graphic presentations.

- TECHNICAL MEMORANDUM. Scientific and technical findings that are preliminary or of specialized interest, e.g., quick release reports, working papers, and bibliographies that contain minimal annotation. Does not contain extensive analysis.

- CONTRACTOR REPORT. Scientific and technical findings by NASA-sponsored contractors and grantees.

- CONFERENCE PUBLICATION. Collected papers from scientific and technical conferences, symposia, seminars, or other meetings sponsored or co-sponsored by NASA.

- SPECIAL PUBLICATION. Scientific, technical, or historical information from NASA programs, projects, and missions, often concerned with subjects having substantial public interest.

- TECHNICAL TRANSLATION. English-language translations of foreign scientific and technical material pertinent to NASA's mission.

Specialized services that complement the STI Program Office's diverse offerings include creating custom thesauri, building customized databases, organizing and publishing research results . . . even providing videos.

For more information about the NASA STI Program Office, see the following:

- Access the NASA STI Program Home Page at ***http://www.sti.nasa.gov***

- Email your question via the Internet to help@sti.nasa.gov

- Fax your question to the NASA STI Help Desk at (301) 621-0134

- Telephone the NASA STI Help Desk at (301) 621-0390

- Write to:
  NASA STI Help Desk
  NASA Center for AeroSpace Information
  7121 Standard Drive
  Hanover, MD 21076-1320

NASA/TM-2000-210541

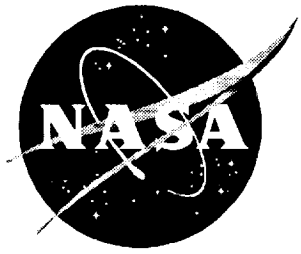

Reynolds Number Effects on the Performance of Lateral Control Devices

Raymond E. Mineck
Langley Research Center, Hampton, Virginia

National Aeronautics and
Space Administration

Langley Research Center
Hampton, Virginia 23681-2199

October 2000

The use of trademarks or names of manufacturers in this report is for accurate reporting and does not constitute an official endorsement, either expressed or implied, of such products or manufacturers by the National Aeronautics and Space Administration.

Available from:

NASA Center for AeroSpace Information (CASI)
7121 Standard Drive
Hanover, MD 21076-1320
(301) 621-0390

National Technical Information Service (NTIS)
5285 Port Royal Road
Springfield, VA 22161-2171
(703) 605-6000

Abstract

The influence of Reynolds number on the performance of outboard spoilers and ailerons was investigated on a generic subsonic transport configuration in the National Transonic Facility over a chord Reynolds number range from 3×10^6 to 30×10^6 and a Mach number range from 0.50 to 0.94. Spoiler deflection angles of 0°, 10°, 15°, and 20° and aileron deflection angles of -10°, 0°, and 10° were tested. Aeroelastic effects were minimized by testing at constant normalized dynamic pressure conditions over intermediate Reynolds number ranges. Results indicated that the increment in rolling moment due to spoiler deflection generally becomes more negative as the Reynolds number increases from 3×10^6 to 22×10^6 with only small changes between Reynolds numbers of 22×10^6 and 30×10^6. The change in the increment in rolling moment coefficient with Reynolds number for the aileron deflected configuration is generally small with a general trend of increasing magnitude with increasing Reynolds number.

Introduction

Lateral control devices are typically designed using empirical tools, analytical methods, and wind tunnel tests. Conventional wind tunnel tests typically provide results at Reynolds numbers significantly below those encountered in flight. Thus, some form of adjustment may be needed to account for the effects of Reynolds number on the results. A series of wind tunnel tests were undertaken to investigate the effect of Reynolds number on the performance of ailerons and spoilers on a generic subsonic transport configuration.

The generic wing-body configuration used in the wind tunnel tests was representative of a subsonic commercial transport configuration. The body was the Pathfinder-I fuselage described in reference 1. The wing, referred to as the "Pathfinder-I Lateral Controls Wing," was based on the Energy Efficient Transport (EET) configuration, described in reference 1. The Lateral Controls Wing had provisions for mounting inboard spoilers and ailerons and outboard spoilers and ailerons. Pressure orifices were installed in chordwise rows on the wing.

The purpose of this report is to present results from two wind tunnel tests that investigated the effects of Reynolds number on the performance of lateral control devices. The first test studied the effect of Reynolds number on the performance of outboard spoilers, and the second test studied the effect of Reynolds number on the performance of outboard ailerons. Results are presented at Mach numbers from 0.50 to 0.94 at Reynolds numbers, based on the mean geometric chord, of 3×10^6, 13×10^6, 22×10^6, and 30×10^6.

Symbols and Abbreviations

All dimensional data are presented in U.S. customary units. The longitudinal force and moment data are presented in coefficient form in the stability axis system. The lateral moment data are presented in coefficient form in the body axis system as shown in figure 1. The moment reference center was located 37.922 inches downstream of the model nose and 1.563 inches below the centerline of the model fuselage. The symbols and abbreviations are defined as follows:

b	reference span, 52.97 in.
c	local chord, in.
$\bar{c}$	mean geometric chord, 5.742 in.
C_D	drag coefficient, $D/q_\infty S$
C_L	lift coefficient, $L/q_\infty S$
C_l	rolling moment coefficient, $M_x/q_\infty Sb$
C_m	pitching moment coefficient, $M_y/q_\infty S\bar{c}$
C_n	yawing moment coefficient, $M_z/q_\infty Sb$
C_p	wing static pressure coefficient, $(p-p_\infty)/q_\infty$
$C_{p.te}$	static pressure coefficient at the wing trailing edge, $(p_{te}-p_\infty)/q_\infty$
D	drag, lbf
E	wing material modulus of elasticity (Young's modulus), lbf/ft^2
EET	Energy Efficient Transport
ESP	electronically scanned pressure
Inter.	intermediate
L	lift, lbf
M_x	rolling moment, in-lbf
M_y	pitching moment, in-lbf
M_z	yawing moment, in-lbf
M_∞	free stream Mach number
NTF	National Transonic Facility
p	local static pressure, lbf/ft^2

p_{te}	static pressure at wing trailing edge, lbf/ft^2
p_∞	free stream static pressure, lbf/ft^2
q_∞	free stream dynamic pressure, lbf/ft^2
$R_{\bar{c}}$	Reynolds number based on mean geometric chord
sta	model streamwise station, in.
S	wing reference (trapezoidal) area, 1.9884 ft^2
T_t	stagnation temperature, °F
V_∞	free stream velocity, ft/sec
X,Y,Z	model axis system
x/c	local chord fraction
y	distance in spanwise direction, positive out the right wing, in.
α	angle of attack, deg
Δ	change in a parameter
δ_a	aileron deflection, positive trailing edge down, deg
δ_s	spoiler deflection, deg
η	wing semispan fraction, $y/b/2$
σ	standard deviation

Experimental Apparatus

Test Facility

The National Transonic Facility (NTF) is a fan-driven, closed-circuit, continuous-flow, pressurized wind tunnel (ref. 2). It may be operated as a conventional wind tunnel using air as a test gas or as a cryogenic wind tunnel using nitrogen as a test gas. When operated as a conventional wind tunnel, heat is removed by a water-cooled heat exchanger located at the upstream end of the settling chamber. When operated as a cryogenic tunnel, heat is removed by the evaporation of liquid nitrogen which is sprayed into the tunnel circuit ahead of the fan. Nitrogen gas is vented to maintain a constant total pressure. NTF capabilities allow testing of aircraft configurations at Mach numbers ranging from low subsonic to low supersonic, at Reynolds numbers up to full-scale flight values (depending on aircraft type and size). The test section is 8.2 feet by 8.2 feet in cross section and 25 feet in length. Longitudinal slots in the floor and ceiling give a wall-openness ratio of 6 percent. The test-section sidewalls are solid. The NTF is capable of an absolute pressure range from 15 psi to 125 psi, a stagnation temperature range from -320°F to 150°F, a Mach number range from 0.2 to 1.2, and a maximum Reynolds number per foot of 146×10^6 at a Mach number of 1.

Free stream turbulence is reduced by four damping screens and the 15:1 contraction ratio between the settling chamber and the test section. An initial assessment of the flow quality in the NTF has been reported in reference 3. Conventional model support is provided by an aft-mounted sting attached to a vertically mounted arc sector. The pitch range of the arc sector is from about -11° to 19°, depending on the test setup. A remotely controlled roll coupling, with a range from -180° to 180°, provides the interface between the arc sector and the sting. The test-section floor, ceiling, and reentry flap angles were fixed during these tests.

Model Description

The generic low-wing subsonic transport wing known as the NTF Pathfinder-I Lateral Controls Wing was used in this investigation. The wing is designed for use with the existing NTF Pathfinder-I subsonic transport model fuselage components (ref. 1). A 10.5-inch fuselage extension plug was inserted between the nose and wing to provide a more realistic ratio of fuselage length to wing span. Wing-fuselage fillets typical of current subsonic transport designs were installed at the wing root. The model is designed to accept inboard and outboard spoilers and ailerons. Photographs of the model installed in the NTF test section are presented in figure 2. Sketches of the model general arrangement, the outboard spoilers, and the outboard ailerons are presented in figure 3.

The wing design, based on the EET wing reported in reference 1, incorporated supercritical airfoil sections with blunt trailing edges. It was manufactured from Vascomax T-200 steel and had a surface finish of 8 microinches for the first 15 percent of the local chord and 16 microinches for the remainder. The planform break is located at $\eta = 0.376$, with extended chord lengths inboard of this station. (See fig. 3(a).) Wing attributes, presented in table 1, were based on the trapezoidal reference planform formed by extending the outboard leading and trailing edge lines to the centerline and to the wingtip station. The cruise design condition is for a lift coefficient of 0.55 at a Mach number of 0.82. Because the wind tunnel model is not a scaled representation of a full-scale aircraft, a cruise Reynolds number is not defined. The model wing was not designed to deform aeroelastically to a specific shape at the cruise condition, since the cruise Reynolds number (and tunnel dynamic pressure) is not defined. The rear portion of the outboard portion of the port wing panel was removable so that different pieces simulating different outboard aileron deflections could be installed. Provisions were also made to install spoilers on the center portion of the port wing panel.

The outboard spoilers consisted of two panels for each of the three spoiler deflections: 10°, 15°, and 20°. Details about the spoilers are presented in figure 3(b). Spoilers were mounted only on the port wing on a 0.550 inch by 2.500 inch pad integral to each spoiler. The angle machined into the pad determined the deflection angle. The pad was machined to match the local wing contour. The spoiler panels were removed for the 0° deflection case. When installed, each spoiler panel was sealed to the wing surface to prevent any flow from going between the spoiler panel and the wing upper surface. The two spoiler panels were always installed with the same deflection angle.

The outboard aileron consisted of a single machined piece for each of the three aileron deflections: -10°, 0°, and 10°. Details of the ailerons are presented in figure 3(c). The trailing edge down deflection was assigned the positive value. When installed, the machined piece for the aileron was sealed to the wing along the upstream edge. Ailerons were mounted only on the port wing panel.

The wing contains 258 static pressure orifices distributed in 7 chordwise rows. (See fig. 3(a).) Nominal chordwise locations in each row are listed in tables 2 and 3. To simplify model fabrication and maximize wing strength, upper surface orifices are located in the port wing panel and lower surface orifices are located in the starboard wing panel. The nominal orifice diameter was 0.015 inch.

Instrumentation

Aerodynamic force and moment data were obtained with a six-component, strain-gage balance. For each wind tunnel test, the NTF balance with the smallest load capacity that exceeded the expected model loads was selected. All NTF balances were not always available because of periodic maintenance such as moisture proofing. Thus, different balances were used for the two tests as shown in table 4. The NTF101B balance was used for the outboard spoiler test and the NTF113B balance was used for the outboard aileron test. The 2σ accuracy of each component of each balance was determined from the measured and applied loads from the balance calibration. The full-scale loads and quoted accuracies as a percent of the full-scale loads are presented in table 4.

The accuracy of the measurement instruments was used to estimate the error bands for the model force and moment coefficients for the loads encountered near the angle of attack for the design lift coefficient using the technique described in reference 4. Error bands for the force and moment coefficients based on the quoted instrumentation accuracies for the two tunnel tests are presented in table 5. As expected, the uncertainty in each of the force and moment coefficients decreases with increasing dynamic pressure. Changes in results smaller than the measurement uncertainty should not be considered significant.

An onboard, heated, single-axis accelerometer package was used to measure the model angle of attack. The accelerometer package has a quoted accuracy of ±0.01° under smooth wind tunnel operating conditions (ref. 5). For the test conditions presented in this report, the model dynamic acceleration was small and was not expected to have a significant impact on the accuracy of the angle of attack measurement.

Wing-pressure measurements were made with six 48-port, electronically scanned pressure (ESP) modules contained in an internal, nose-mounted, heated enclosure. The upper surface (port wing) pressures were measured using modules having a full-scale pressure range of ±45 psid; the lower surface (starboard wing) pressures were measured using modules having a range of ±30 psid. The quoted accuracy of the modules was ±0.20 percent of full-scale pressure. The modules were calibrated immediately before each series of runs. Body cavity pressures were measured at two locations inside the fuselage cavity using an ESP module with a full-scale pressure range of ±2.5 psid.

The wind tunnel total and static pressures were measured using two banks of quartz Bourdon tube transducers referenced to a vacuum. A controller selects the smallest transducer from each bank capable of measuring the total and the static pressures. The manufacturer's quoted accuracy for these pressure transducers is ±0.012 percent of reading plus ±0.006 percent of full scale. Since data were obtained at three levels of dynamic pressure (to be discussed later), different transducers in each bank were used depending on the test conditions. For the low level dynamic pressure data, 30 psi transducers were used for both the total and static pressure measurements. For the intermediate level dynamic pressure data, 50 psi transducers were used for both the total and static pressure measurements. For the high level dynamic pressure data, a 100 psi transducer was used for the total pressure measurement and a 50 psi transducer was used for the static pressure measurement. The tunnel total temperature was measured with a platinum resistance thermometer with an accuracy of ±0.2°F.

Procedures

Data Reduction and Corrections

Information on NTF instrumentation devices, tunnel process and data-acquisition systems, and data-reduction algorithms are provided in reference 6. Balance output is sensitive to the balance temperature as well as the

balance longitudinal temperature gradient. Balance readings were compensated for changes in balance temperature between the wind-on and wind-off conditions. Also, temperature gradients within the balance were minimized by allowing the balance to approach thermal equilibrium with the tunnel flow before recording any data. Balance temperature gradients of less than 10°F were maintained throughout these tests. Wind-off data were acquired prior to and following each set of runs to monitor balance electrical zero shifts over the course of a set of runs. The ending wind-off point was used for all data reduction because the thermal state of the balance (for both temperature and temperature gradient) at the end of a set of runs was generally more representative of the wind-on conditions.

Axial force and drag were corrected to the condition of free stream static pressure acting in the body cavity. No corrections were required for normal force or pitching moment for the static pressure acting in the body cavity. A buoyancy correction was applied to the drag coefficient based on the longitudinal Mach number gradient measured in the test section during the tunnel calibration. The data used in this report were not corrected for test-section wall interference or for sting interference.

The model angle of attack was corrected for upflow in the test section, with the upflow angle determined from data acquired with the model in both upright and inverted orientations at a given set of tunnel conditions. In each test, an upright and inverted run was obtained for each Reynolds number at the design Mach number, 0.82, and the resulting upflow correction applied across the Mach number range except for the results at a Mach number of 0.50. Additional upright and inverted runs at a Mach number of 0.50 were used to correct the data at that Mach number. Upflow angles ranged from about 0.13° to about 0.18°.

Tests

The test program was designed to investigate the effects of Reynolds number at transonic speeds on the performance of different lateral control devices. The Mach number range covered speeds from below the design Mach number to above the maximum operating Mach number of a typical subsonic commercial transport. The Mach number range for the outboard spoiler test was from 0.70 to 0.94 and for the outboard aileron test was from 0.50 to 0.94. The lowest Reynolds number was representative of the Reynolds numbers obtained on similarly sized models in conventional transonic wind tunnels ($R_{\bar{c}} = 3\times10^6$). The highest Reynolds number was representative of a moderate sized commercial transport at cruise ($R_{\bar{c}} = 30\times10^6$). Two additional Reynolds numbers ($R_{\bar{c}} = 13\times10^6$ and $R_{\bar{c}} = 22\times10^6$) were included to assess Reynolds number effects. At each test condition, the angle of attack was varied from about -2° (approximately the angle of zero lift) to about 6° (onset of model pitch angle dynamics). The test matrix for the outboard spoilers is presented in table 6 and the test matrix for the outboard ailerons is presented in table 7.

The wind tunnel model wing will deform under load. Testing at different dynamic pressures will yield different model loads and, consequently, different model deformations. The effects of model deformation should be removed from the experimental results. Static aeroelastic deformation of the wing depends on the applied load and the material stiffness. An indicator of static aeroelastic deformation is the nondimensional ratio of dynamic pressure (q_∞) to the modulus of elasticity (E) for the metal that was used in the wing. The parameter q_∞/E is appropriate for characterizing aeroelastic condition because the material stiffness E increases as the temperature decreases. To eliminate the effect of static aeroelastic deformation, the model should be tested at constant q_∞/E.

Although the operating characteristics of the NTF allow independent variation of Mach number, Reynolds number, and dynamic pressure, constraints from the NTF operating envelope prevent testing at a constant dynamic pressure across the full range of desired Mach numbers and Reynolds numbers. The NTF operating envelope for the Pathfinder-I Lateral Controls Model at a Mach number of 0.82, shown in figure 4, demonstrates the problem. One option is to test at a high dynamic pressure ($q_\infty/E = 0.61\times10^{-6}$) over a reduced Reynolds number range from about 7×10^6 to 30×10^6. Extensive testing at such high levels of dynamic pressure is not preferred because of the high liquid nitrogen consumption. The desired test matrix could not be completed at this high dynamic pressure because the required liquid nitrogen exceeded the amount available for the test. An alternate approach that limits the testing required at the high dynamic pressure was selected. This approach provides Reynolds number effects at three levels of dynamic pressure and static aeroelastic (i.e., dynamic pressure) effects at two intermediate Reynolds numbers as noted by the solid circles in figure 4. The results at Reynolds numbers of 3×10^6 and 13×10^6 are obtained at the baseline $q_\infty/E = 0.28\times10^{-6}$ (low range), the results at a Reynolds number of 22×10^6 are obtained at $q_\infty/E = 0.45\times10^{-6}$ (intermediate range), and the results at a Reynolds number of 30×10^6 are obtained at $q_\infty/E = 0.61\times10^{-6}$ (high range). The results for a Reynolds number of 22×10^6 are corrected for the static aeroelastic increment between $q_\infty/E = 0.45\times10^{-6}$ and $q_\infty/E = 0.28\times0^{-6}$. Similarly, the results for a Reynolds number of 30×10^6 are corrected for two static aeroelastic increments: the first between $q_\infty/E = 0.61\times10^{-6}$ and $q_\infty/E = 0.45\times10^{-6}$ and the second

between $q_\infty/E = 0.45\times10^{-6}$ and $q_\infty/E = 0.28\times10^{-6}$. Details of the corrections as well as uncorrected and corrected longitudinal aerodynamic characteristics of the Pathfinder-I Lateral Controls Wing with the controls undeflected are presented in the Appendix.

Each time the model is assembled, small differences in the clean (no deflected control surface) wing are possible, leading to small differences in the baseline rolling moment coefficients. Also, small manufacturing differences created small asymmetries in the model. To minimize these effects, the effect of control surface deflection was determined from the difference between the results with the control surface deflected and the results with the control surface set to 0° (clean wing). Separate clean wing data were obtained for each test.

Clean wing data were not obtained during the outboard spoiler test at the intermediate dynamic pressure level at a Reynolds number of 13×10^6 and the high dynamic pressure at a Reynolds number of 22×10^6 for Mach numbers from 0.70 to 0.88. (See table 6.) Estimated clean wing data were needed to determine the increments in the force and moment coefficients due to spoiler deflection. Examination of the increments in the force and moment coefficients from three other wind tunnel tests of the Lateral Controls Wing due to increasing the dynamic pressure from the low to the intermediate levels and from the intermediate to high levels showed similar static aeroelastic effects for each test. Since the static aeroelastic increments are relatively independent of the test, the missing clean wing data were estimated by adding the average static aeroelastic increment from the other three Lateral Controls Wing tests to the available clean wing data from the outboard spoiler test.

The outboard spoiler and aileron tests did not include a complete set of results at a Reynolds number of 13×10^6 for $\delta_s = 10°$ and $\delta_a = 10°$. Without the static aeroelastic increment at that Reynolds number, the results at the two higher Reynolds numbers could not be corrected using the standard procedure described in the Appendix. The aeroelastic increment between the intermediate and high dynamic pressure levels at a Reynolds number of 22×10^6 was used to calculate the sensitivity of each of the force and moment coefficients to a change in the dynamic pressure. This sensitivity was used to correct the results at a Reynolds number of 22×10^6 at the intermediate dynamic pressure level to the baseline dynamic pressure level. In a similar fashion, the sensitivity was used to correct the results at a Reynolds number of 30×10^6 at the high dynamic pressure level to the baseline dynamic pressure level. This procedure was tested on the complete set of results for $\delta_s = 20°$ and found to provide reasonable agreement with results from the standard correction procedure. An example of the modified aeroelastic correction procedure is described in the Appendix.

All polars were obtained in a "pitch-pause" mode in which the model is pitched to the next angle of attack in the series, transients in the flow and instrumentation are allowed to damp out, and the data are then recorded before repeating the cycle.

Wing pressure data acquisition required ESP hardware (tubing for the reference pressure, calibration pressure, and control pressure and electrical wires for data acquisition and control) to bridge the balance. Previous test experiences (e.g., ref. 7) indicated that the presence of the ESP instrumentation had a small effect on the lift and pitching moment measurements but could have a significant effect on the drag measurements. Thus, drag data from the NTF measured with the ESP hardware present have been used with caution and are frequently excluded in the analysis of the test results.

The results at the two lower Reynolds numbers, 3×10^6 and 13×10^6, were obtained with the boundary layer transition location artificially fixed on the nose of the model and on the wing upper and lower surfaces. Epoxy disks were selected for the trip strips because they provide a repeatable configuration unlike grit (ref. 8). The disks, 0.0035 inch high and 0.045 inch in diameter, were installed with the disk centers 0.100 inch apart. Disk height was determined using the method described in reference 9. The ring of disks on the fuselage nose was located 1.00 inch downstream of the nose (sta = -9.5 in.). The rows of disks on each surface of the wing were laid out in two straight lines—from near the wing root to the leading edge break and from the leading edge break to near the tip—as shown in figure 5. The trip location varies from about $x/c = 0.05$ at the root to about $x/c = 0.10$ at the tip. Natural boundary layer transition (strips of trip disks removed) was used for tests at the two higher Reynolds numbers, 22×10^6 and 30×10^6, since transition is estimated to occur within the first 5 percent of the local chord.

Repeatability

The Lateral Controls Wing has been tested three times with the wing-fuselage fillets: investigating outboard spoilers, inboard ailerons, and outboard ailerons. Repeat runs were obtained at a Mach number of 0.82 and a Reynolds number of 3×10^6 for the clean wing during each test. These runs were analyzed to assess the data repeatability using the regression statistical analysis of reference 10. The statistical analysis was applied over an angle of attack range from -1° to 3°. The estimated mean value was calculated from a fourth-order polynomial regression equation fitted to the results. From the

measured data and the estimated mean value, the residual error, the 95-percent confidence interval, and the 95-percent prediction interval were determined. The 95-percent confidence interval is the bounds about the estimated mean value that encompass the true mean with a 95-percent probability. The 95-percent prediction interval is the bounds about the estimated mean value that will contain a single future measurement with a 95-percent probability. The confidence interval is related to the location of the true mean and the prediction interval is a measure of the data scatter. As defined in reference 10, confidence and prediction intervals are inversely proportional to the number of measurements in the data set and the local density of the measurements. Thus, at the ends of the intervals, the local density of the points decreases and the confidence and prediction intervals widen. The results from the statistical analysis are presented in figure 6. In general, the repeatability is good, with the confidence interval similar in magnitude to the measurement uncertainty.

Results and Discussion

Outboard spoilers

The effect of outboard spoiler deflection for the force and moment coefficients was determined from the increment (difference) in the coefficient with the spoiler deflected and with the clean wing. The increment is denoted by a delta (Δ) preceding the coefficient. The effect of Reynolds number on the increments in the force and moment coefficients is presented in figures 7 and 8 for spoiler deflections of 10° and 20°. For the lower angles of attack, the increment in rolling moment coefficient due to spoiler deflection is relatively constant at the lowest Mach number of 0.70. The level becomes more negative as the Reynolds number increases from 3×10^6 to 22×10^6. A smaller change is found between Reynolds numbers of 22×10^6 and 30×10^6. It should be noted that these changes in rolling moment coefficient are larger than the test-to-test repeatability ($\approx$0.0002) and the uncertainty in the rolling moment coefficient ($\approx$0.0001 to $\approx$0.0003). As the angle of attack increases above 5°, the increment in rolling moment coefficient becomes less negative. Model pitch dynamics frequently occurred in this part of the test envelope, limiting the extent of the angle of attack range. As the Mach number increases, the region of less negative rolling moment coefficients occurs at smaller angles of attack so that eventually the relatively constant rolling moment coefficient portion ceases. The yawing moment, pitching moment, and lift coefficient increments show the expected trends. In regions where the increment in rolling moment coefficient is relatively constant, the yawing moment coefficient and the lift coefficient increments are negative and the pitching moment coefficient increment is positive. In regions where the increment in rolling moment coefficient is becoming less negative, the yawing moment and lift coefficient increments are also becoming less negative and the pitching moment coefficient increment is becoming less positive.

The basic results from figures 7 and 8 were curve fit, and fitted values at angles of attack of -1.5°, 0.0°, and 2.0° were cross-plotted to determine the variation of the increment in rolling moment coefficient with Reynolds number for two spoiler deflections and the results are presented in figure 9. The angle for zero lift is about -1.5° and the angle for design lift is about 2.0° at the design Mach number of 0.82. In most cases, the increment in rolling moment coefficient due to spoiler deflection becomes more negative as the Reynolds number increases from 3×10^6 to 22×10^6. Typically, there is only a small change in the rolling moment coefficient between Reynolds numbers of 22×10^6 and 30×10^6. The influence of Reynolds number on the increment in rolling moment coefficient is generally larger for the 20° spoiler deflection.

The basic results from figures 7 and 8 along with the results for a spoiler deflection of 15° were cross-plotted at the same angles of attack to determine the variation of the increment in rolling moment coefficient with spoiler deflection, and the results are presented in figure 10. In general, spoiler roll control power, as determined from the slopes of the curves, decreases at the higher Mach numbers. Increasing the Reynolds number generally increased the roll control power.

Reynolds number will have an influence on the wing pressure distributions. Direct comparisons of the pressure distributions on the wing for the different spoiler deflections are not possible because of the differences in the angle of attack for the data at a given Reynolds number, dynamic pressure, and Mach number. At each combination of Reynolds number, dynamic pressure, and Mach number, the pressure coefficient from each pressure orifice was curve fit as a function of angle of attack and fitted values selected at four angles of attack: -1.5°, 0°, 2°, and either 3.5° or 4° (depending on the maximum measured angle of attack). Results at Reynolds numbers of 22×10^6 and 30×10^6 were corrected for static aeroelastic effects in a manner similar to that used for the force and moment data.

The effect of Reynolds number on the trailing edge pressure distributions with and without the spoilers deflected is presented in figure 11. Since there was an incomplete set of clean wing data, the undeflected results were taken from the starboard wing panel. For the clean wing, the trailing edge pressure coefficient becomes more positive (less negative) as the Reynolds number

increases. Separated flow regions tend to become smaller as the Reynolds number increases. (See, for example, α=4° at M_∞=0.82.) For the spoiler deflected, there is a significant separated flow region downstream of the spoiler, as shown by the negative pressure coefficients at η=-0.44 to η=-0.69. (The spoiler hinge line extended from η=-0.430 to η=-0.669.) Up through a Mach number of 0.85, the peak negative pressure coefficient becomes less negative with increasing Reynolds number. The spanwise pressure coefficient distribution does not change drastically with increasing angle of attack. At the higher angles of attack, especially at the higher Mach numbers, a separated flow region developed on the clean wing near the mid-span portion of the wing. This region grew with increasing Mach number and angle of attack. The loss of lift on the clean wing panel from the separated flow region increases so as to reduce the effectiveness of the spoiler on the opposite wing panel.

Two chordwise rows of pressure orifices, at η=-0.509 and η=-0.630, crossed the spanwise stations covered by the spoilers. Because there was an incomplete set of clean wing data, aeroelastic corrections to the upper surface pressure data at the two higher Reynolds numbers were not possible. The effect of Reynolds number on the upper surface chordwise pressure distributions is presented in figures 12 and 13 for the two spanwise rows covered by the spoilers. In general, the only significant effect on the pressure distribution of increasing the Reynolds number was to shift the shock aft. This happened both with and without the spoilers deflected.

Outboard ailerons

The effect of Reynolds number on the increments in the force and moment coefficients is presented in figures 14 and 15 for aileron deflections of -10° and 10°. For the angles of attack used in this investigation, the increment in rolling moment coefficient due to aileron deflection was relatively constant for Mach numbers through 0.82. For Mach numbers from 0.80 through 0.91, the magnitude of the increment in the rolling moment coefficient was smallest at a Reynolds number of 3×10^6 and generally increased as the Reynolds number increased. As expected, for the positive aileron deflection, the increment in lift coefficient was positive and the increment in pitching moment coefficient was negative. The negative aileron deflection had the opposite effect.

The basic results from figures 14 and 15 were curve fit and cross-plotted at angles of attack of -1.25°, 0°, and 2° to determine the increment in rolling moment coefficient with Reynolds number for both aileron deflection angles and the results are presented in figure 16. The effect of Reynolds number on the increment in rolling moment coefficient is generally small with a general trend of increasing magnitude with increasing Reynolds number.

The basic results from figures 14 and 15 were curve fit and cross-plotted at angles of attack of -1.25°, 0°, and 2° to determine the increment in rolling moment coefficient with aileron deflection angle for constant Reynolds number and the results are presented in figure 17. In general, the aileron control power increases with Reynolds number and is larger for the negative aileron deflection.

Pressure data were not obtained for the two lower Reynolds numbers in the outboard aileron test; therefore the effect of Reynolds number on the trailing edge pressure coefficient distribution and the chordwise pressure coefficient distribution could not be determined.

Conclusions

Data from two tests of a wing-body configuration in the NTF have been analyzed to study the effect of Reynolds number on the performance of lateral control devices. The results indicated the following conclusions:

1. In most cases, the increment in rolling moment due to spoiler deflection becomes more negative as the Reynolds number increases from 3×10^6 to 22×10^6. Typically, there is only a small change in the increment in rolling moment coefficient between Reynolds numbers of 22×10^6 and 30×10^6. The influence of Reynolds number on the increment in rolling moment coefficient is generally larger for the 20° spoiler deflection.

2. For the clean wing configuration, the trailing edge pressure became more positive (less negative) as the Reynolds number increases. Separated flow regions tended to become smaller as the Reynolds number increased.

3. For the spoiler-deflected configuration, there is a significant separated flow region downstream of the spoiler. Up through a Mach number of 0.85, the peak negative pressure coefficient becomes less negative with increasing Reynolds number. The spanwise pressure coefficient distribution does not change drastically with increasing angle of attack.

4. For the aileron-deflected configuration, the effect of Reynolds number on the increment in rolling moment coefficient is generally small with a general trend of increasing magnitude with increasing Reynolds number.

Appendix

Procedure To Correct Results for Changes in Dynamic Pressure

Test results were obtained at three levels of dynamic pressure. The different applied loads on the model for the three dynamic pressure levels led to three different model shapes. A procedure has been developed and applied to the data to correct the results at the shapes for the two higher dynamic pressures to the shape at the lowest dynamic pressure. This Appendix presents the uncorrected longitudinal force and moment coefficients, examples of the correction procedure applied to the intermediate and high dynamic pressure data, and the corrected longitudinal force and moment coefficients.

The uncorrected longitudinal force and moment coefficient data are presented in figure A1 at constant Mach number. Trends shown are typical for subsonic configurations tested in the NTF. Increases in Reynolds number at a constant dynamic pressure typically lead to an increase in the lift coefficient at a given angle of attack and a more negative (less positive) pitching moment coefficient at a given lift coefficient. The thinner boundary layer, especially over the aft portion of the wing, leads to a greater effective aft camber, increasing the lift and the nose-down moment. Increases in Reynolds number lead to decreases in the drag coefficient as the skin friction coefficient decreases with increasing Reynolds number. Increases in dynamic pressure have the opposite effect on the lift and pitching moment coefficients. Increased load on the wing leads to increased vertical displacements, especially on the outer portion of the wing. Since the wing elastic axis is swept, the vertical displacements lead to an increased nose-down local twist angle, reduced lift, and reduced nose-down pitching moment. Increasing dynamic pressure has a mixed effect on the drag because of the changes in the wing profile and induced drags. Typically, the effects of dynamic pressure (i.e., static aeroelastic deformation) and Reynolds number are of similar orders of magnitude and often of opposite sign for tests such as this.

Standard Correction Procedure

The procedure used to correct results for changes in dynamic pressure is the same for each of the model force and moment coefficients. The correction to the pitching moment coefficient at a Mach number of 0.70 is selected as an example, since the effects are clearly visible in the data in figure A1(b). A subset of these measured results along with results from the procedure are presented in figure A2. A second-order, polynomial curve is fitted to segments of the pitching moment coefficient data as a function of the angle of attack for each polar. From the curve fits, the pitching moment coefficient is determined at even increments of 0.2° over the experimental data range. The experimental data are indicated by the large, open symbols and the fitted points are indicated by the solid dots connected by solid, straight lines in figure A2. The difference in the fitted points at a constant angle of attack and Reynolds number is used to determine the change in the pitching moment coefficient associated with the change in dynamic pressure. This is done for the increment between the intermediate and low dynamic pressures ($\Delta_{i\text{-}l}$) at a Reynolds number of 13×10^6 (top left plot of fig. A2) and between the high and intermediate dynamic pressures ($\Delta_{h\text{-}i}$) at a Reynolds number of 22×10^6 (top right plot of fig. A2). The results at an angle of attack of 1° are

$$\Delta_{i\text{-}l}C_m = -.07150-(-.07894) = 0.00744$$

$$\Delta_{i\text{-}l}q_\infty/E = 0.4003\times10^{-6}-0.2483\times10^{-6} = 0.1520\times10^{-6}$$

$$\Delta_{h\text{-}i}C_m = -.07216-(-.07686) = 0.00470$$

$$\Delta_{h\text{-}i}q_\infty/E = 0.5479\times10^{-6}-0.4073\times10^{-6} = 0.1406\times10^{-6}$$

The increments in pitching moment coefficient are divided by the associated change in dynamic pressure to determine a sensitivity factor for aeroelastic effects between the intermediate and low dynamic pressure levels and a sensitivity factor between the high and intermediate dynamic pressure levels.

A single step procedure is used to correct the results at a Reynolds number of 22×10^6 and the intermediate dynamic pressure ($q_\infty/E = 0.4073\times10^{-6}$) to the low dynamic pressure. The required change in dynamic pressure is

$$\Delta_{req}q_\infty/E = 0.4073\times10^{-6}-0.2483\times10^{-6}= 0.1590\times10^{-6}$$

The single correction to the low dynamic pressure level for the pitching moment coefficient (Δ_1C_m) is the pitching moment coefficient sensitivity factor between the intermediate and low dynamic pressures multiplied by the required change in dynamic pressure:

$$\Delta_1C_m = (\Delta_{i\text{-}l}C_m)/(\Delta_{i\text{-}l}q_\infty/E)\times(\Delta_{req}q_\infty/E)$$
$$=.00744/(.1520\times10^{-6})\times(.1590\times10^{-6})=-0.00779$$

As shown in the lower left plot of figure A2 (solid dots connected by dashed line), the pitching moment at a Reynolds number of 22×10^6 corrected to the low dynamic pressure is

$$C_m = -0.07686-0.00779 = -0.08465$$

A two step procedure is used to correct the results at a Reynolds number of 30×10^6 and the high dynamic pressure level ($q_\infty/E = 0.5523\times10^{-6}$) to the low dynamic pressure level. The first step corrects for the increment between the high and intermediate dynamic pressure levels and the second step corrects for the increment

between the intermediate and low dynamic pressure levels. The required change in dynamic pressure for the first step is

$$\Delta_{req}q_\infty/E = 0.5523\times10^{-6}-0.4073\times10^{-6}= 0.1450\times10^{-6}$$

The first correction, from the high to the intermediate dynamic pressure level, for the pitching moment coefficient (Δ_1C_m) is the pitching moment coefficient sensitivity factor between the high and intermediate dynamic pressures multiplied by the required change in dynamic pressure:

$$\Delta_1C_m = (\Delta_{h\text{-}i}C_m)/(\Delta_{h\text{-}i}q_\infty/E)\times(\Delta_{req}q_\infty/E)$$
$$=0.00470/(.1406\times10^{-6})\times(.1450\times10^{-6})=-0.00485$$

The required change in dynamic pressure for the second step is

$$\Delta_{req}q_\infty/E = 0.4073\times10^{-6}-0.2483\times10^{-6}= 0.1590\times10^{-6}$$

The second correction, from the intermediate to the low dynamic pressure level, for the pitching moment coefficient (Δ_2C_m) is the pitching moment coefficient sensitivity factor between the intermediate and low dynamic pressure levels multiplied by the required change in dynamic pressure:

$$\Delta_2C_m = (\Delta_{i\text{-}l}C_m)/(\Delta_{i\text{-}l}q_\infty/E)\times(\Delta_{req}q_\infty/E)$$
$$=0.00744/(.1520\times10^{-6})\times(.1590\times10^{-6})=-0.00779$$

The corrected pitching moment coefficient is the pitching moment coefficient at the high dynamic pressure level summed with the corrections obtained from the first and second steps. As shown in the lower right plot of figure A2, the pitching moment coefficient at a Reynolds number of 30×10^6 corrected to the low dynamic pressure is

$$C_m = -0.06352-0.00485-0.00779 = -0.07616$$

These two procedures were used to correct the measured data at Reynolds numbers of 22×10^6 and 30×10^6 to the low dynamic pressure. Second-order, polynomial curves were fitted to the measured data at Reynolds numbers of 3×10^6 and 13×10^6 at the low dynamic pressure. These results, all at or corrected to the low dynamic pressure level, are presented in figure A3. The results show the expected trends with Reynolds number; that is, lift and the nose down moment coefficients increase and the drag coefficient decreases with increasing Reynolds number.

Modified Correction Procedure

No measured results were available for the configuration with the outboard aileron deflected 10° at a Reynolds number of 13×10^6. Thus, the normal procedure to correct the data at 22×10^6 and 30×10^6 could not be used. For this special case, a modified one step method was applied that used the increment in the measured model force or moment coefficient between the intermediate and high dynamic pressures to extrapolate to the low dynamic pressure level. For the results at a Reynolds number of 22×10^6 and the intermediate dynamic pressure ($q_\infty/E = 0.4073\times10^{-6}$), the required correction for dynamic pressure is

$$\Delta_{req}q_\infty/E = 0.4073\times10^{-6}-0.2483\times10^{-6} = 0.1590\times10^{-6}$$

The only sensitivity factor available is between the high and intermediate dynamic pressure levels. The single correction (Δ_1) to the pitching moment coefficient is the product of the sensitivity factor between the high and intermediate dynamic pressure levels and the required change between the intermediate and low dynamic pressure levels:

$$\Delta_1C_m= 0.00470/(0.1406\times10^{-6})\times(0.1590\times10^{-6})=0.00532$$

The corrected pitching moment coefficient is

$$C_m = -.07686 - 0.00532 = -0.08218$$

This value is reasonably close to the corrected value of -0.08465 from the standard correction procedure in the previous section.

For the results at a Reynolds number of 30×10^6 and the high dynamic pressure ($q_\infty/E = 0.5523\times10^{-6}$), the required correction for dynamic pressure is

$$\Delta_{req}q_\infty/E = 0.5523\times10^{-6}-0.2483\times10^{-6} = 0.3040\times10^{-6}$$

The only sensitivity factor available is between the high and intermediate dynamic pressure levels. The single correction (Δ_1) to the pitching moment coefficient is the product of the sensitivity factor between the high and intermediate dynamic pressure levels and the required change between the high and low dynamic pressure levels:

$$\Delta_1C_m= 0.00470/(0.1406\times10^{-6})\times(0.3040\times10^{-6}) = 0.01016$$

The corrected pitching moment coefficient is

$$C_m = -.06352 - 0.01016 = -0.07368$$

This value is reasonably close to the corrected value of -0.07616 from the standard correction procedure in the previous section. The modified procedure does a reasonable job of correcting the results at the higher Reynolds numbers when the part of the data required for the dynamic pressure correction is missing.

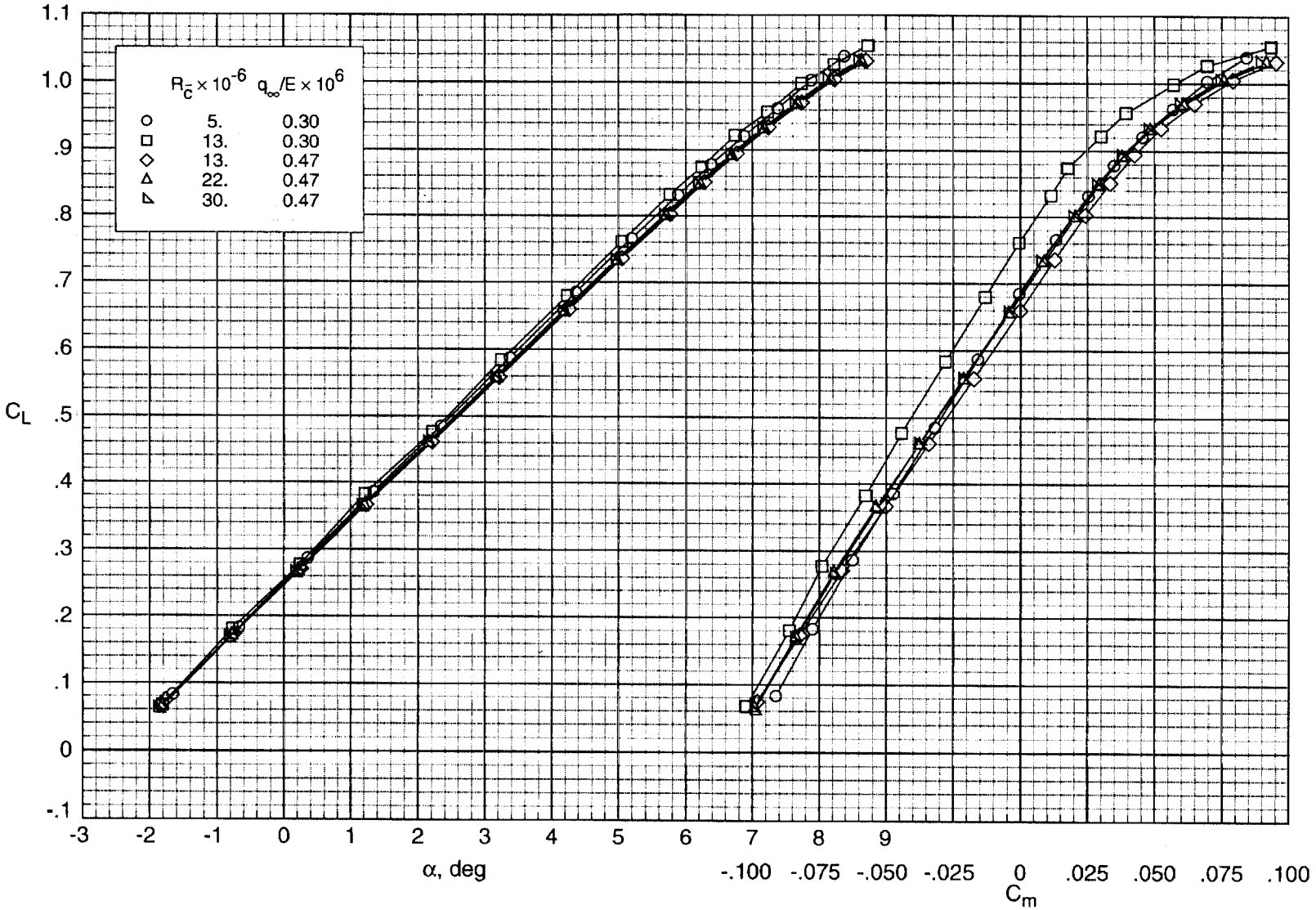

(a) $M_\infty = 0.50$.

Figure A1. Measured (uncorrected) longitudinal aerodynamic characteristics of the model.

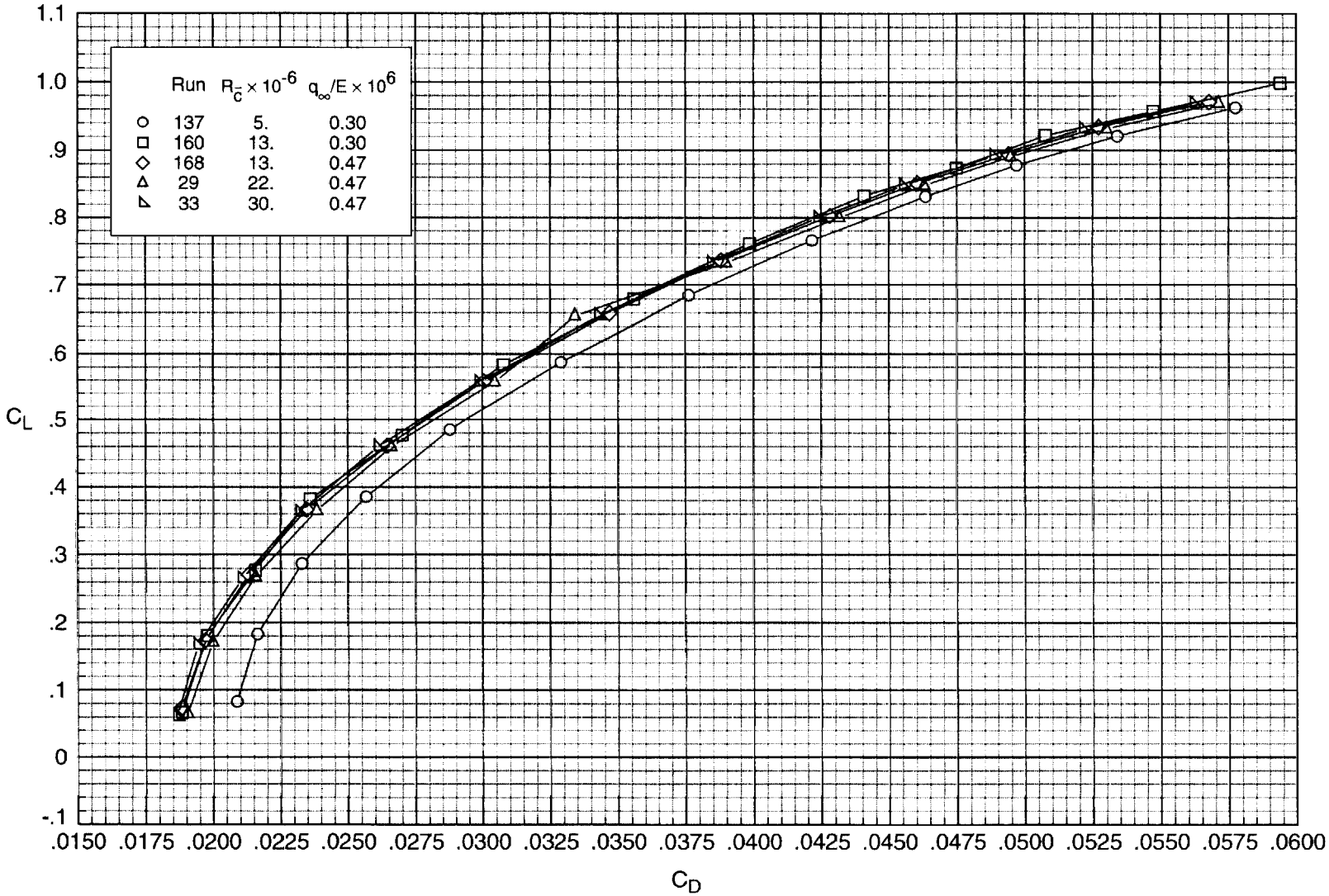

(a) Concluded.

Figure A1. Continued.

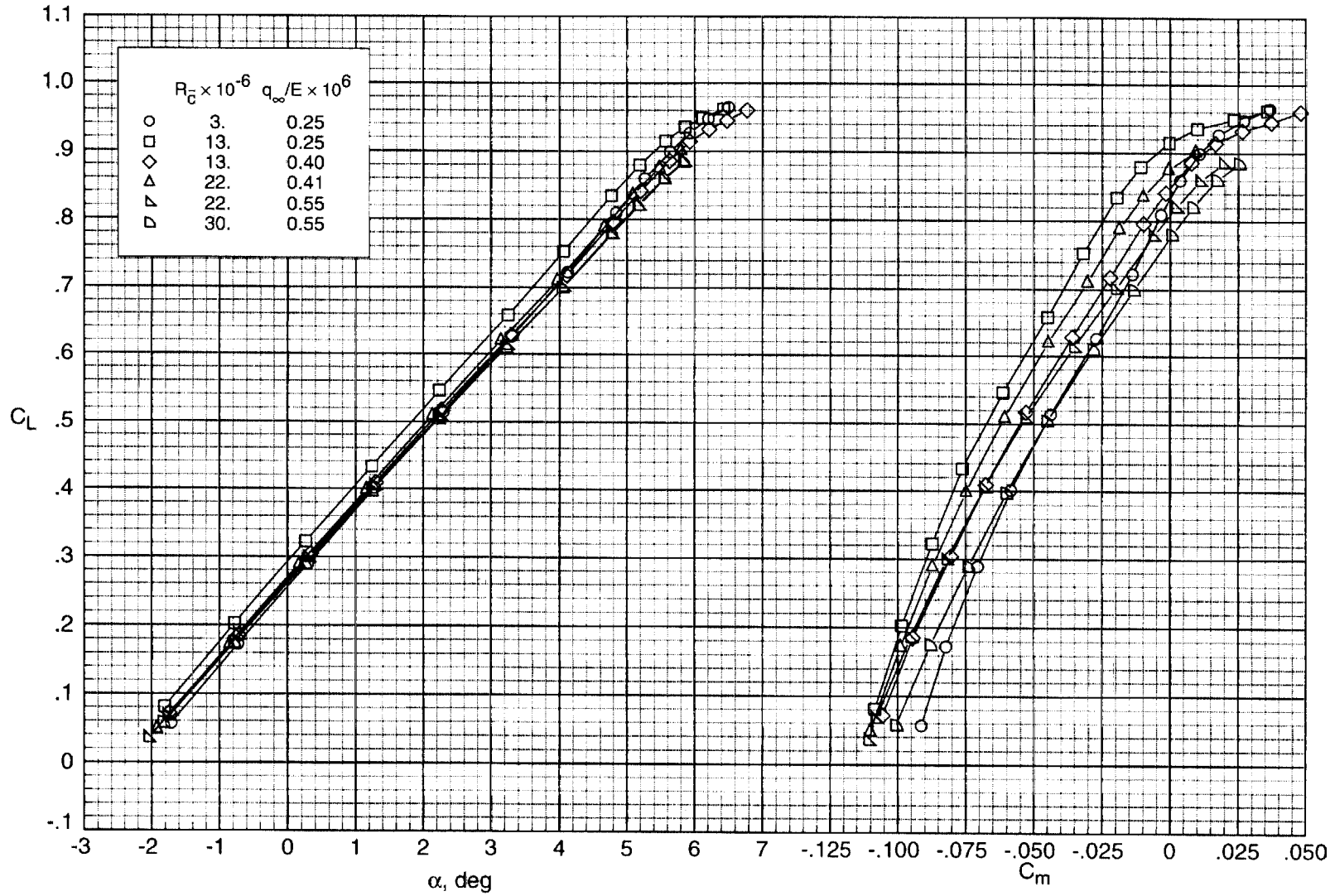

(b) $M_\infty = 0.70$.

Figure A1. Continued.

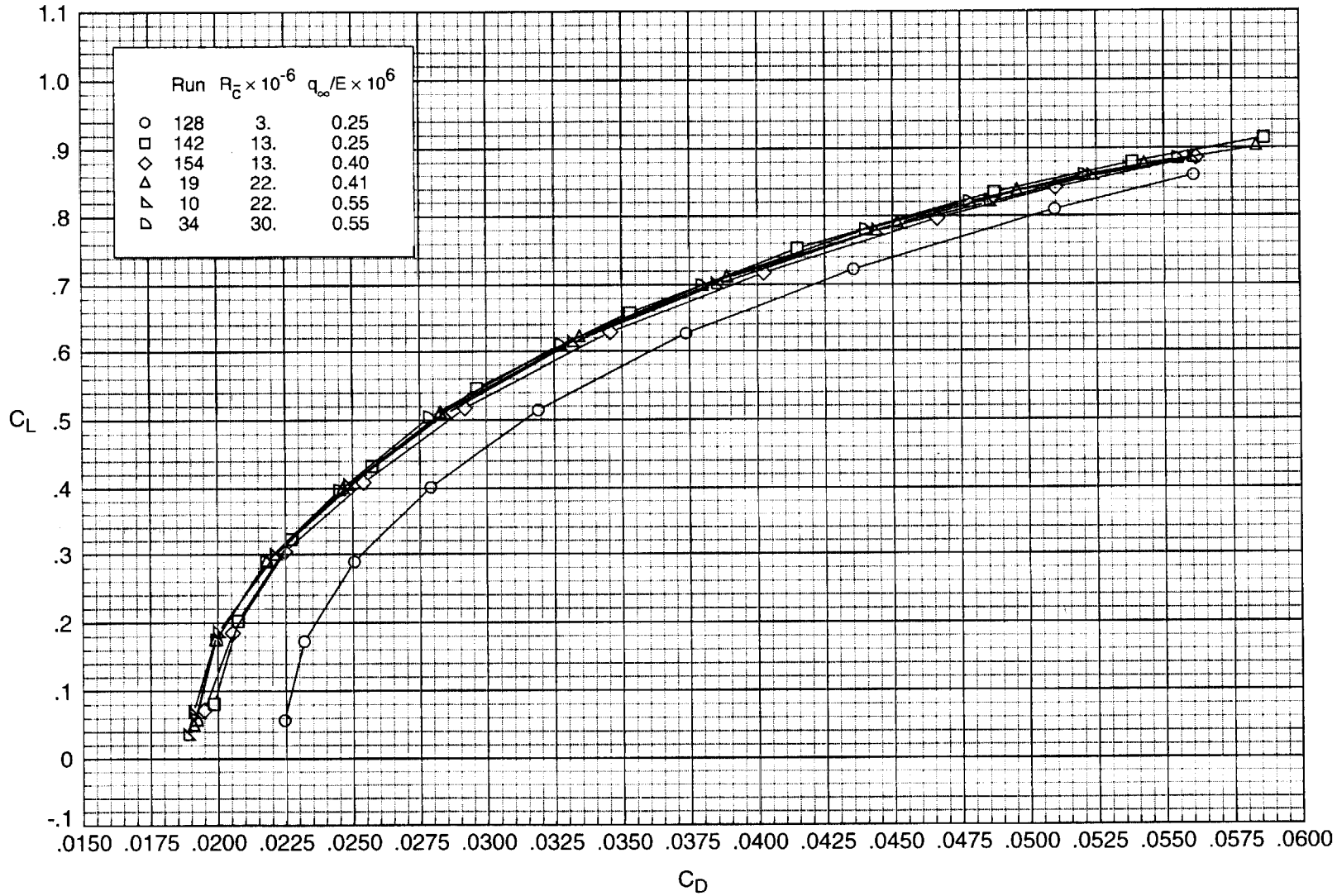

(b) Concluded.

Figure A1. Continued.

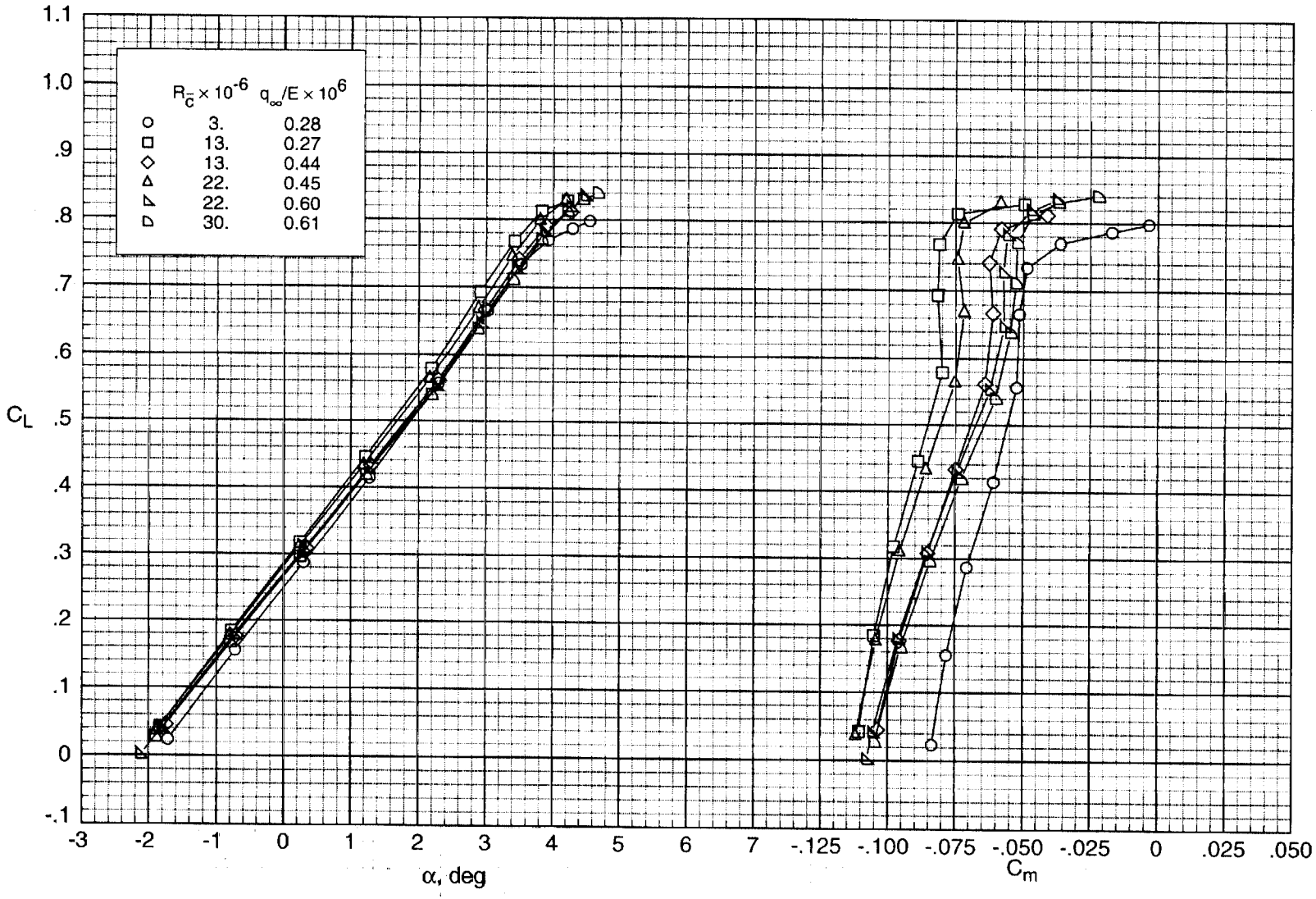

(c) $M_\infty = 0.80$.

Figure A1. Continued.

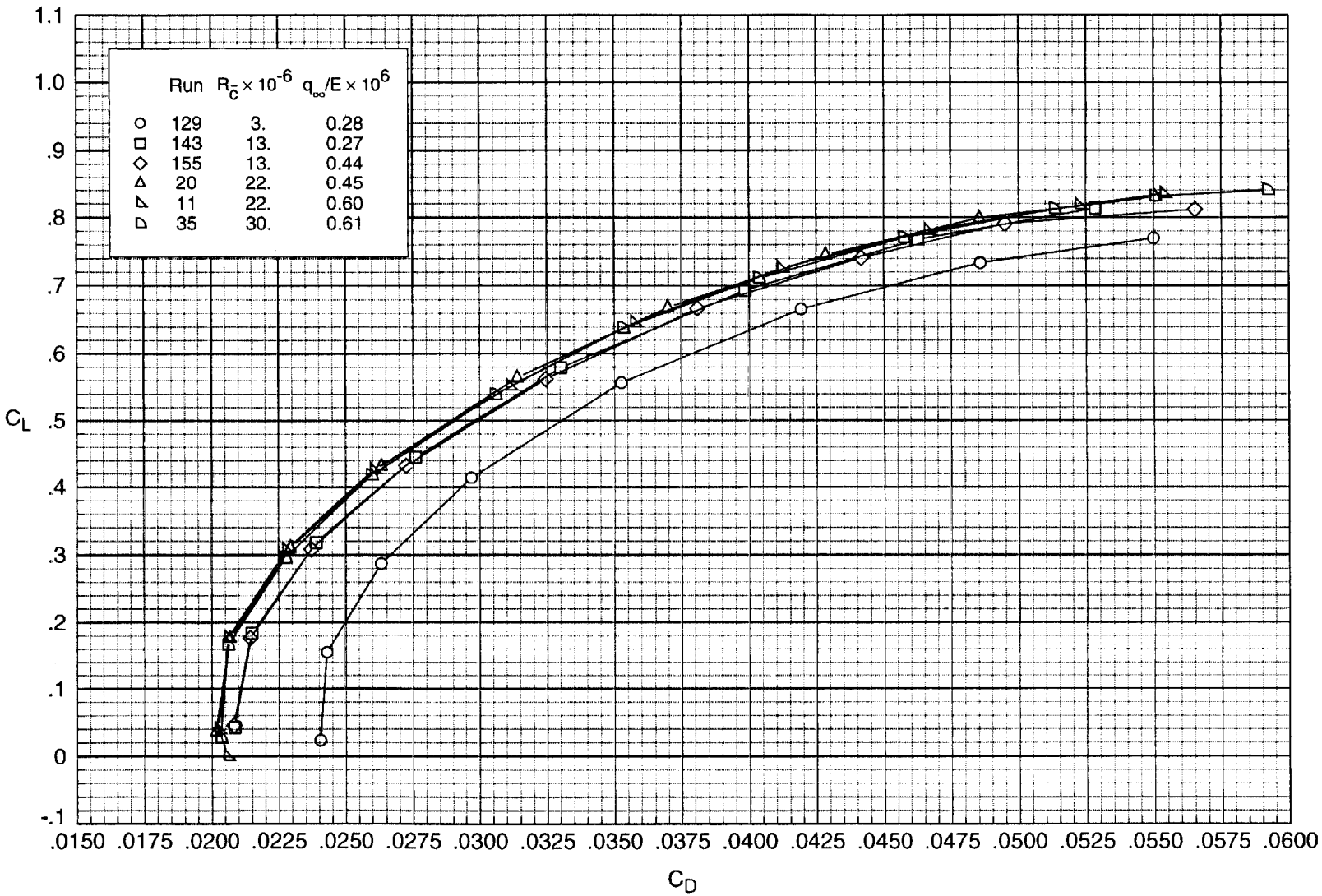

(c) Concluded.

Figure A1. Continued.

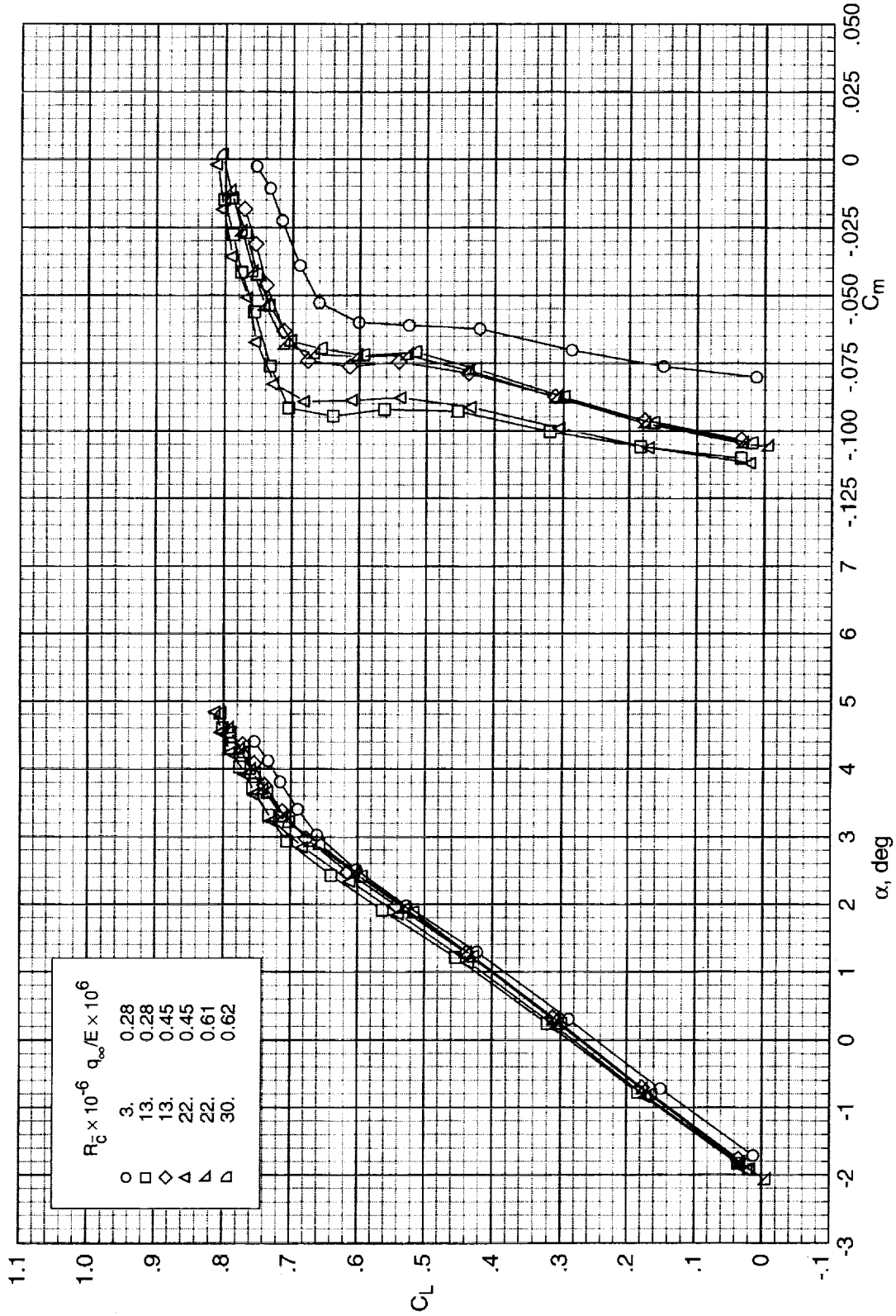

(d) $M_\infty = 0.82$.

Figure A1. Continued.

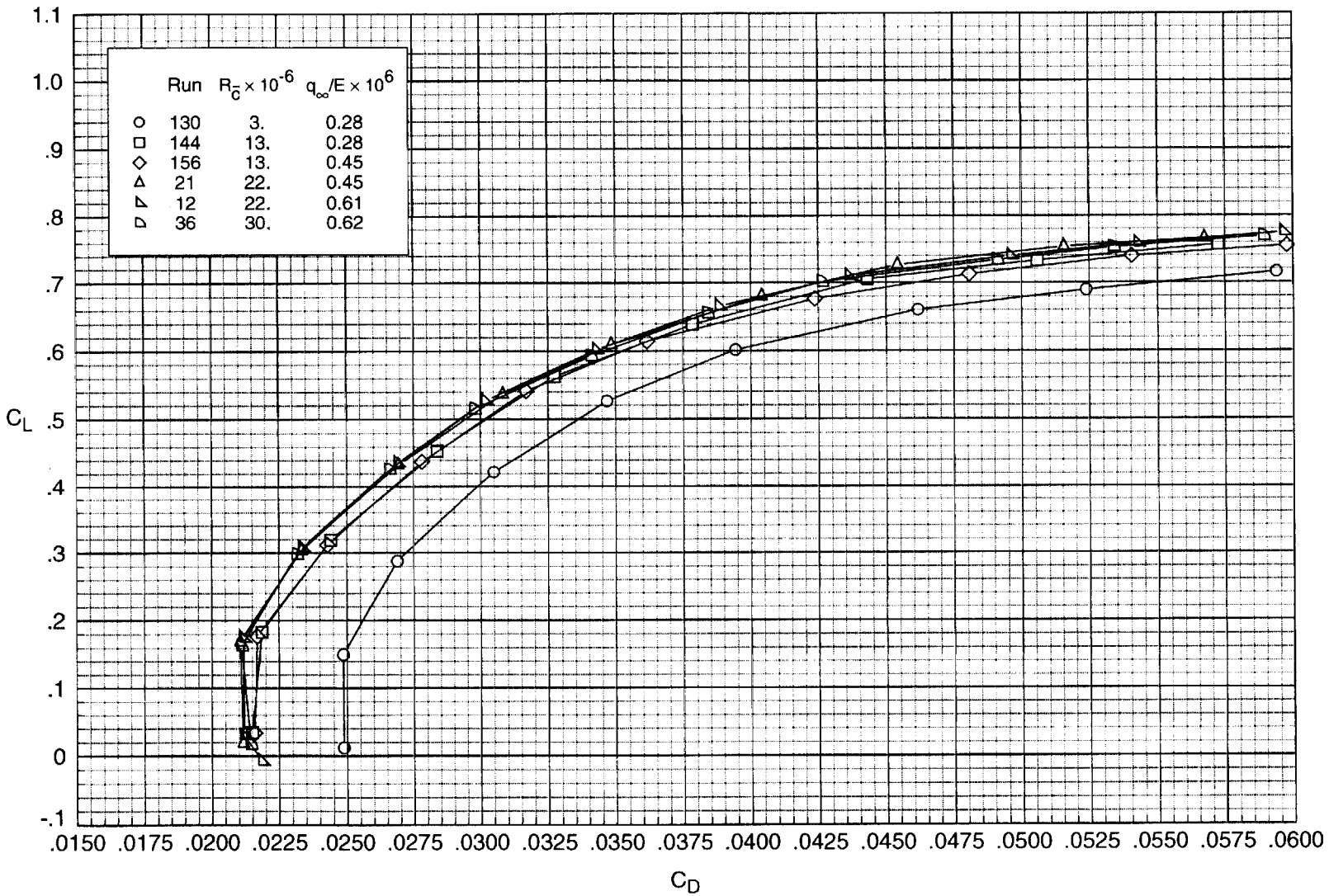

(d) Concluded.

Figure A1. Continued.

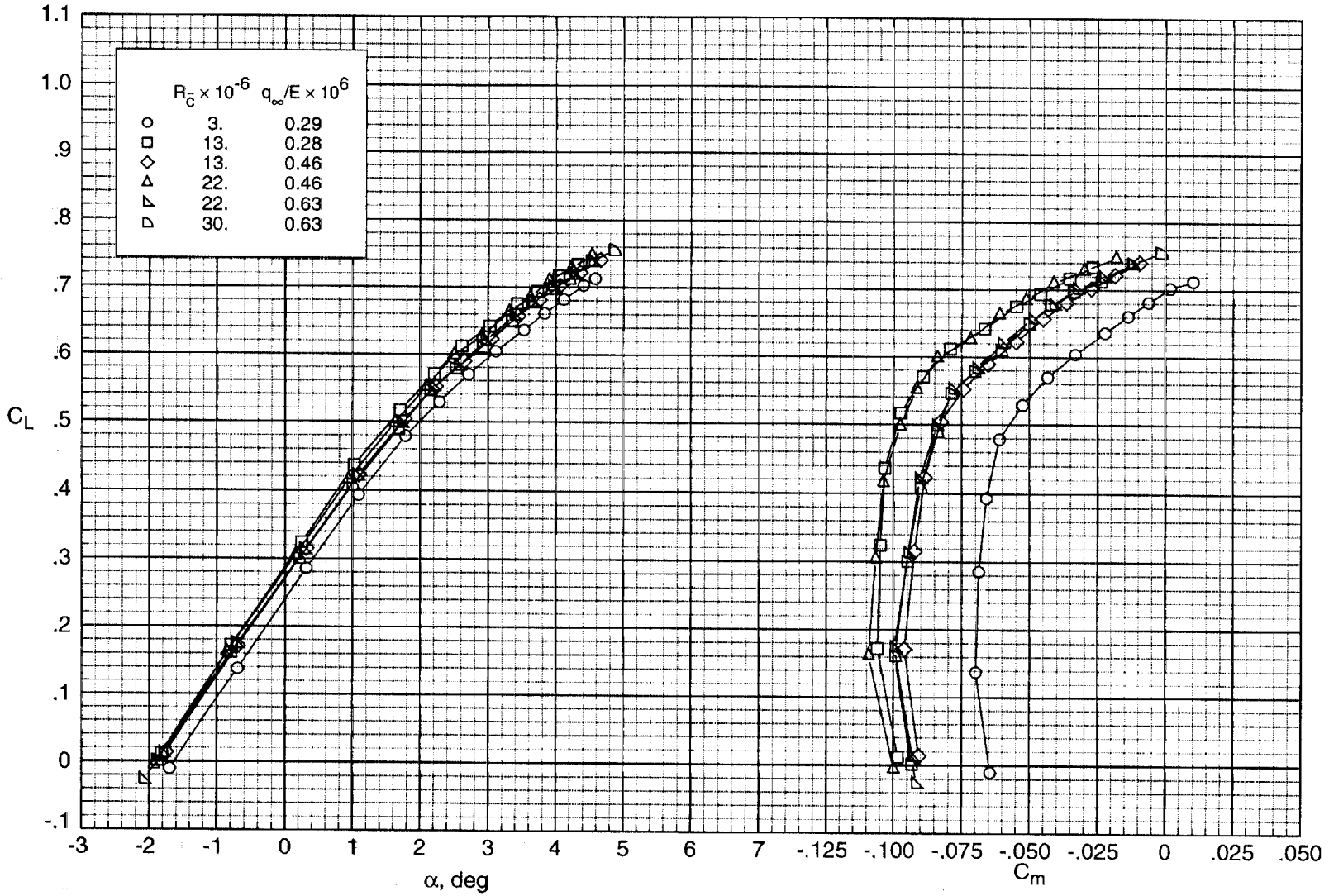

(e) $M_\infty = 0.85$.

Figure A1. Continued.

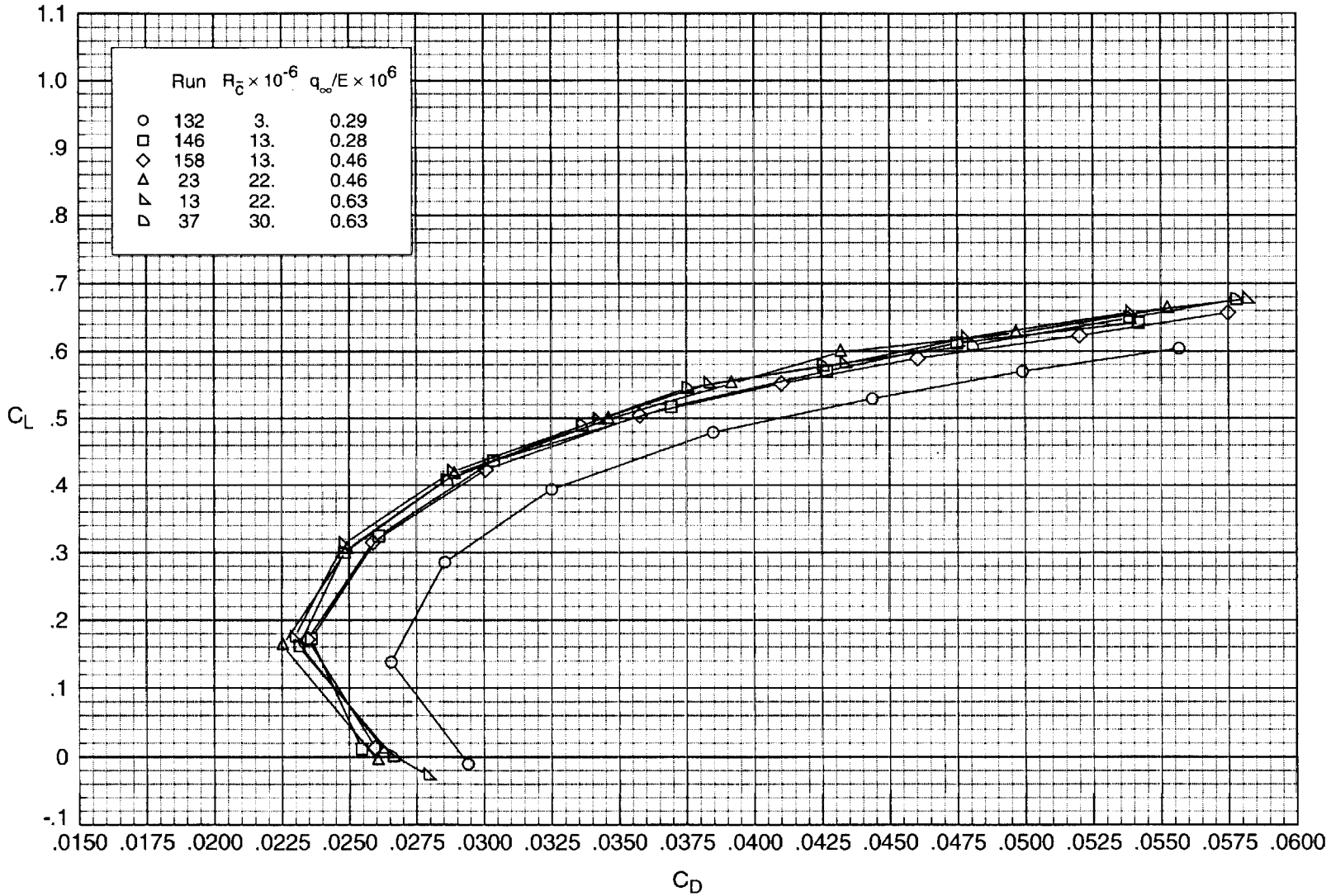

(e) Concluded.

Figure A1. Continued.

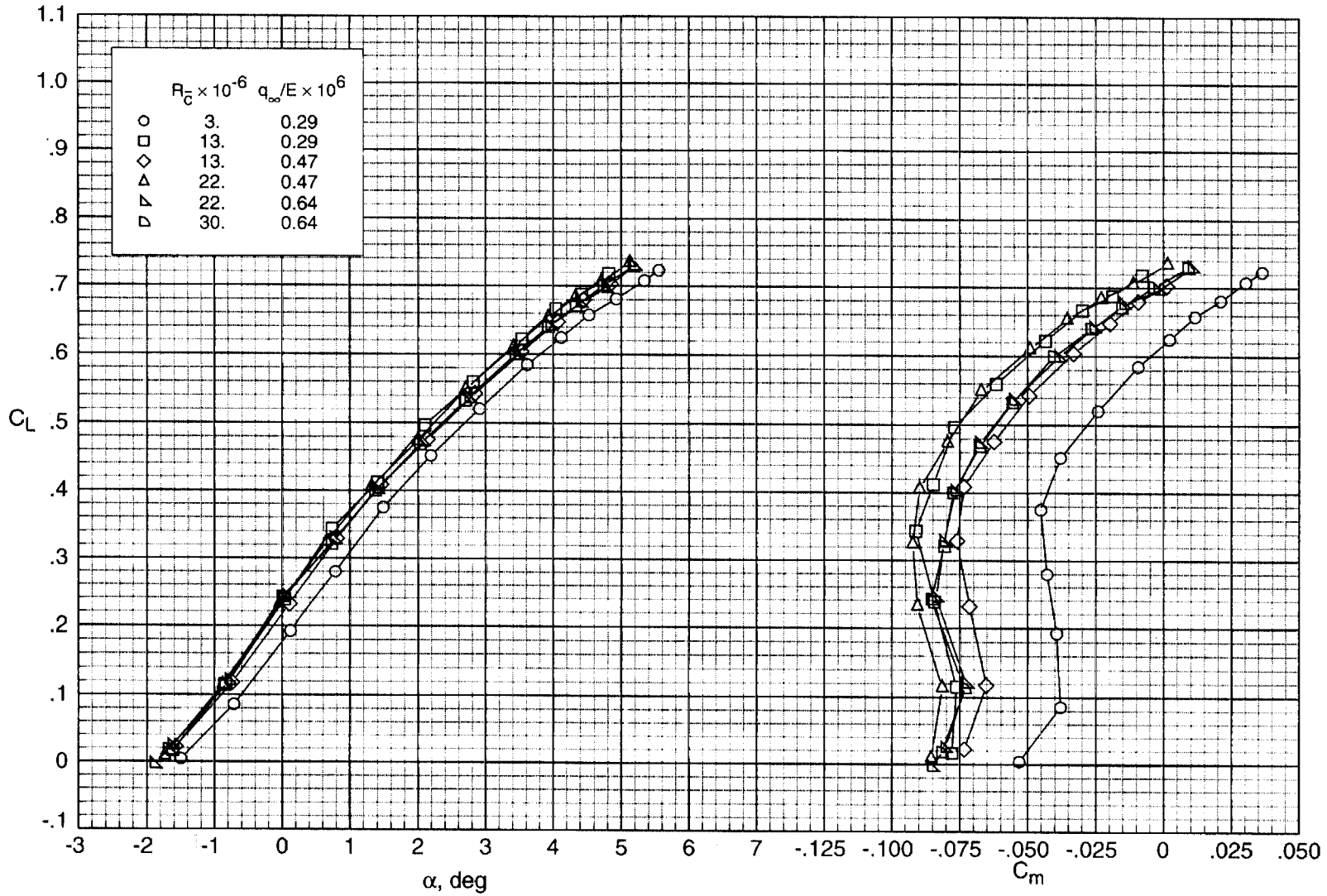

(f) $M_\infty = 0.88$.

Figure A1. Continued.

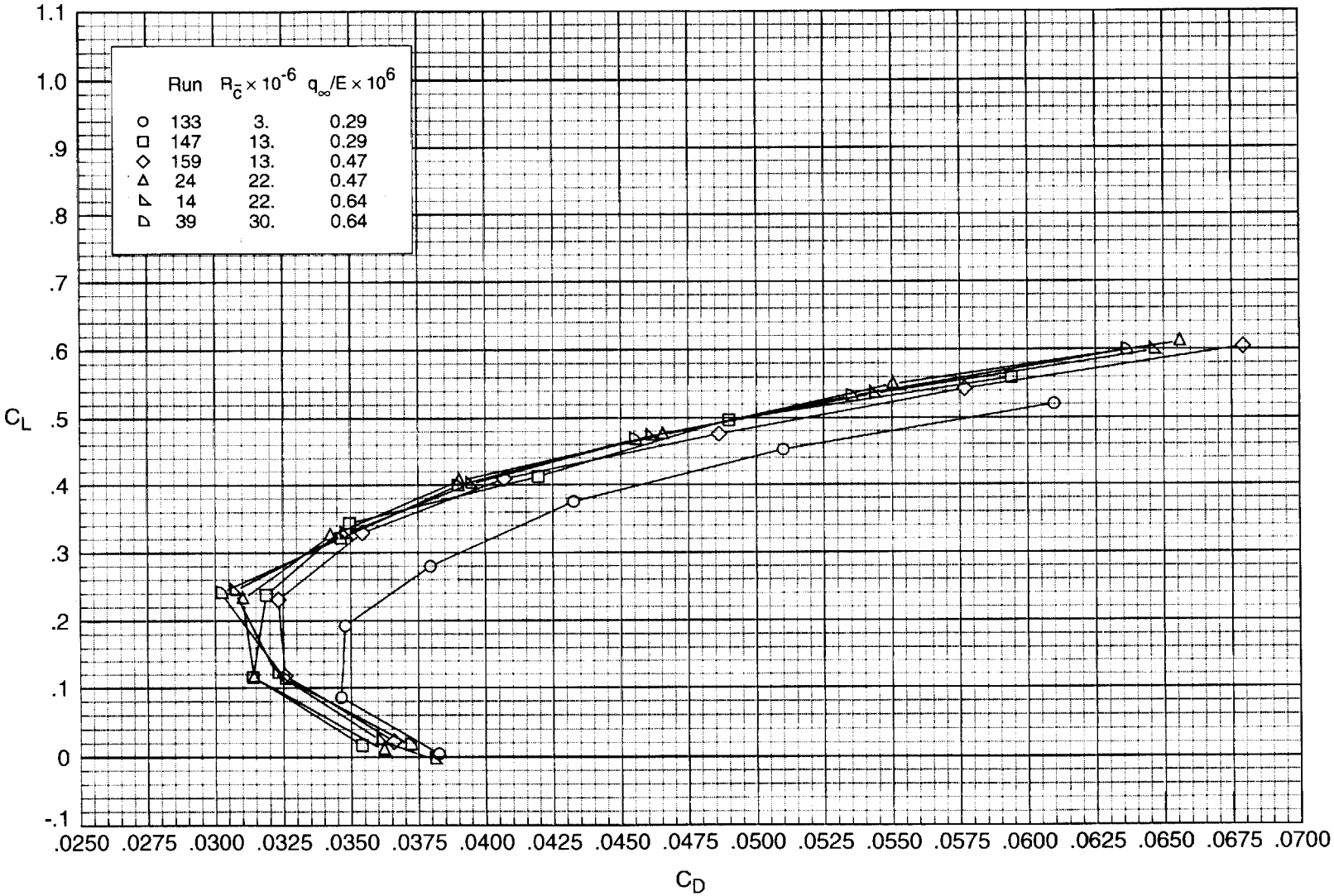

(f) Concluded.

Figure A1. Continued.

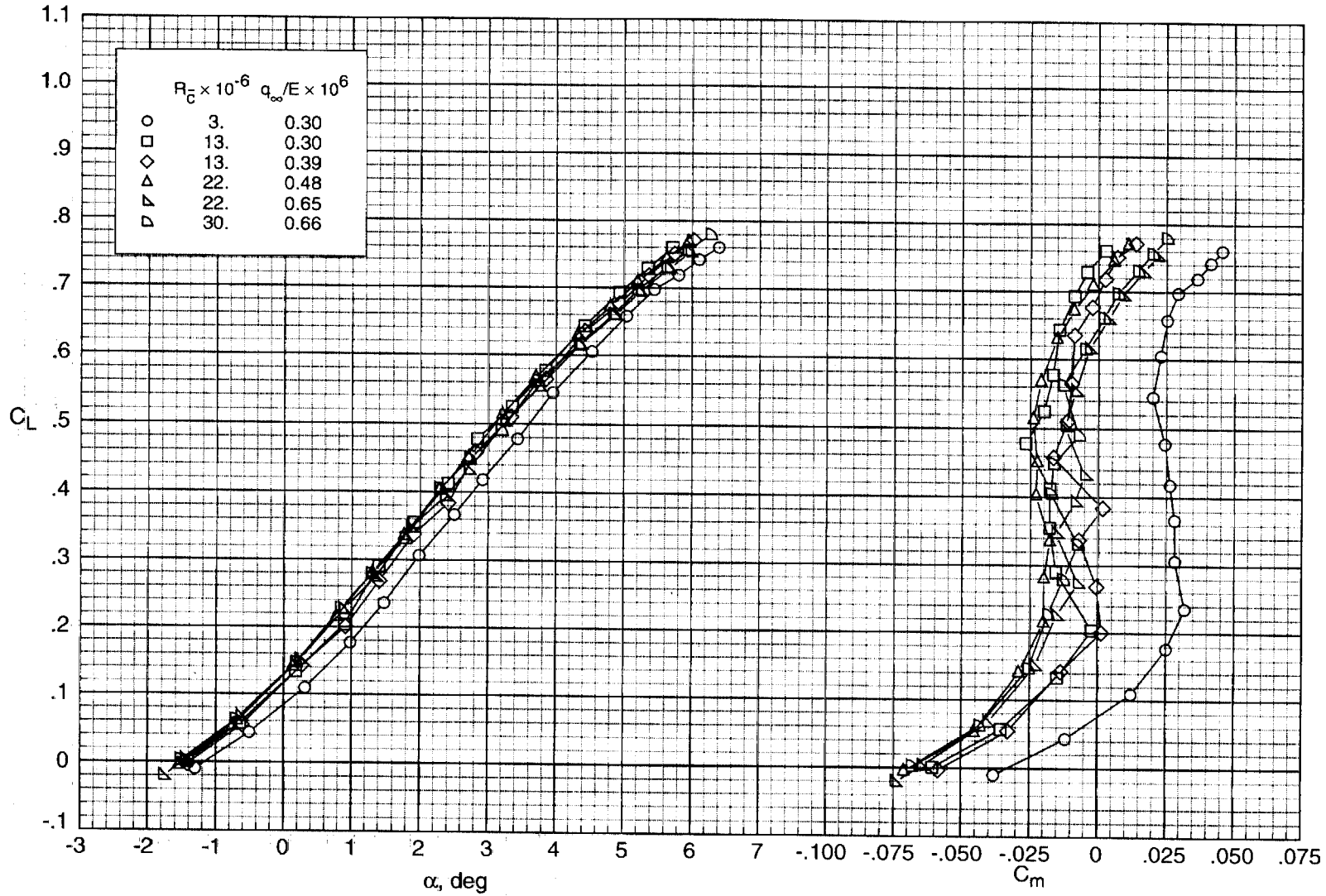

(g) $M_\infty = 0.91$.

Figure A1. Continued.

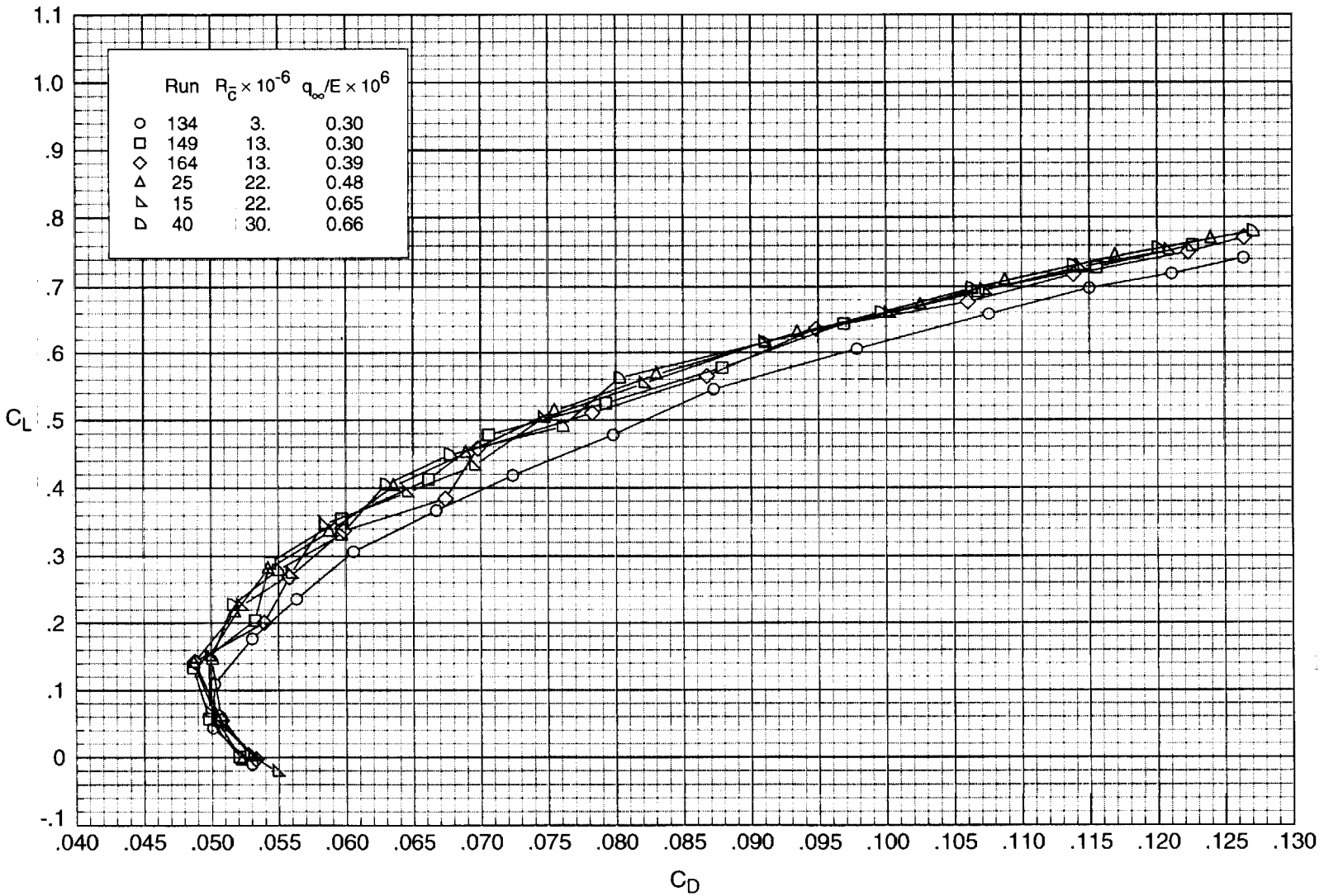

(g) Concluded.

Figure A1. Continued.

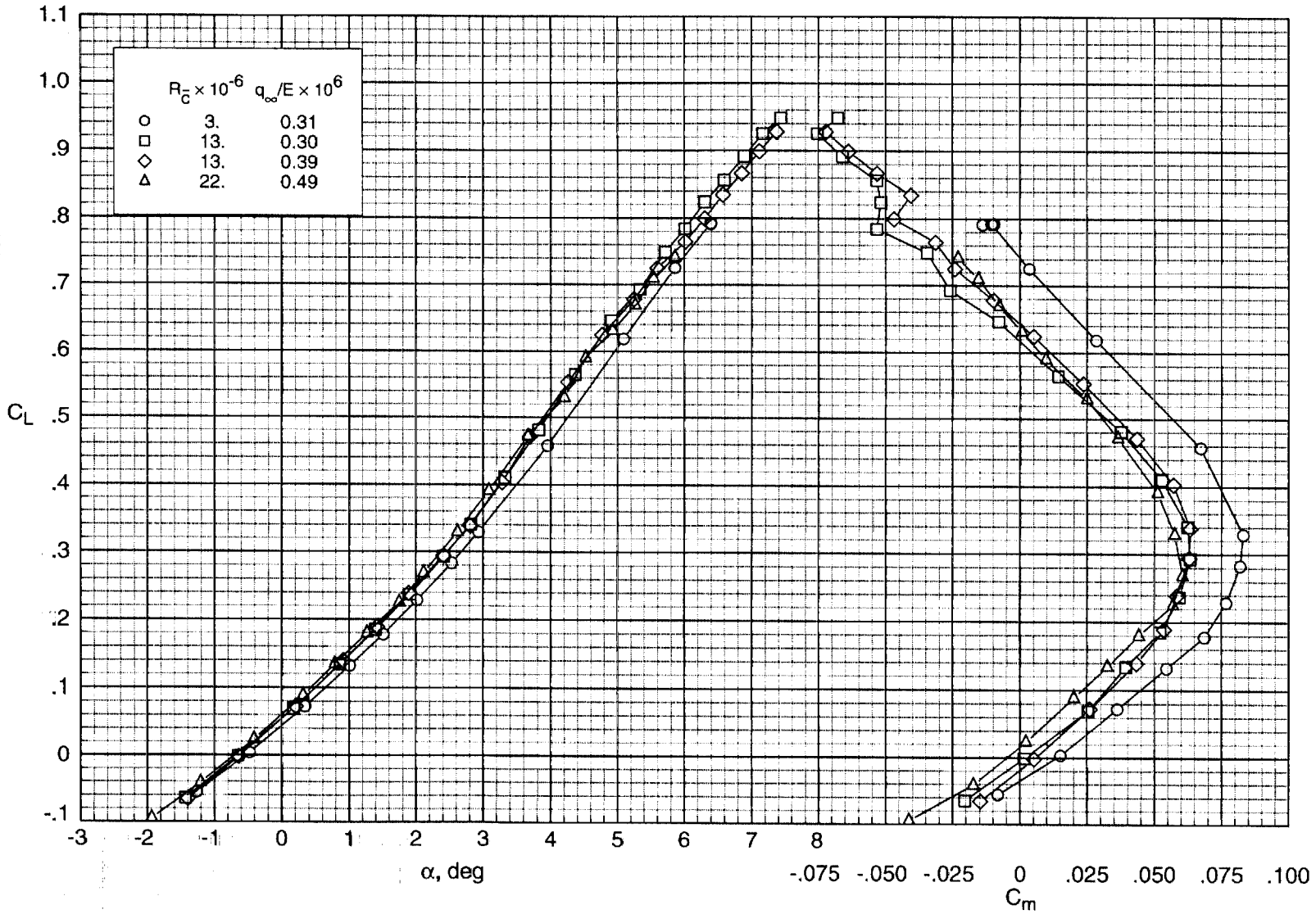

(h) $M_\infty = 0.94$.

Figure A1. Continued.

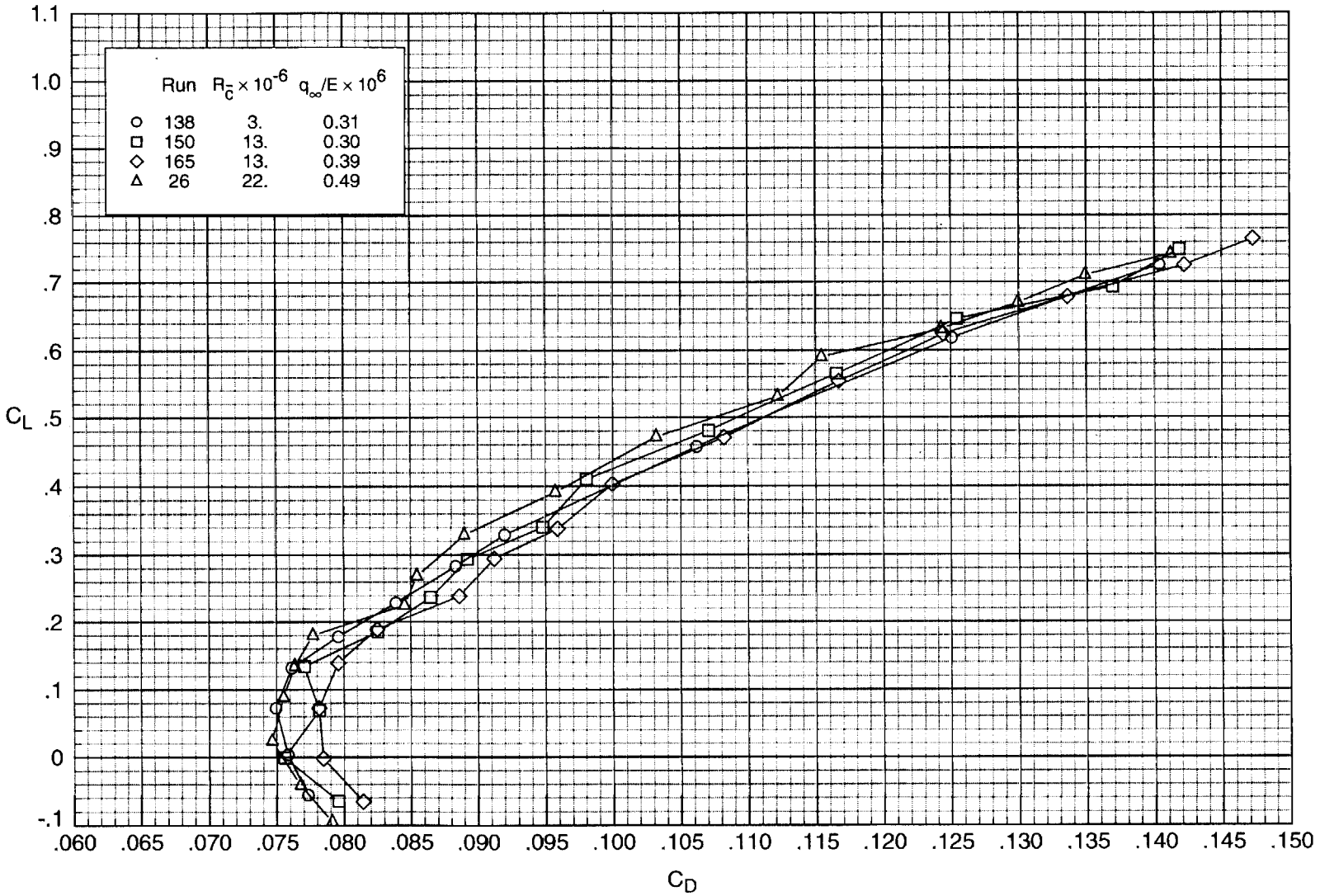

(h) Concluded.

Figure A1. Concluded.

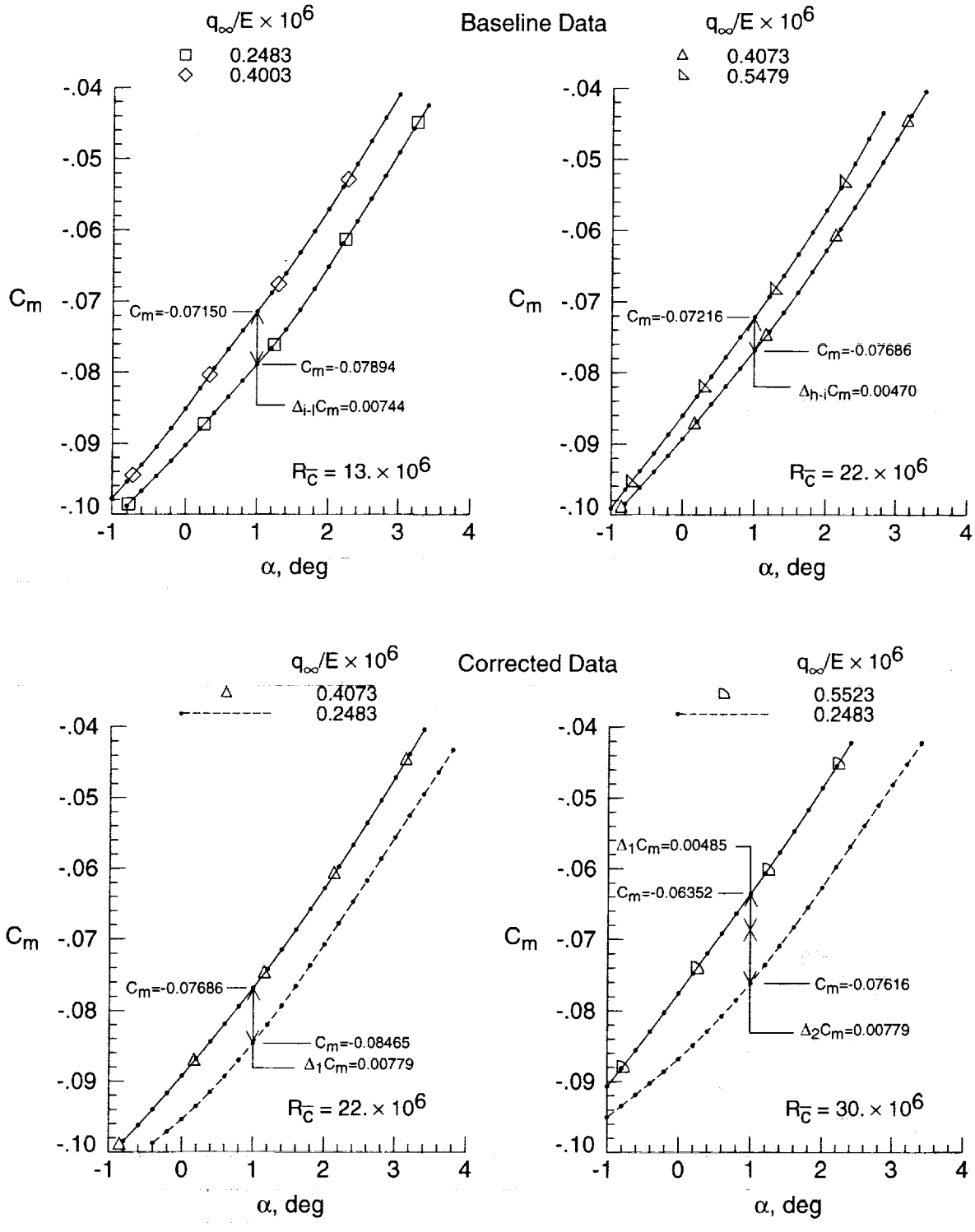

Figure A2. Illustration of steps in the baseline process to correct force and moment coefficients for static aeroelastic effects. Dots are curve-fit values.

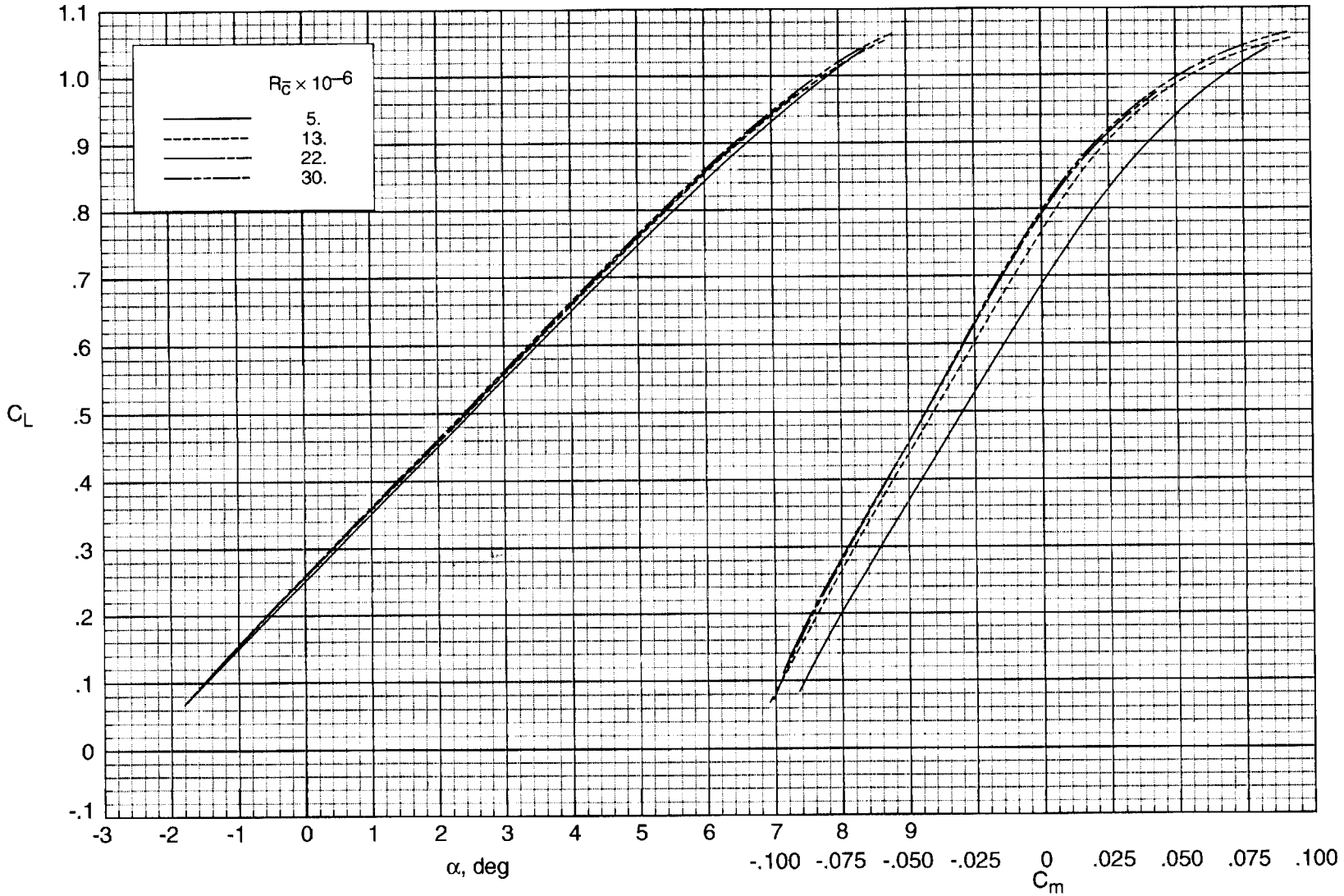

(a) $M_\infty = 0.50$.

Figure A3. Measured (corrected) longitudinal aerodynamic characteristics of the model.

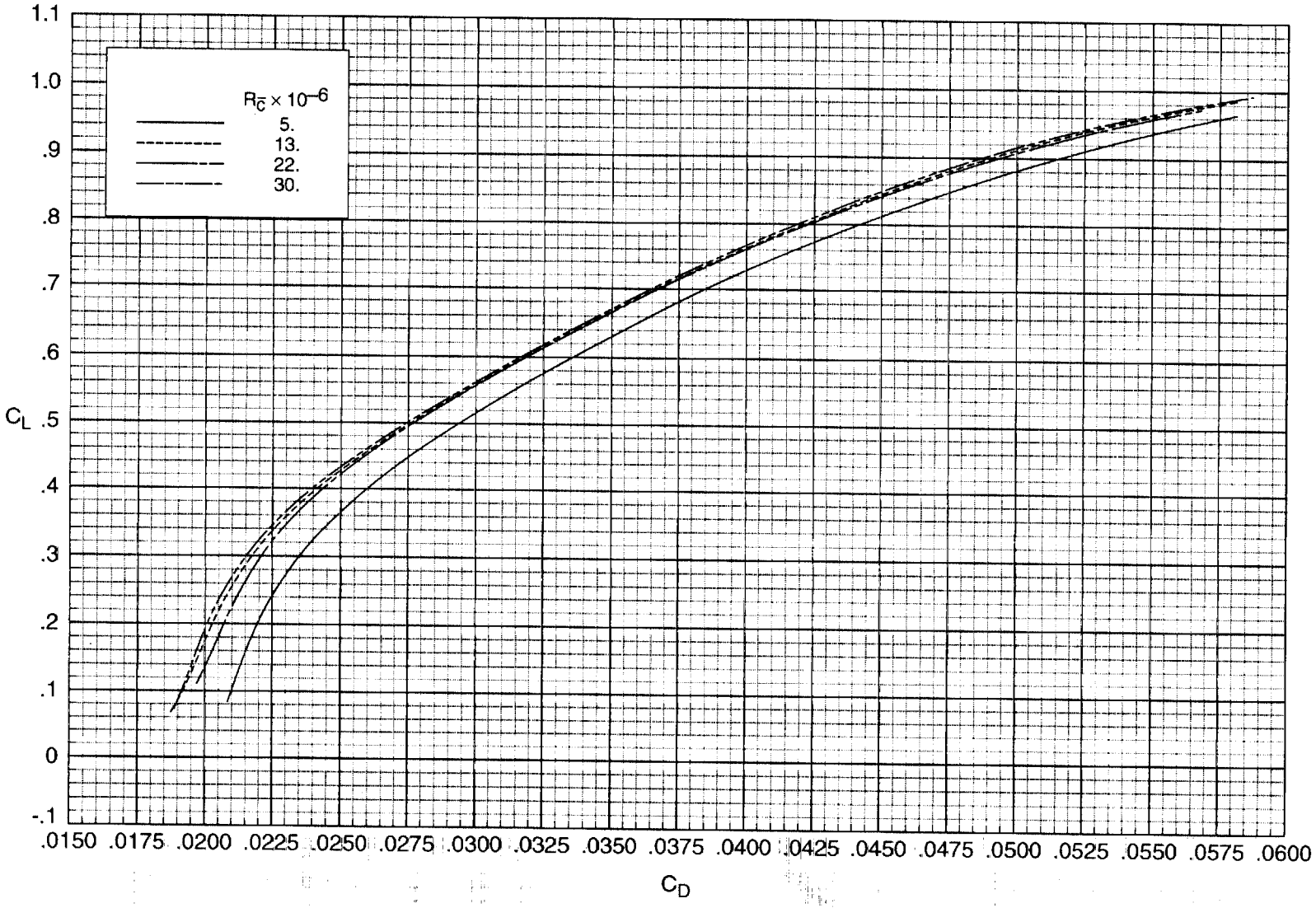

(a) Concluded.

Figure A3. Continued.

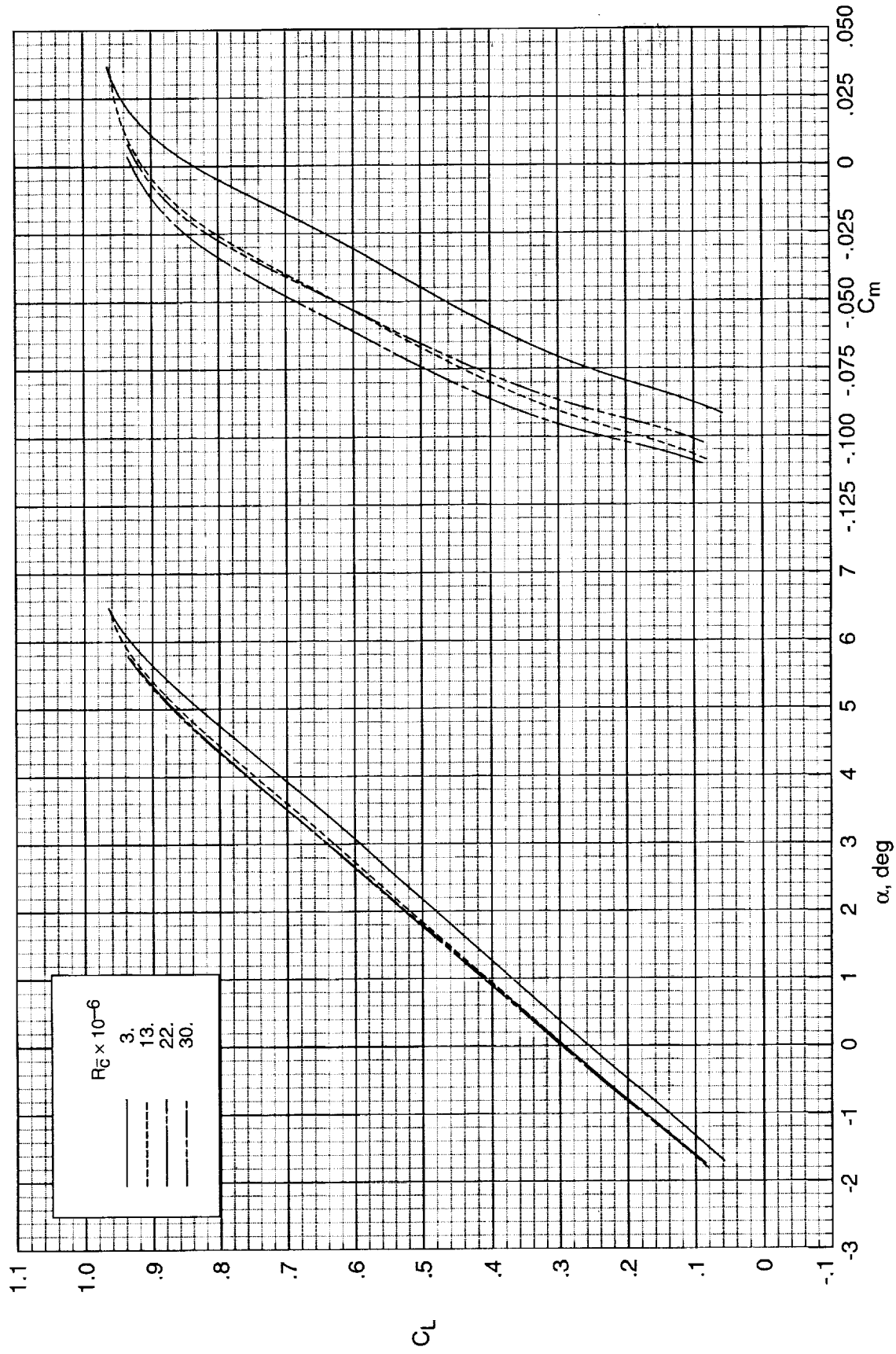

(b) $M_\infty = 0.70$.

Figure A3. Continued.

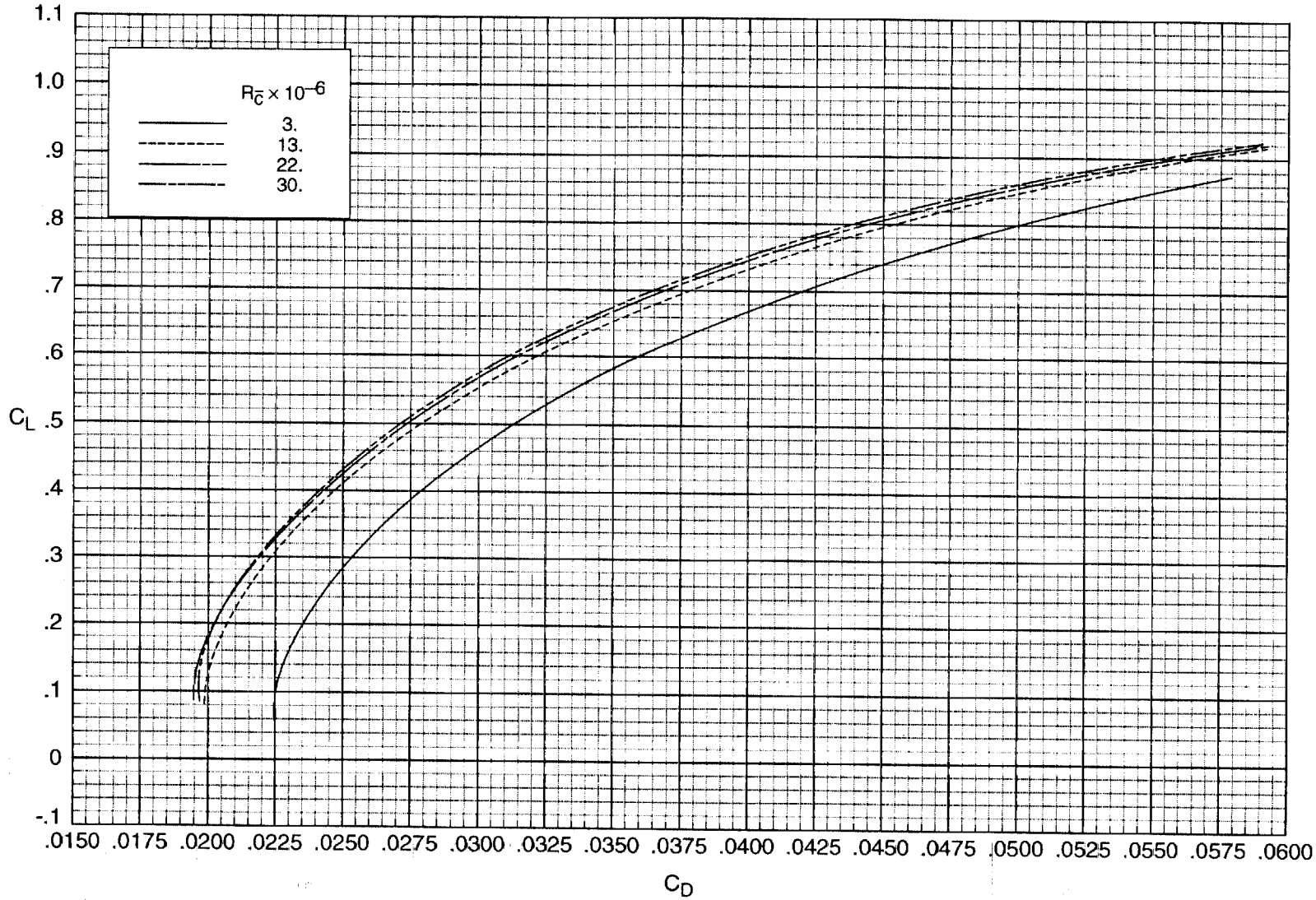

(b) Concluded.

Figure A3. Continued.

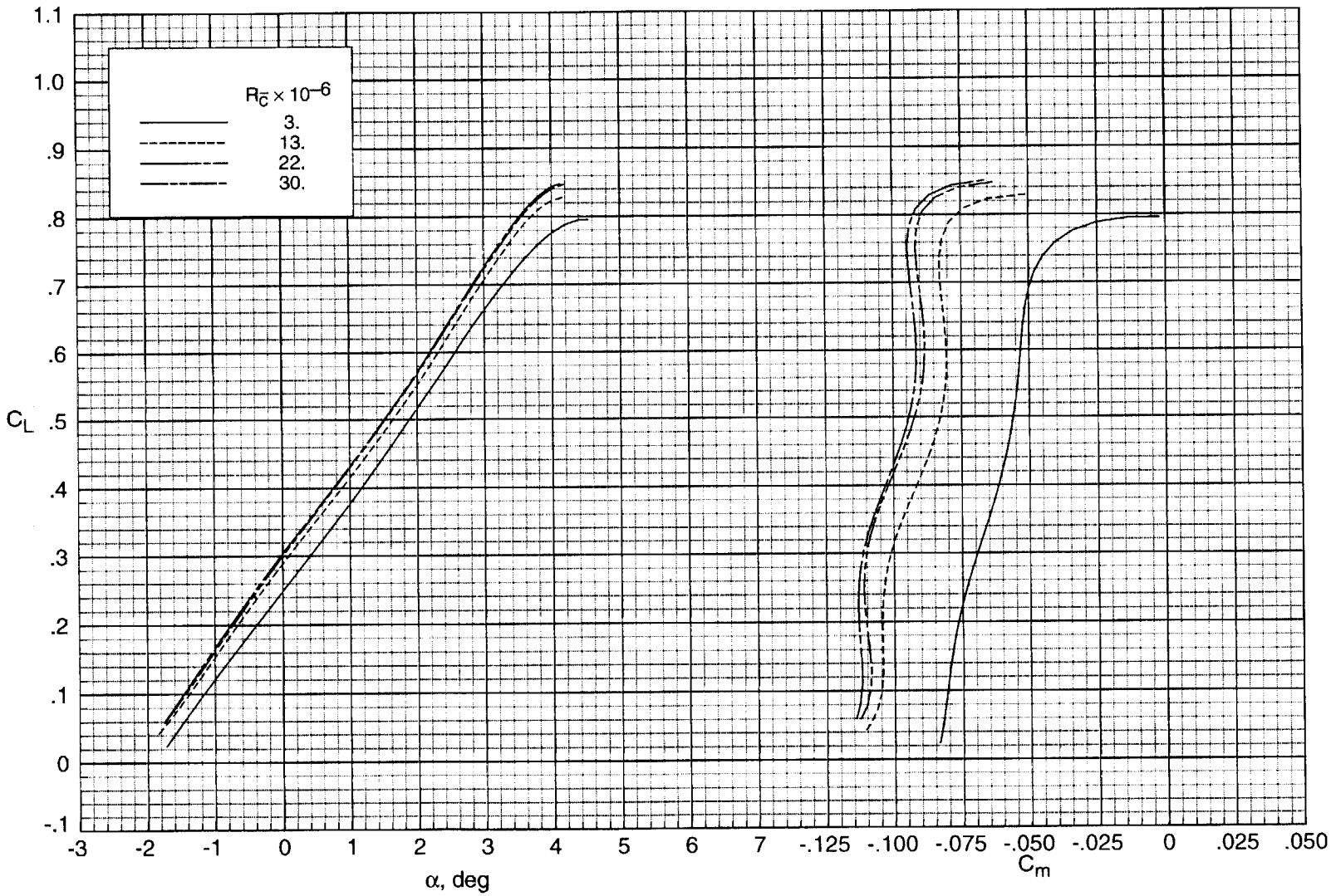

(c) $M_\infty = 0.80$.

Figure A3. Continued.

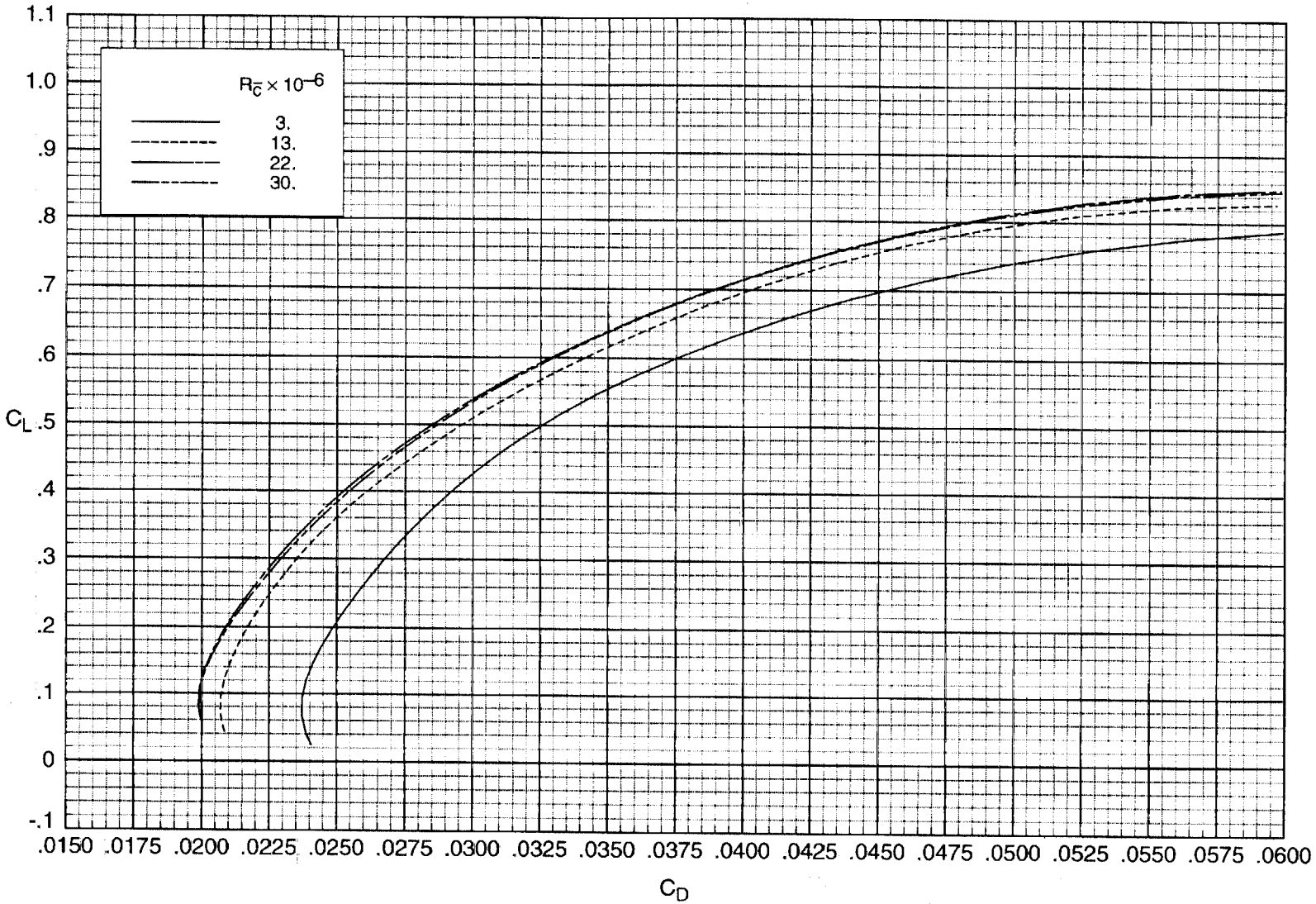

(c) Concluded.

Figure A3. Continued.

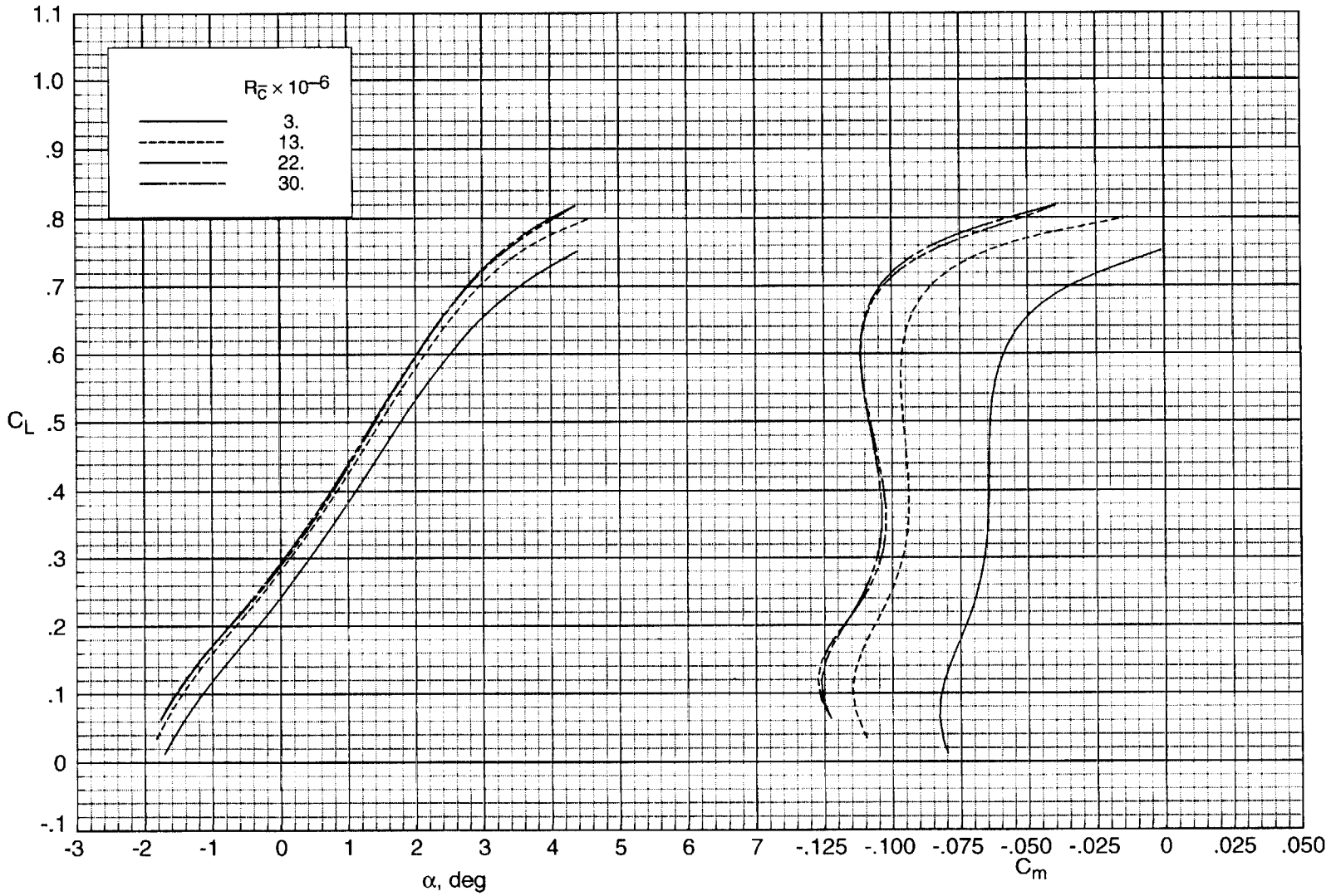

(d) $M_\infty = 0.82$.

Figure A3. Continued.

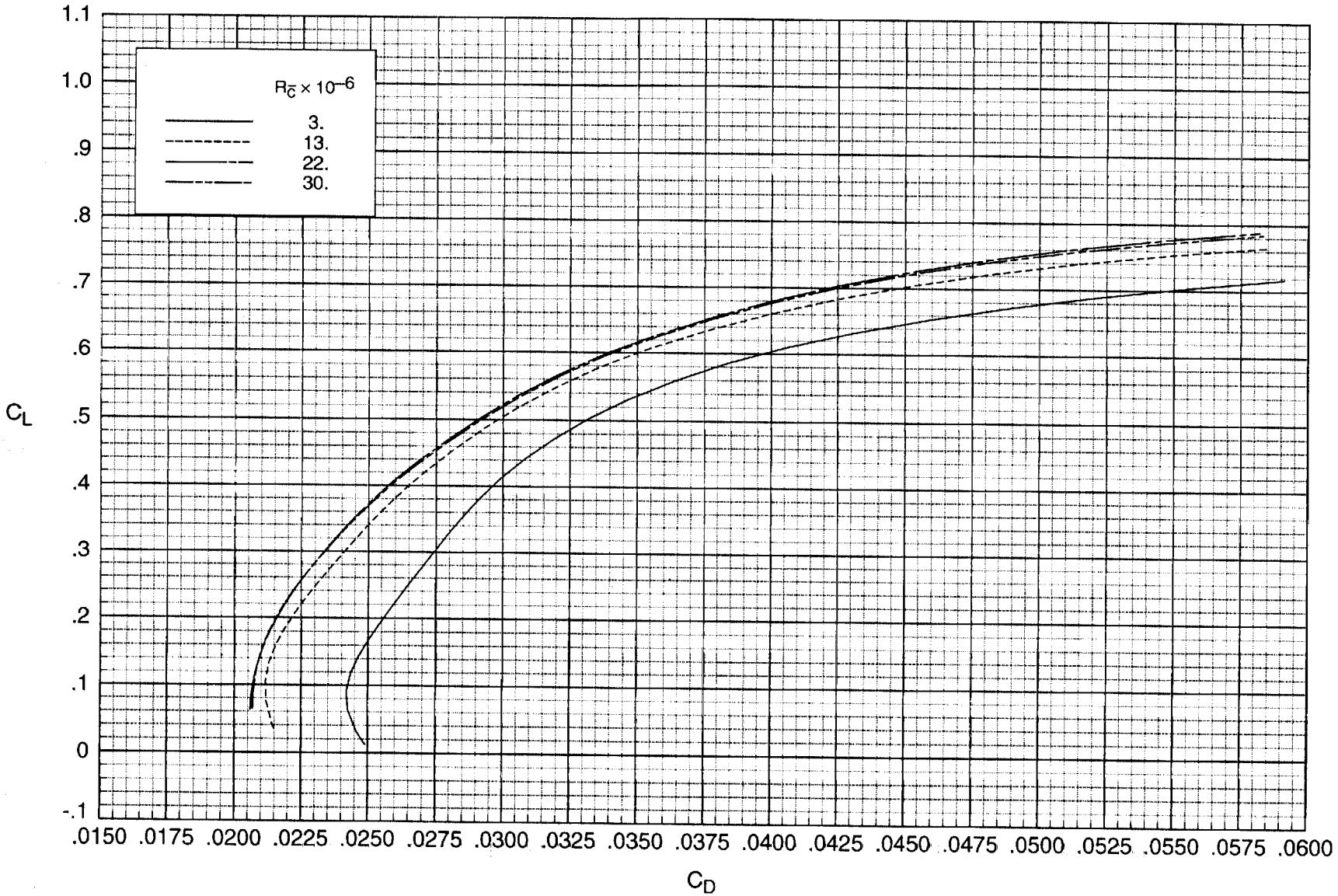

(d) Concluded.

Figure A3. Continued.

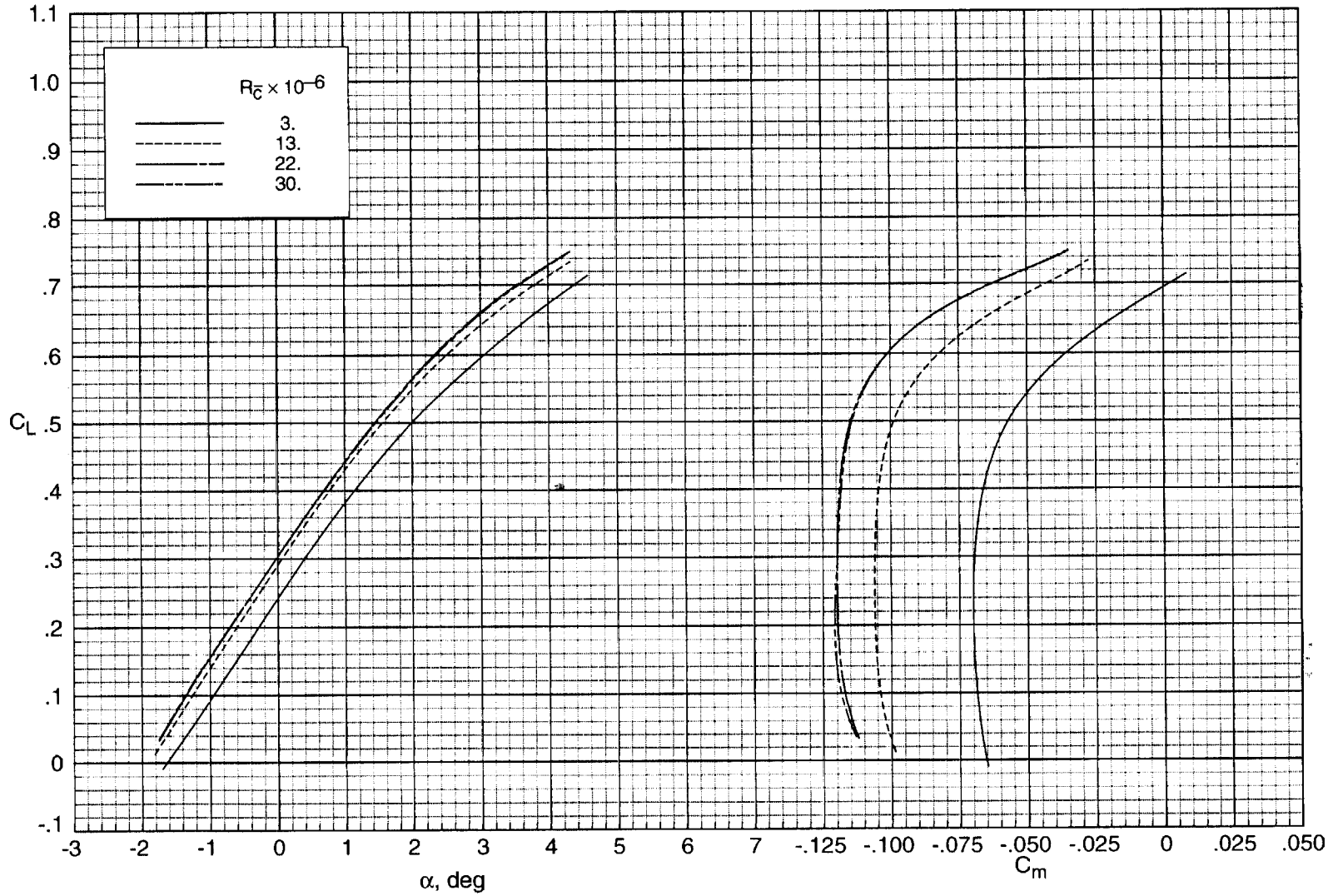

(e) $M_\infty = 0.85$.

Figure A3. Continued.

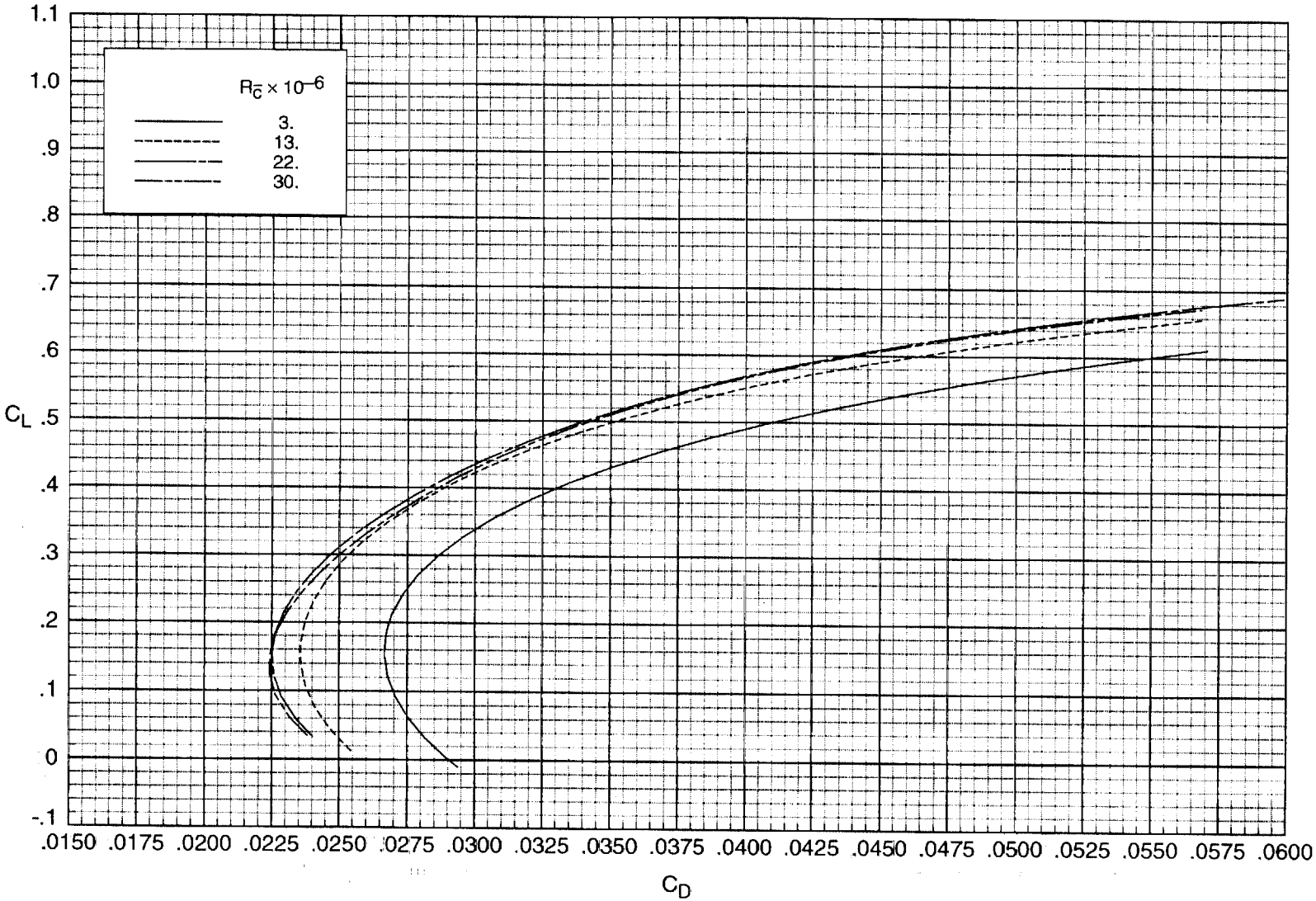

(e) Concluded.

Figure A3. Continued.

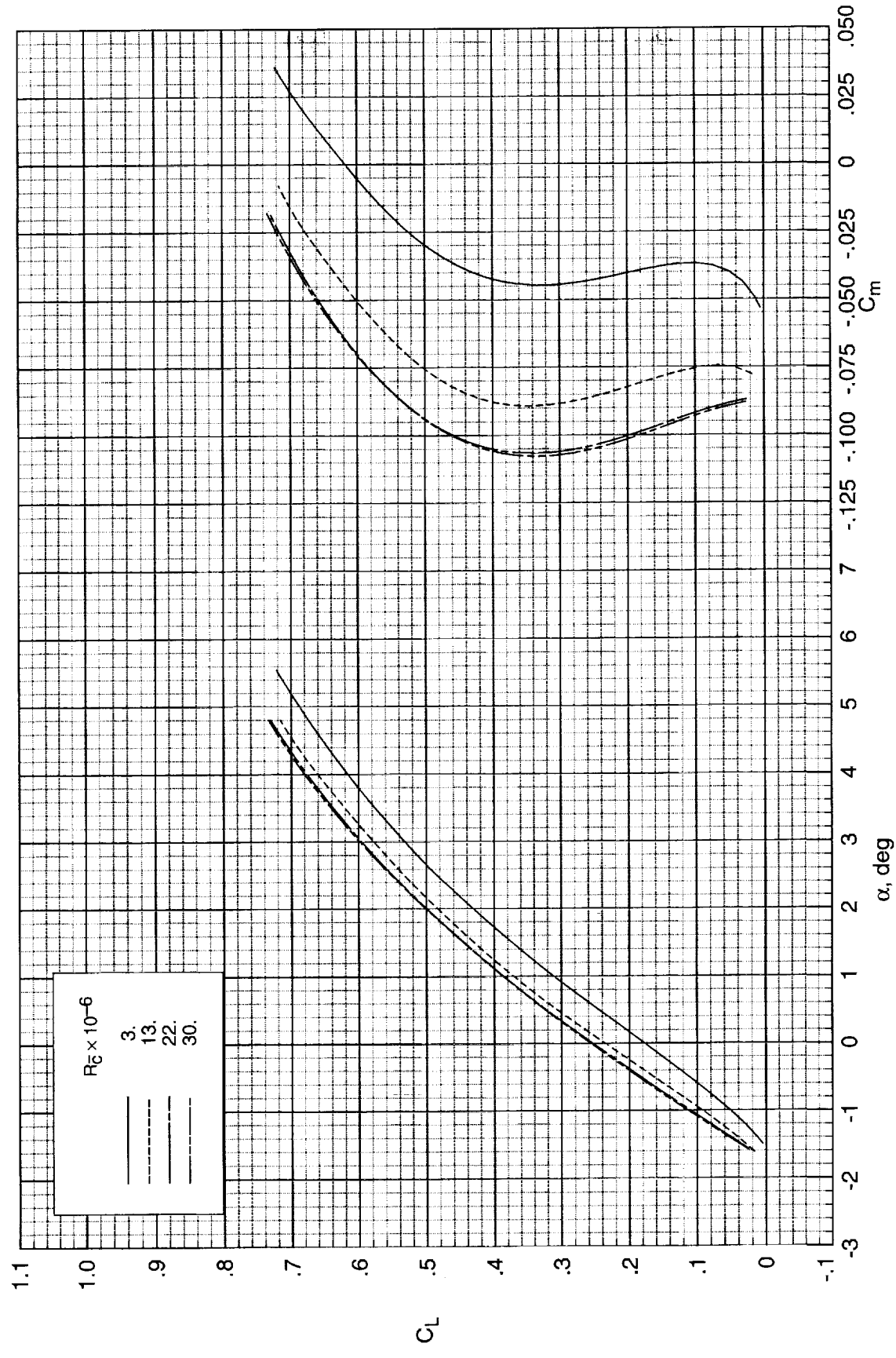

(f) $M_\infty = 0.88$.

Figure A3. Continued.

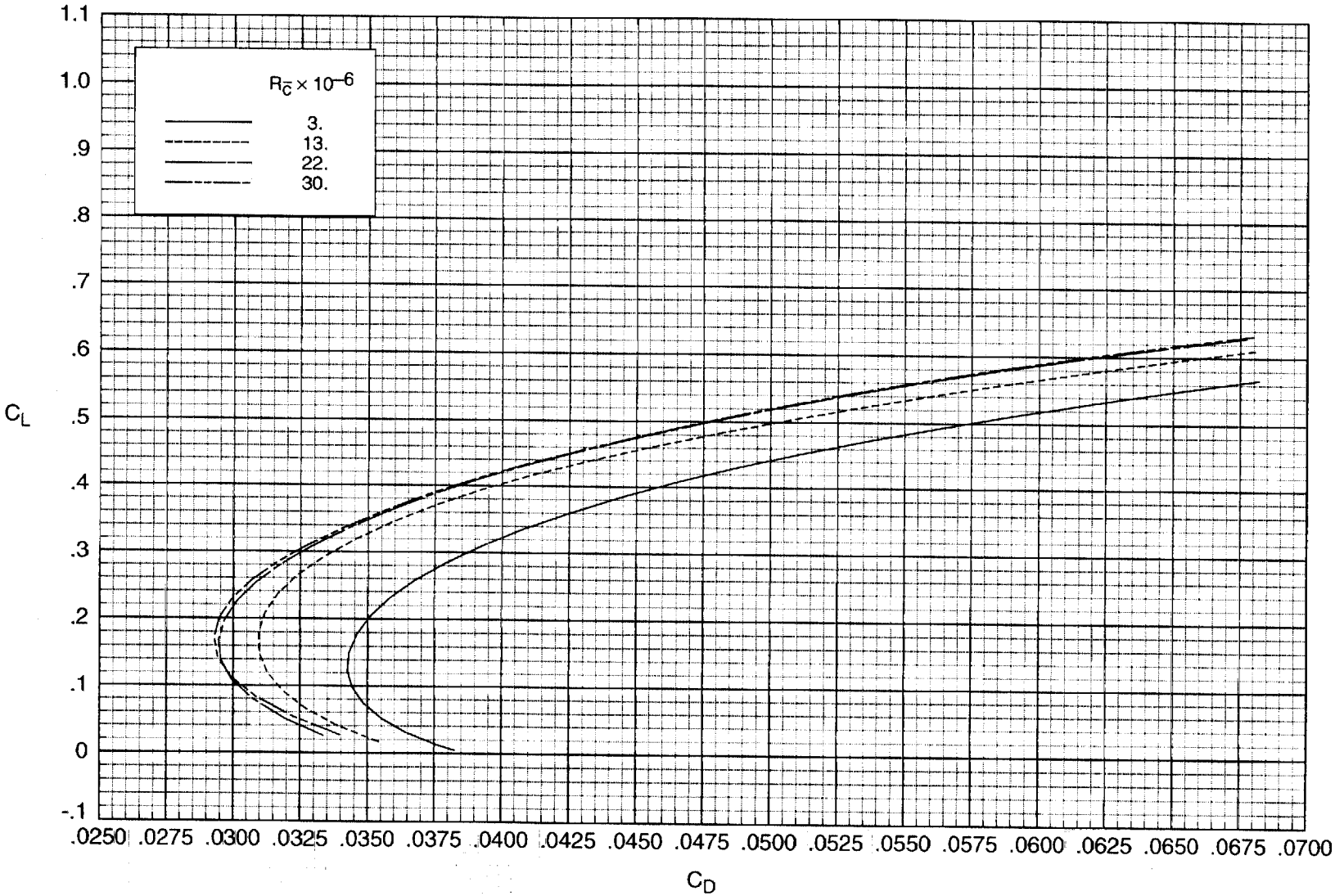

(f) Concluded.

Figure A3. Continued.

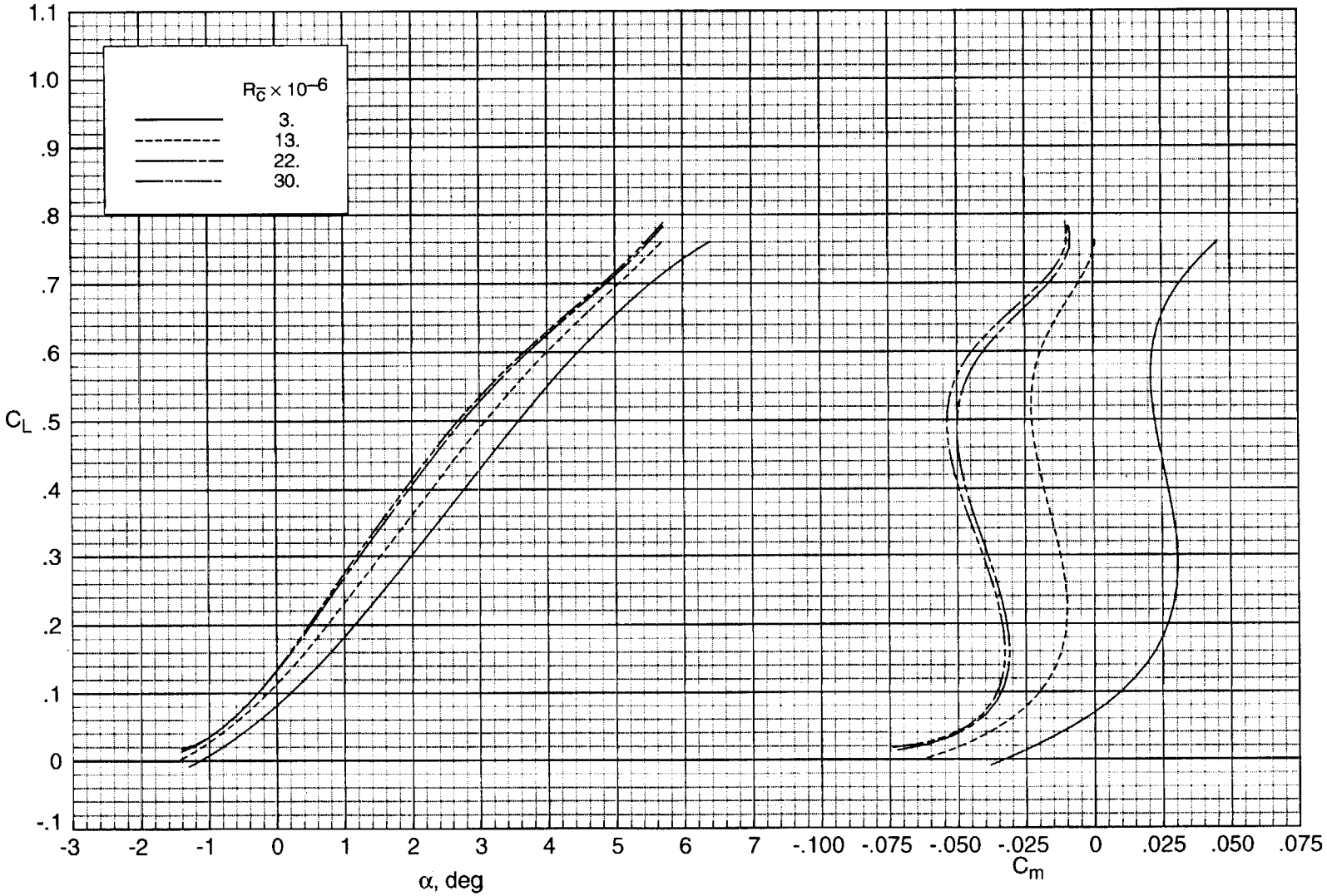

(g) $M_\infty = 0.91$.

Figure A3. Continued.

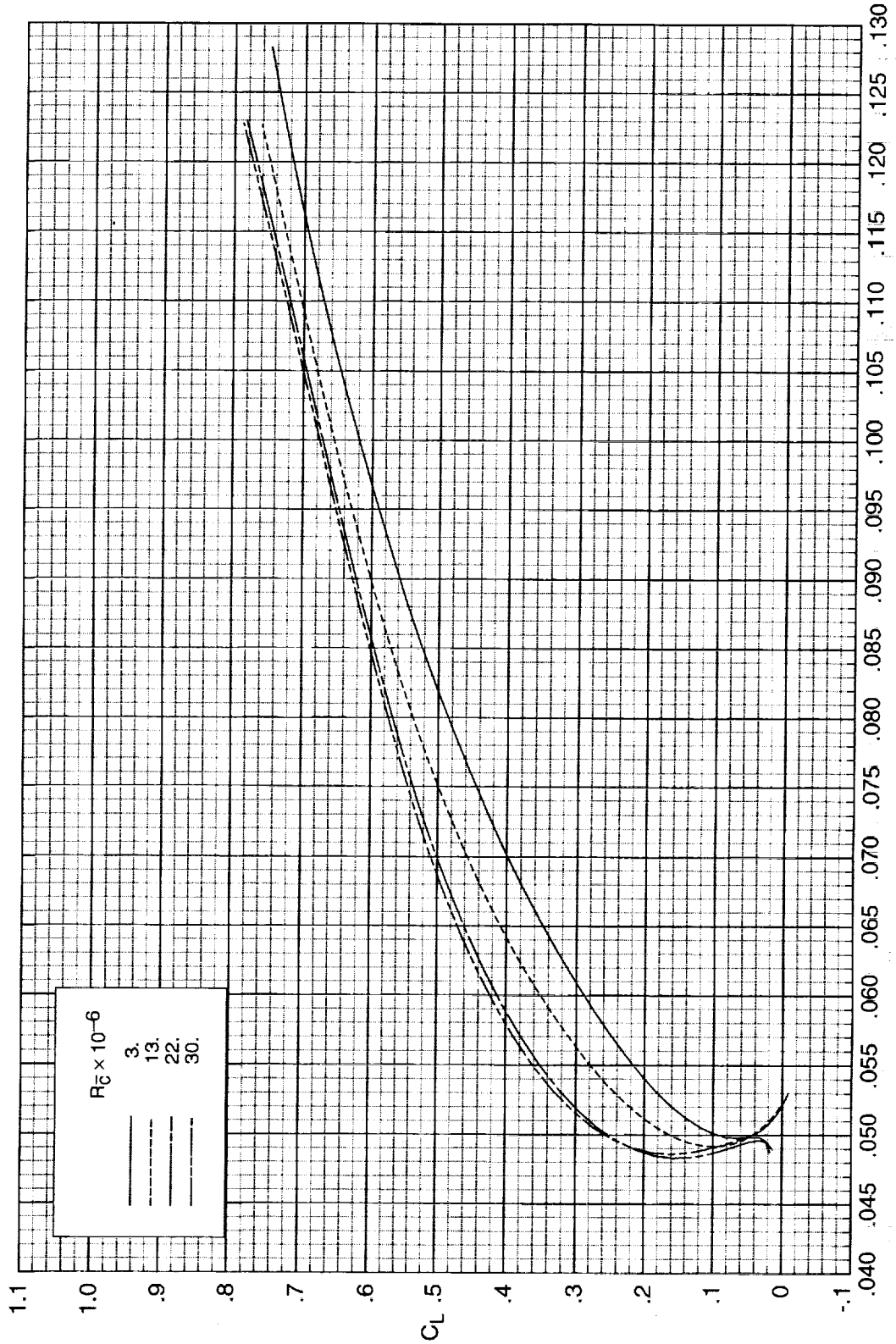

(g) Concluded.

Figure A3. Continued.

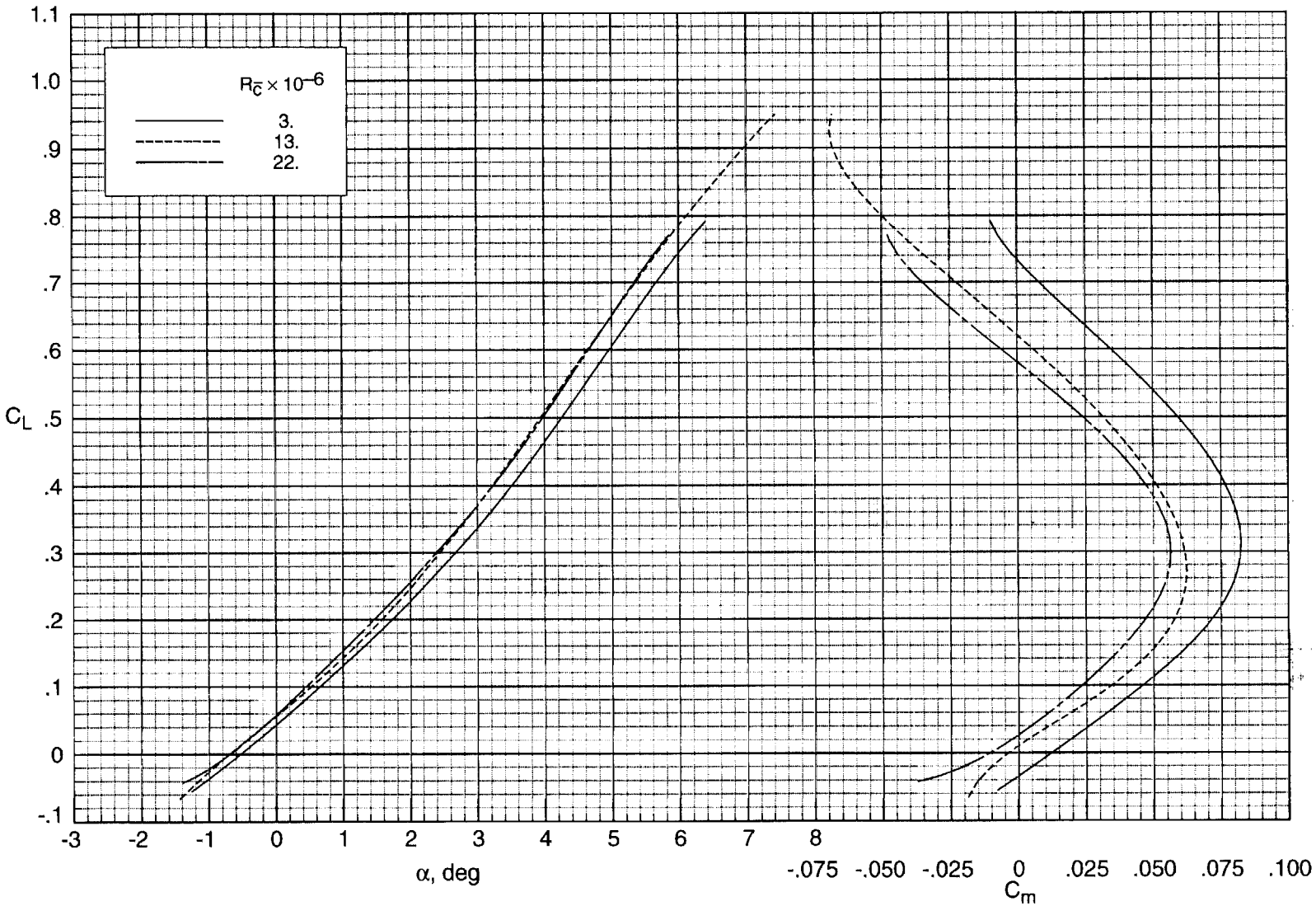

(h) $M_\infty = 0.94$.

Figure A3. Continued.

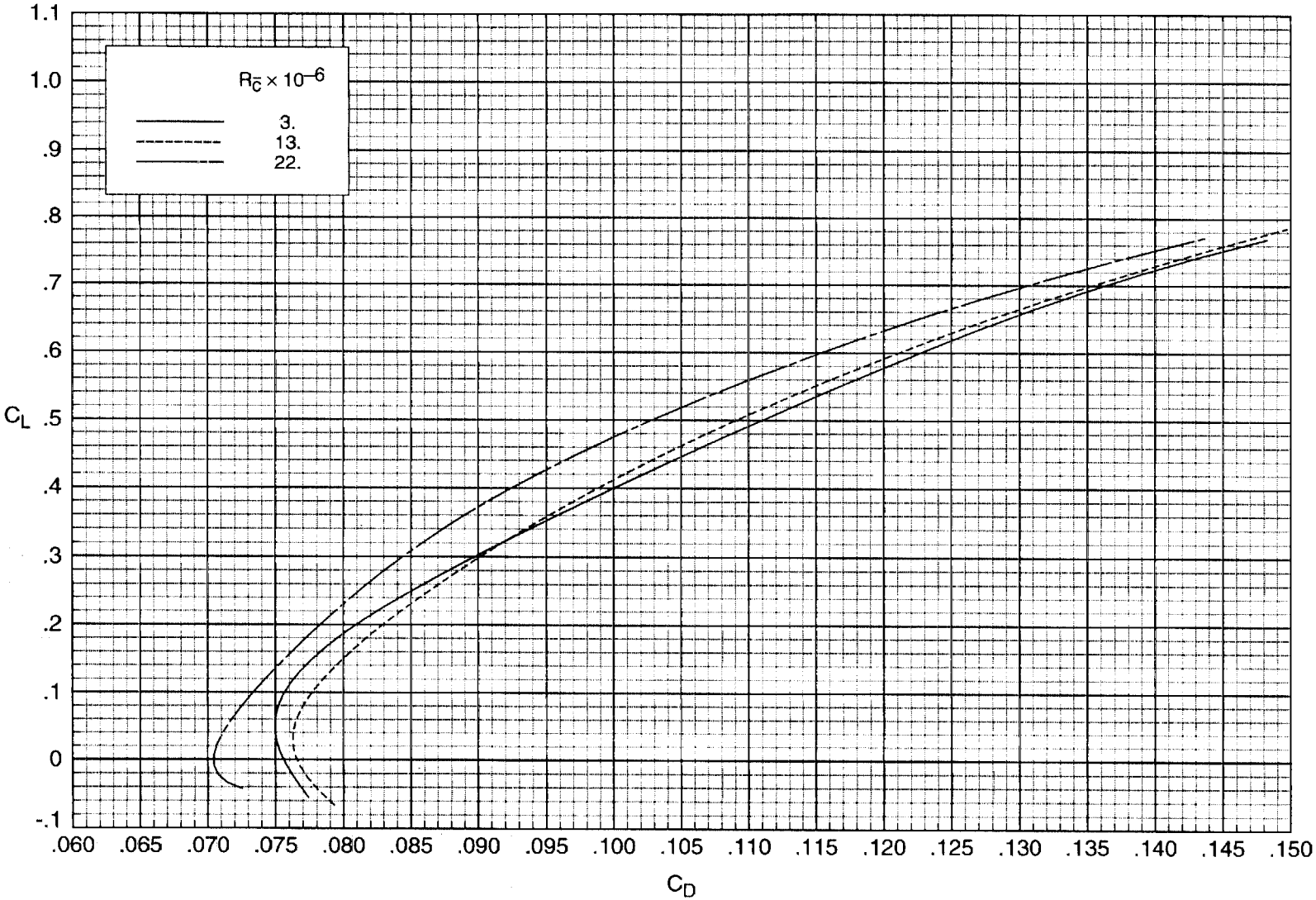

(h) Concluded.

Figure A3. Concluded.

References

1. Jacobs, Peter F.; and Gloss, Blair B.: *Longitudinal Aerodynamic Characteristics of a Subsonic, Energy-Efficient Transport Configuration in the National Transonic Facility.* NASA TP-2922, Aug. 1989.

2. Fuller, D. E.; Gloss, B. B.; and Nystrom, D.: *Guide to Users of the National Transonic Facility.* NASA TM-83124, 1981.

3. Igoe, William B.: *Analysis of Fluctuating Static Pressure Measurements in the National Transonic Facility.* NASA TP-3475, Mar. 1996. (Also available as Analysis of Fluctuating Static Pressure Measurements of a Large High Reynolds Number Transonic Cryogenic Wind Tunnel. Ph.D Diss., George Washington Univ., May 1993.)

4. Coleman, Hugh W.; and Steele, W. Glenn: *Experimentation and Uncertainty Analysis for Engineers.* John Wiley and Sons, 1989.

5. Finley, Tom D.; and Tcheng, Ping: Model Attitude Measurements at NASA Langley Research Center. AIAA-92-0763, Jan. 1992.

6. Foster, Jean M.; and Adcock, Jerry B.: *User's Guide for the National Transonic Facility Research Data System.* NASA TM-110242, Apr. 1996.

7. Al-Saadi, Jassim A.: *Effect of Reynolds Number, Boundary-Layer Transition, and Aeroelasticity on Longitudinal Aerodynamic Characteristics of a Subsonic Transport Wing.* NASA TP-3655, 1997.

8. Chan, Y. Y.: *Comparison of Boundary Layer Trips of Disks and Grit Types on Airfoil Performance at Transonic Speeds.* NASZ-AN-56 (NRC-29908), National Aeronautical Establishment (Ottawa, Ontario), Dec. 1988.

9. Braslow, Albert L.; and Knox, Eugene C.: *Simplified Method for Determination of Critical Height of Distributed Roughness Particles for Boundary Layer Transition at Mach Numbers From 0 to 5.* NACA TN 4363, 1958.

10. Wahls, R. A.; Adcock, J. B.; Witkowski, D. P.; and Wright, F. L.: *A Longitudinal Aerodynamic Data Repeatability Study for a Commercial Transport Model Test in the National Transonic Facility.* NASA TP-3522, Aug. 1995.

Table 1. Description of the Model

Body:

Maximum diameter, in. 5.75
Length, in. 60.5

Wing (based on trapezoidal planform):

Aspect ratio. 9.8
Taper ratio 0.4
Sweep, quarter chord, deg 30.0
Dihedral, deg 5.0
Mean geometric chord, in. 5.742
Span, in. 52.97
Reference area, ft^2 . . . . . .1.9884

Table 2. Design Location for the Lower Surface Orifices

x/c for row at η =						
0.140	0.275	0.375	0.509	0.630	0.790	0.922
0.025	0.025	0.025	0.025	0.025	0.025	0.025
	0.050	0.050				
0.075	0.075	0.075	0.075	0.075	0.075	0.075
	0.100	0.100				
0.125	0.125	0.125	0.125	0.125	0.125	0.125
	0.150	0.150				
0.200	0.200	0.200	0.200	0.200	0.200	0.200
0.300	0.300	0.300	0.300	0.300	0.300	0.300
0.400	0.400	0.400	0.400	0.400	0.400	0.400
0.500	0.500	0.500	0.500	0.500	0.500	0.500
0.600	0.600	0.600	0.600	0.590	0.580	0.600
0.700	0.700	0.700	0.700	0.700	0.700	0.700
0.800	0.800	0.800	0.800	0.800	0.800	0.800
0.900	0.900	0.900	0.900	0.900	0.900	0.900
0.950	0.950	0.950	0.950	0.950	0.950	0.950
1.000	1.000	1.000	1.000	1.000	1.000	1.000

Table 3. Design Location for the Upper Surface Orifices

x/c for row at η =						
0.140	0.275	0.375	0.509	0.630	0.790	0.922
0.000	0.000	0.000	0.000	0.000	0.000	0.000
	0.025	0.025				
0.050	0.050	0.050	0.050	0.050	0.050	0.050
	0.075	0.075				
0.100	0.100	0.100	0.100	0.100	0.100	0.100
0.150	0.150	0.150	0.150	0.150	0.150	0.150
0.200	0.200	0.200	0.200	0.200	0.200	0.200
	0.250	0.250	0.250	0.250	0.250	0.250
0.300	0.300	0.300	0.300	0.300	0.300	0.300
	0.350	0.350	0.350	0.350	0.350	0.350
0.400	0.400	0.400	0.400	0.400	0.400	0.400
0.450	0.440	0.440	0.440	0.440	0.440	0.440
0.500	0.480	0.480	0.480	0.480	0.480	0.480
	0.520	0.520	0.520	0.520	0.520	0.520
0.550	0.560	0.560	0.560	0.560	0.560	0.560
0.600	0.600	0.600	0.600	0.600	0.600	0.600
0.640	0.640	0.640	0.640	0.640	0.640	0.640
0.680	0.680	0.680	0.680	0.670	0.680	0.680
0.720	0.720	0.720	0.715	0.695	0.730	0.730
	0.750			0.740	0.760	0.760
0.770	0.780	0.770	0.760	0.780	0.790	0.790
0.820	0.820	0.830	0.820	0.830	0.845	0.825
						0.855
0.880	0.880	0.880	0.880	0.880	0.875	0.890
					0.905	
0.940	0.940	0.940	0.940	0.940	0.950	0.940
1.000	1.000	1.000	1.000	1.000	1.000	1.000

Table 4. Balance Full-Scale Load and Accuracy as a Percent of Full Scale

Measured Component	Value for—			
	Outboard spoiler test with NTF101B balance calibrated on 6/8/95		Outboard aileron test with NTF113B balance calibrated on 7/27/95	
	Full-scale load	Accuracy percent of full scale	Full-scale load	Accuracy percent of full scale
Normal force	6500 lb	±0.10%	6500 lb	±0.08%
Axial force	700 lb	±0.18%	400 lb	±0.28%
Pitching moment	13,000 in-lb	±0.12%	13,000 in-lb	±0.09%
Rolling moment	9,000 in-lb	±0.35%	9,000 in-lb	±0.22%
Yawing moment	6500 in-lb	±0.31%	6500 in-lb	±0.14%
Side force	4000 lb	±0.21%	4000 lb	±0.19%

Table 5. Uncertainty in the Model Force and Moment Coefficients

Coefficient	Uncertainty at $q_\infty/E \approx$		
	0.28×10^{-6}	0.45×10^{-6}	0.62×10^{-6}
Outboard spoiler			
C_L	0.0031	0.0019	0.0014
C_D	0.00063	0.00041	0.00033
C_m	0.0013	0.0008	0.0006
C_l	0.00030	0.00018	0.00013
C_n	0.00018	0.00011	0.00008
Outboard aileron			
C_L	0.0025	0.0016	0.0011
C_D	0.00056	0.00038	0.00030
C_m	0.0010	0.0006	0.0004
C_l	0.00019	0.00012	0.00008
C_n	0.00008	0.00005	0.00004

Table 6. Test Conditions for Outboard Spoiler Test

M_∞	Spoiler deflection angle, deg, at $R_{\bar{c}}\times10^{-6}$ of —					
	3 with—	13 with—	13 with—	22 with—	22 with—	30 with—
	Low q_∞ level	Low q_∞ level	Inter. q_∞ level	Inter. q_∞ level	High q_∞ level	High q_∞ level
0.70	0, 10, 15, 20	0, 20	20	0, 10, 20	10, 20	0, 10, 20
0.80	0, 10, 15, 20	0, 20	20	0, 10, 20	10, 20	0, 10, 20
0.82	0, 10, 15, 20	0, 10, 20	20	0, 10, 20	10, 20	0, 10, 20
0.85	0, 10, 15, 20	0, 10, 20	20	0, 10, 20	10, 20	0, 10, 20
0.88	0, 10, 15, 20	0, 10, 20	20	0, 10, 20	10, 20	0, 10, 20
0.91	0, 10, 15, 20	0, 10, 20	20	0, 10, 20	0, 10, 20	0, 10, 20
0.94	0, 10, 15, 20	0, 10, 20	20	0, 10, 20	0, 10, 20	0, 10, 20

Table 7. Test Conditions for Outboard Aileron Test

M_∞	Aileron deflection angle, deg, at $R_c \times 10^{-6}$ of —						
	3 with—	13 with—	13 with—	22 with—	22 with—	30 with—	30 with—
	Low q_∞ level	Low q_∞ level	Inter. q_∞ level	Inter. q_∞ level	High q_∞ level	Inter. q_∞ level	High q_∞ level
0.50	-10, 0, 10	-10, 0	-10, 0	-10, 0, 10		-10, 0, 10	
0.70	-10, 0, 10	-10, 0	-10, 0	-10, 0, 10	-10, 0, 10		-10, 0, 10
0.80	-10, 0, 10	-10, 0	-10, 0	-10, 0, 10	-10, 0		-10, 0
0.82	-10, 0, 10	-10, 0	-10, 0	-10, 0, 10	-10, 0, 10		-10, 0, 10
0.85	-10, 0, 10	-10, 0	-10, 0	-10, 0, 10	-10, 0		-10, 0
0.88	-10, 0, 10	-10, 0	-10, 0	-10, 0, 10	-10, 0, 10		-10, 0, 10
0.91	-10, 0, 10	-10, 0	-10, 0	-10, 0, 10	-10, 0		-10, 0, 10
0.94	-10, 0, 10	-10, 0	-10, 0	-10, 0, 10			

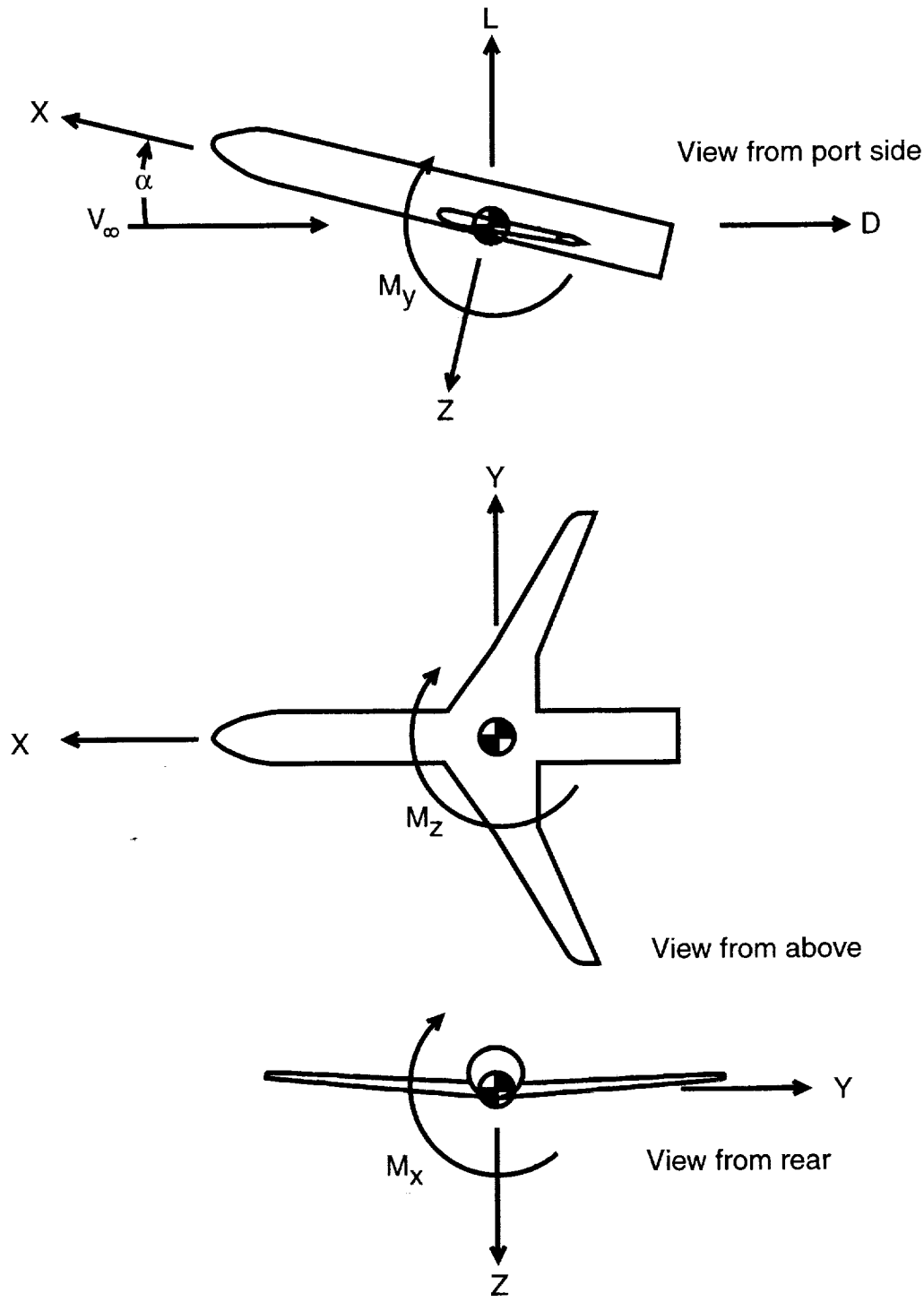

Figure 1. Body axes and sign conventions.

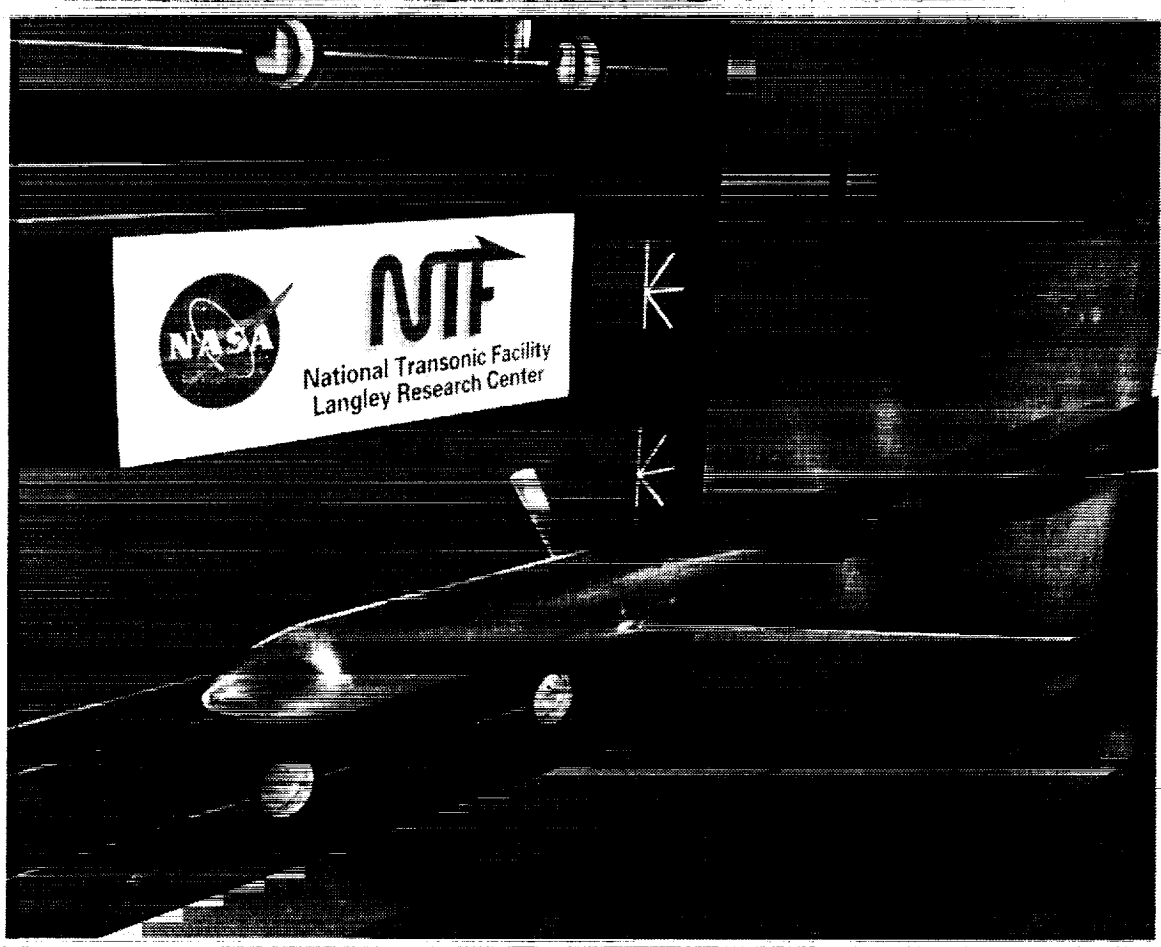

(a) Model installed in the NTF test section.

Figure 2. Photographs of the Pathfinder-I Lateral Controls Wing model.

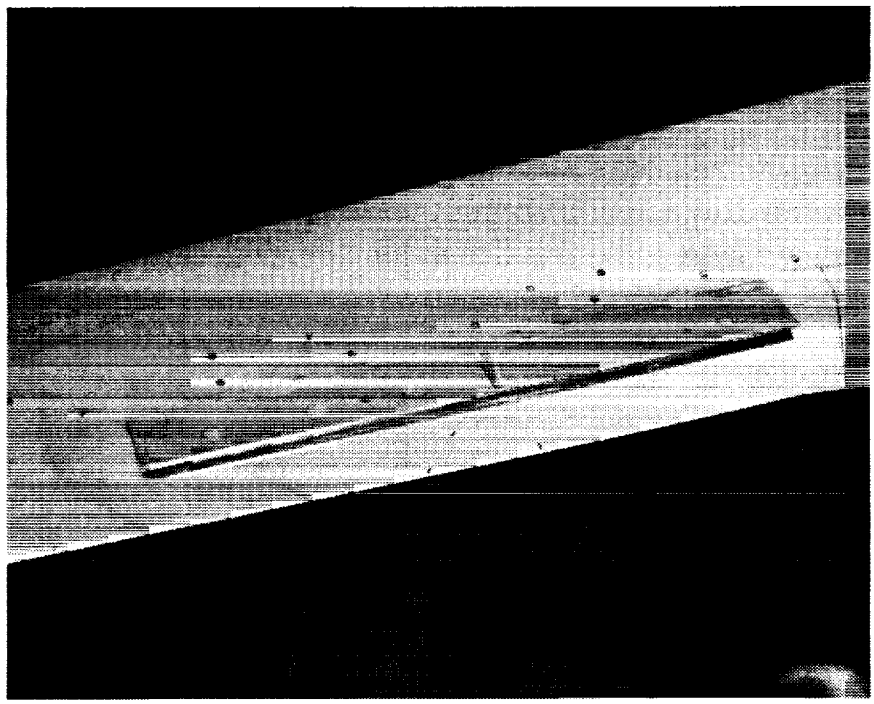

L95-04483

(b) Outboard spoilers.

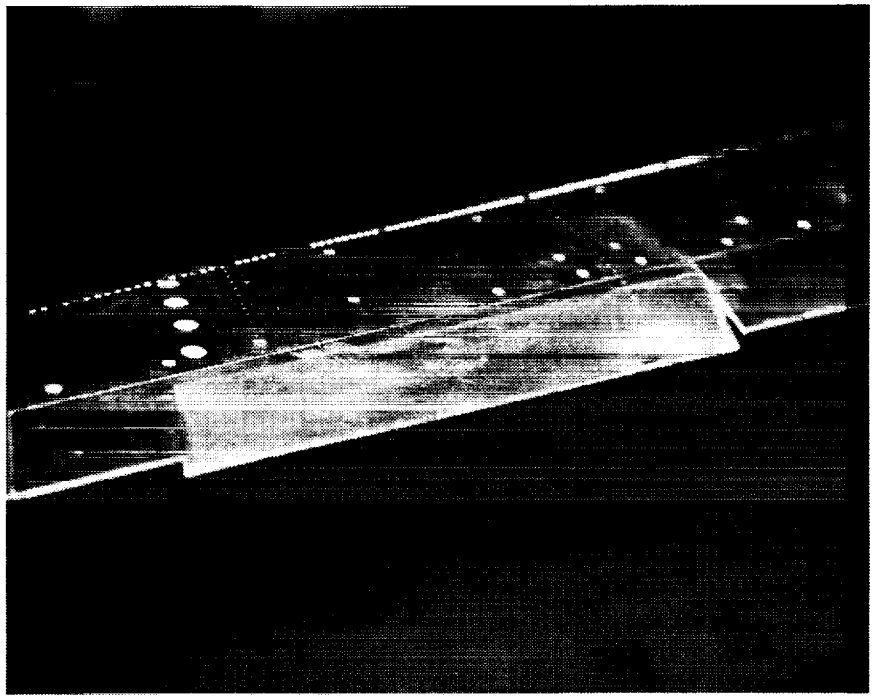

L96-02694

(c) Outboard aileron.

Figure 2. Concluded.

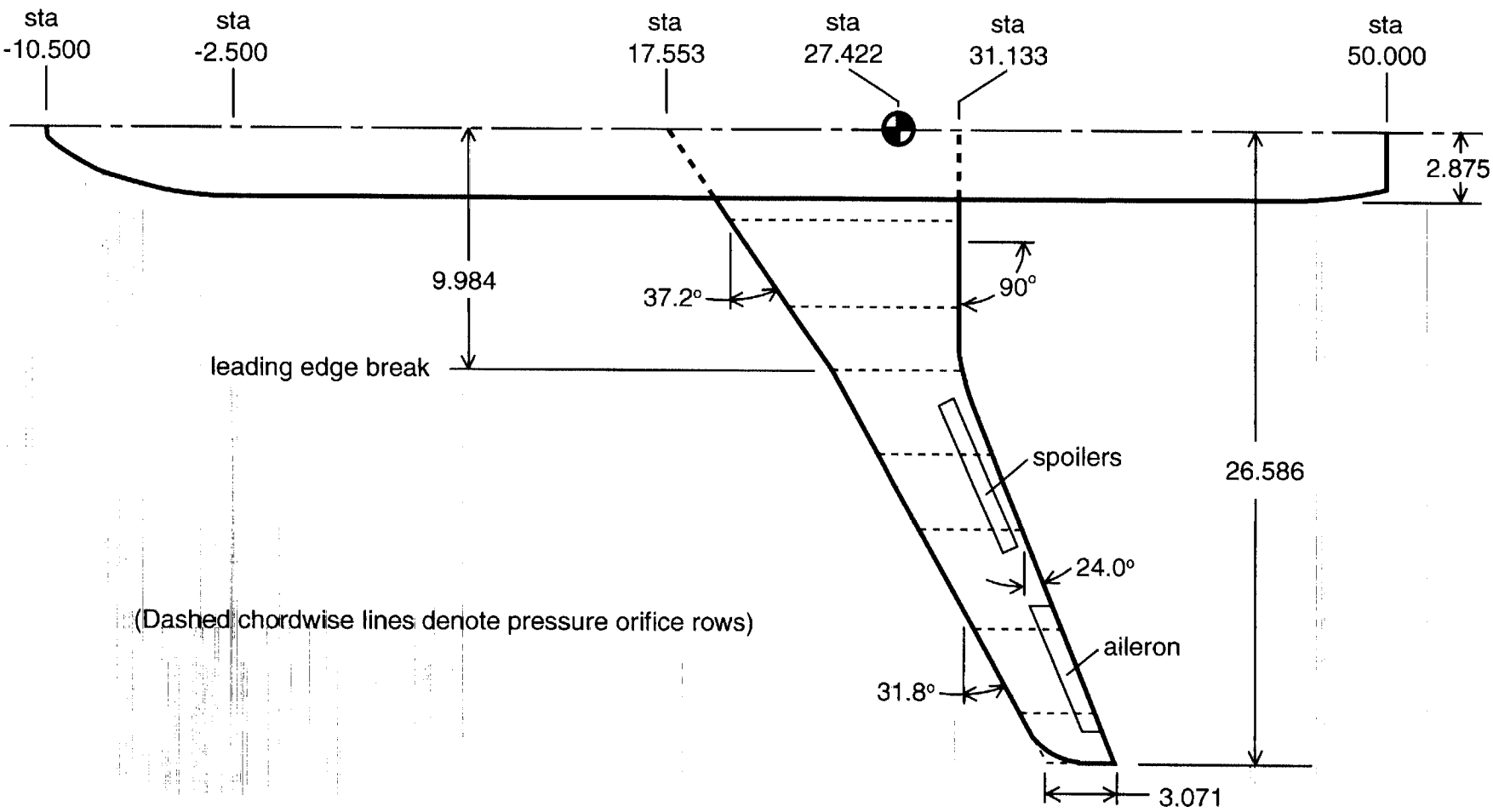

(a) General layout.

Figure 3. Sketches of the Pathfinder-I Lateral Controls Wing Model. All linear dimensions are in inches.

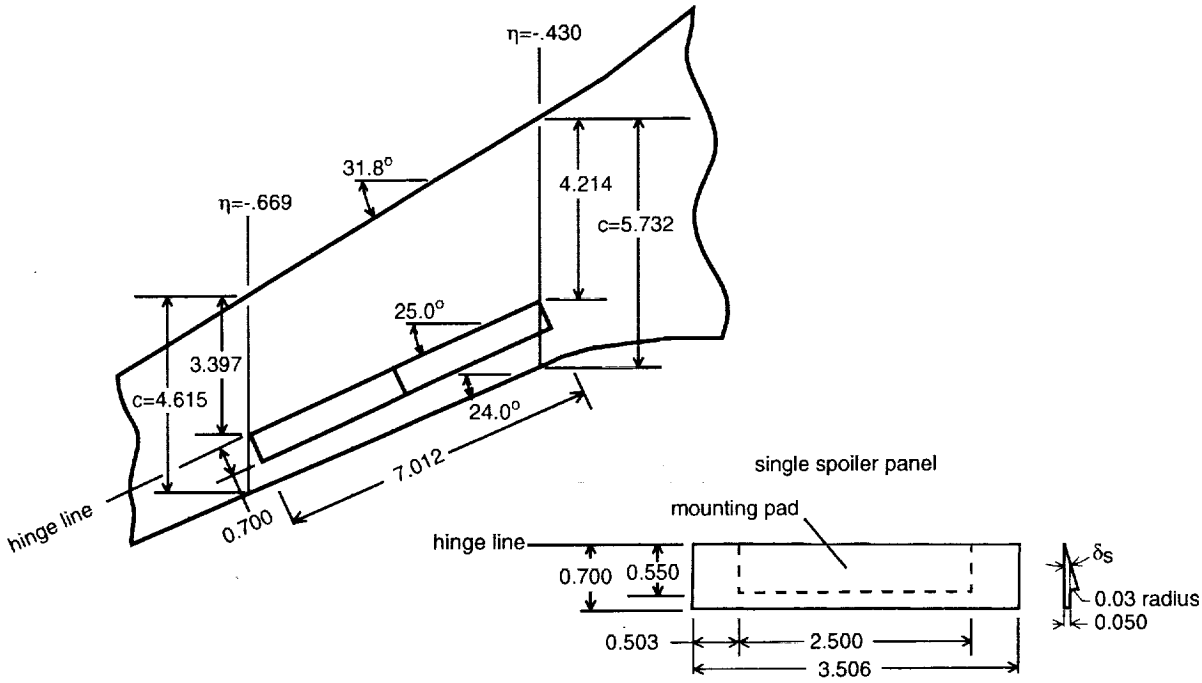

(b) Outboard spoiler details.

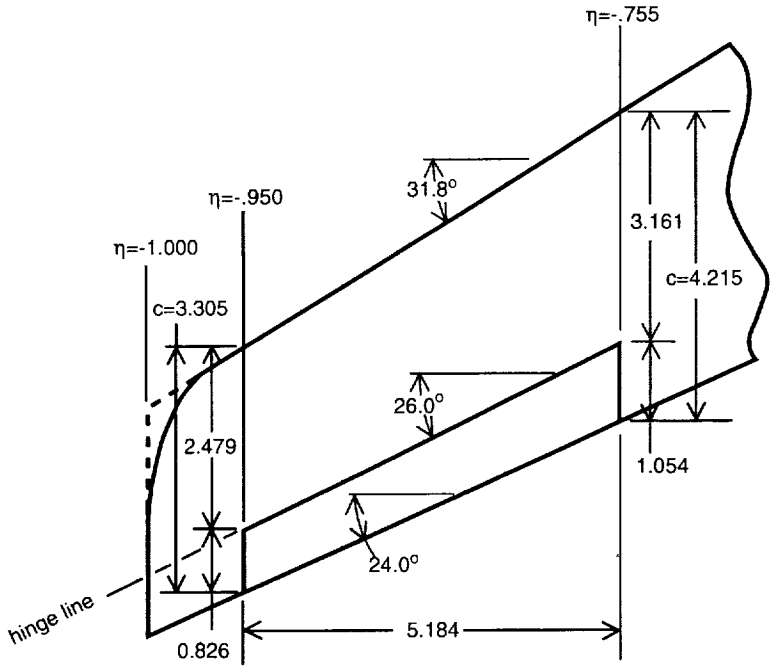

(c) Outboard aileron details.

Figure 3. Concluded.

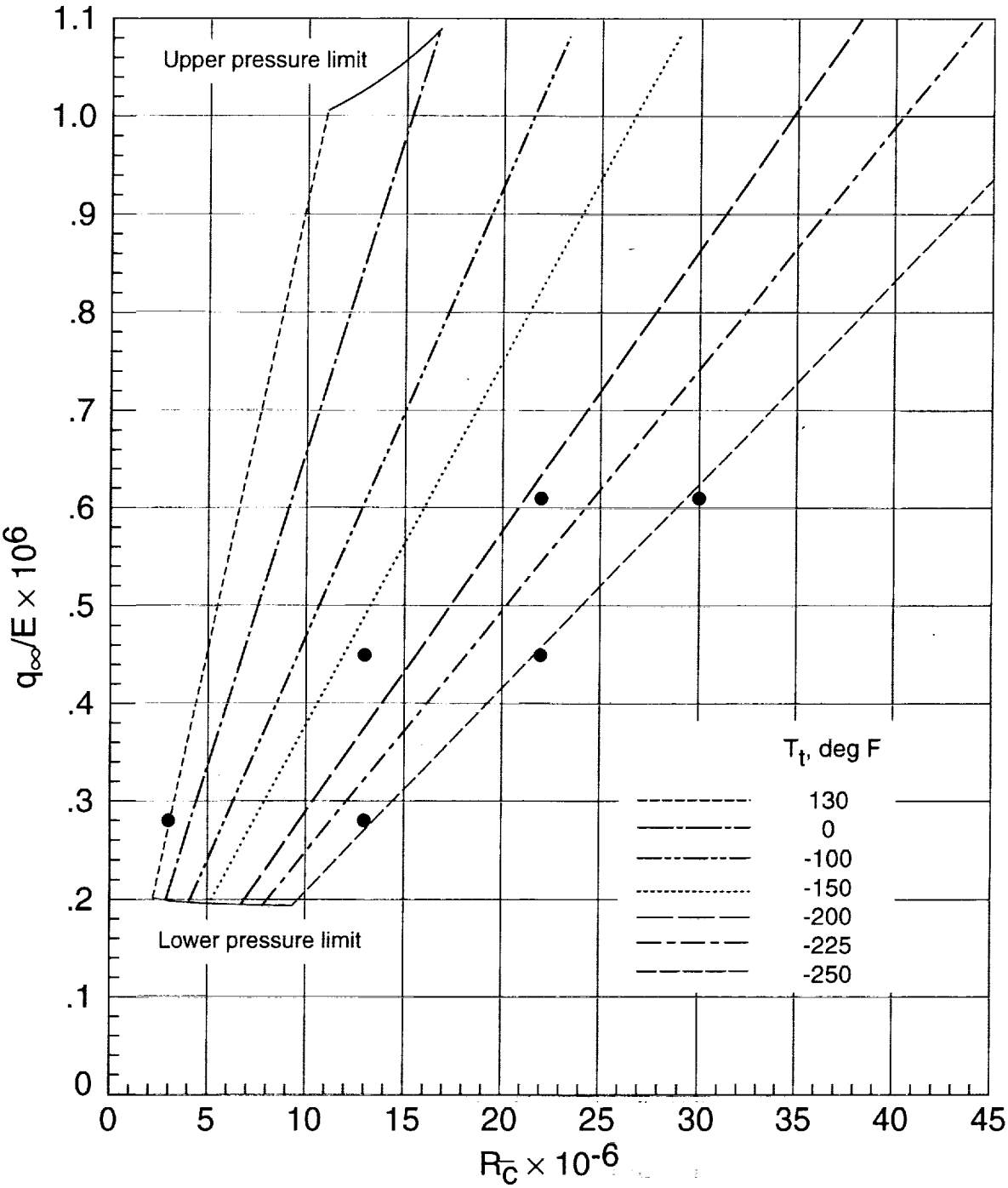

Figure 4. NTF operating envelope and nominal test conditions for the Pathfinder -I Lateral Controls Wing. $M_\infty = 0.82$.

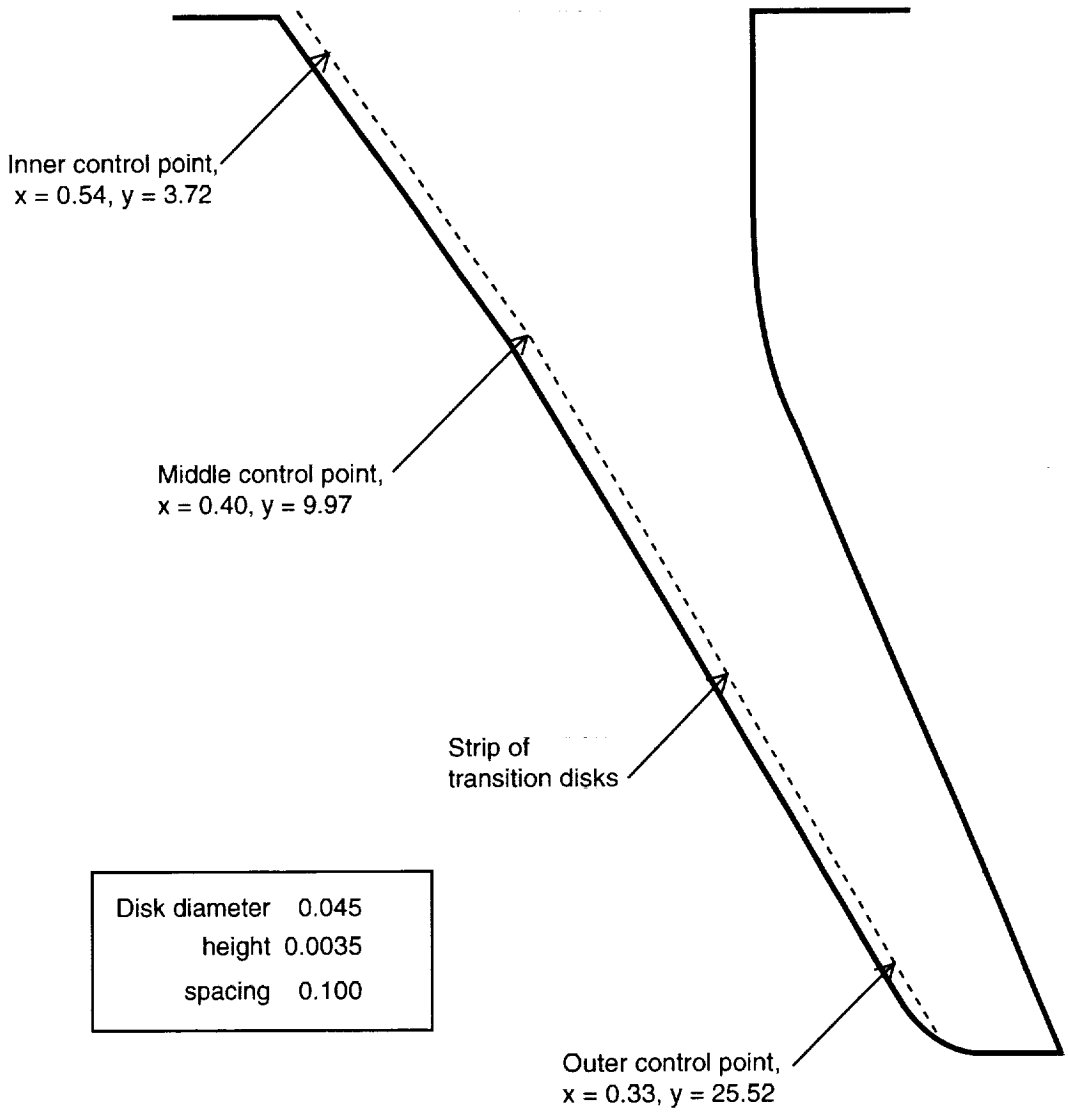

Figure 5. Location of boundary layer transition disks on the wing. All dimensions in inches.

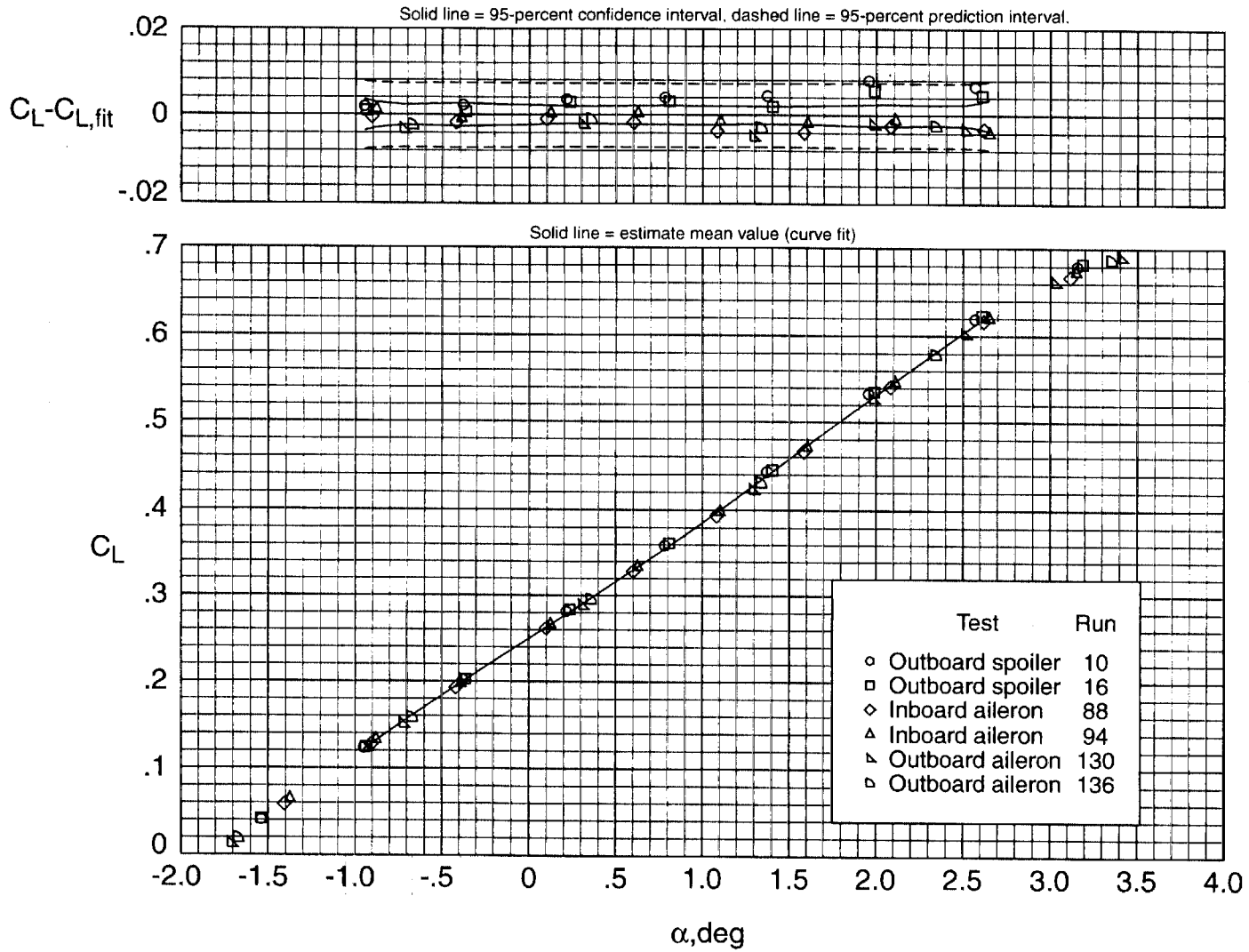

(a) Lift coefficient.

Figure 6. Test-to-test repeatability of the force and moment coefficients. $M_\infty = 0.82$; $R_{\bar{c}} = 3\times10^6$, $q_\infty/E = 0.28\times10^{-6}$.

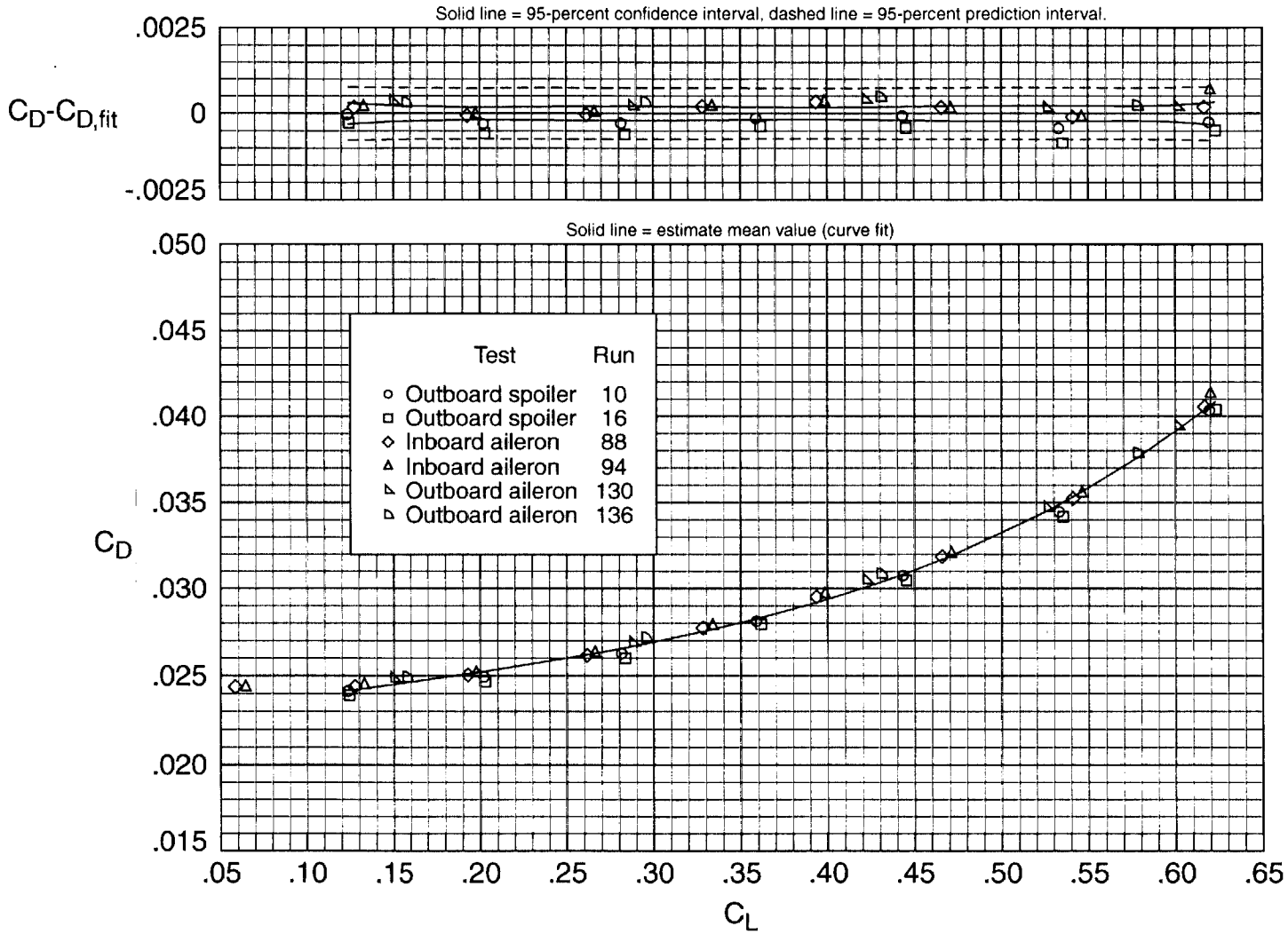

(b) Drag coefficient.

Figure 6. Continued.

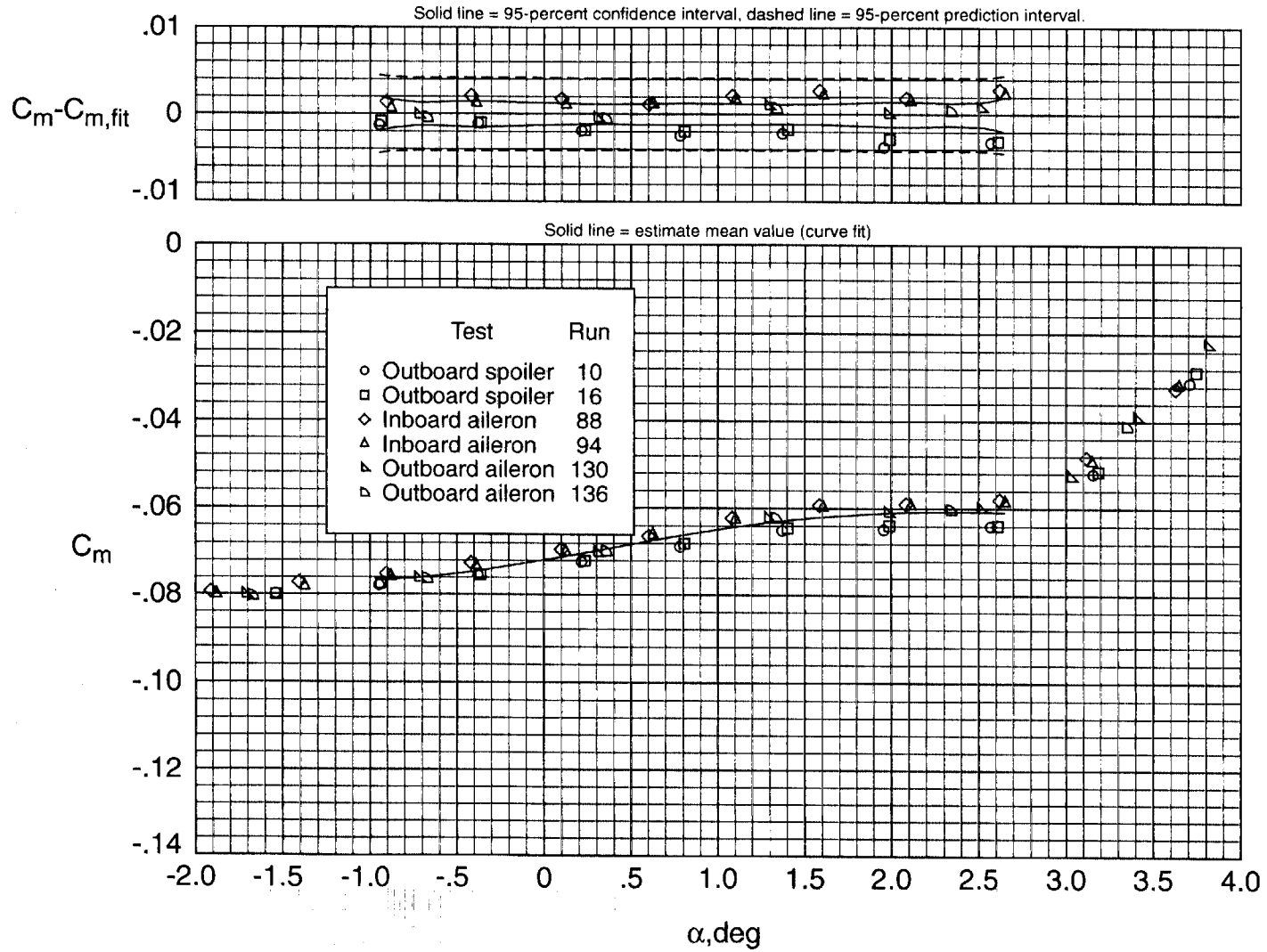

(c) Pitching moment coefficient.

Figure 6. Continued.

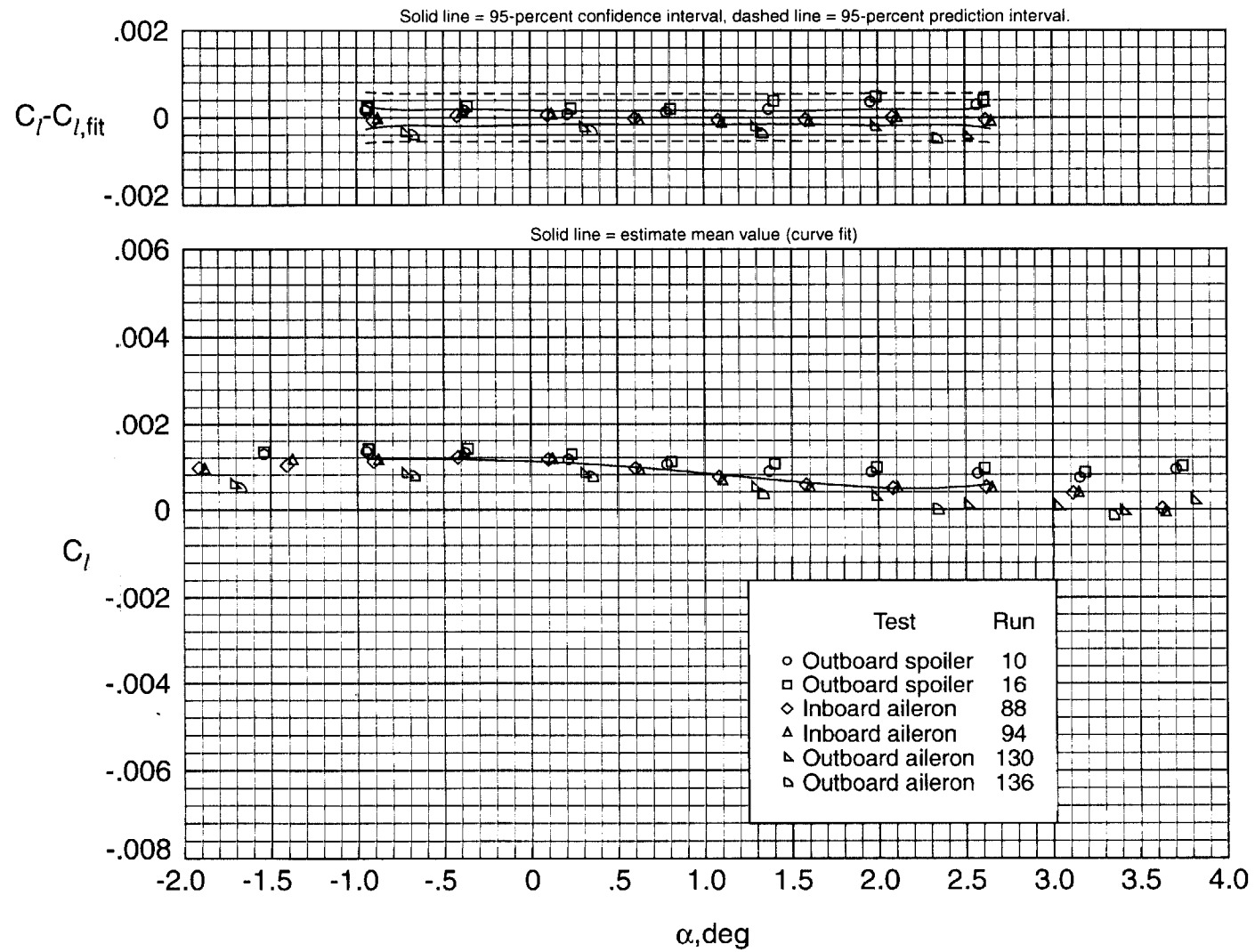

(d) Rolling moment coefficient.

Figure 6. Continued.

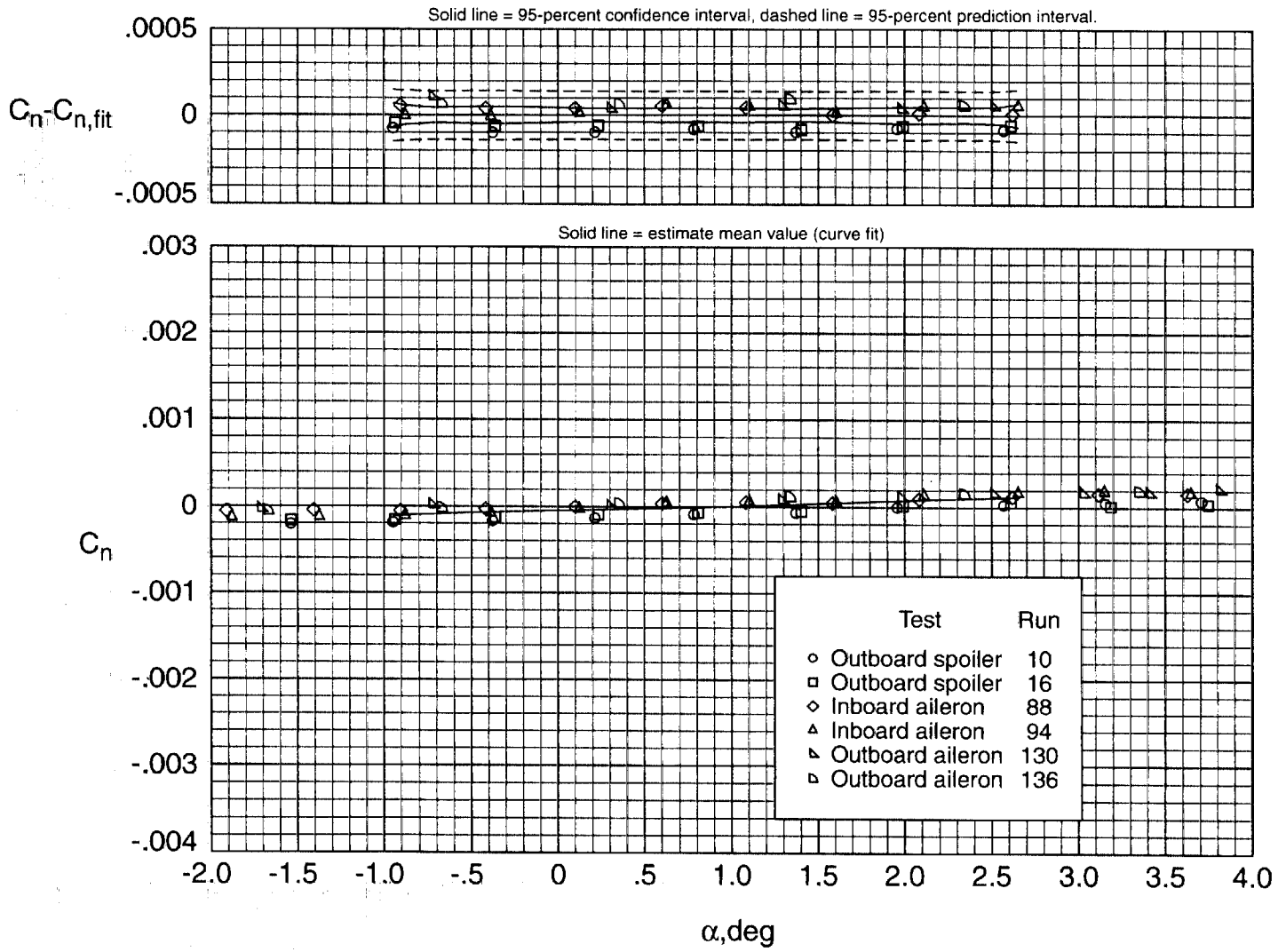

(e) Yawing moment coefficient.

Figure 6. Concluded.

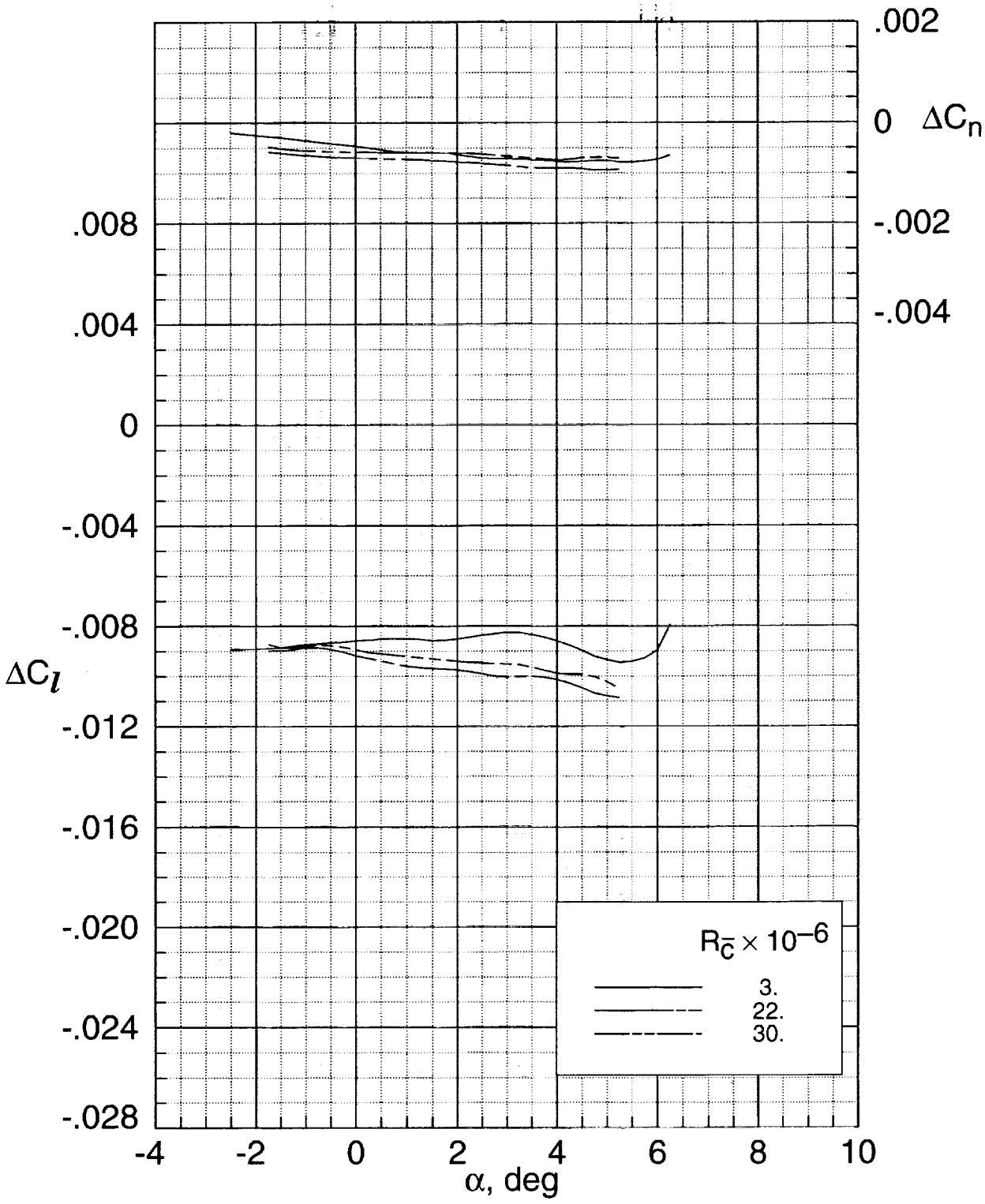

(a) $M_\infty = 0.70$.

Figure 7. Effect of Reynolds number on the aerodynamic characteristics with the outboard spoilers for $\delta_s = 10°$.

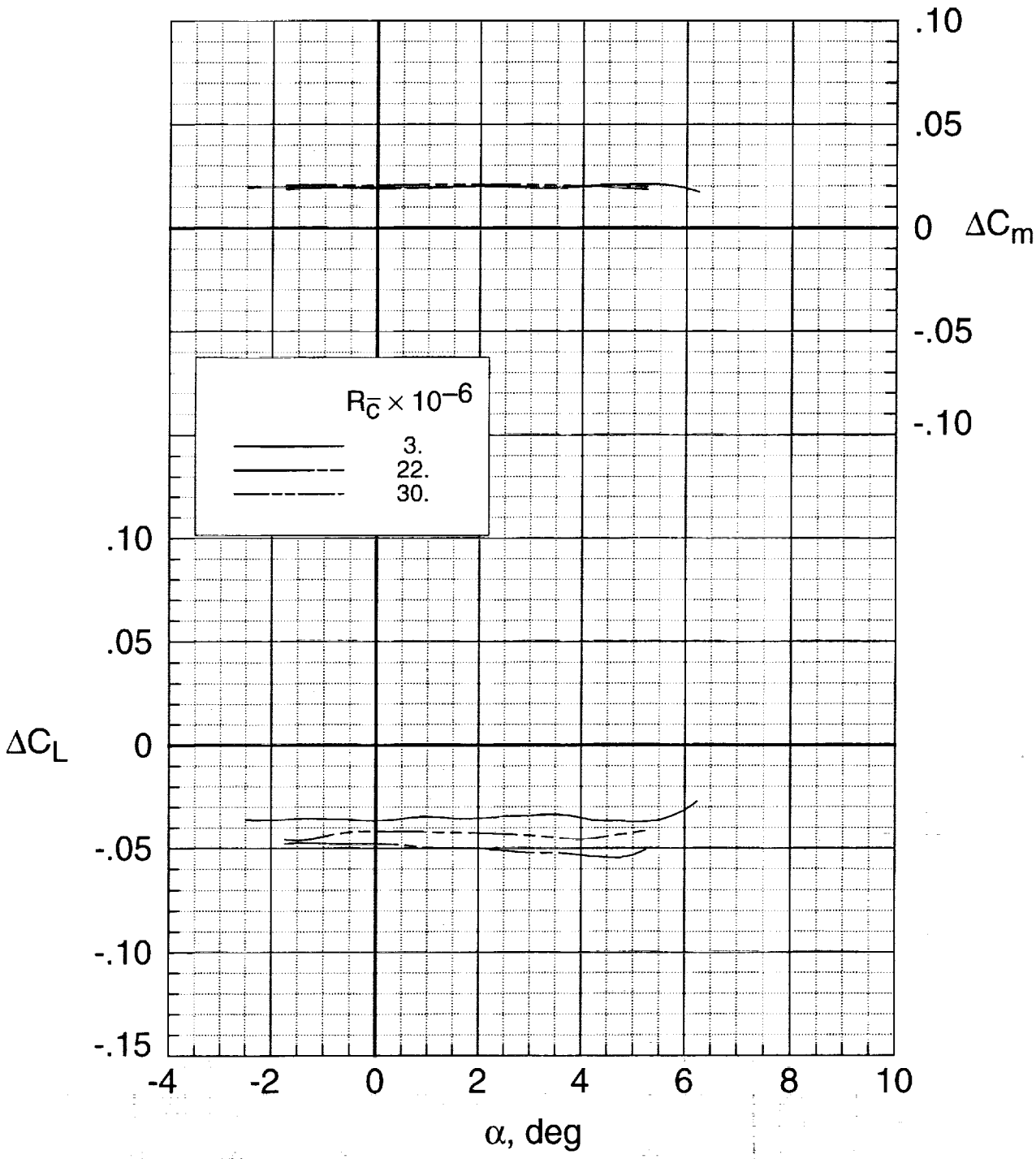

(a) Concluded.

Figure 7. Continued.

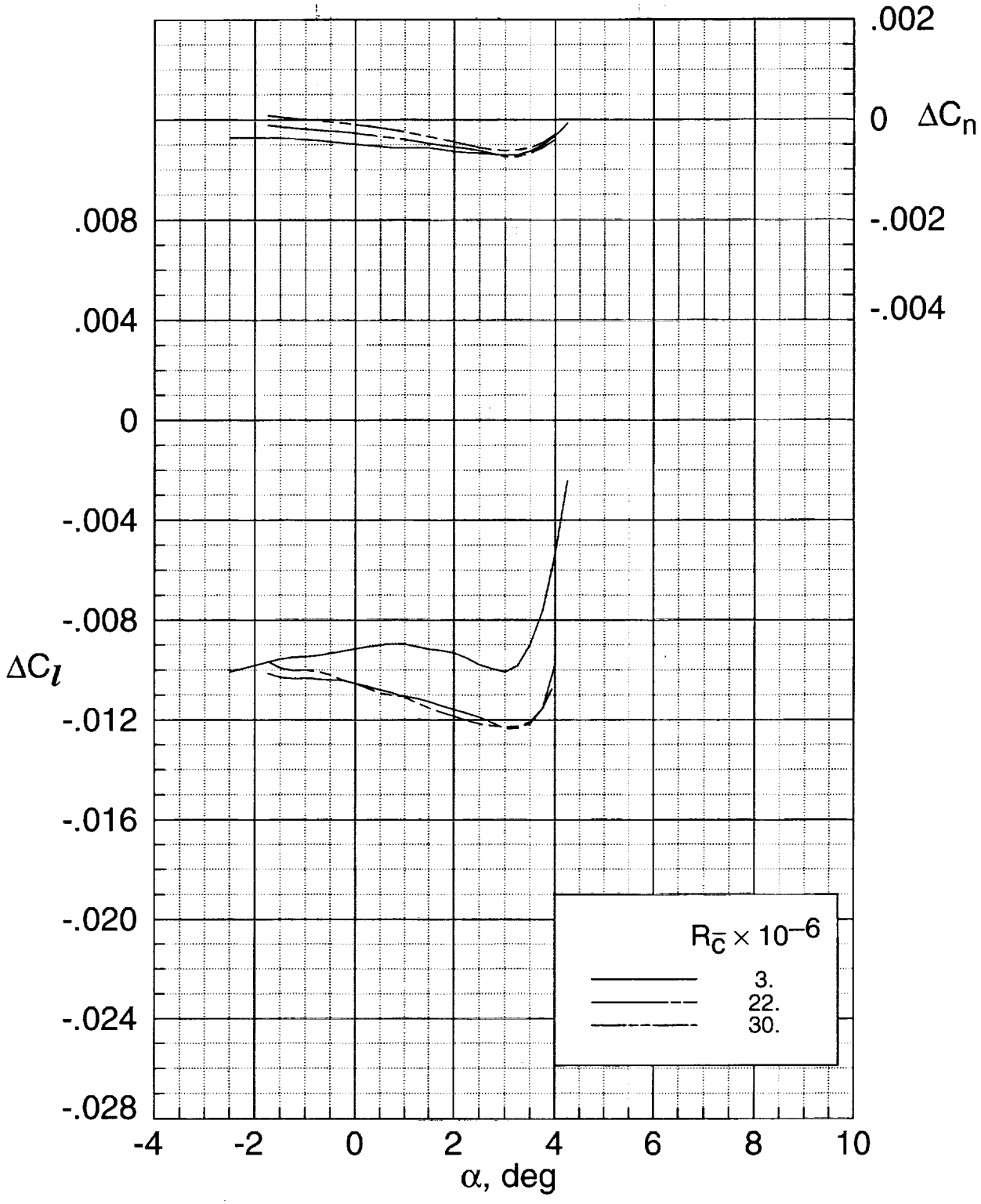

(b) $M_\infty = 0.80$.

Figure 7. Continued.

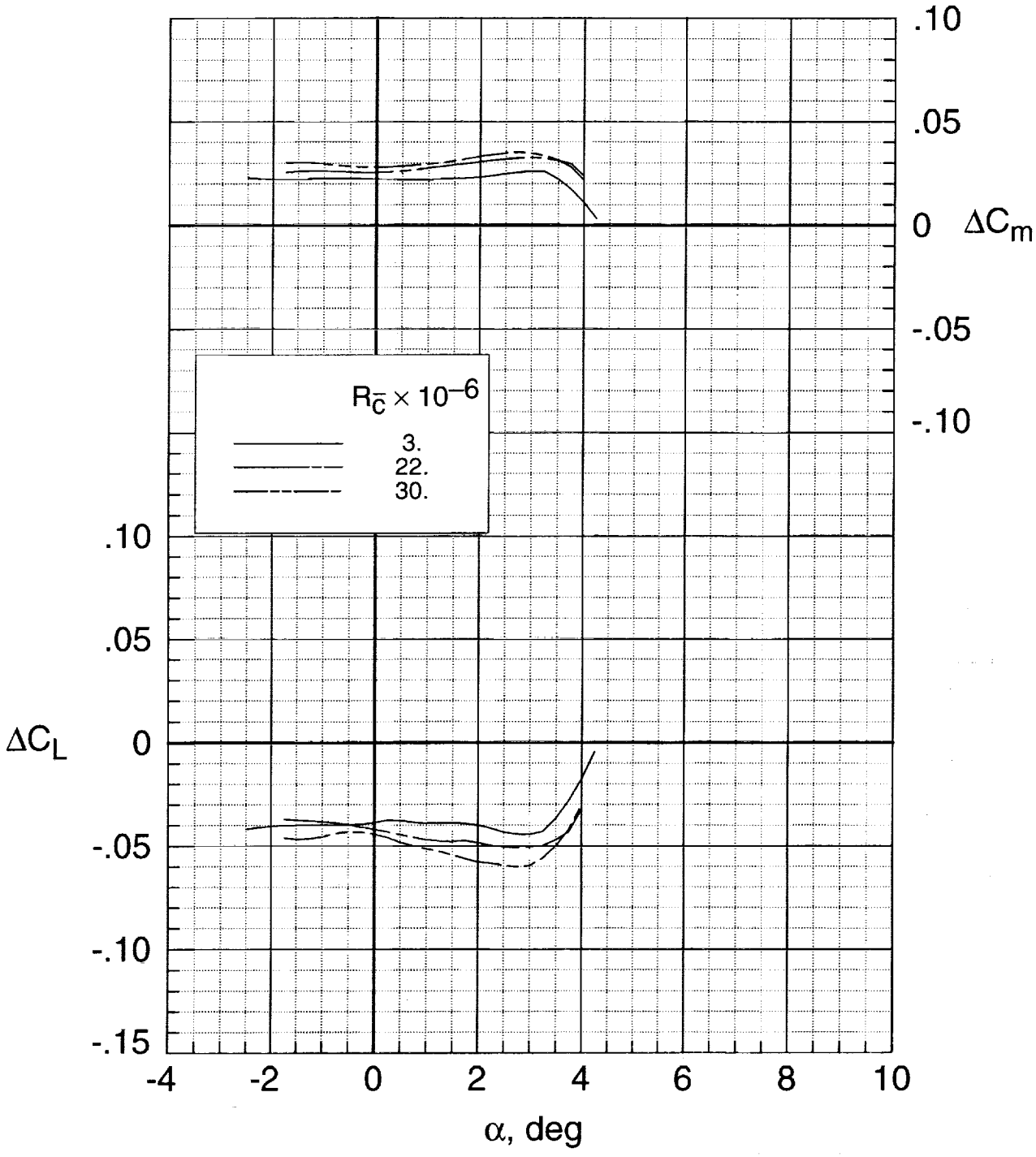

(b) Concluded.

Figure 7. Continued.

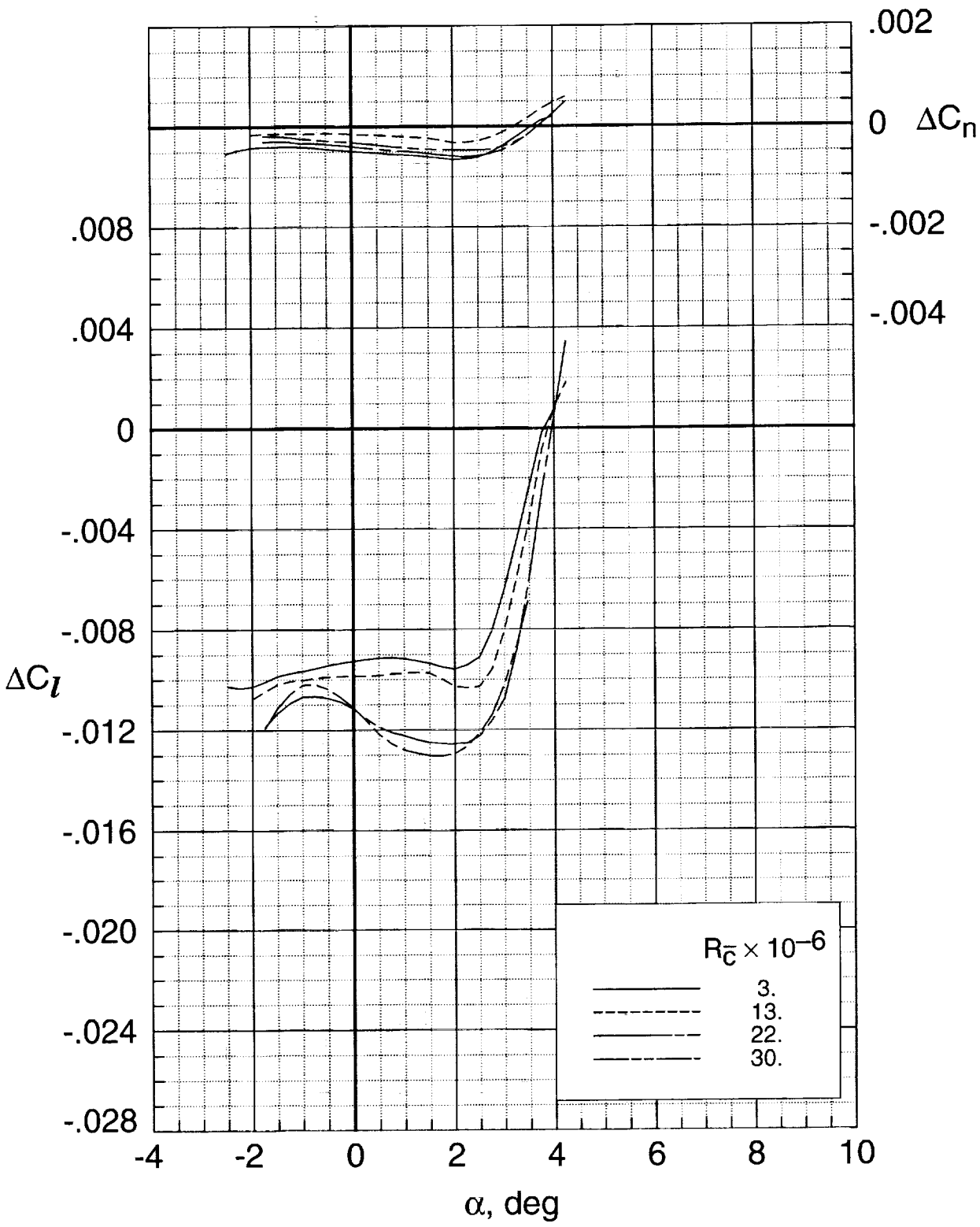

(c) $M_\infty = 0.82$.

Figure 7. Continued.

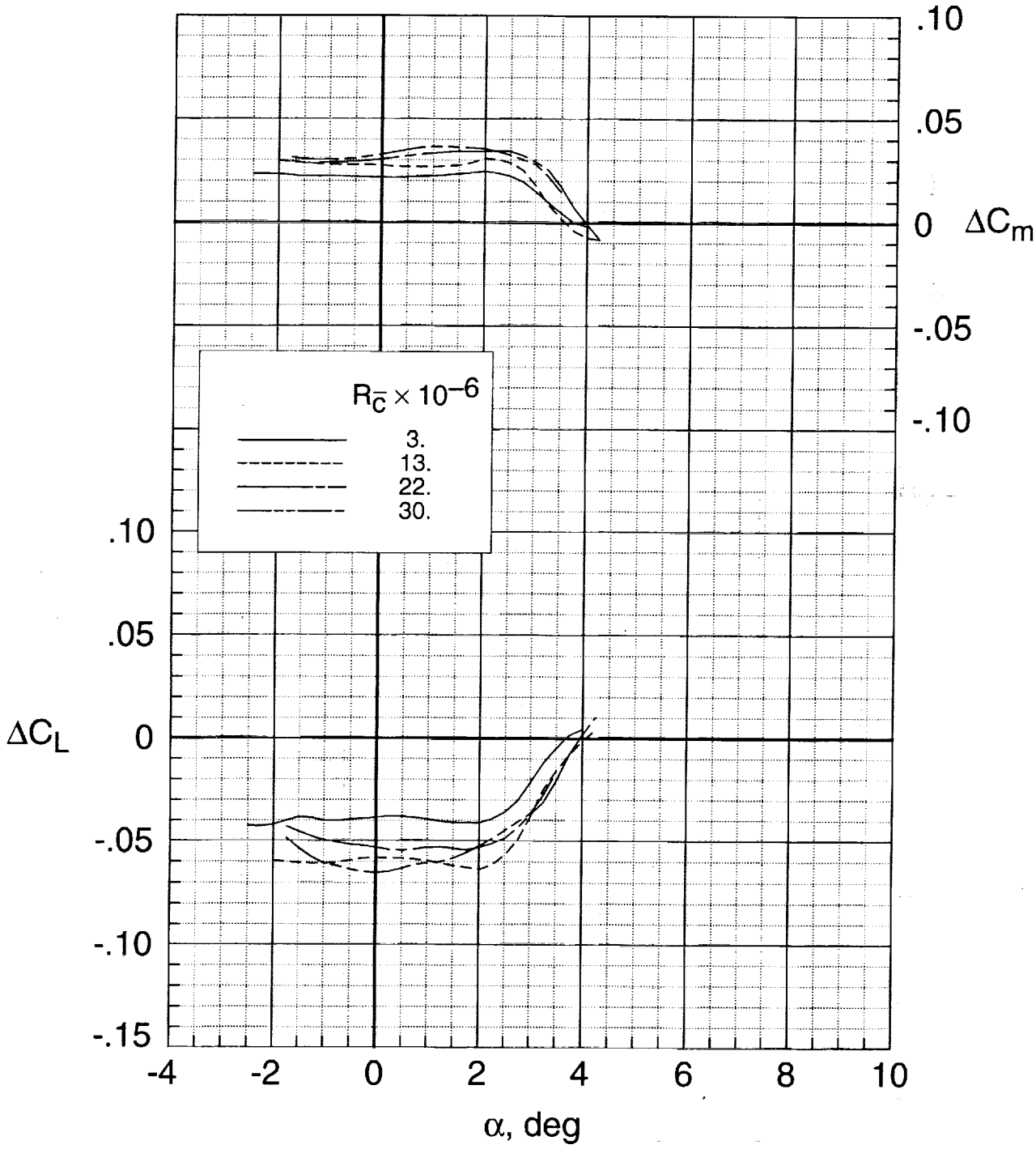

(c) Concluded.

Figure 7. Continued.

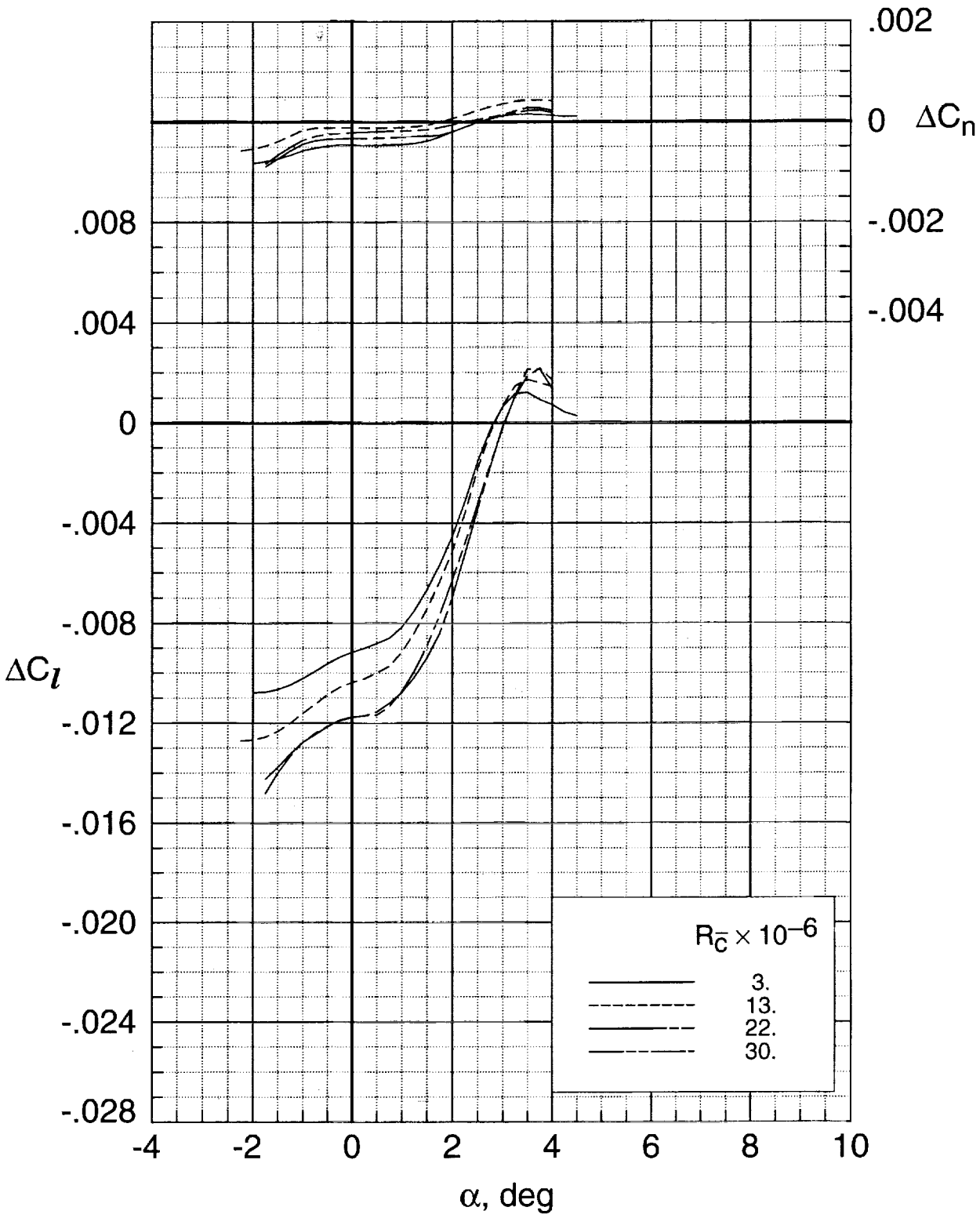

(d) $M_\infty = 0.85$.

Figure 7. Continued.

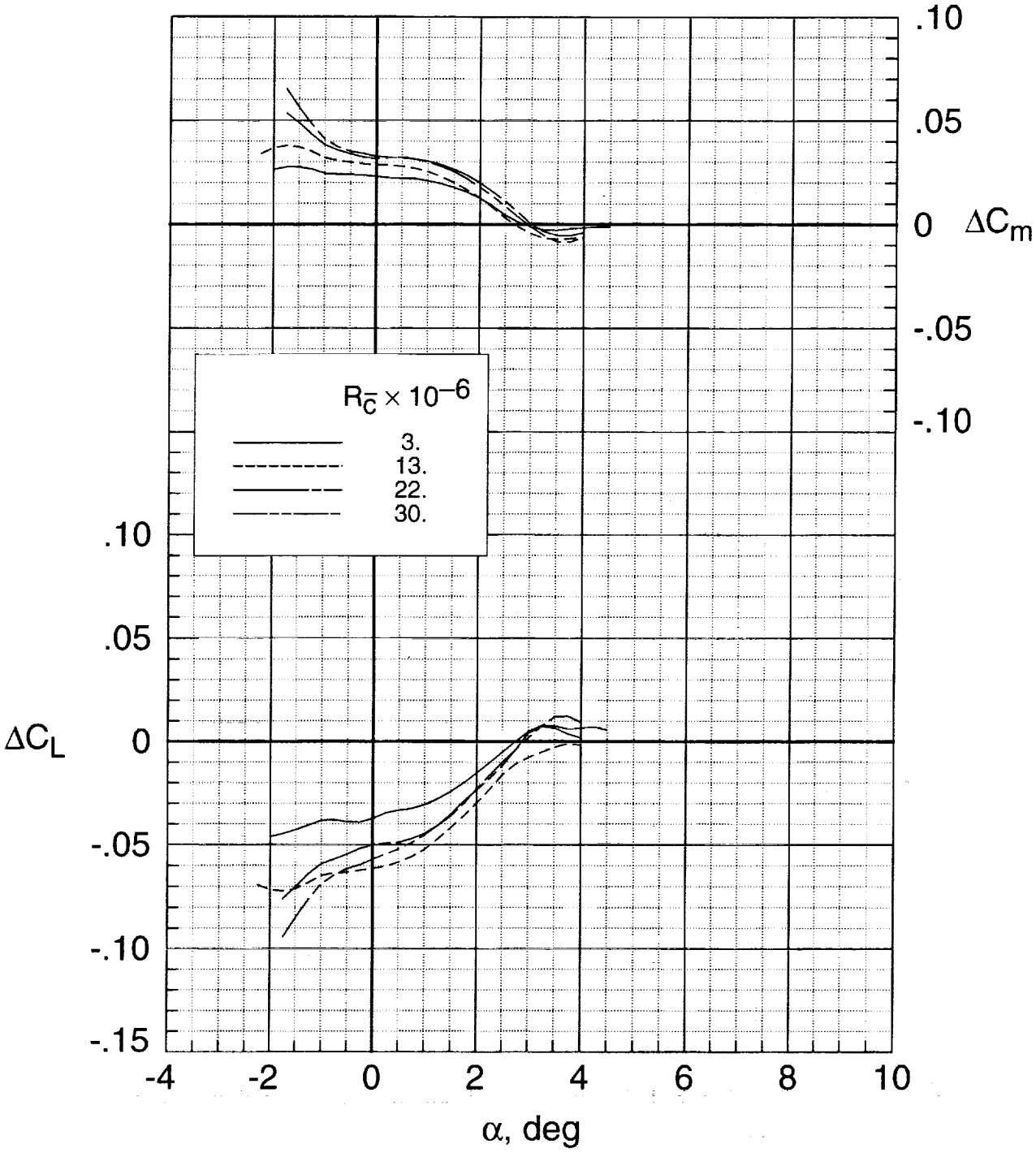

(d) Concluded.

Figure 7. Continued.

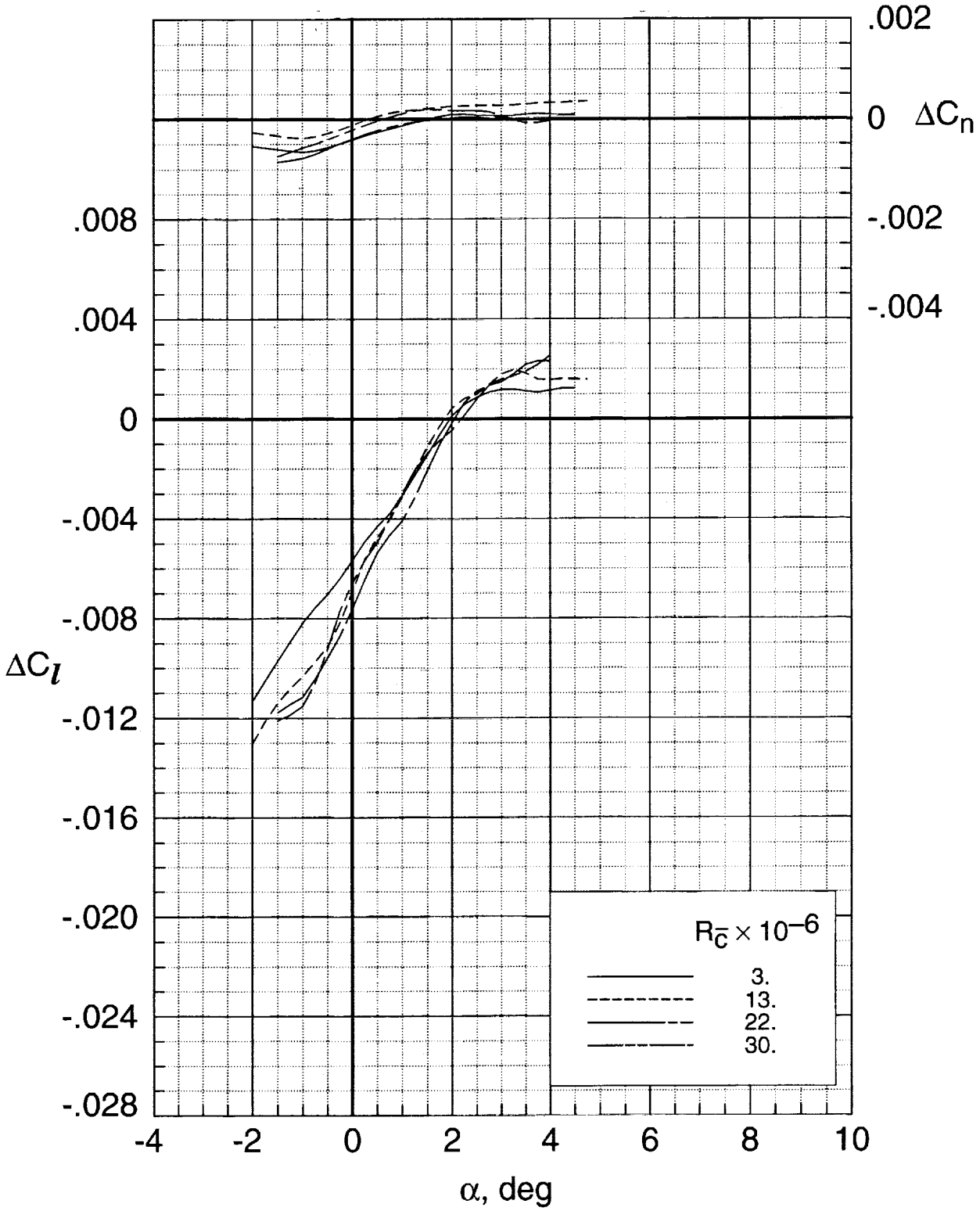

(e) $M_\infty = 0.88$.

Figure 7. Continued.

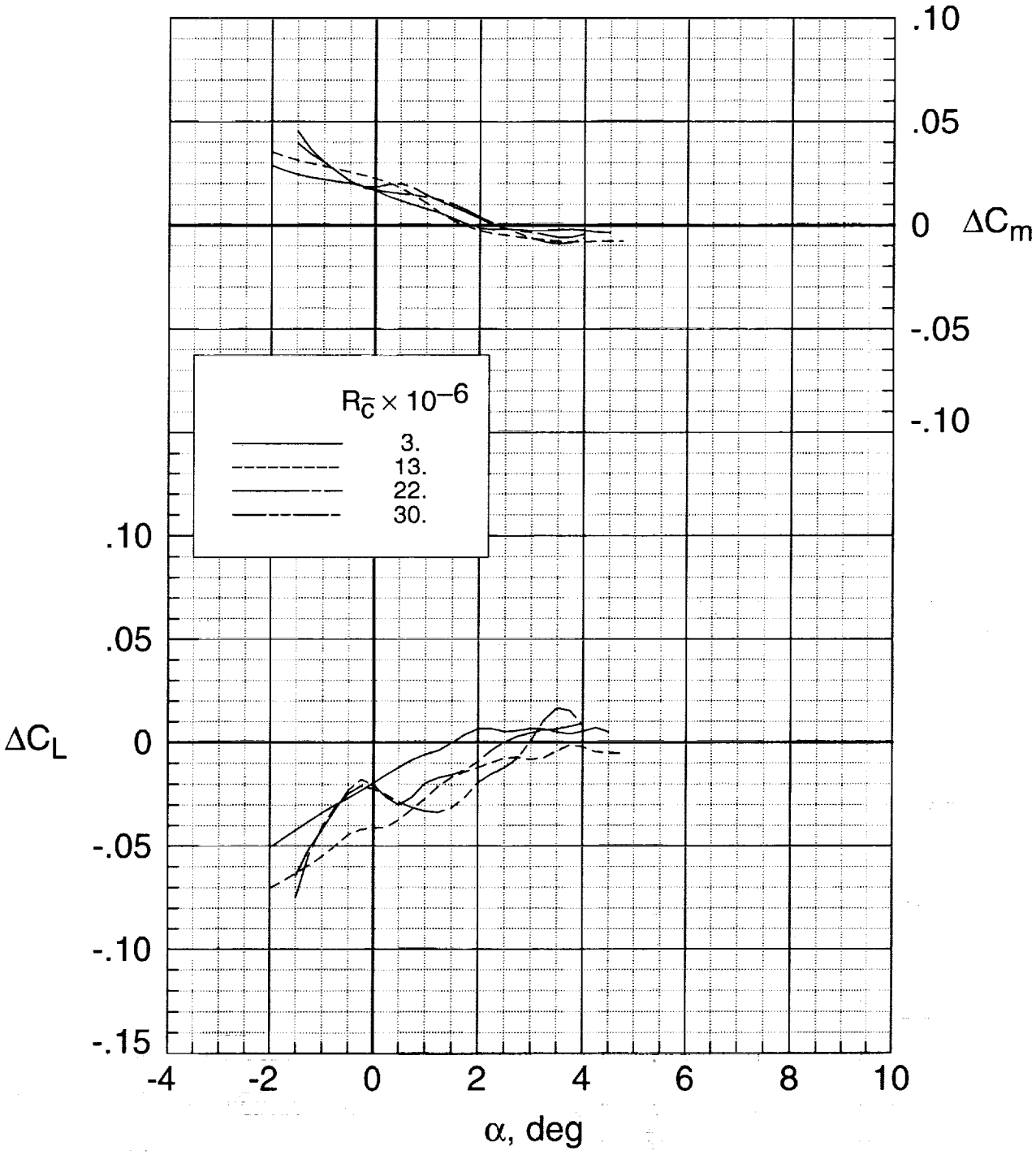

(e) Concluded.

Figure 7. Continued.

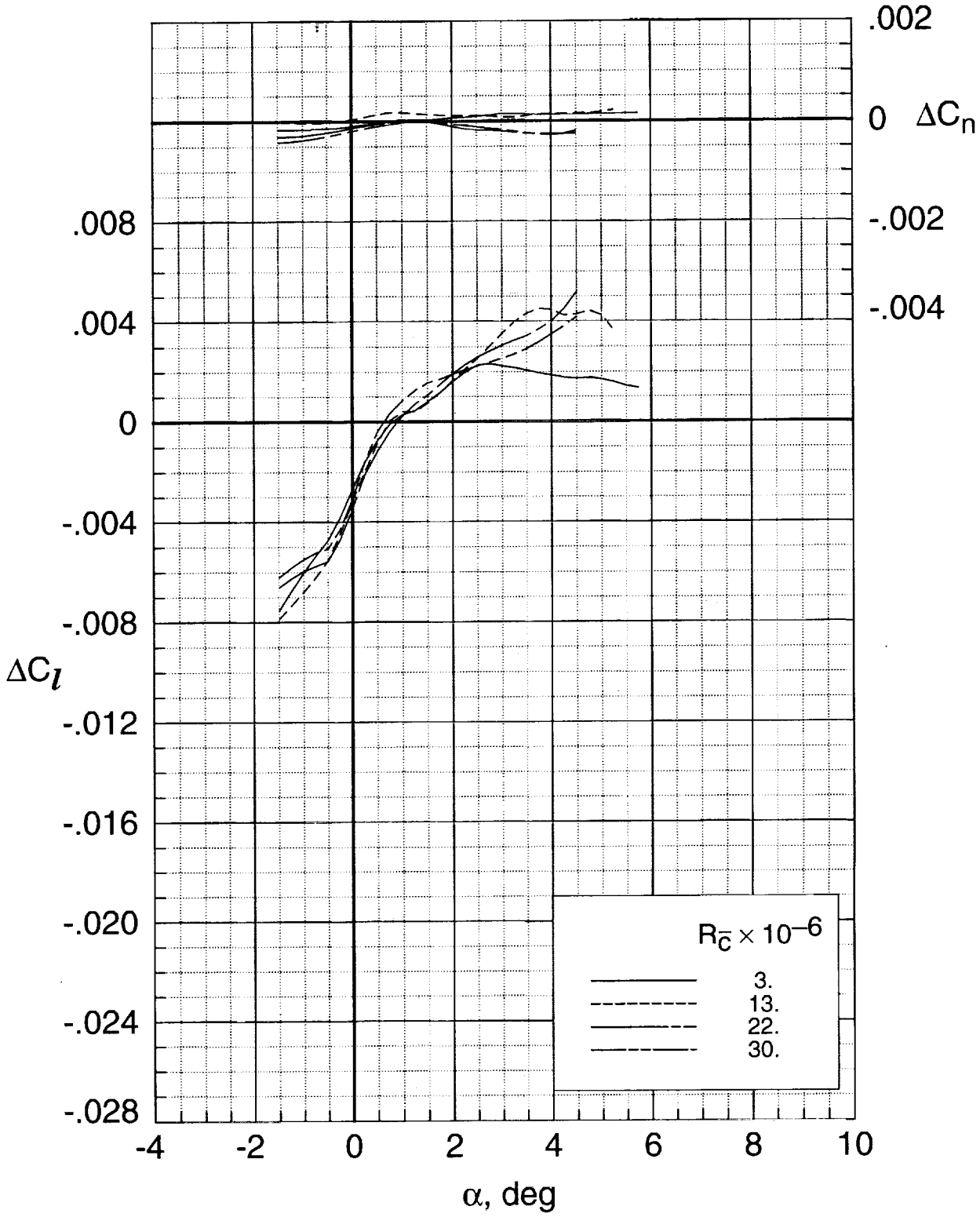

(f) $M_\infty = 0.91$.

Figure 7. Continued.

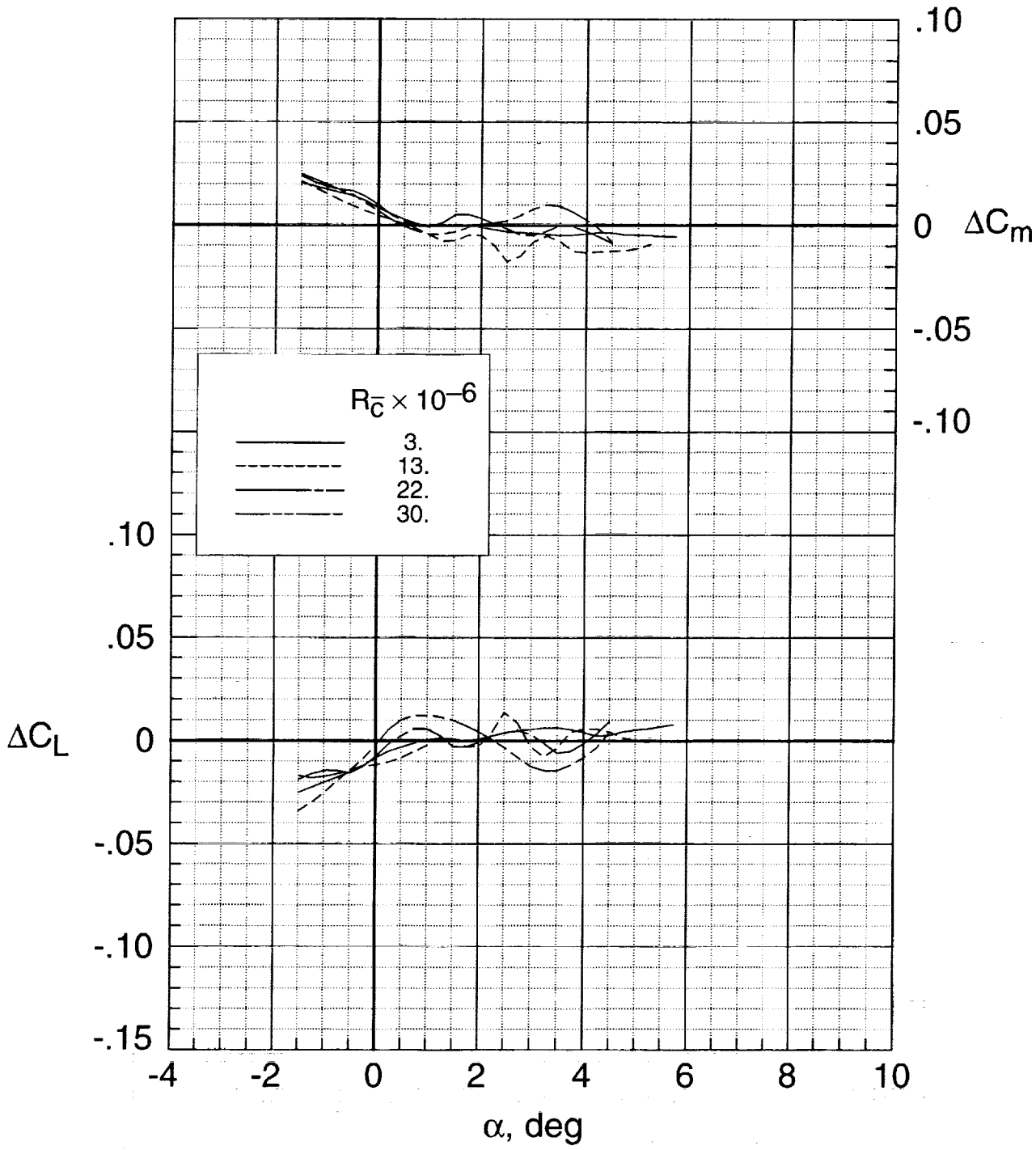

(f) Concluded.

Figure 7. Continued.

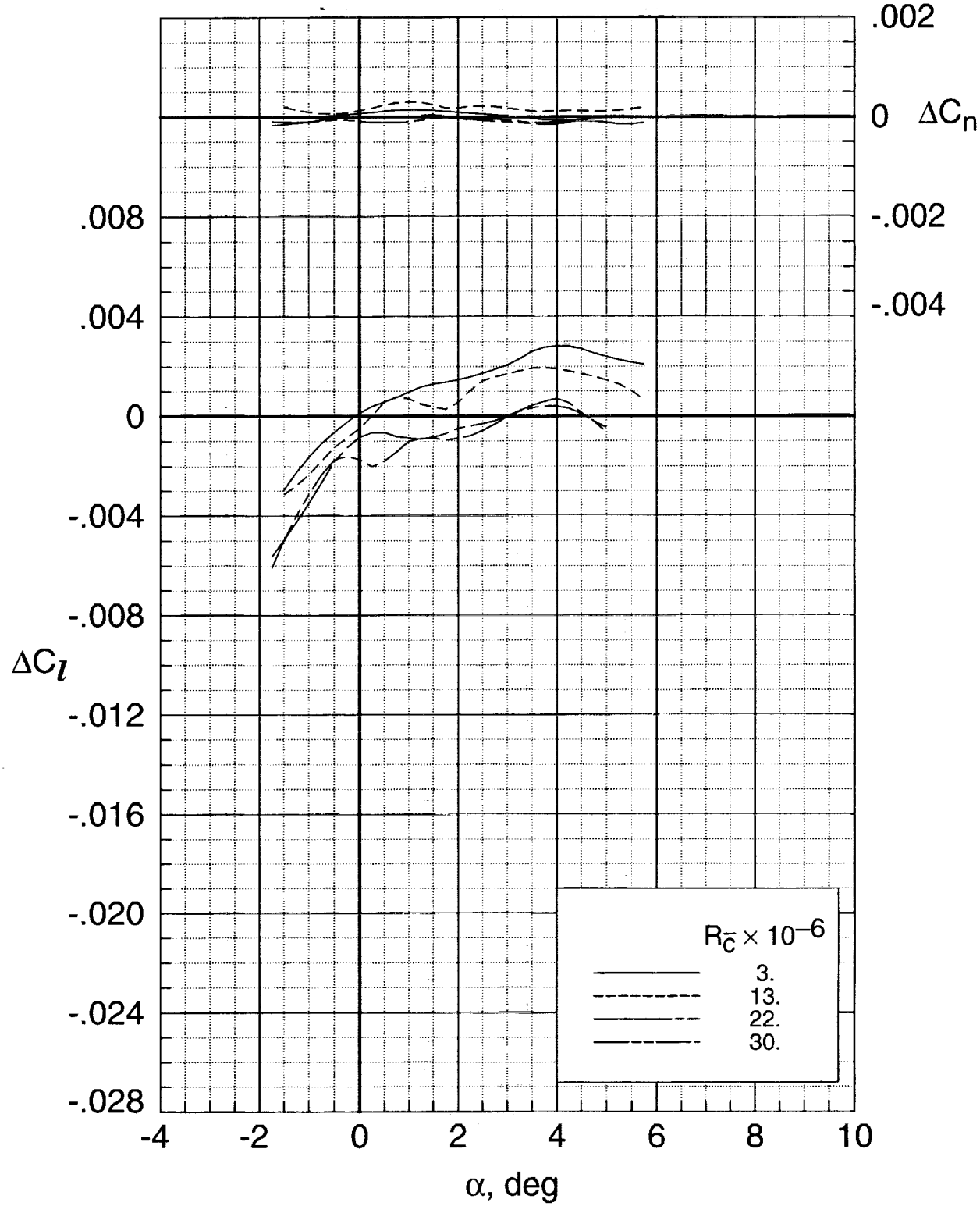

(g) $M_\infty = 0.94$.

Figure 7. Continued.

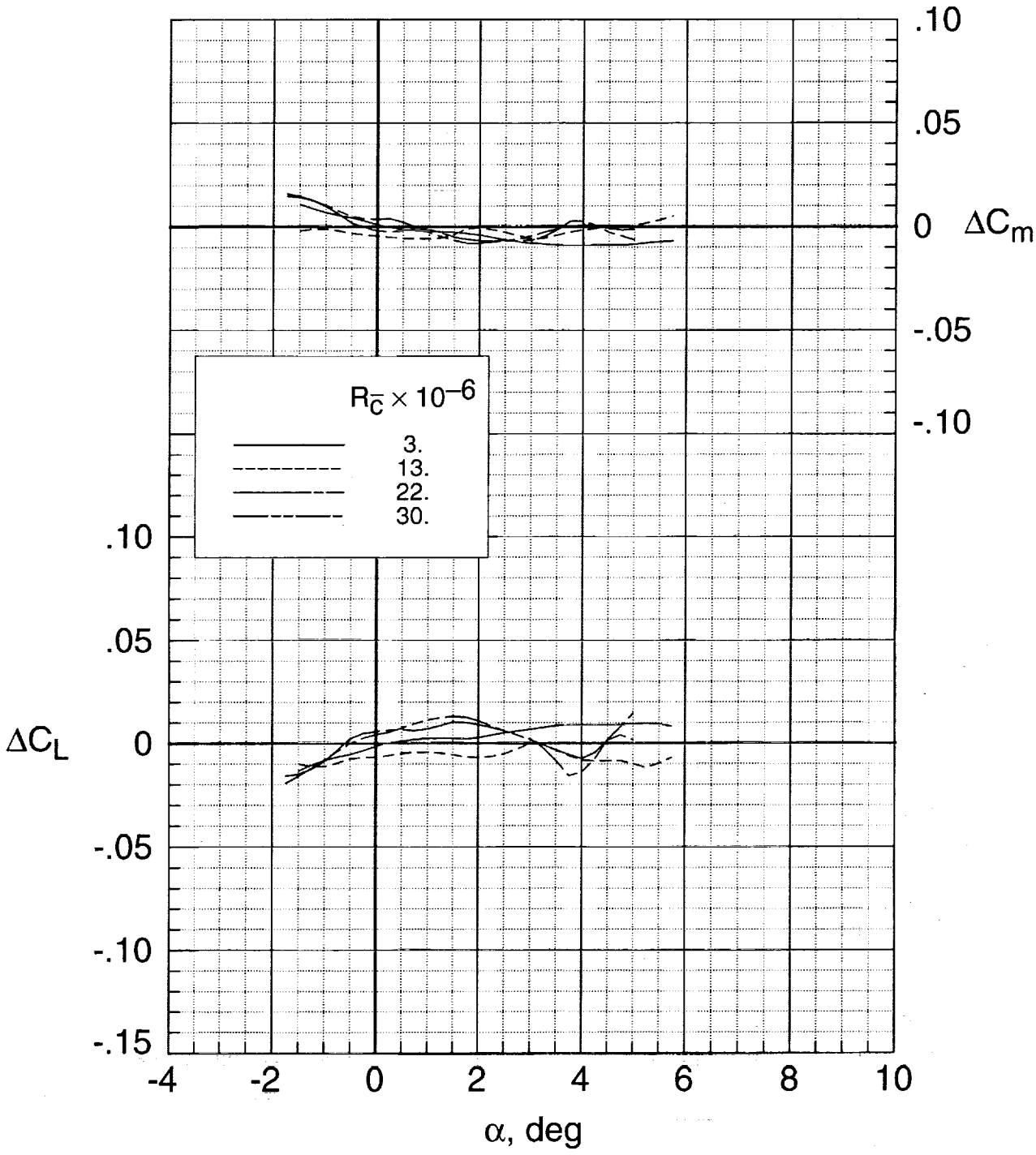

(g) Concluded.

Figure 7. Concluded.

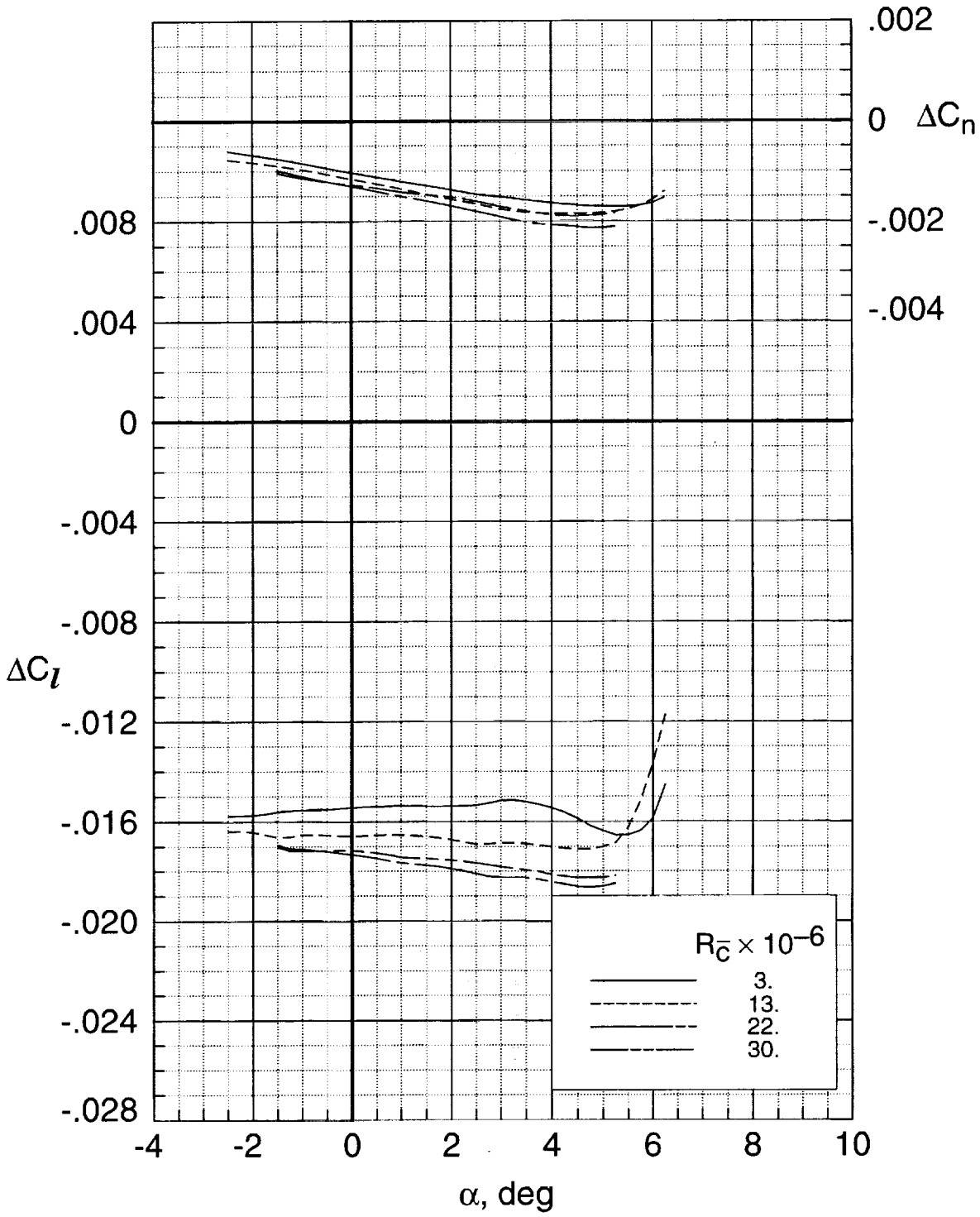

(a) $M_\infty = 0.70$.

Figure 8. Effect of Reynolds number on the aerodynamic characteristics with the outboard spoilers for $\delta_s = 20°$.

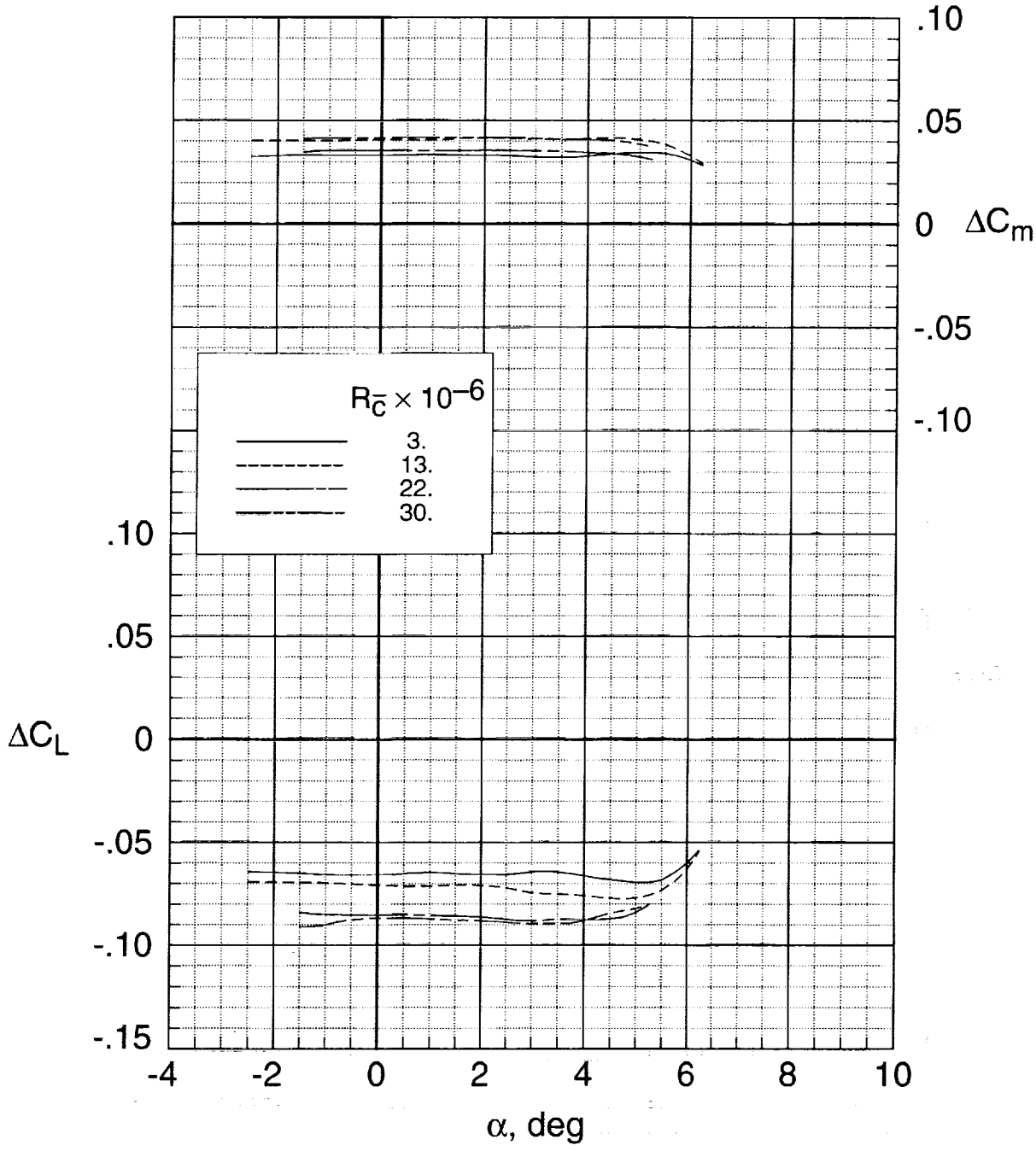

(a) Concluded.

Figure 8. Continued.

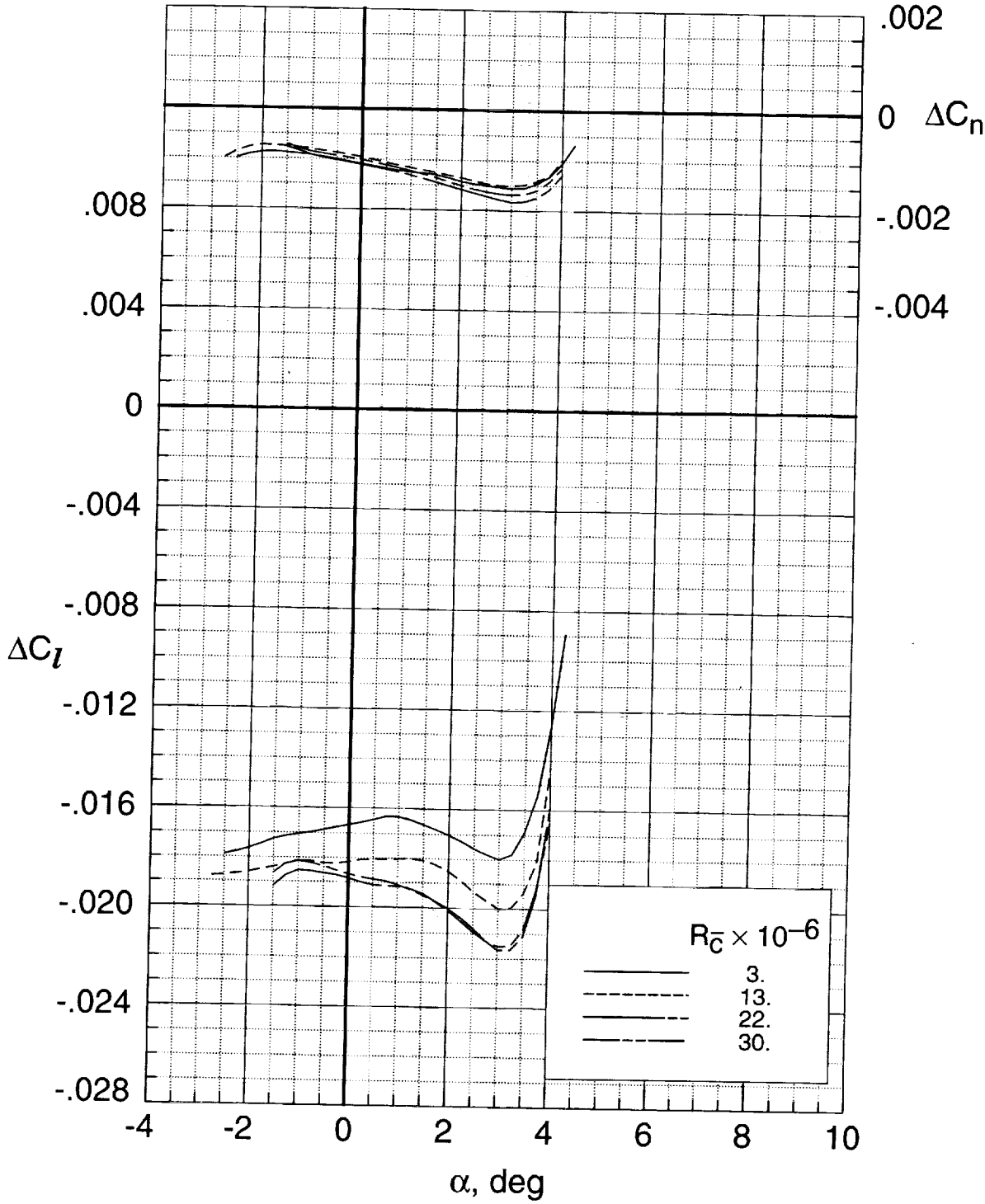

(b) $M_\infty = 0.80$.

Figure 8. Continued.

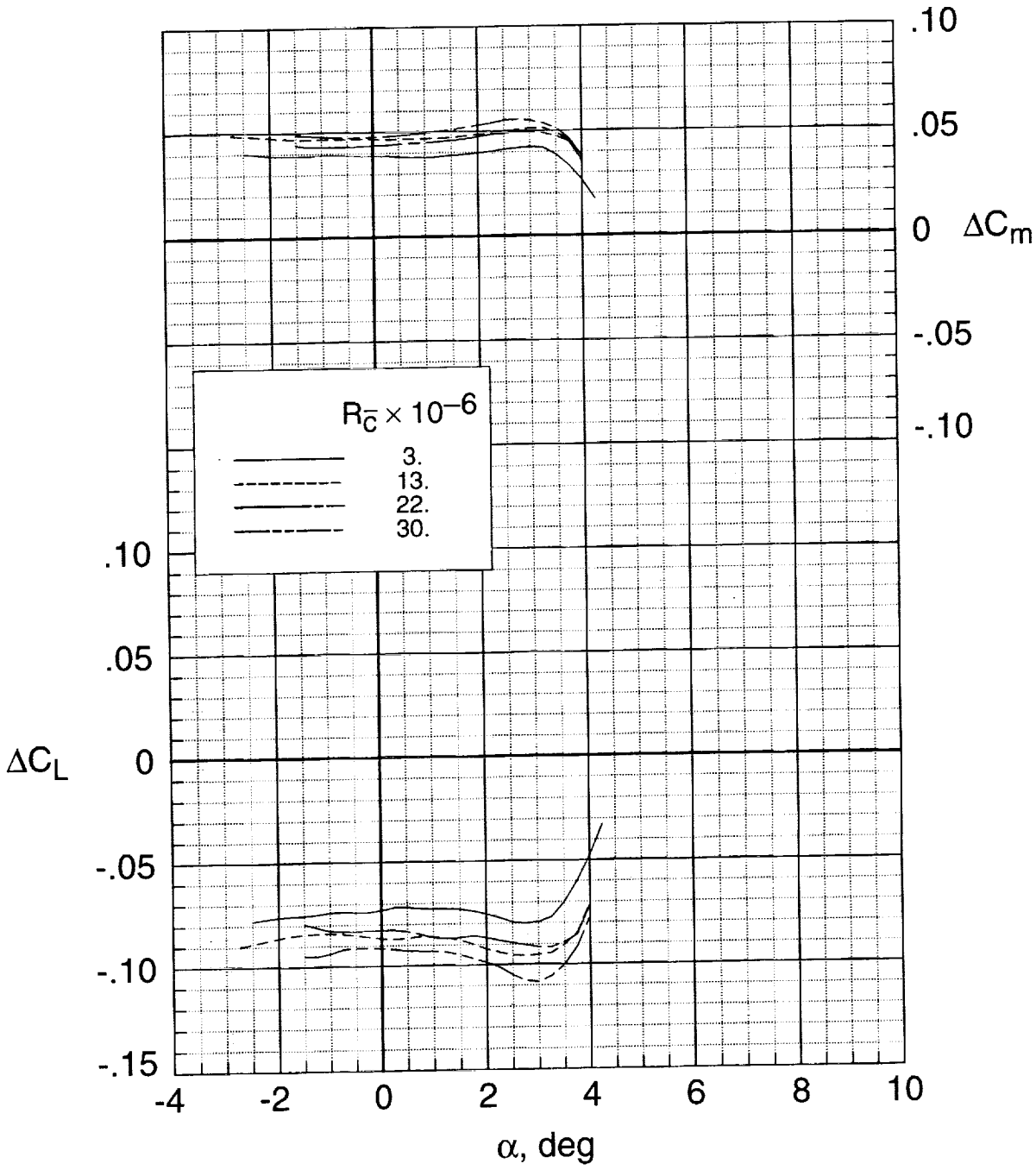

(b) Concluded.

Figure 8. Continued.

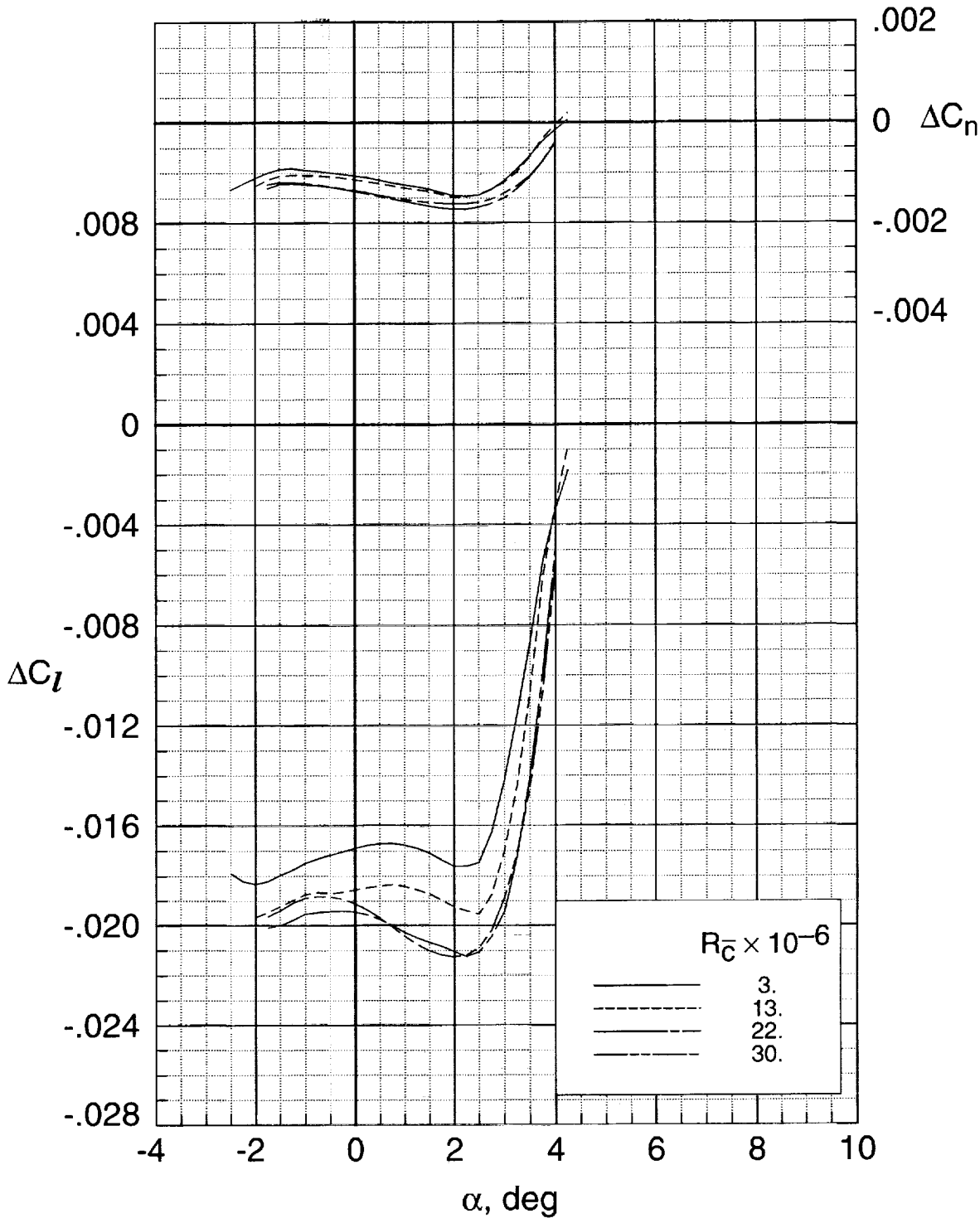

(c) $M_\infty = 0.82$.

Figure 8. Continued.

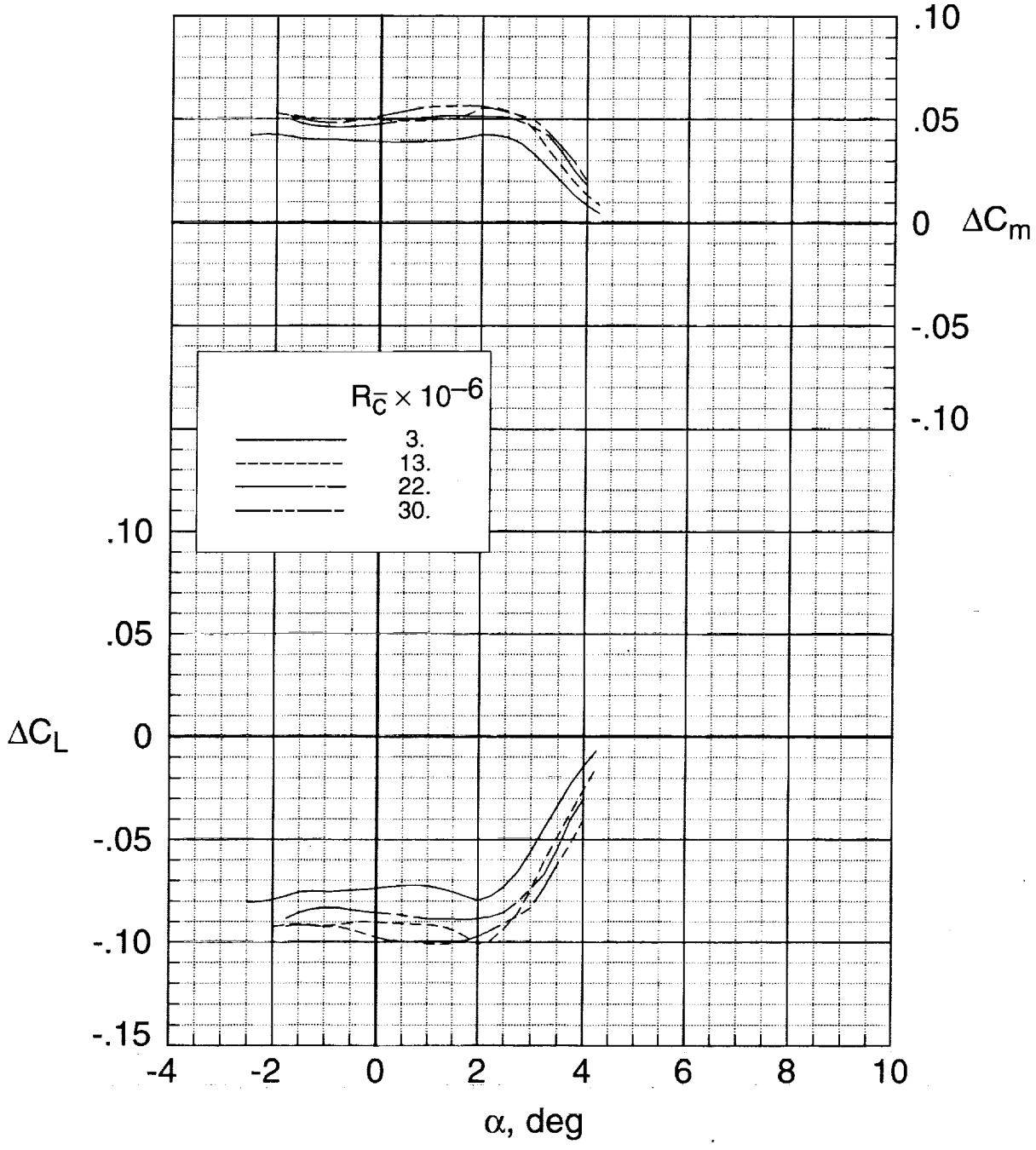

(c) Concluded.

Figure 8. Continued.

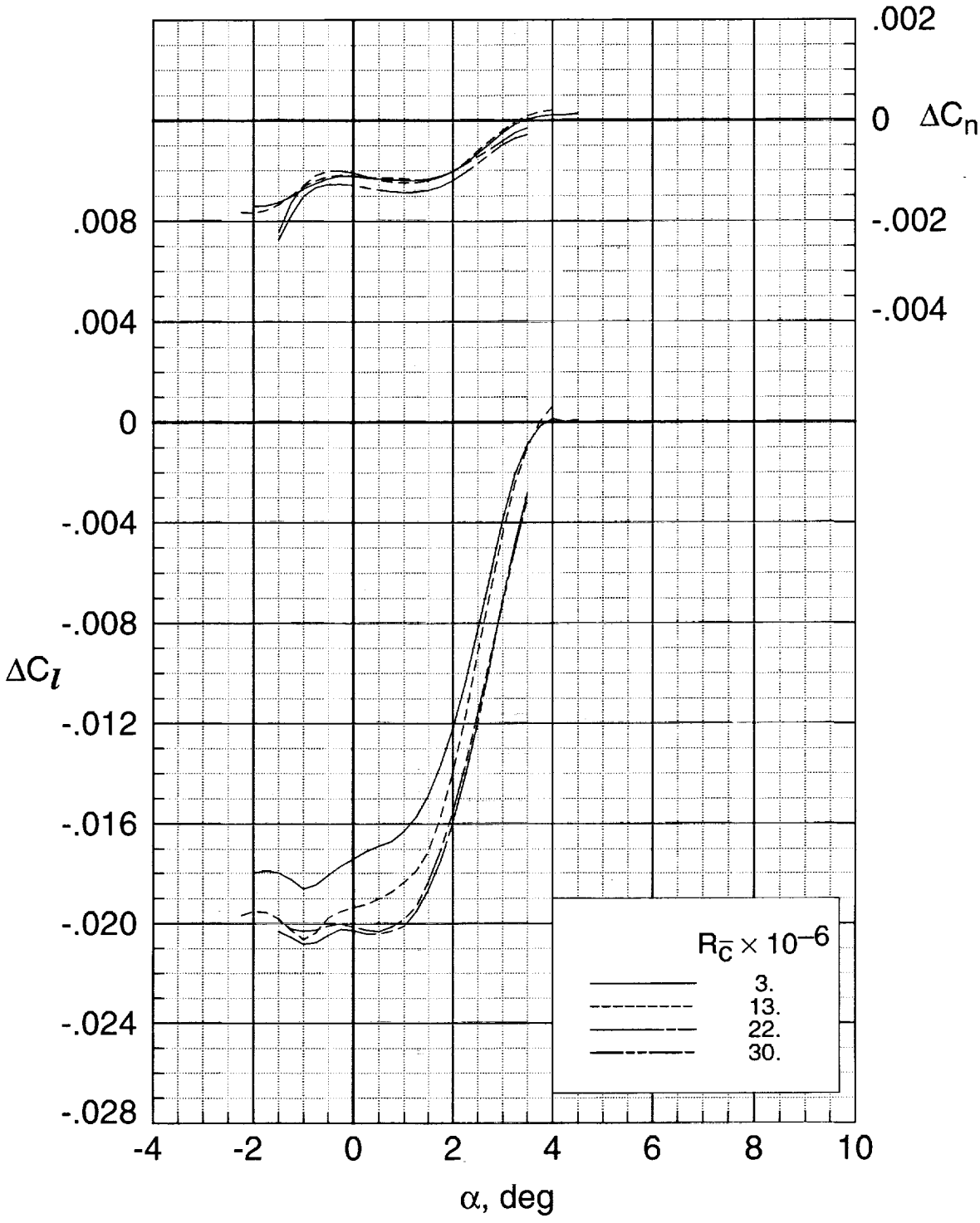

(d) $M_\infty = 0.85$.

Figure 8. Continued.

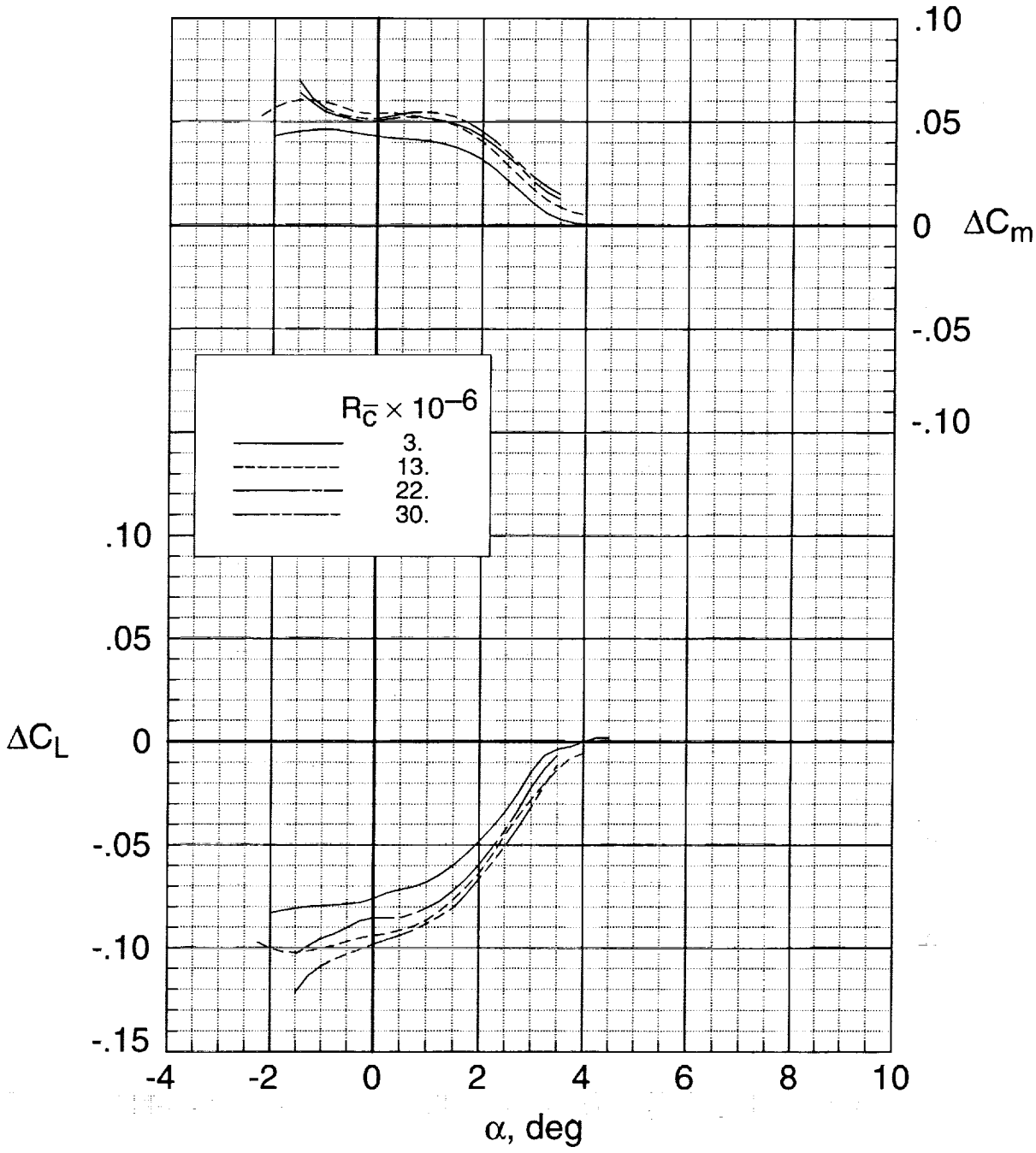

(d) Concluded.

Figure 8. Continued.

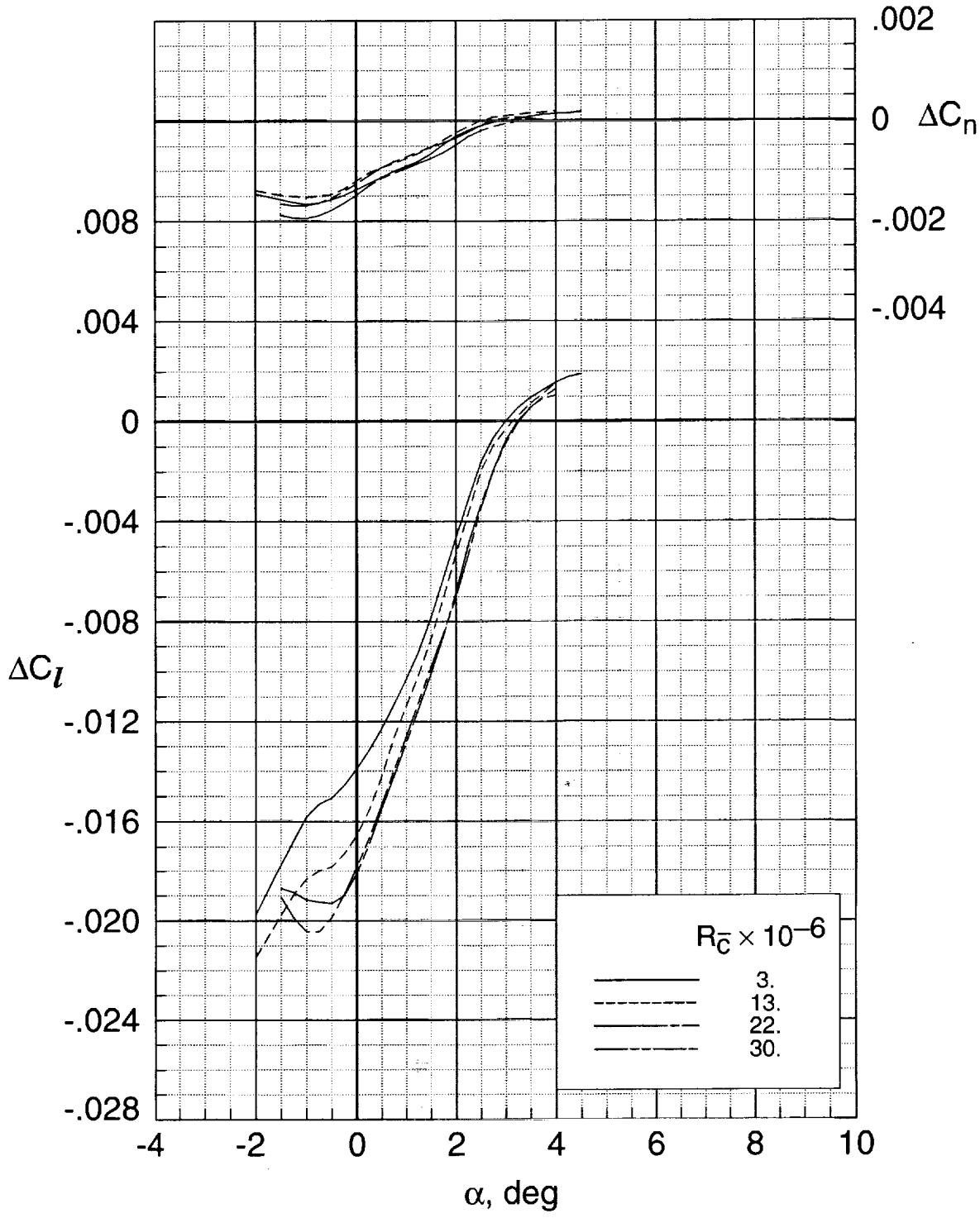

(c) $M_\infty = 0.88$.

Figure 8. Continued.

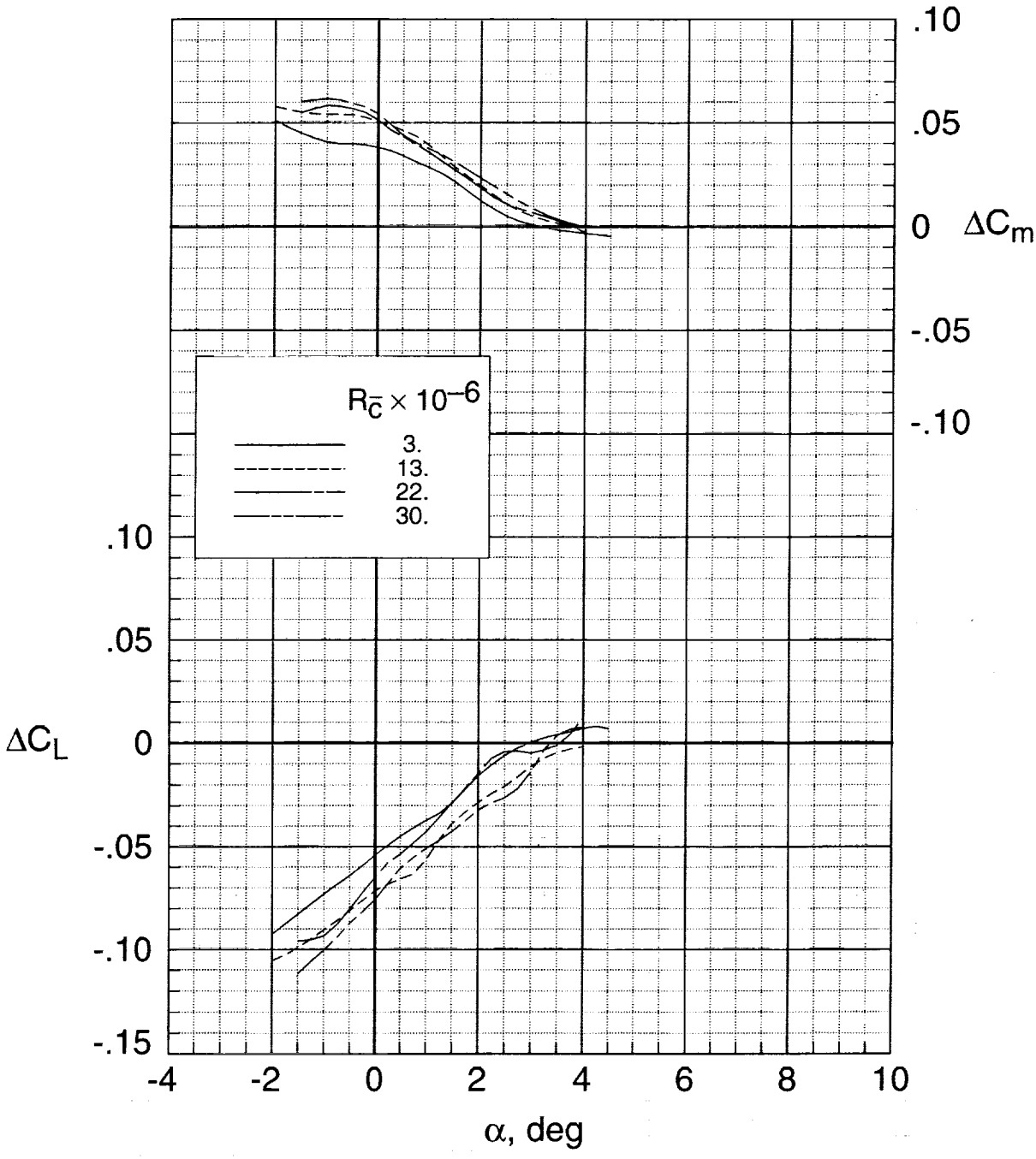

(e) Concluded.

Figure 8. Continued.

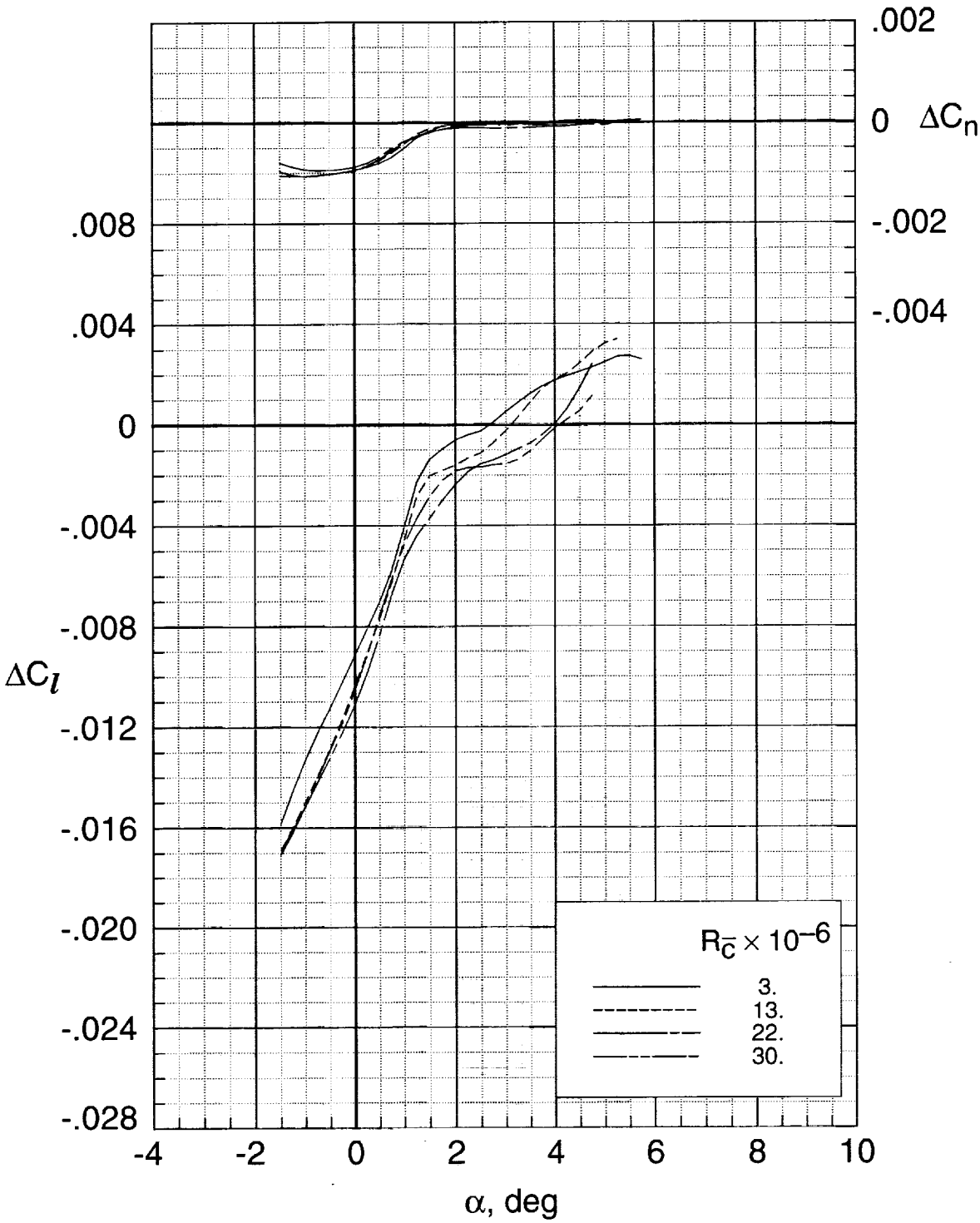

(f) $M_\infty = 0.91$.

Figure 8. Continued.

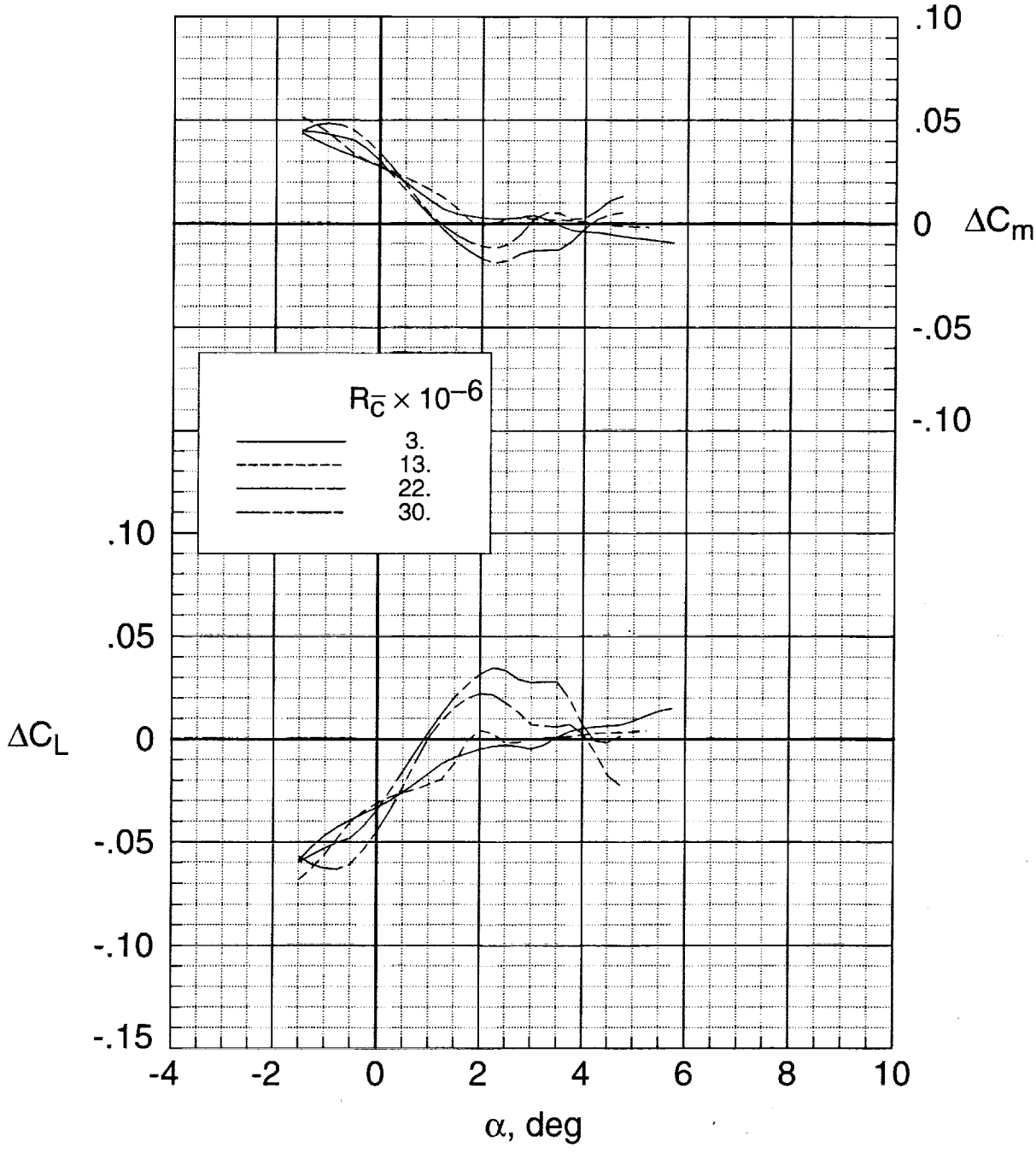

(f) Concluded.

Figure 8. Continued.

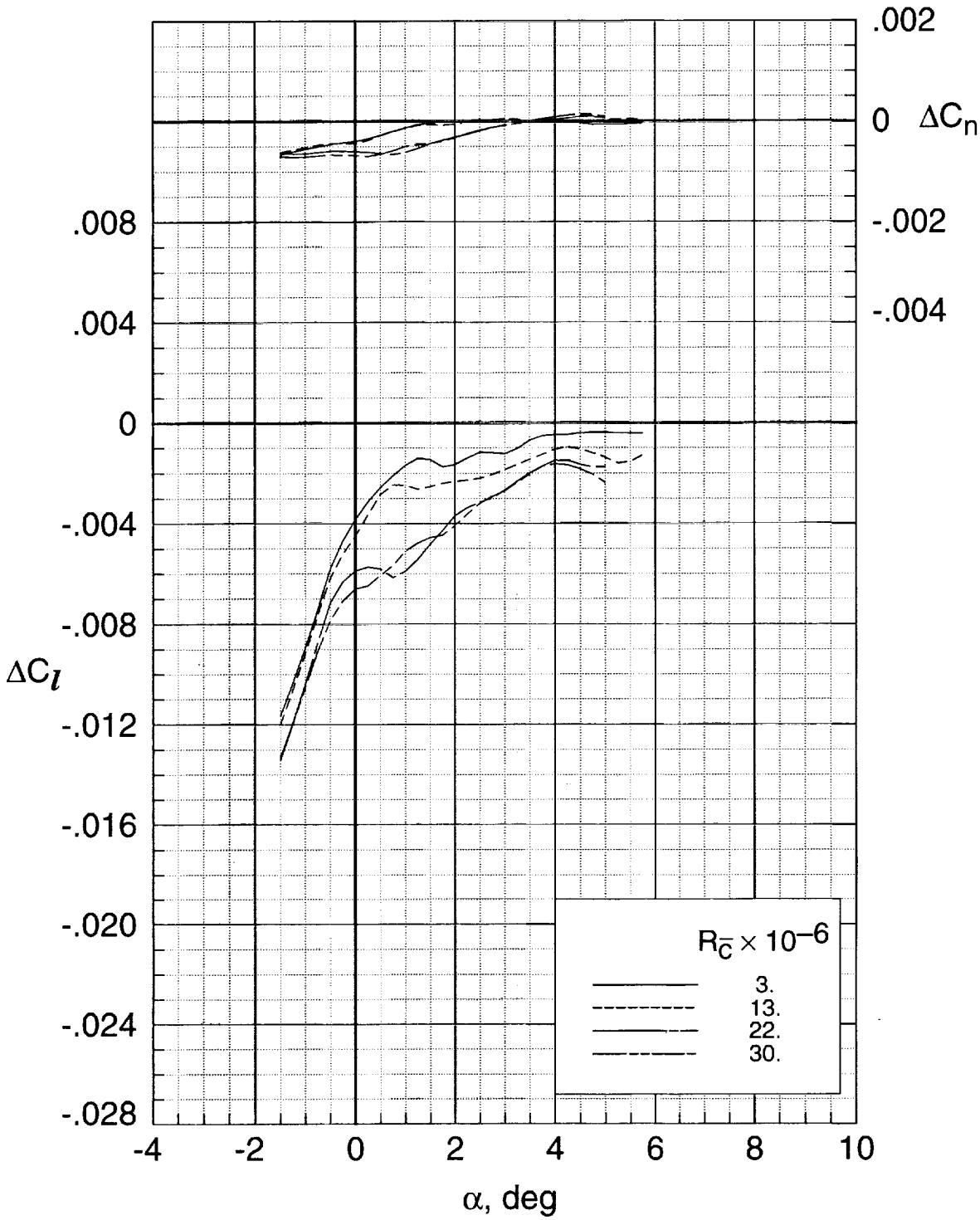

(g) $M_\infty = 0.94$.

Figure 8. Continued.

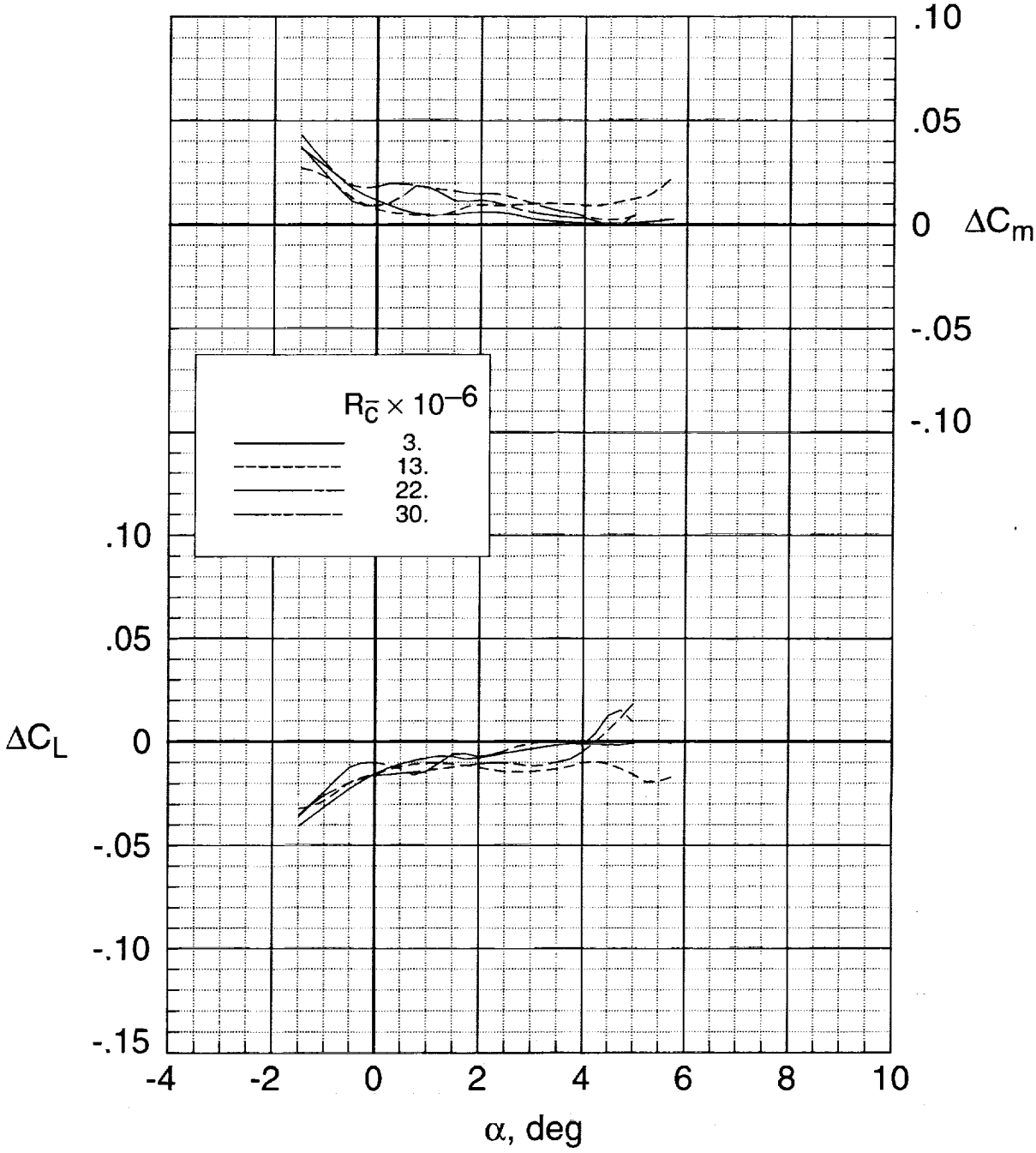

(g) Concluded.

Figure 8. Concluded.

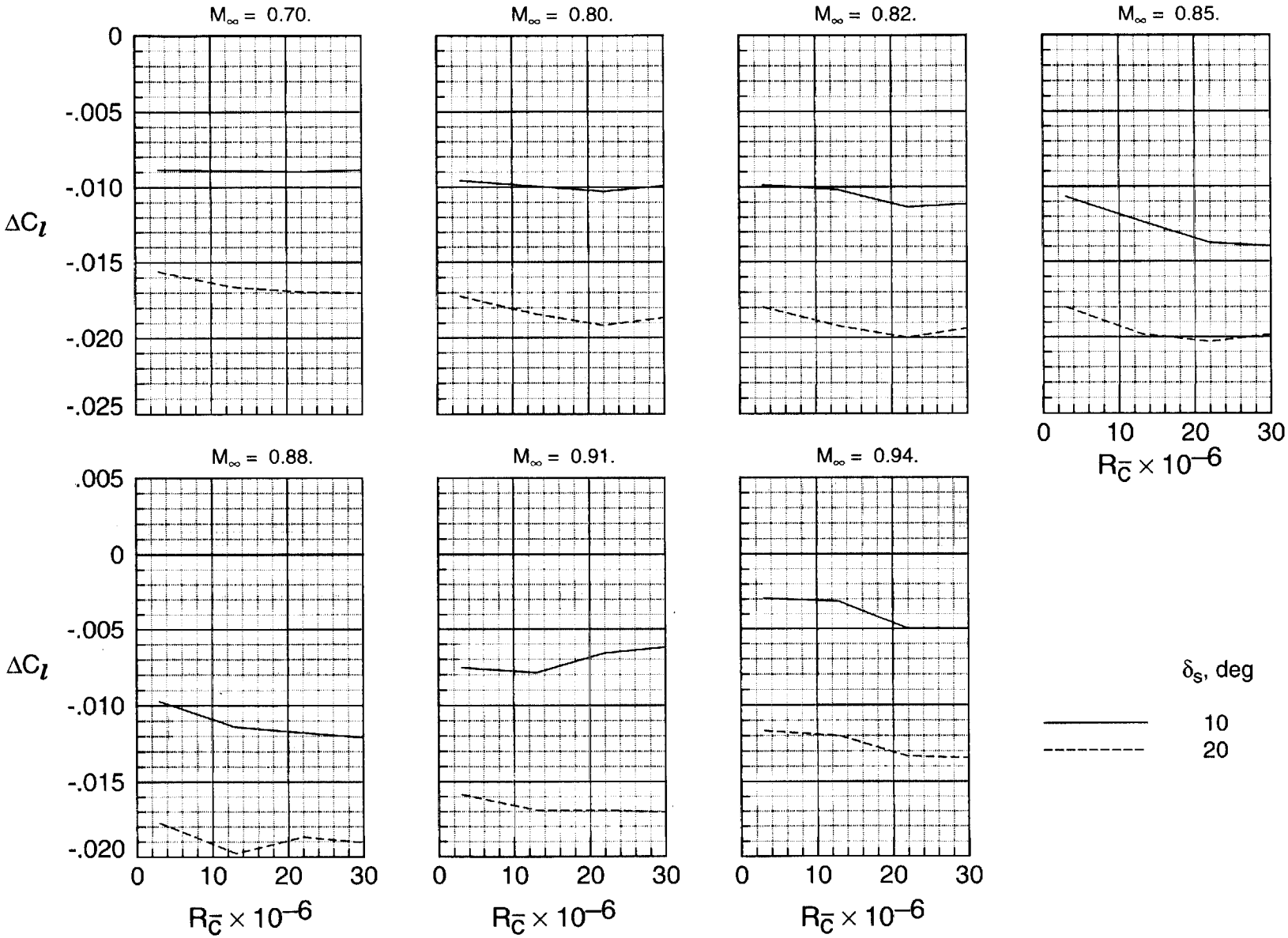

(a) $\alpha = -1.5°$.

Figure 9. Effect of spoiler deflection on the rolling moment coefficient increment.

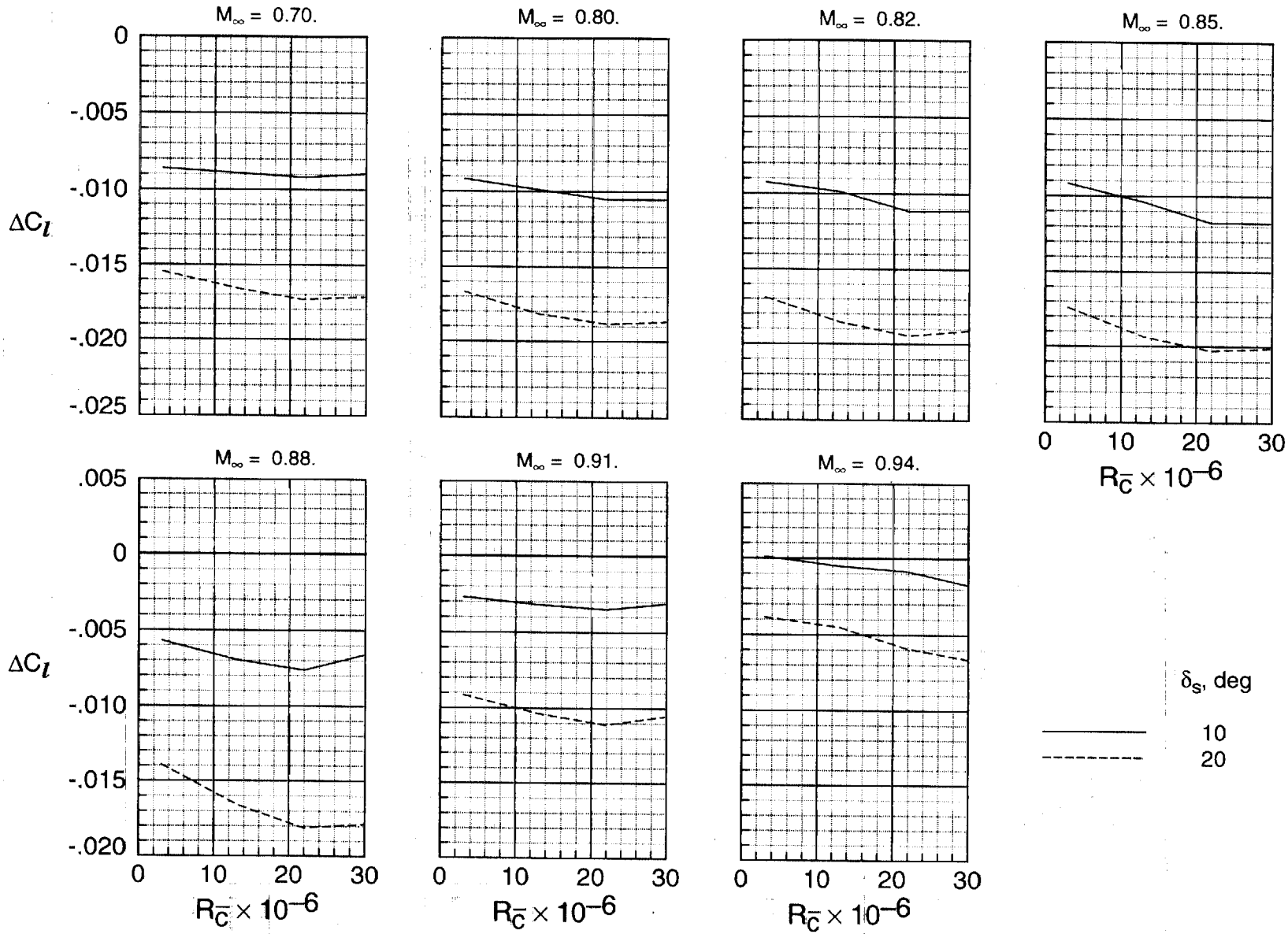

(b) $\alpha = 0.0°$.

Figure 9. Continued.

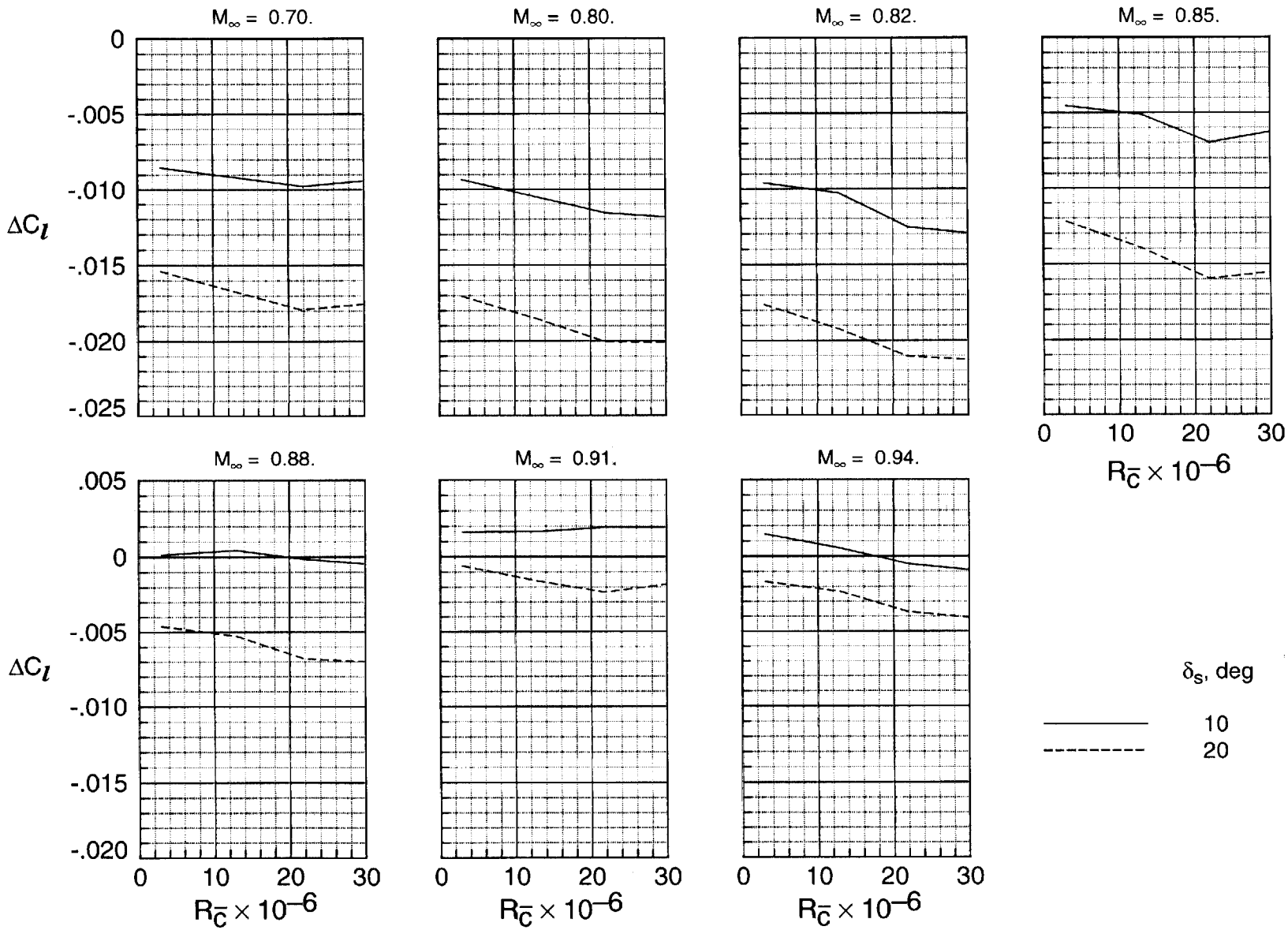

(c) $\alpha = 2.0°$.

Figure 9. Concluded.

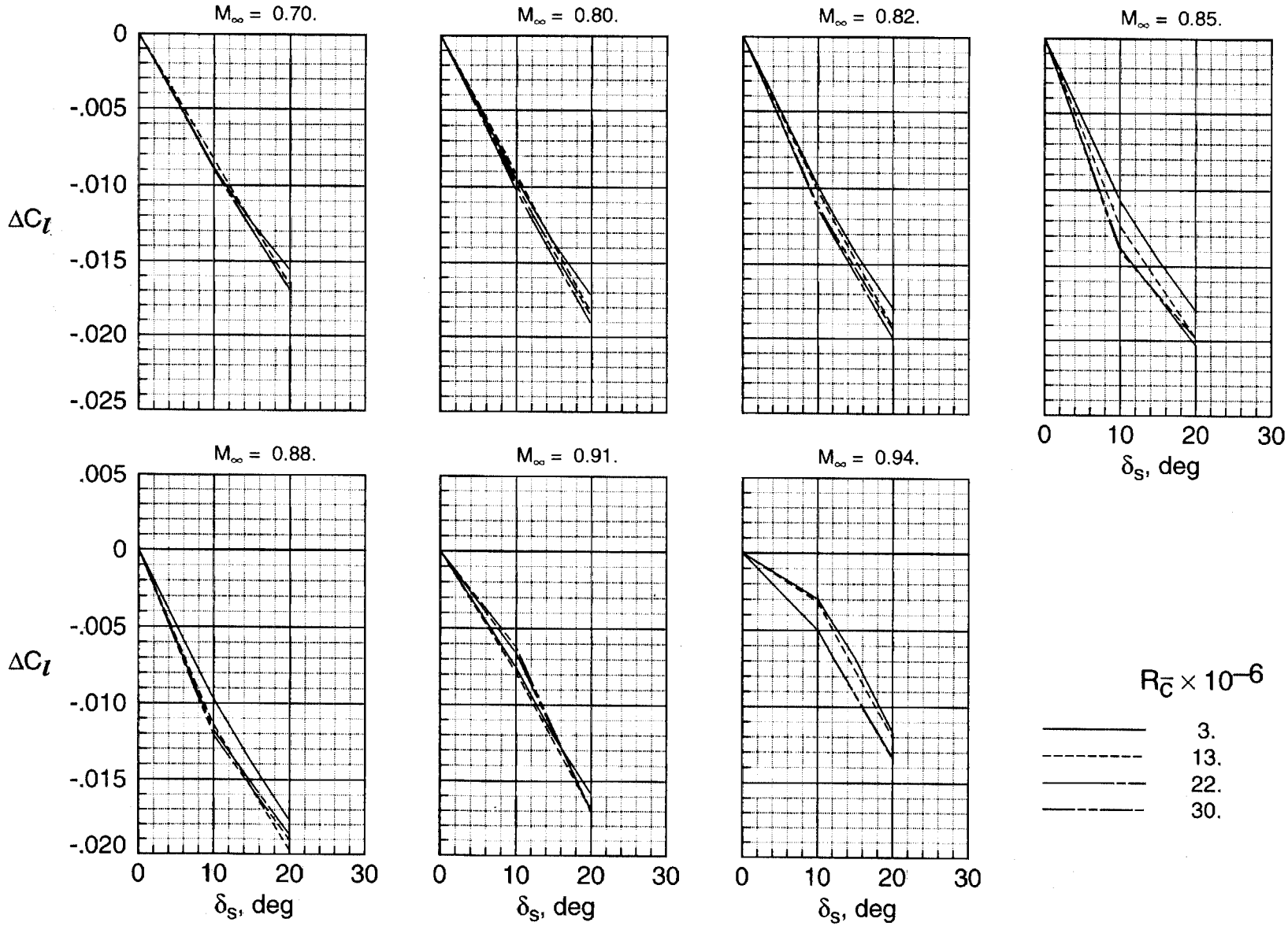

(a) $\alpha = -1.5°$.

Figure 10. Effect of Reynolds number on the spoiler control power.

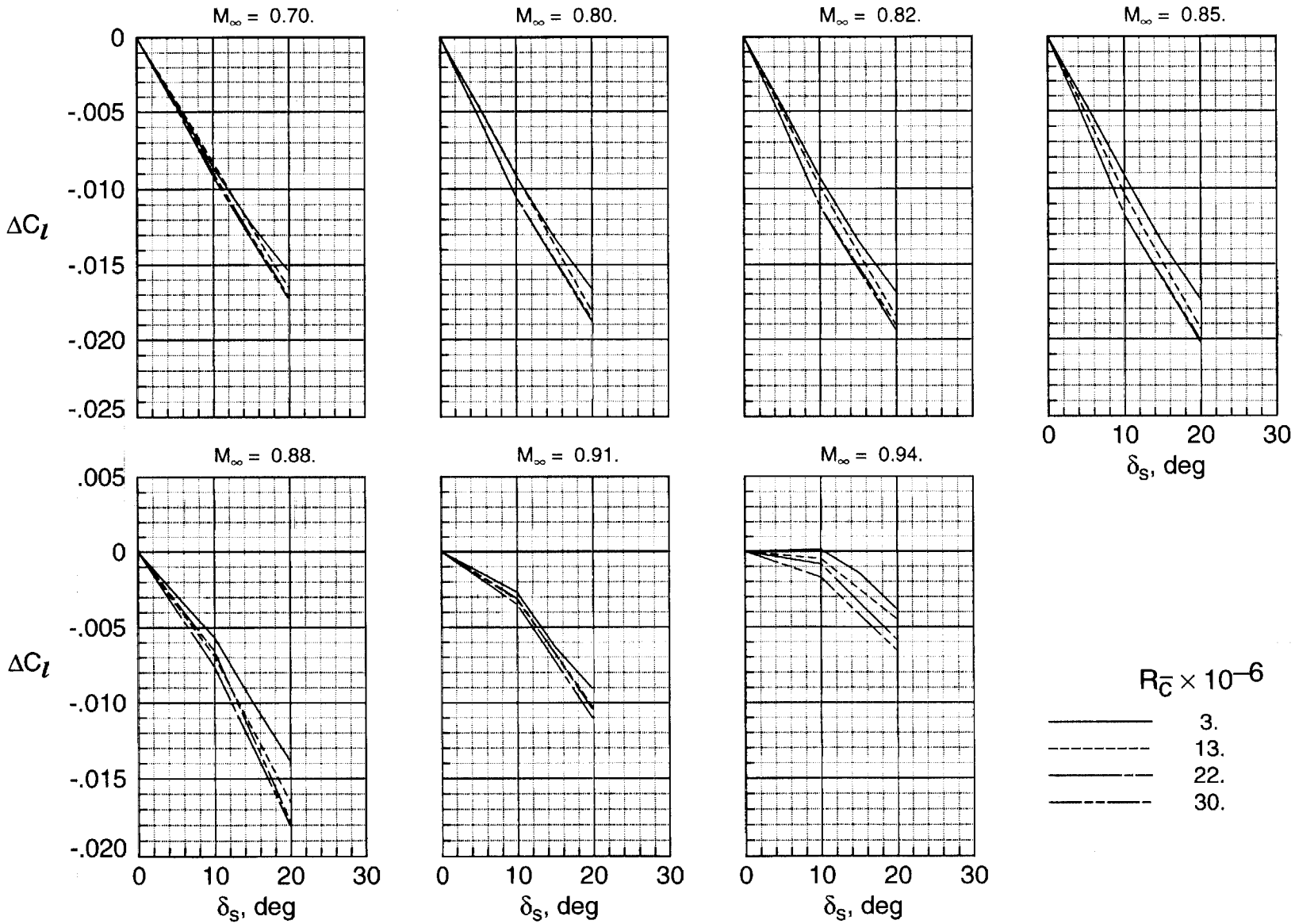

(b) $\alpha = 0.0°$.

Figure 10. Continued.

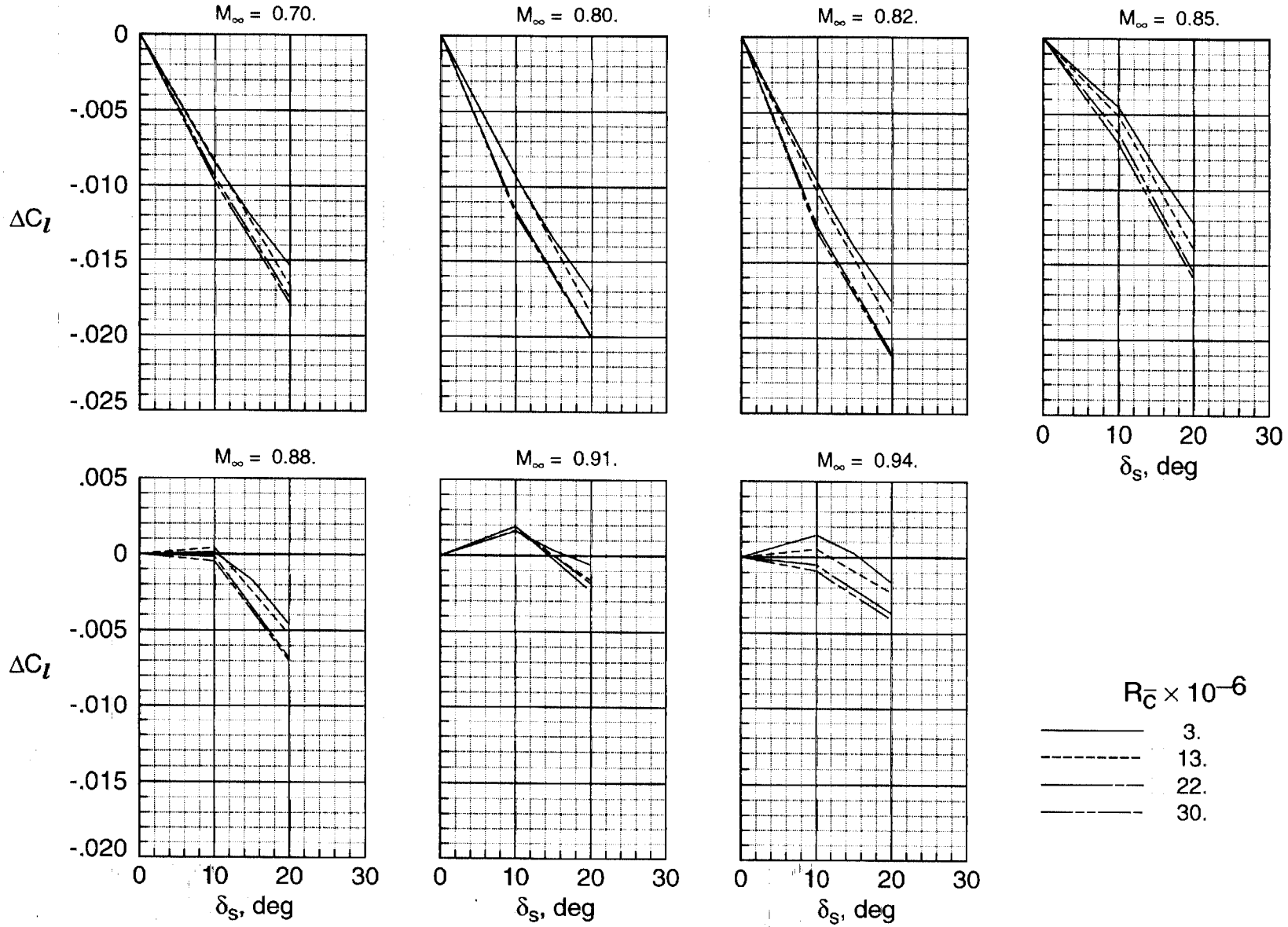

(c) $\alpha = 2.0°$.

Figure 10. Concluded.

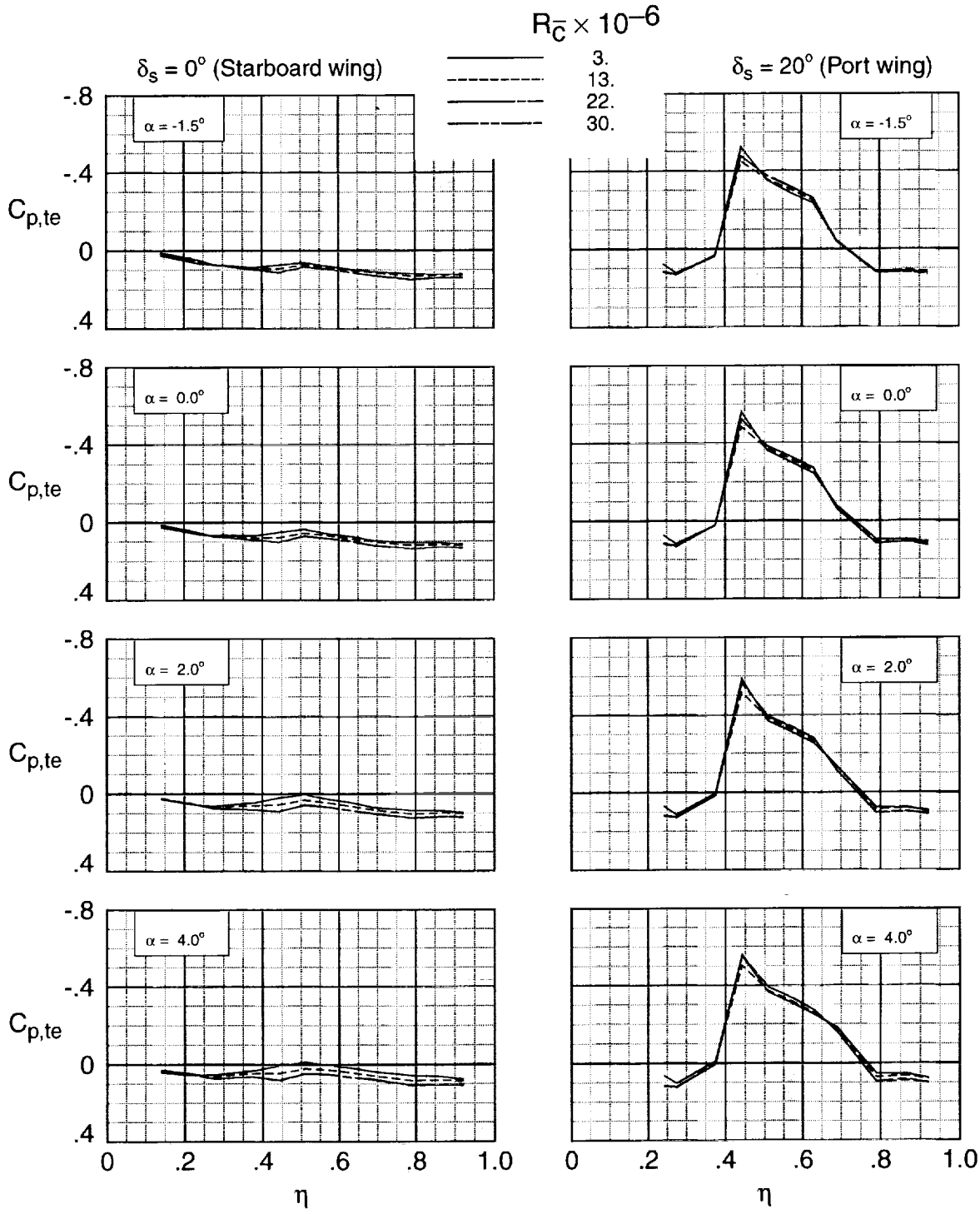

(a) $M_\infty = 0.70$.

Figure 11. Effect of Reynolds number on the trailing edge pressure distribution.

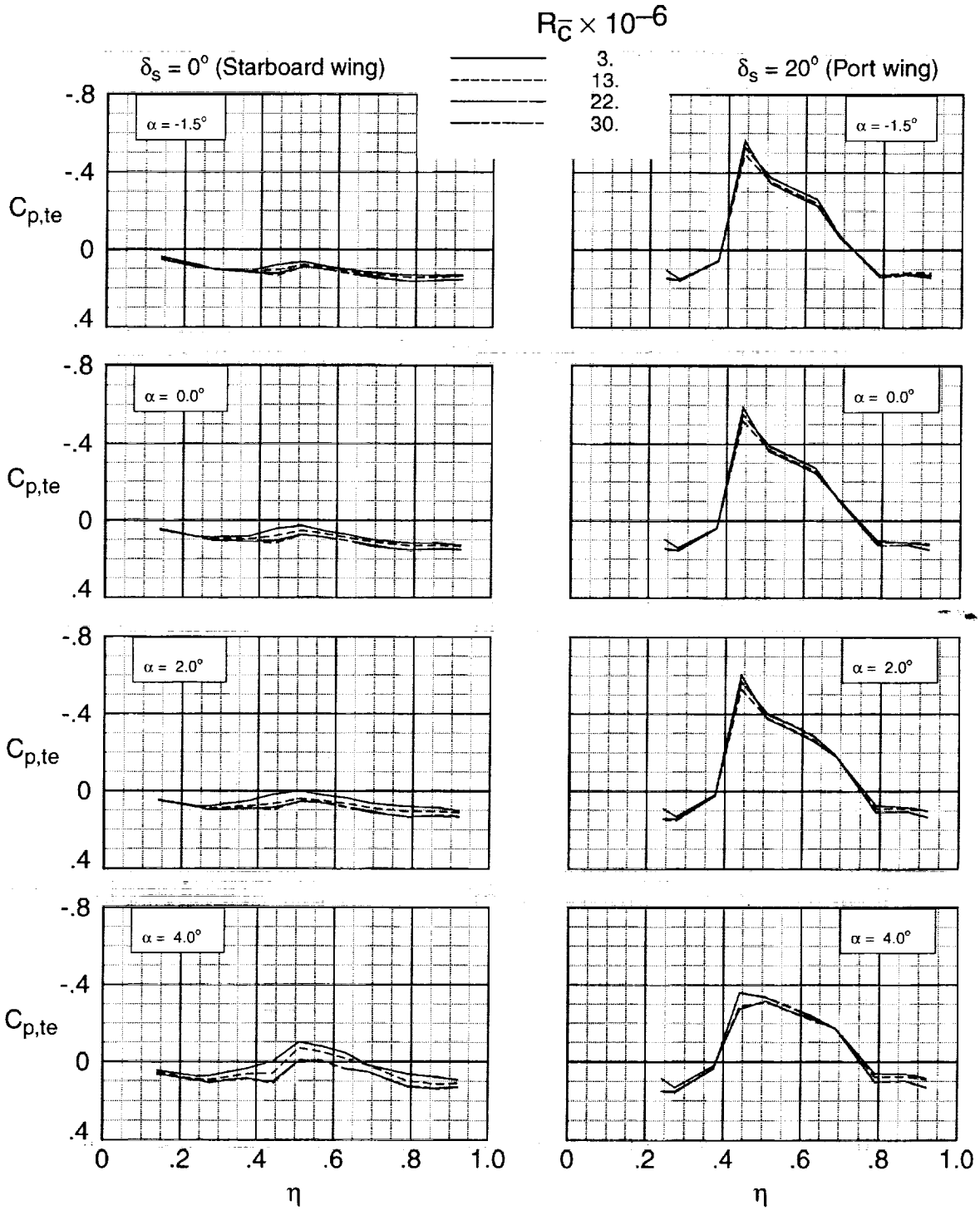

(b) $M_\infty = 0.80$.

Figure 11. Continued.

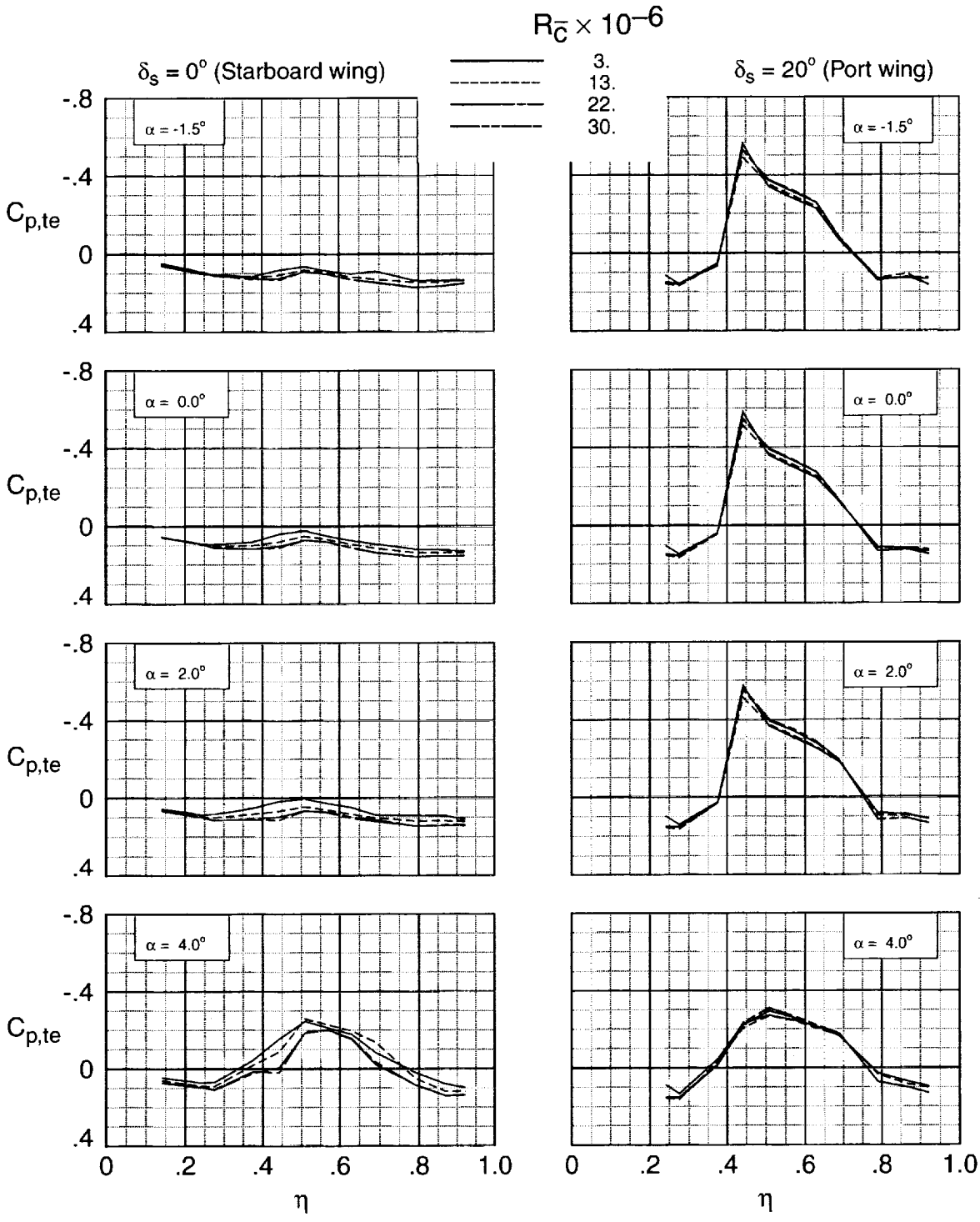

(c) $M_\infty = 0.82$.

Figure 11. Continued.

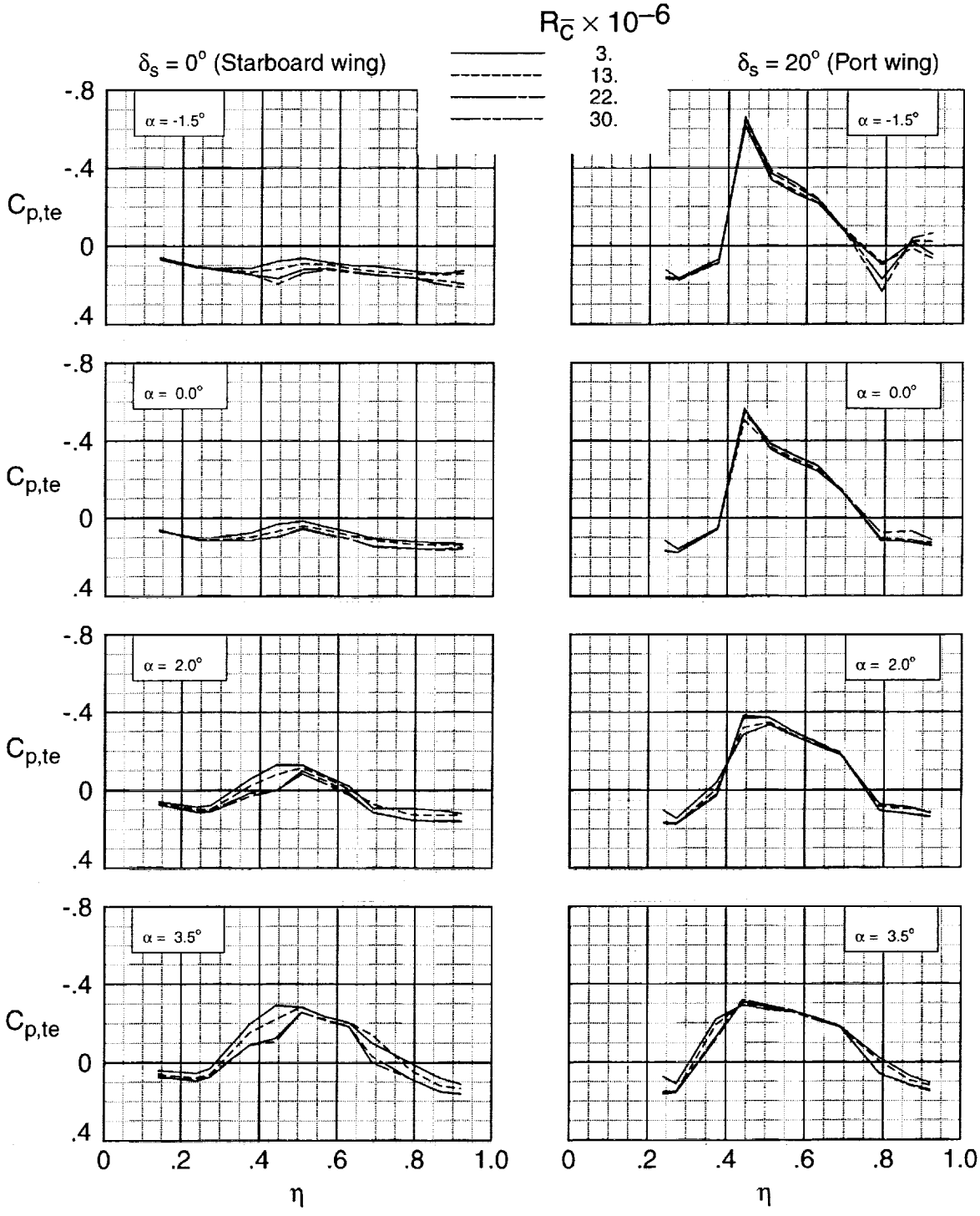

(d) $M_\infty = 0.85$.

Figure 11. Continued.

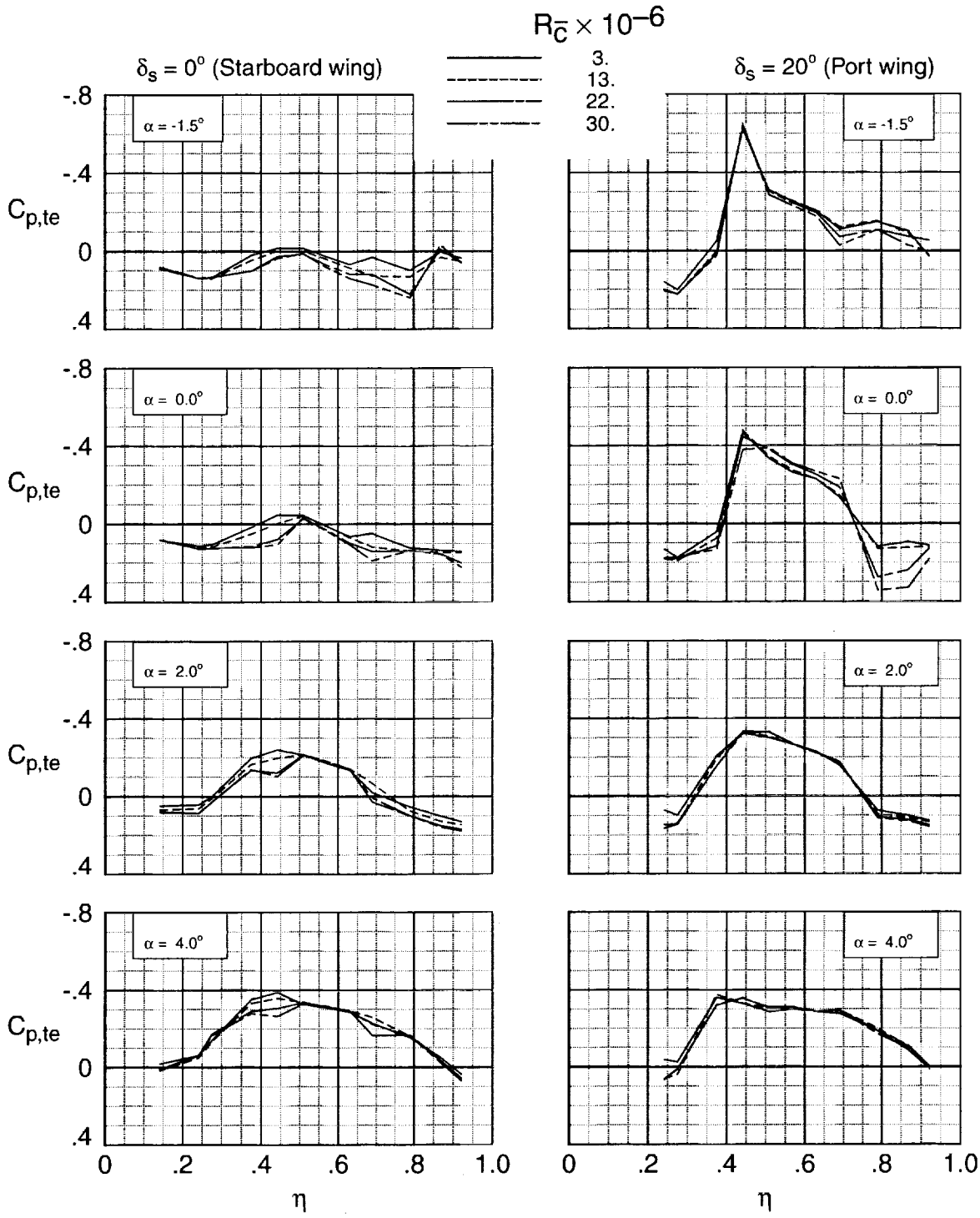

(e) $M_\infty = 0.88$.

Figure 11. Continued.

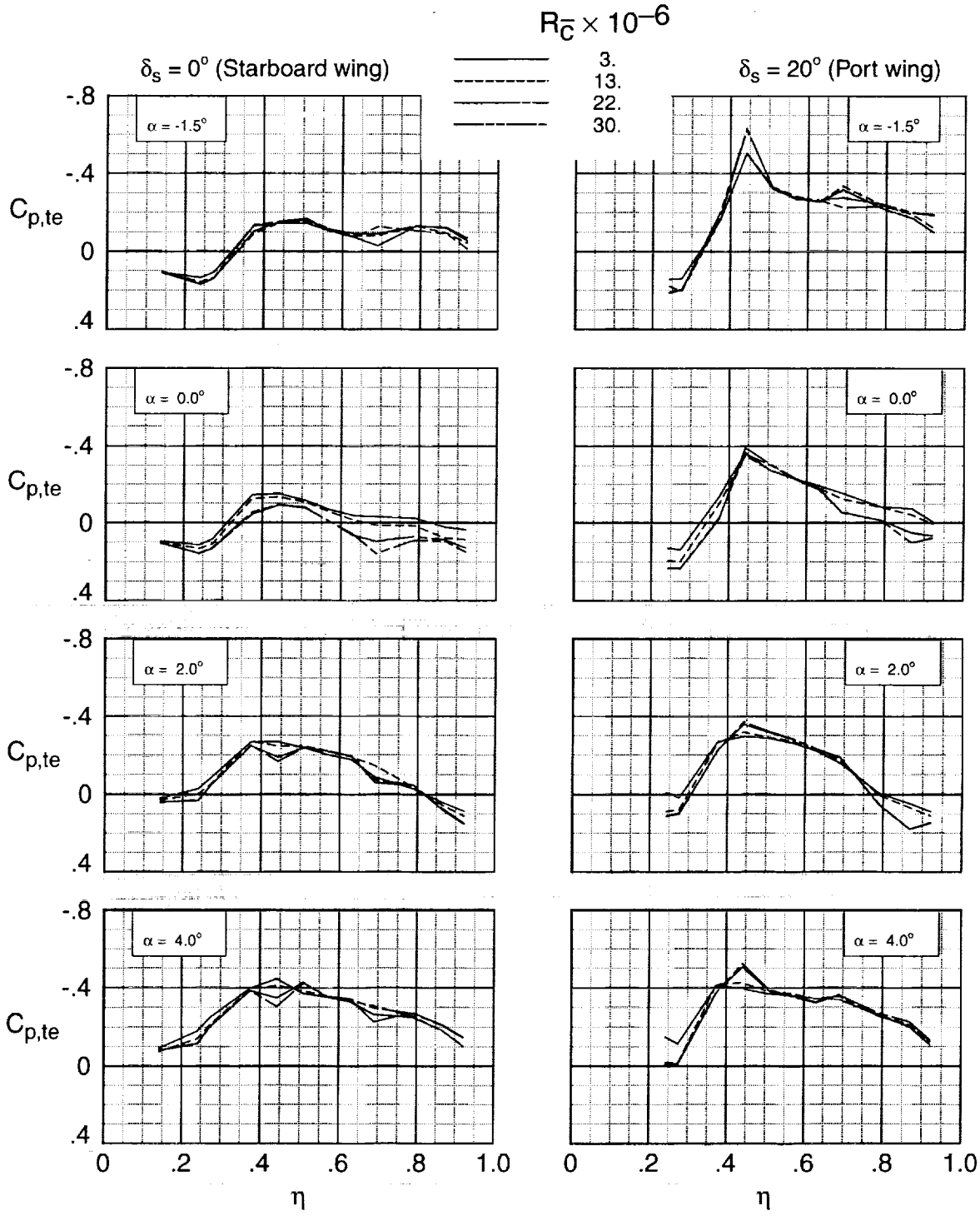

(f) $M_\infty = 0.91$.

Figure 11. Continued.

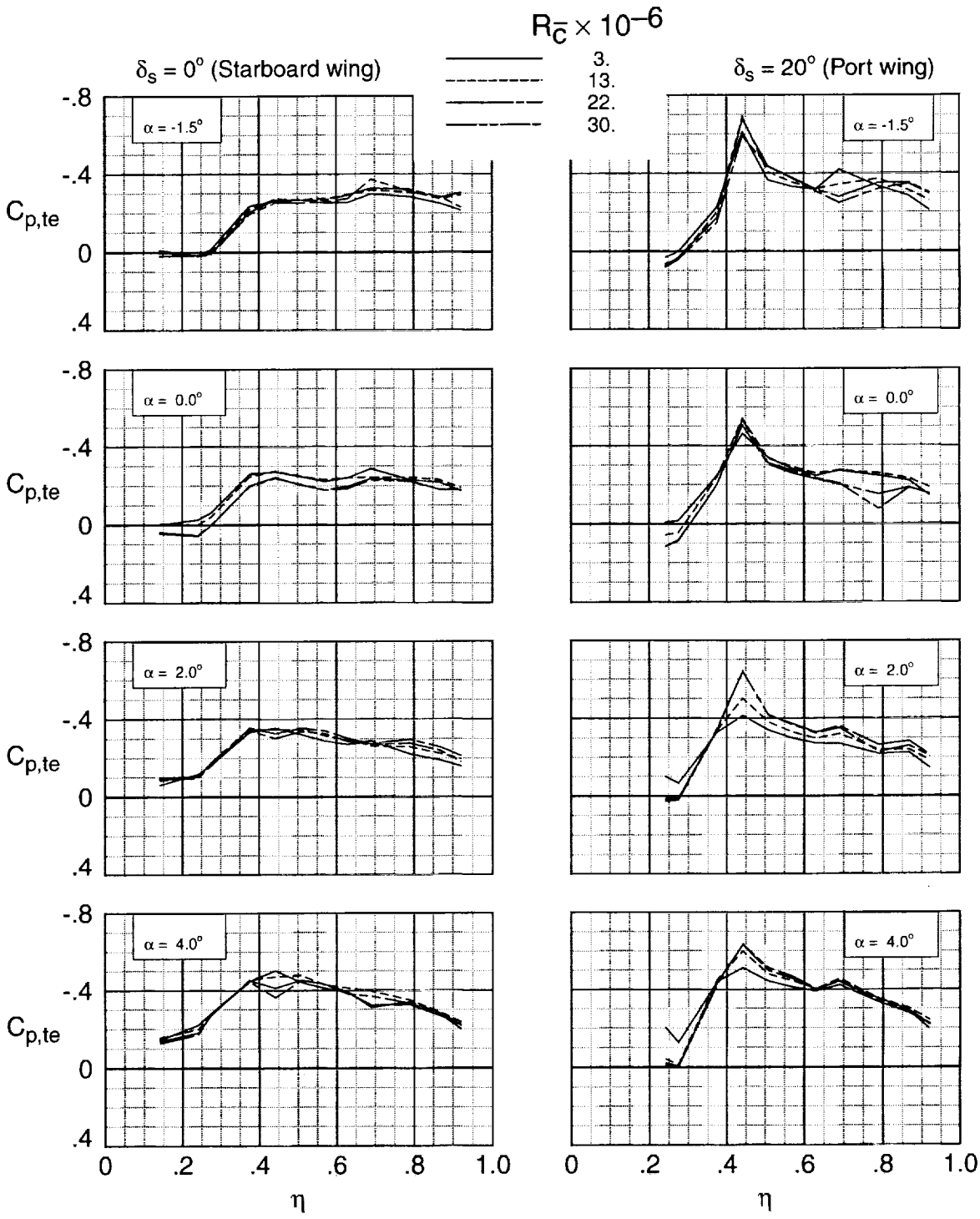

(g) $M_\infty = 0.94$.

Figure 11. Concluded.

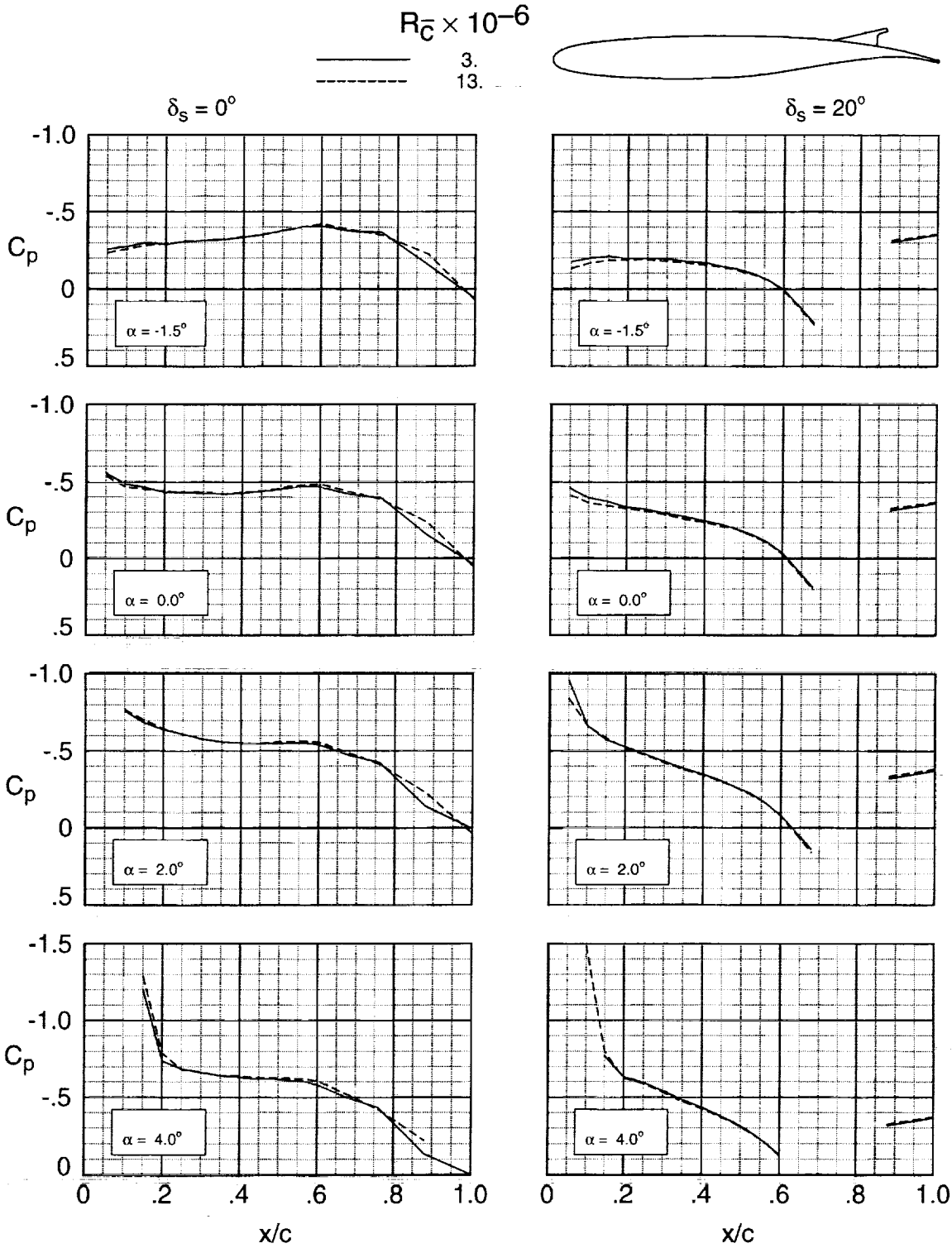

(a) $M_\infty = 0.70$.

Figure 12. Effect of Reynolds number on the chordwise pressure distribution for $\eta = 0.509$.

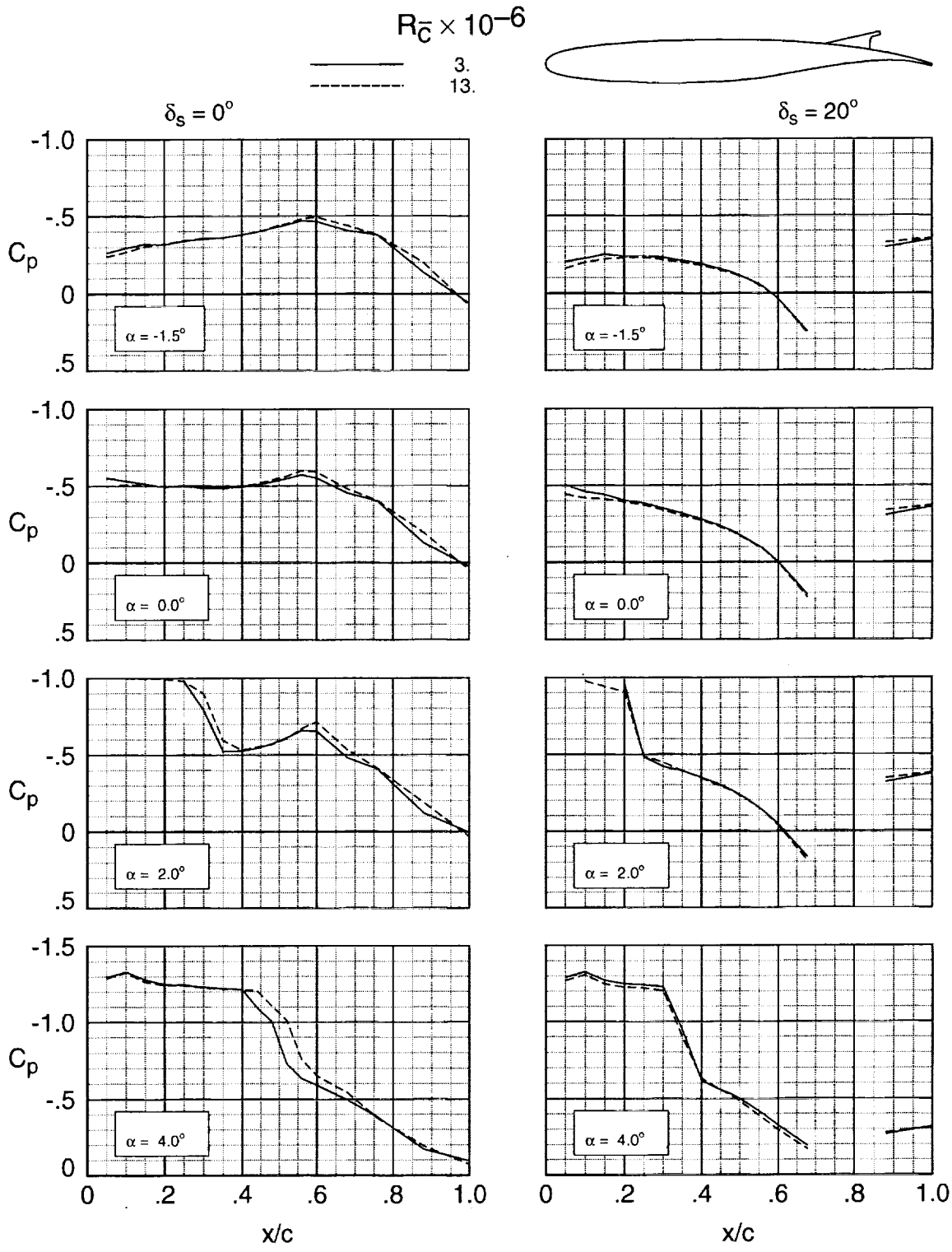

(b) $M_\infty = 0.80$.

Figure 12. Continued.

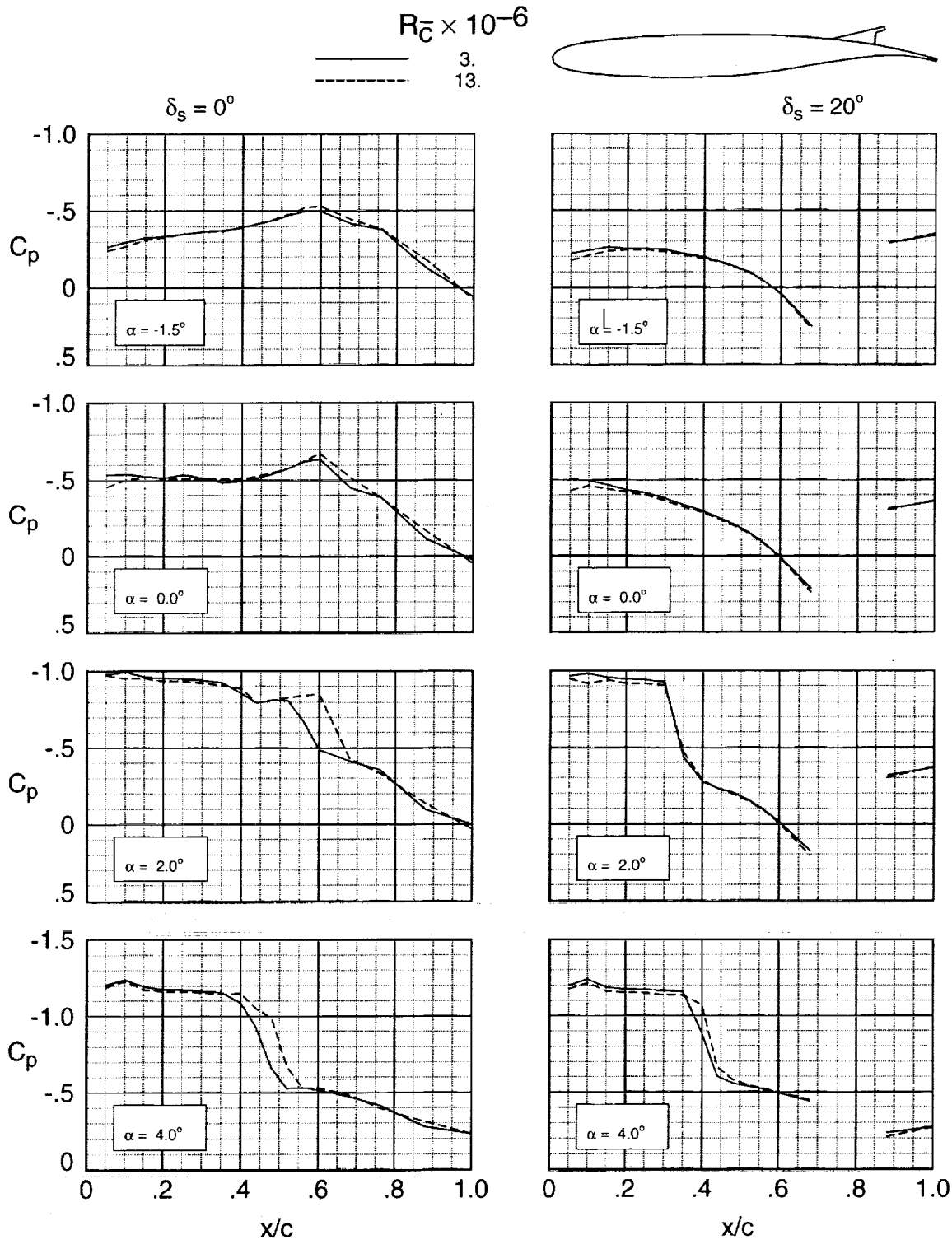

(c) $M_\infty = 0.82$.

Figure 12. Continued.

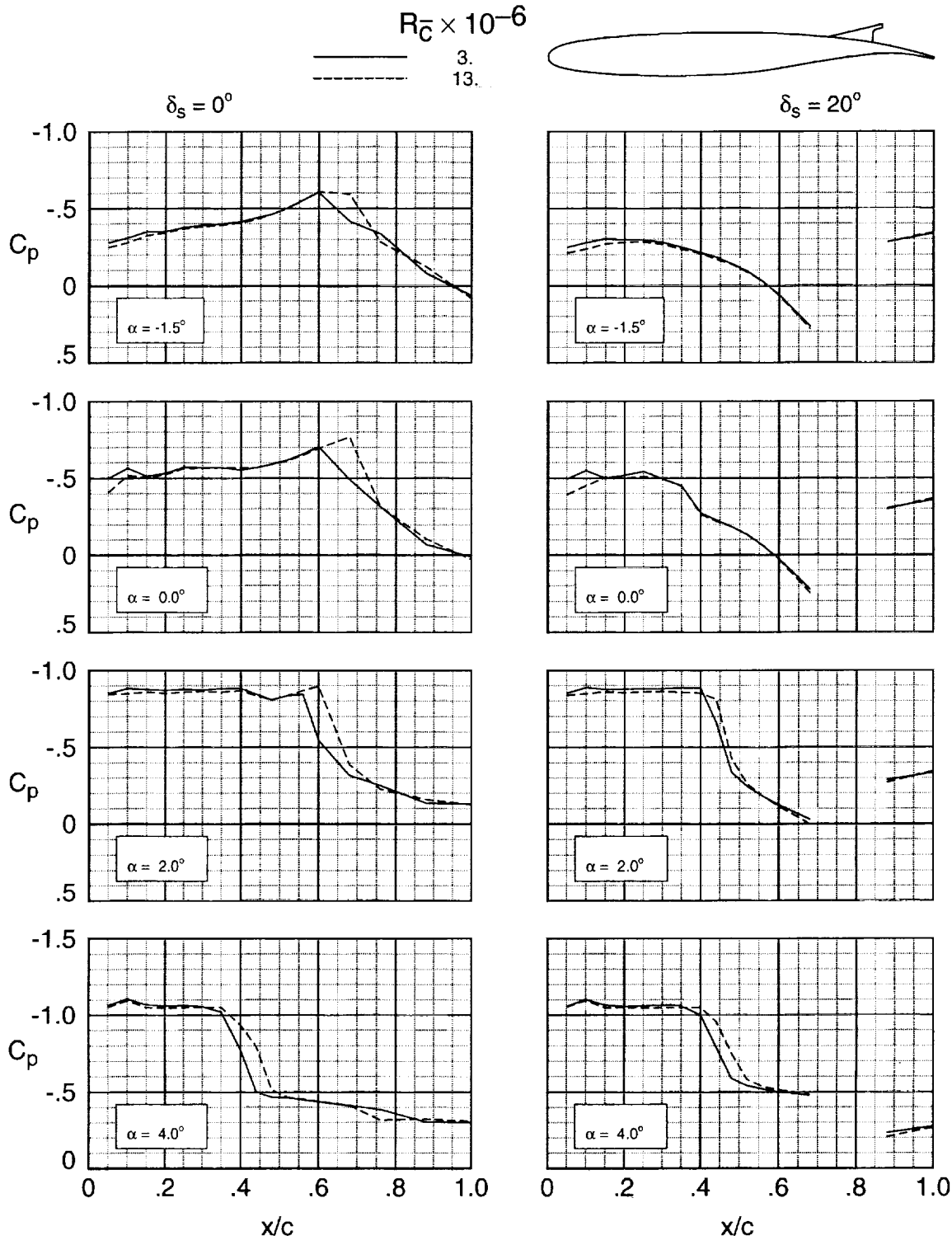

(d) $M_\infty = 0.85$.

Figure 12. Continued.

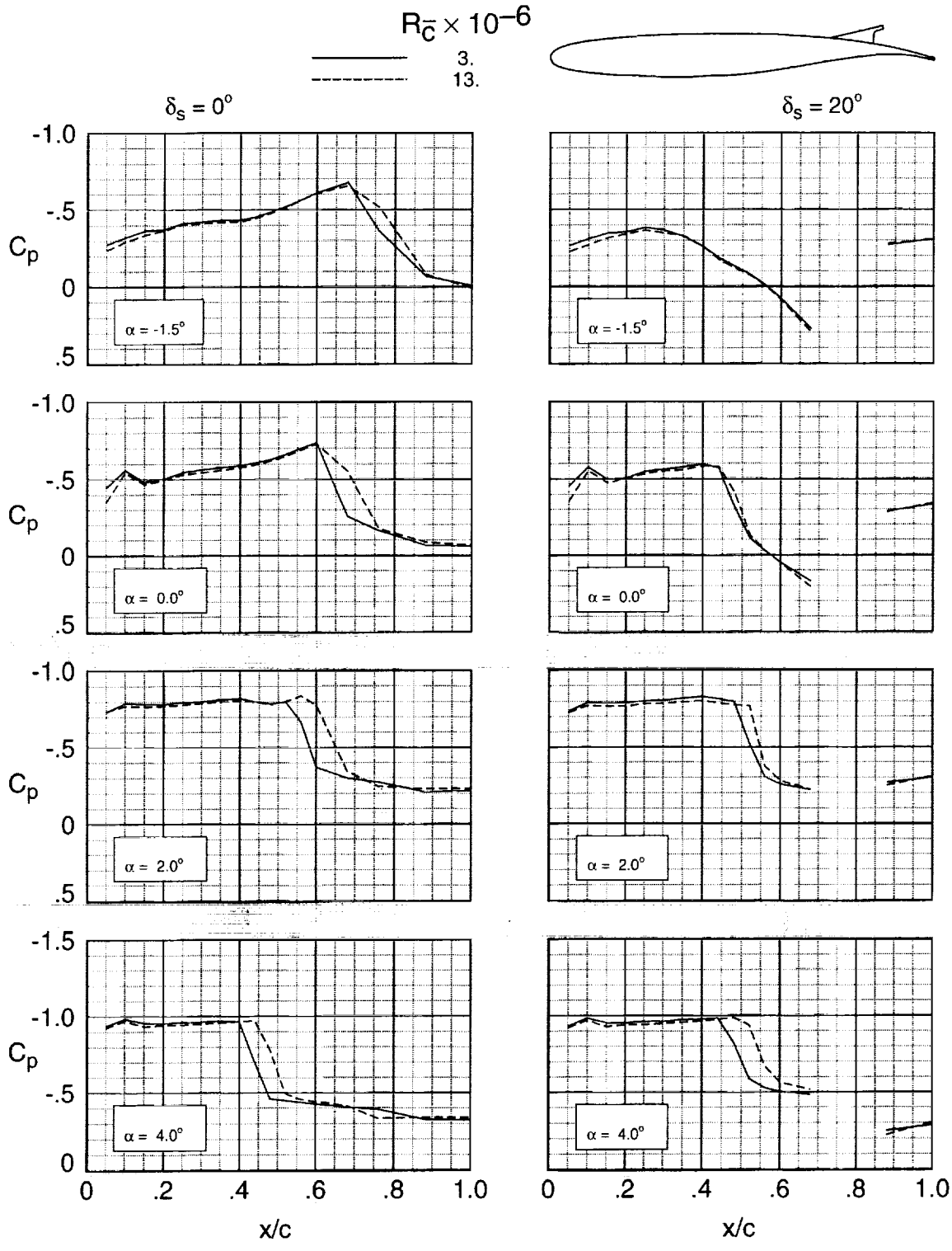

(e) $M_\infty = 0.88$.

Figure 12. Continued.

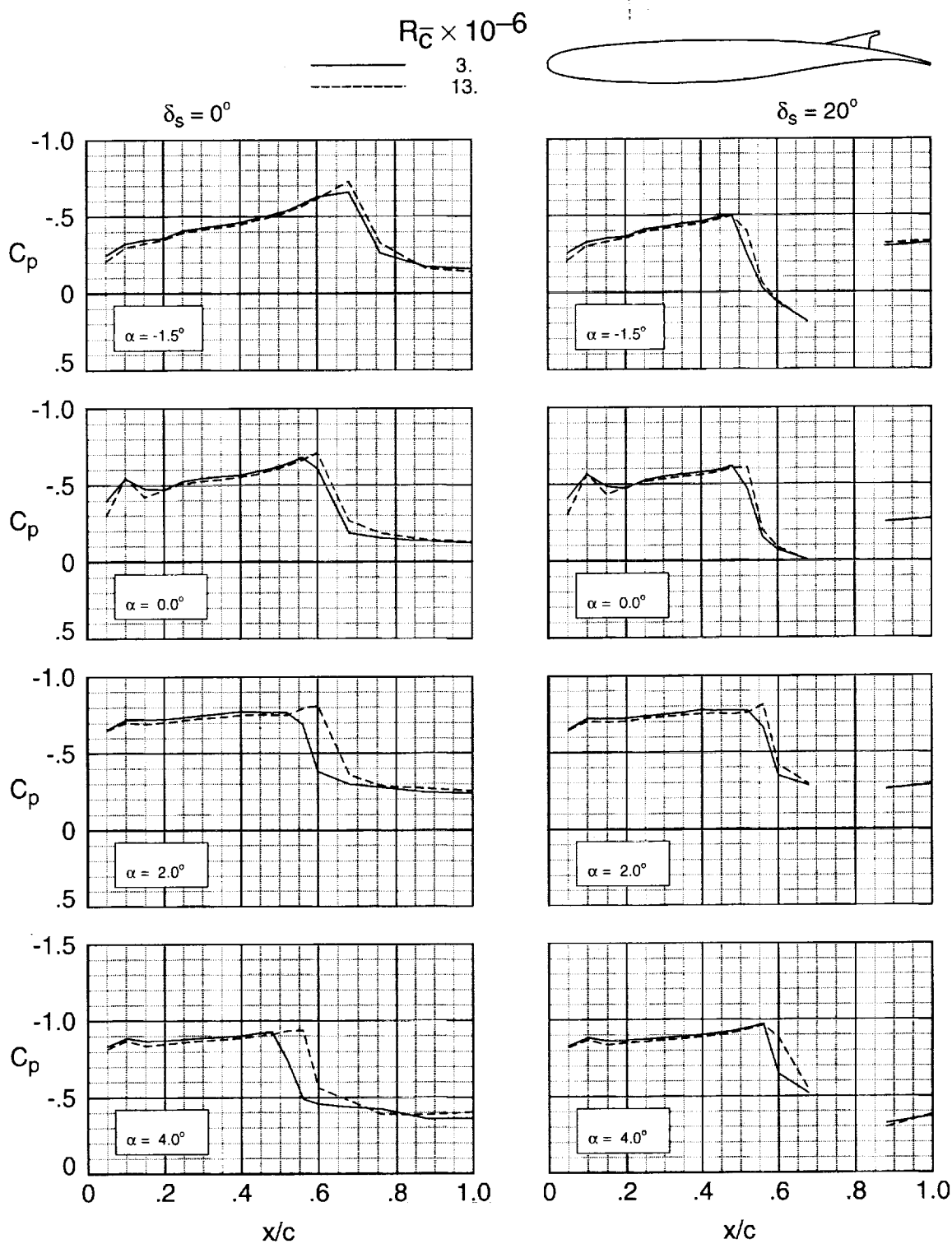

(f) $M_\infty = 0.91$.

Figure 12. Continued.

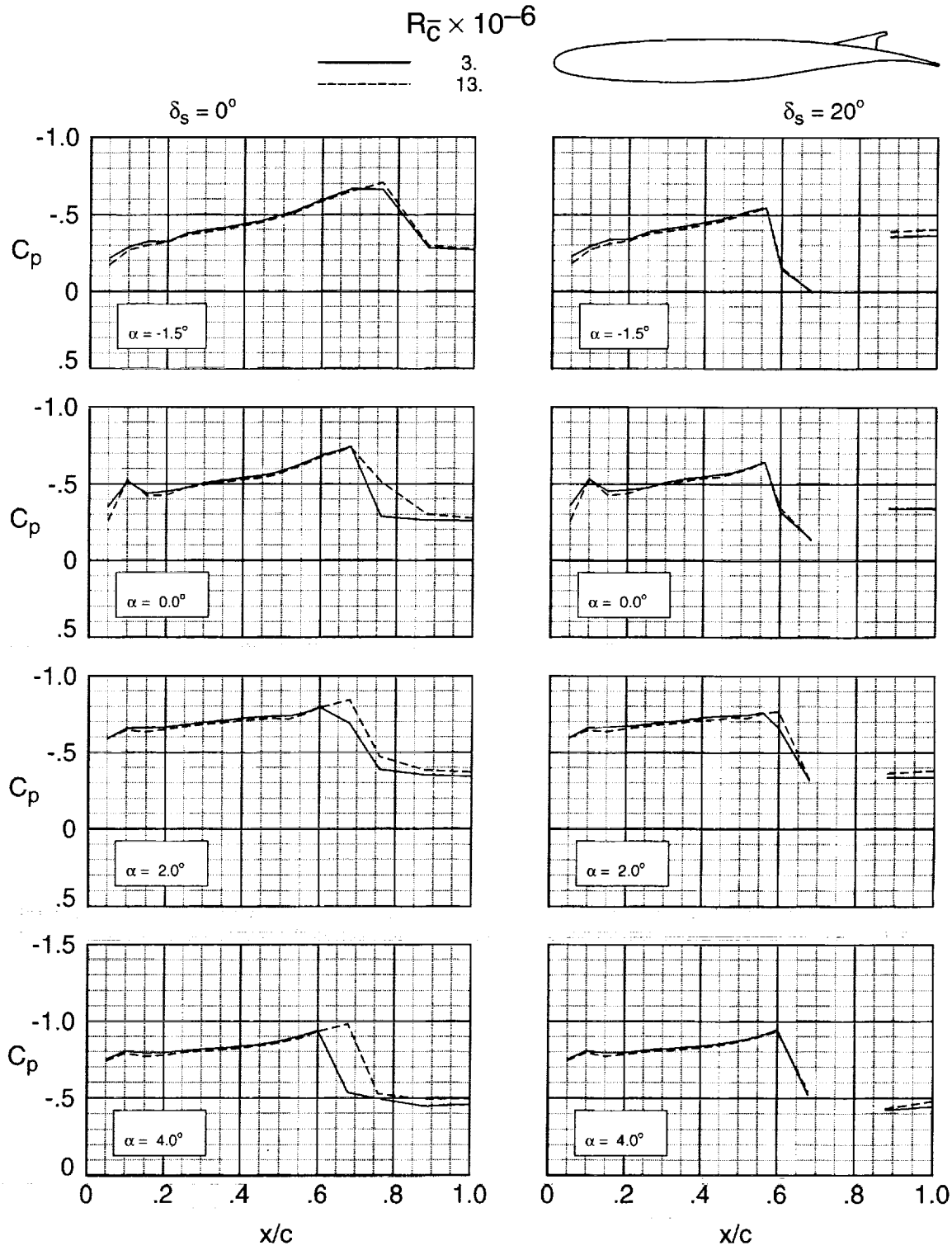

(g) $M_\infty = 0.94$.

Figure 12. Concluded.

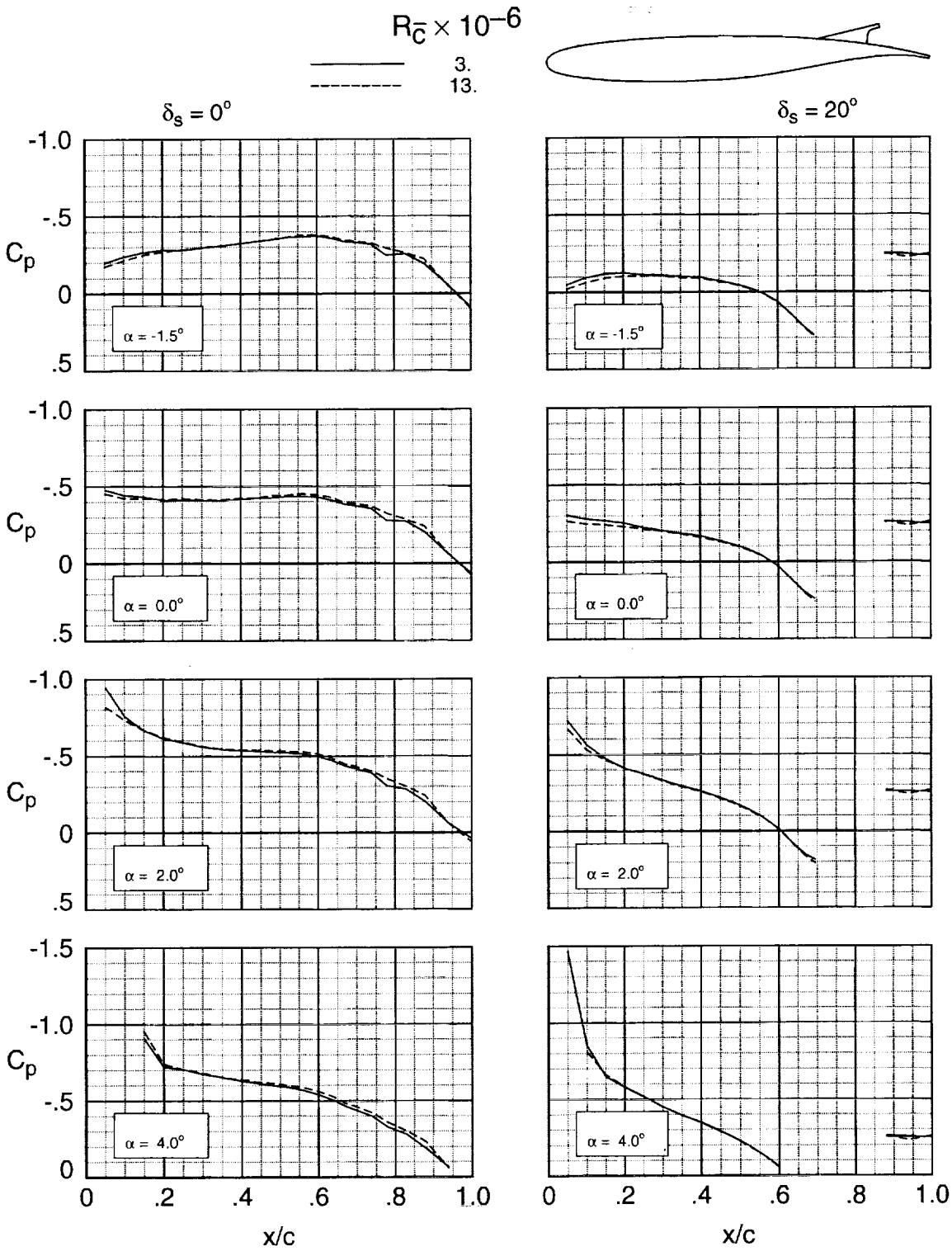

(a) $M_\infty = 0.70$.

Figure 13. Effect of Reynolds number on the chordwise pressure distribution for $\eta = 0.630$.

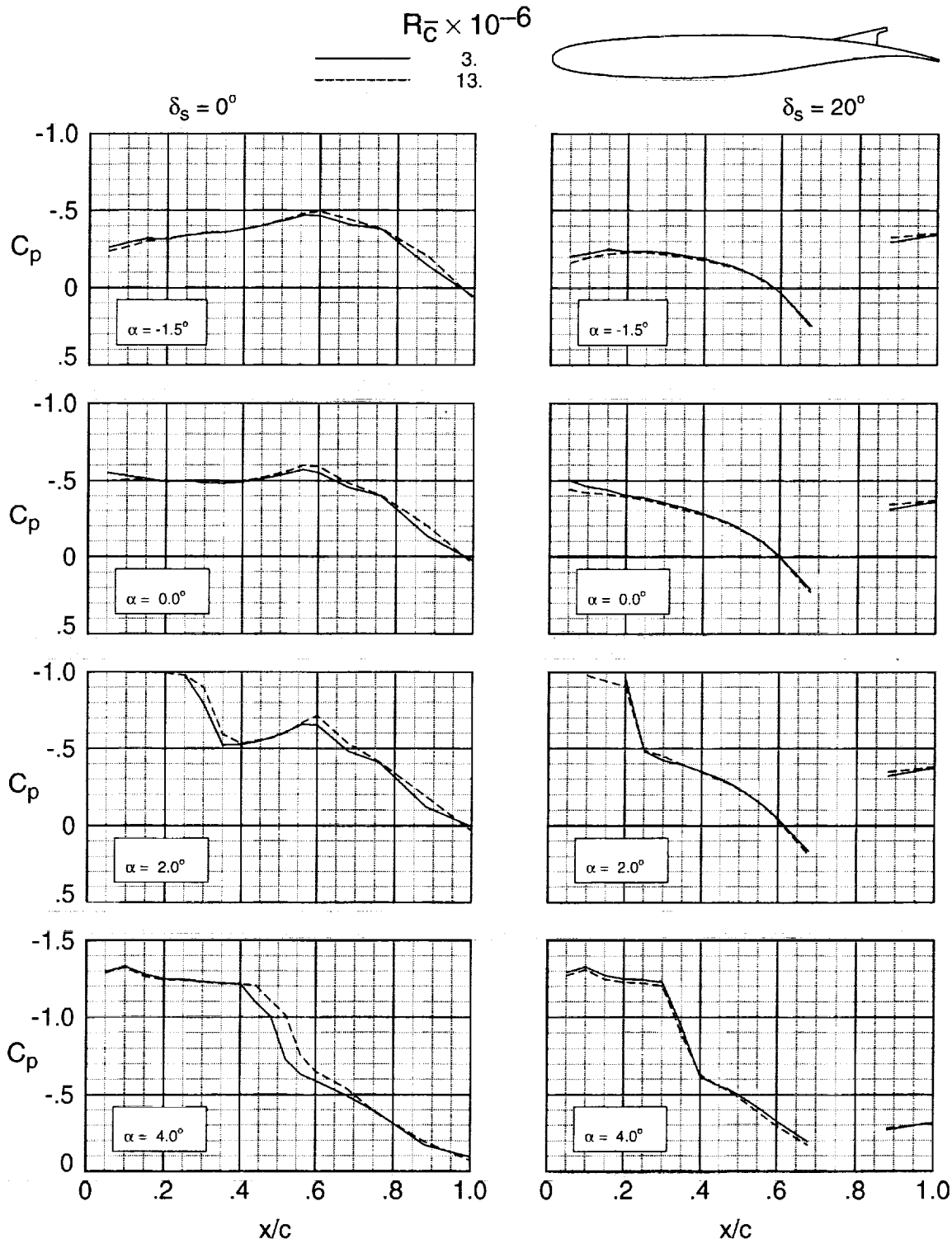

(b) $M_\infty = 0.80$.

Figure 13. Continued.

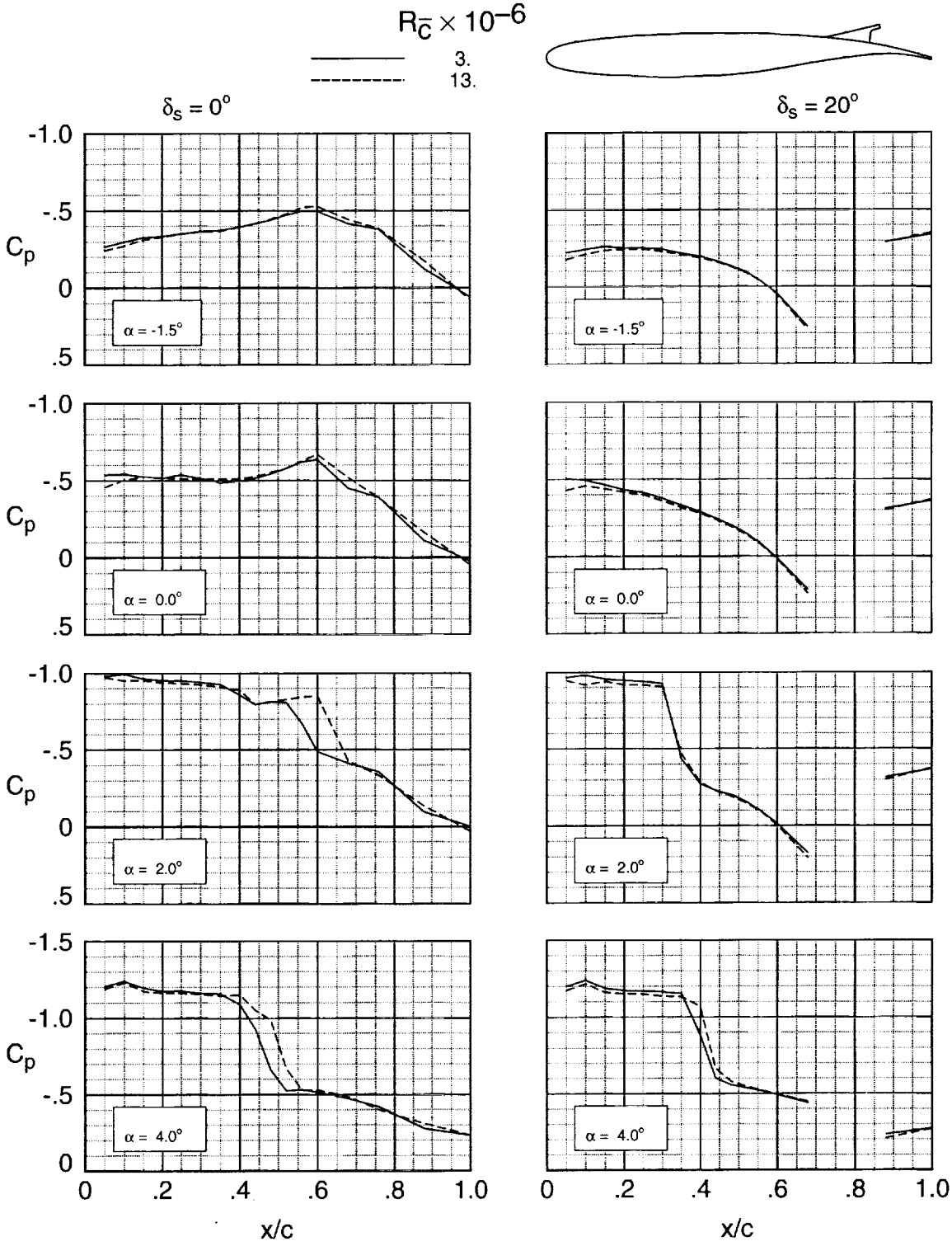

(c) $M_\infty = 0.82$.

Figure 13. Continued.

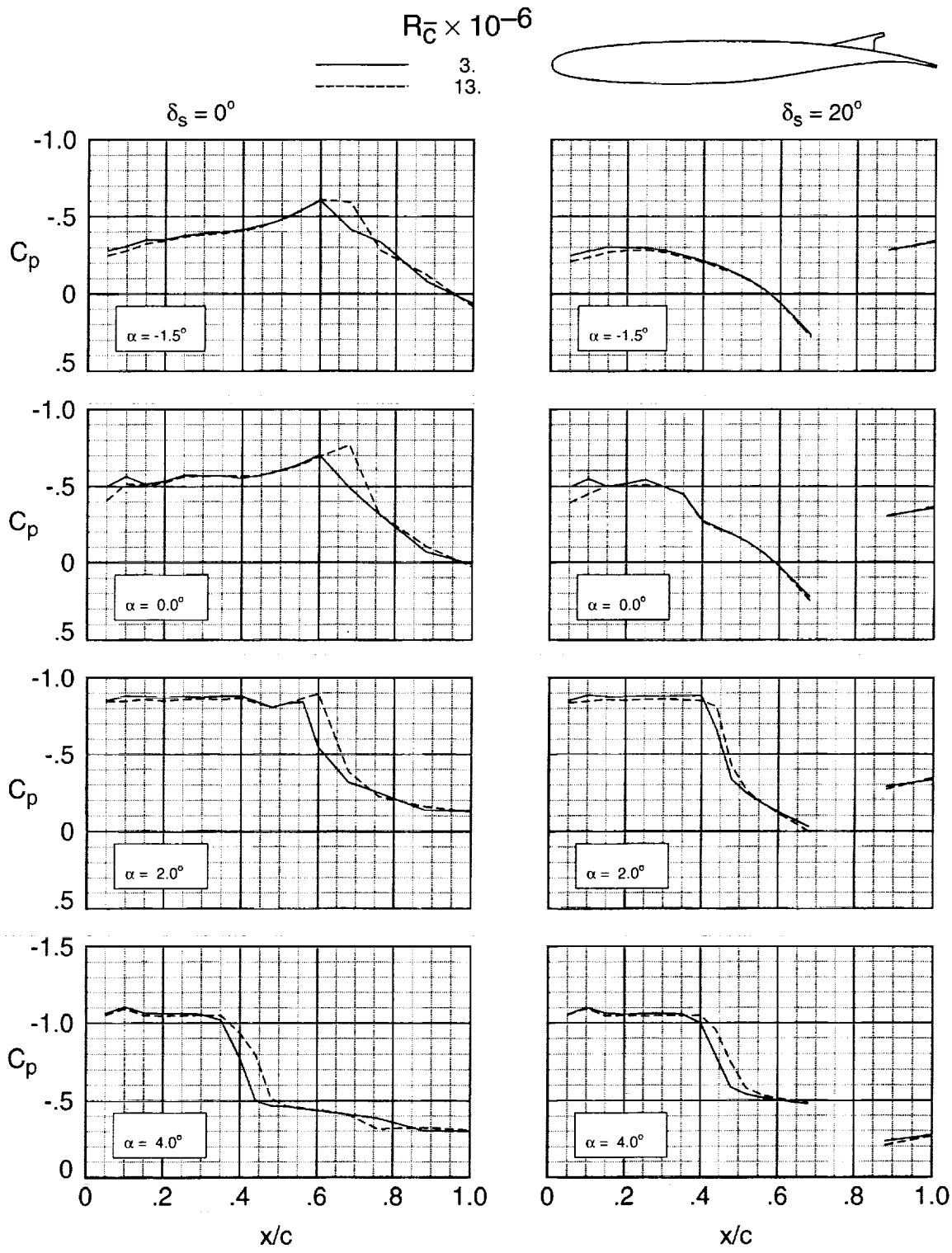

(d) $M_\infty = 0.85$.

Figure 13. Continued.

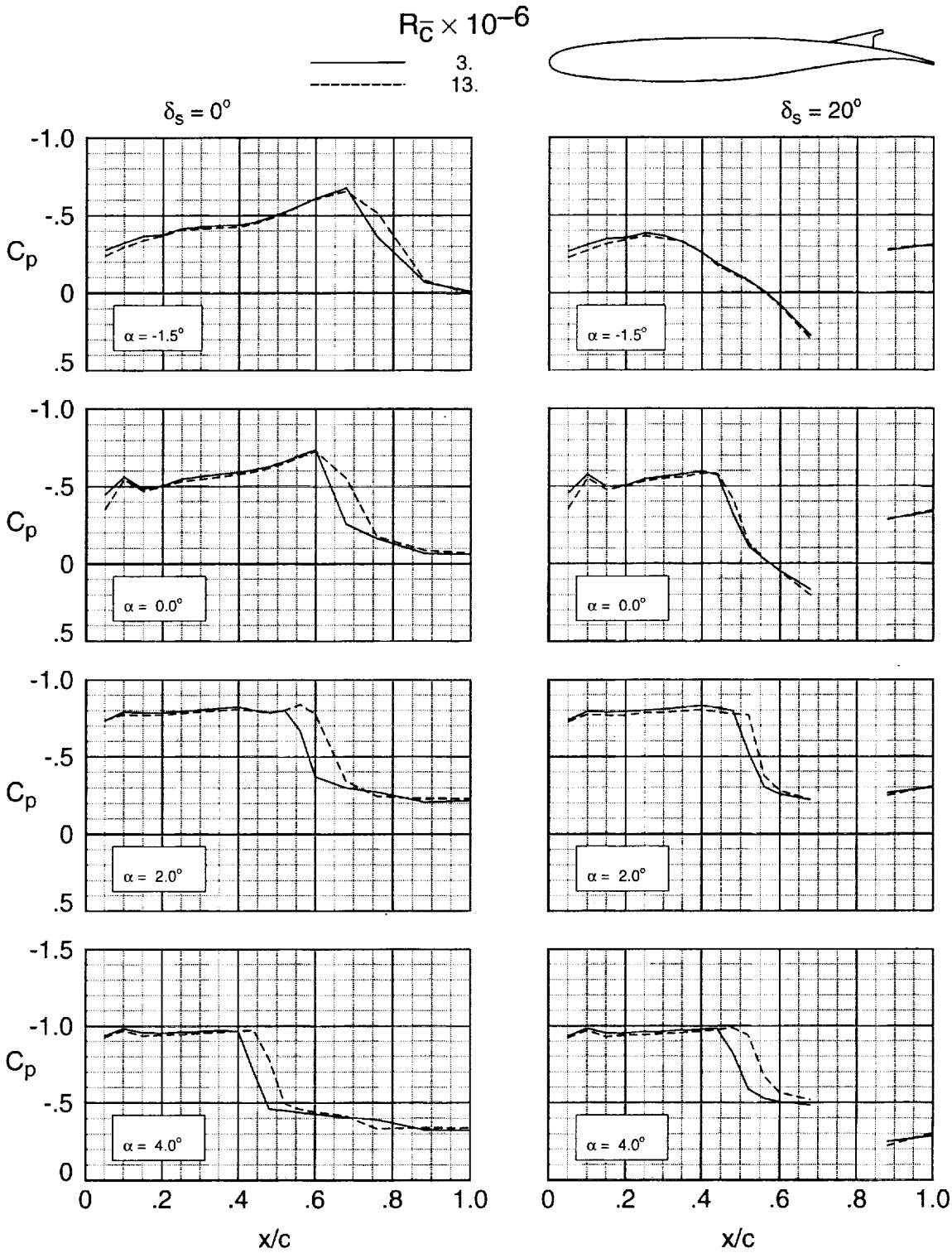

(e) $M_\infty = 0.88$.

Figure 13. Continued.

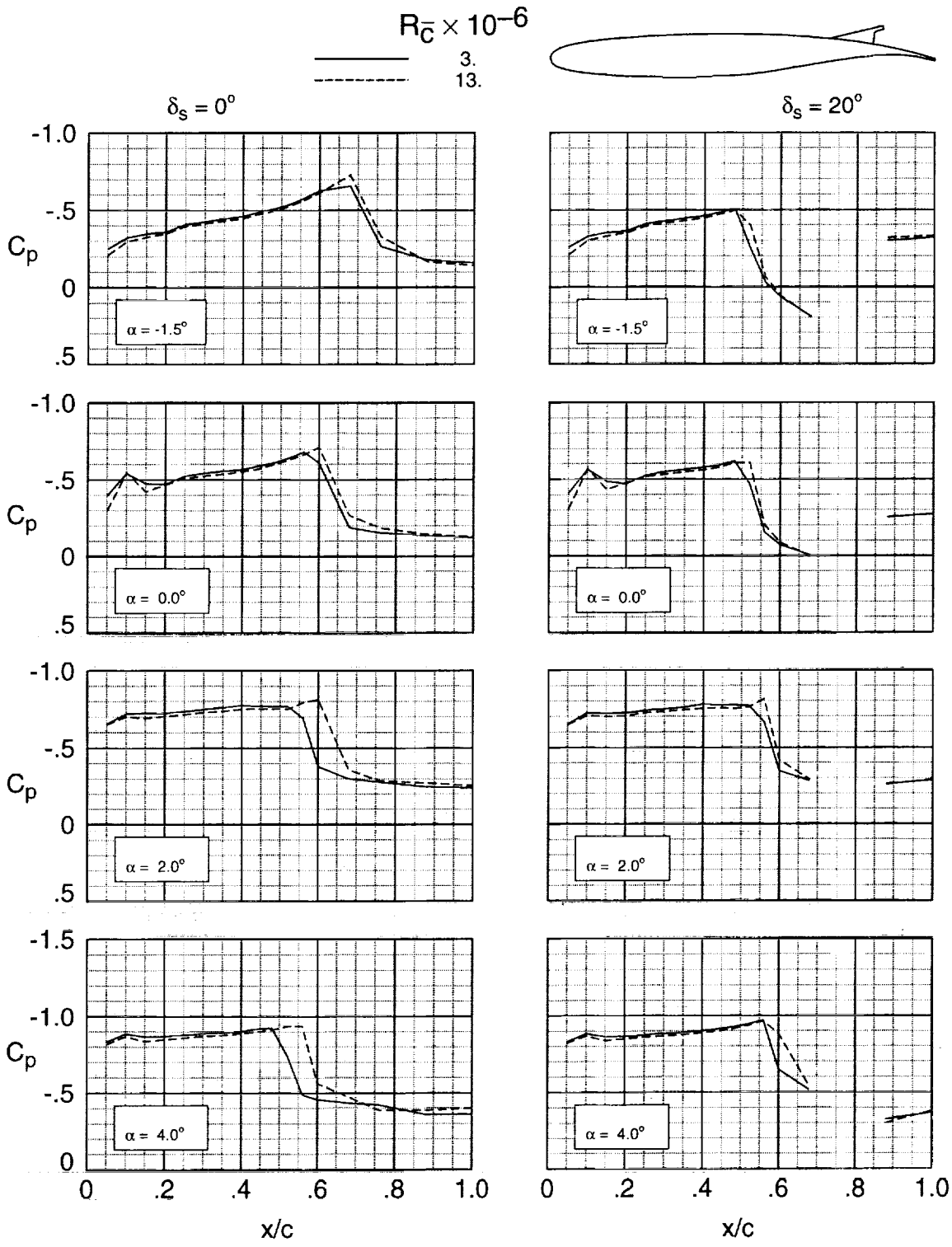

(f) $M_\infty = 0.91$.

Figure 13. Continued.

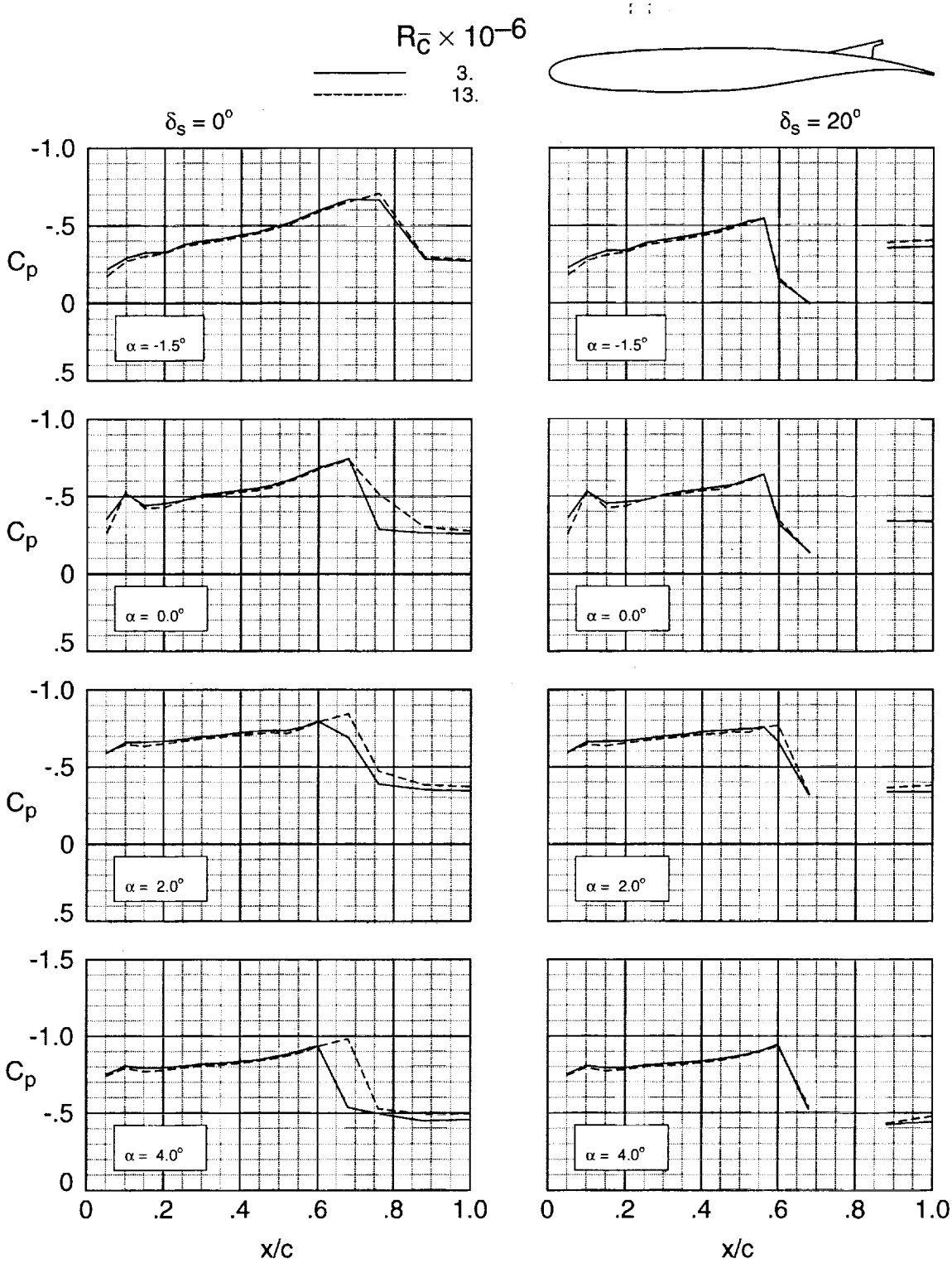

(g) $M_\infty = 0.94$.

Figure 13. Concluded.

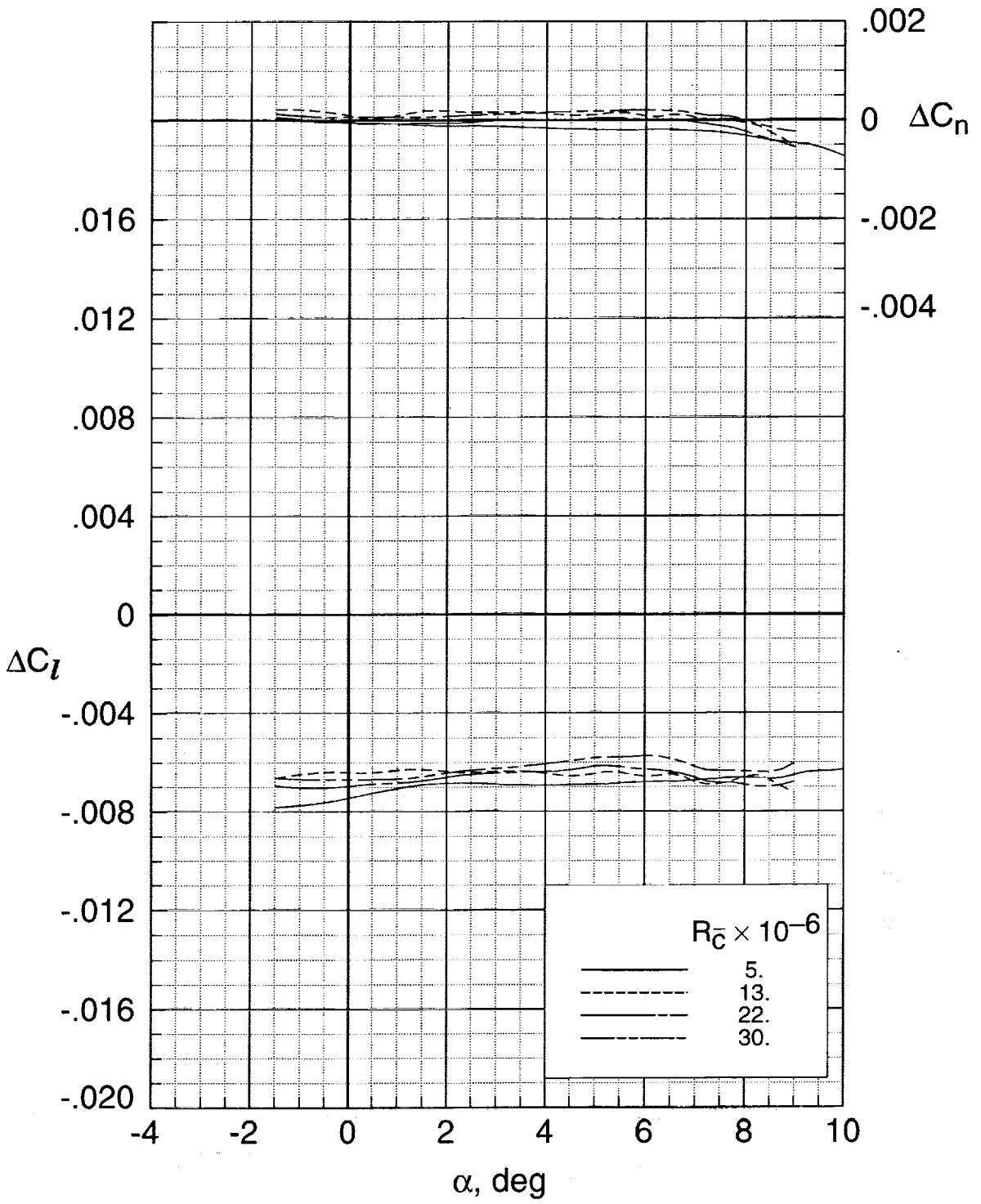

(a) $M_\infty = 0.50$.

Figure 14. Effect of Reynolds number on the aerodynamic characteristics with the outboard ailerons for $\delta_a = -10°$.

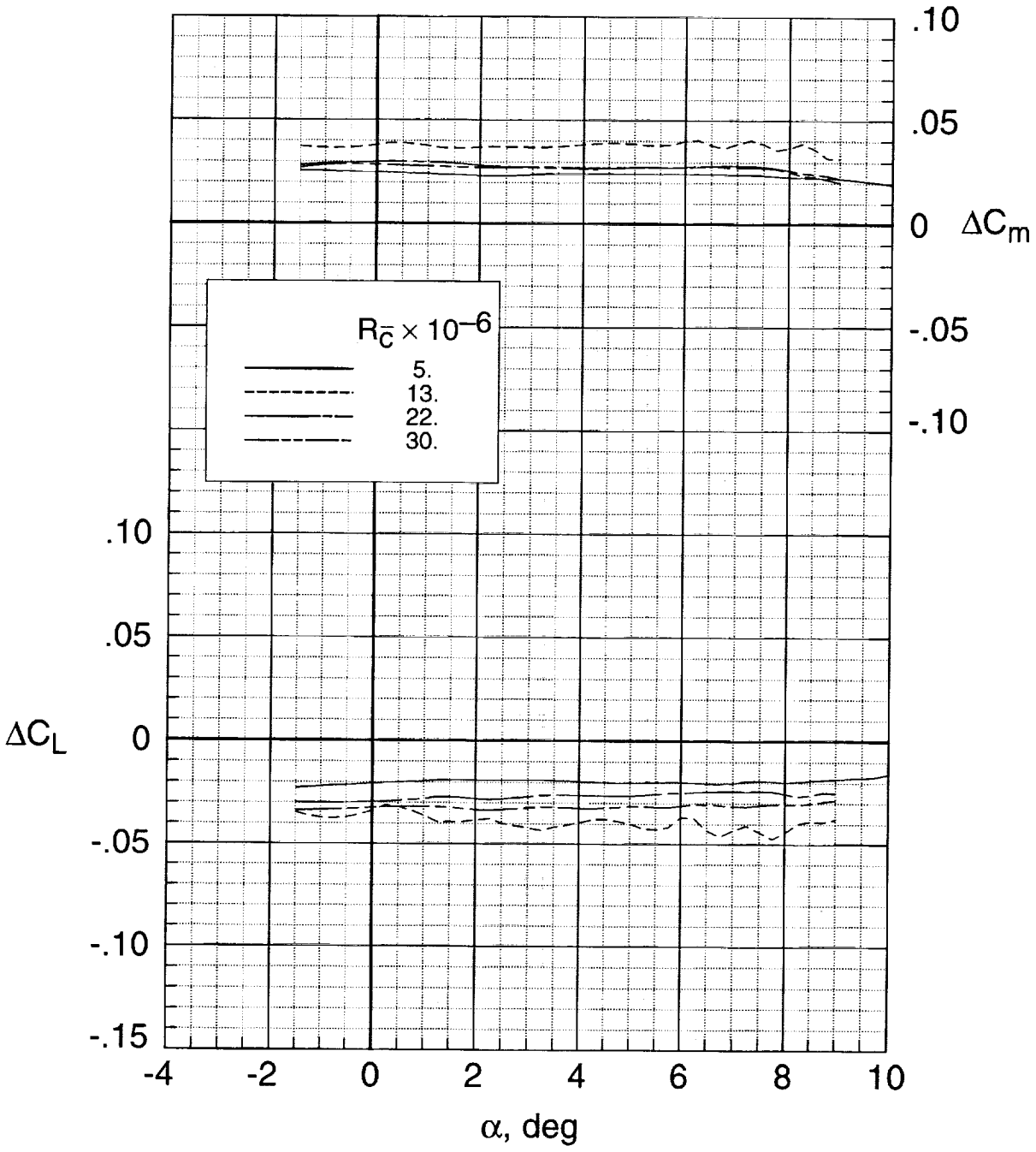

(a) Concluded.

Figure 14. Continued.

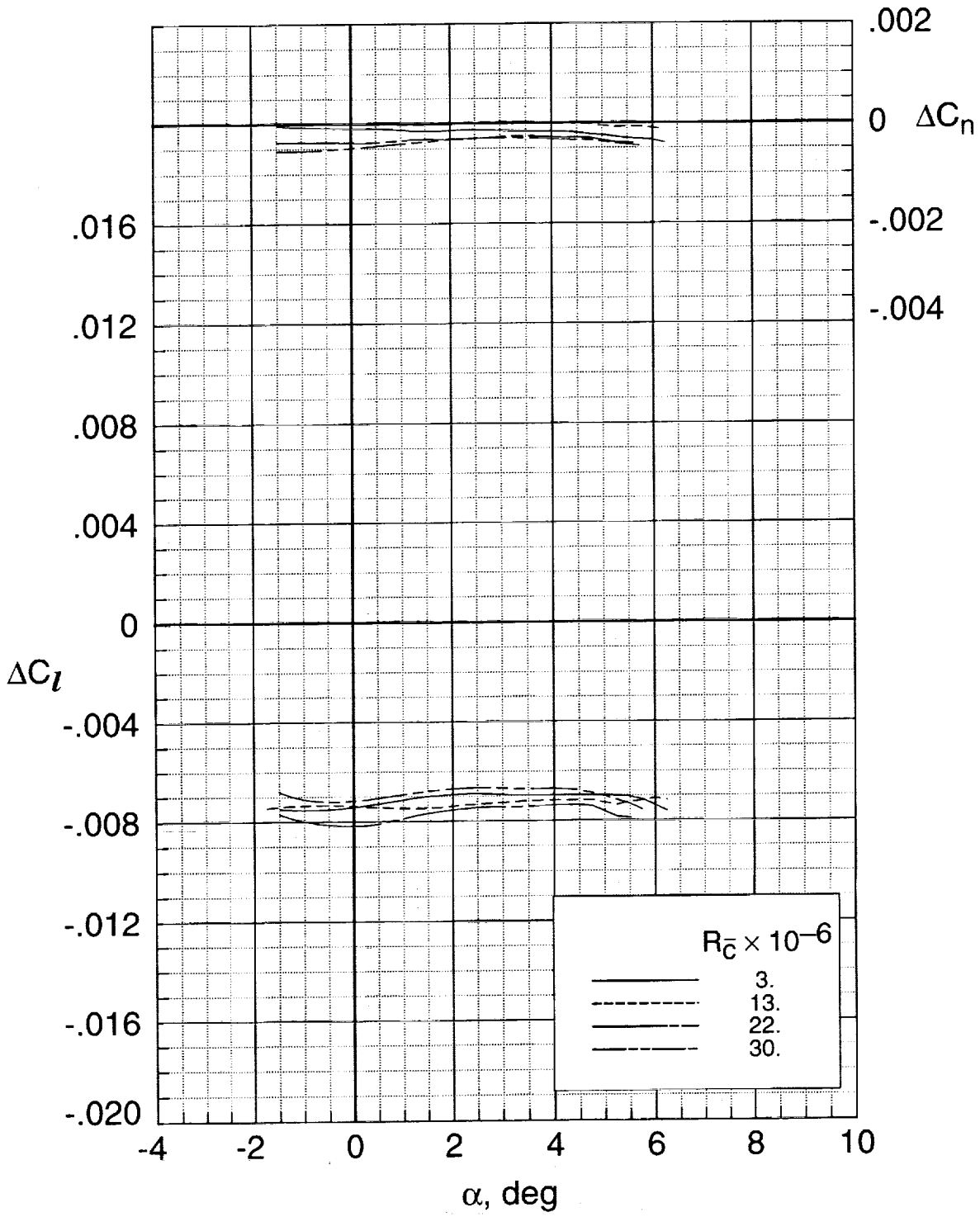

(b) $M_\infty = 0.70$.

Figure 14. Continued.

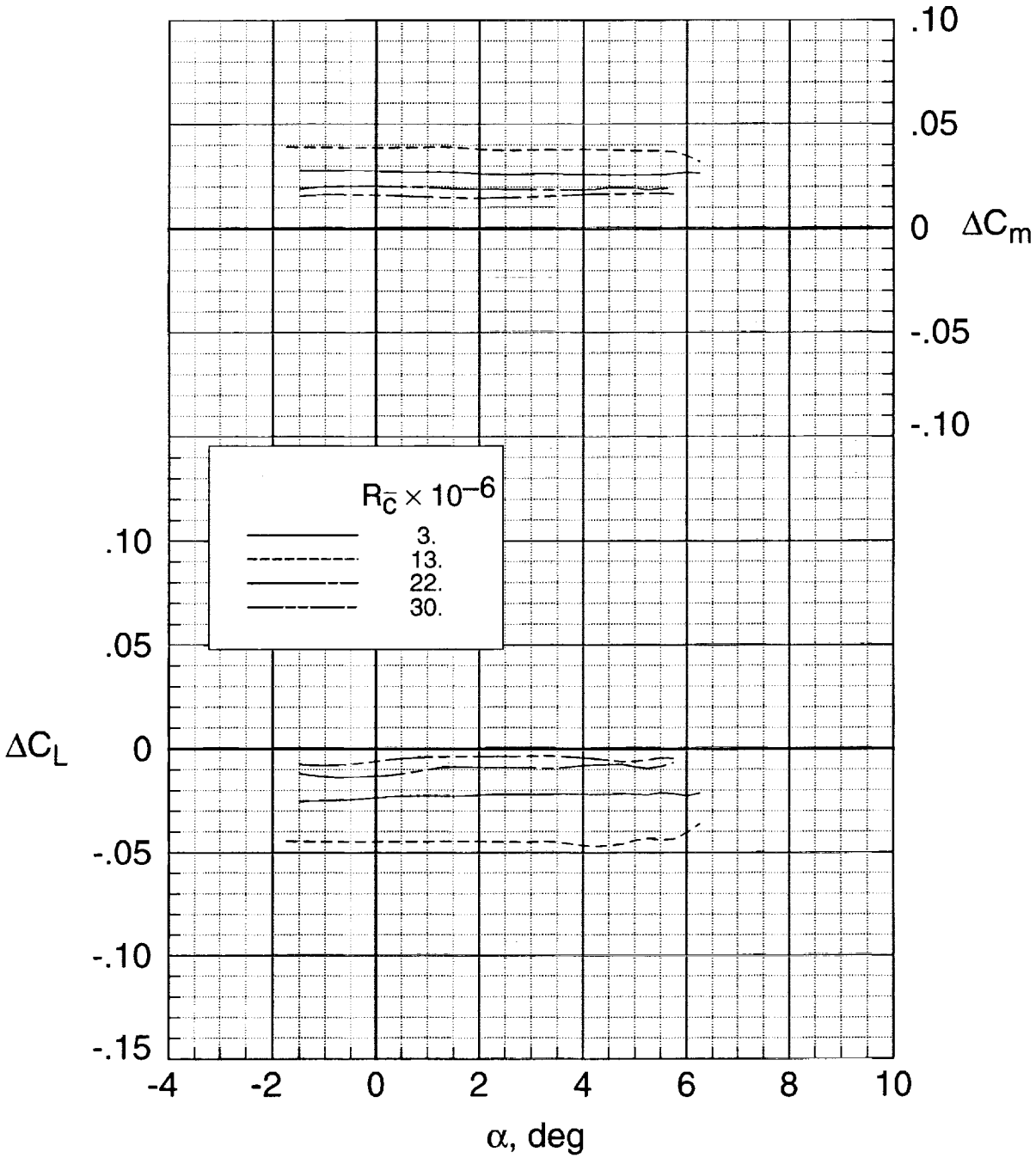

(b) Concluded.

Figure 14. Continued.

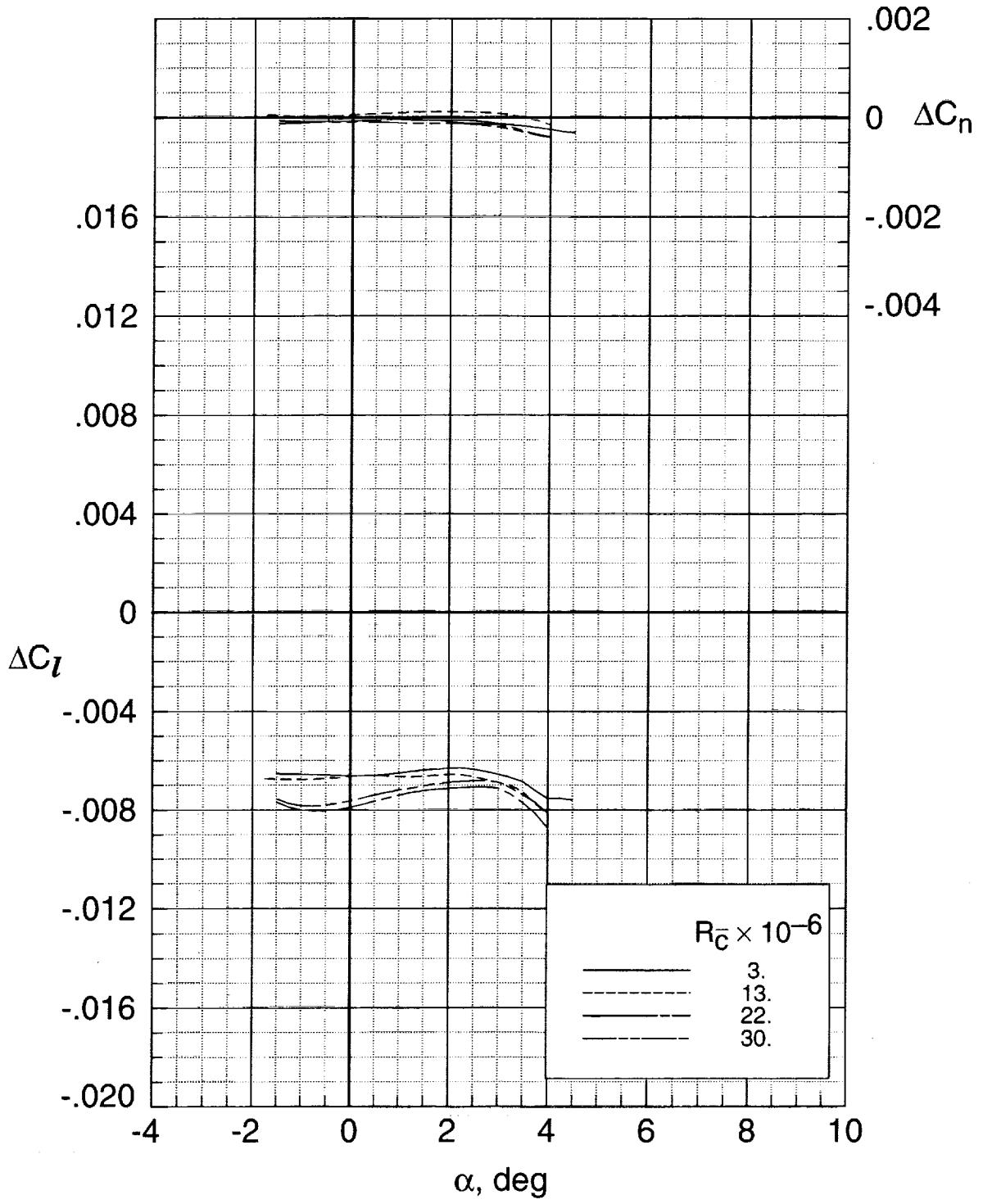

(c) $M_\infty = 0.80$.

Figure 14. Continued.

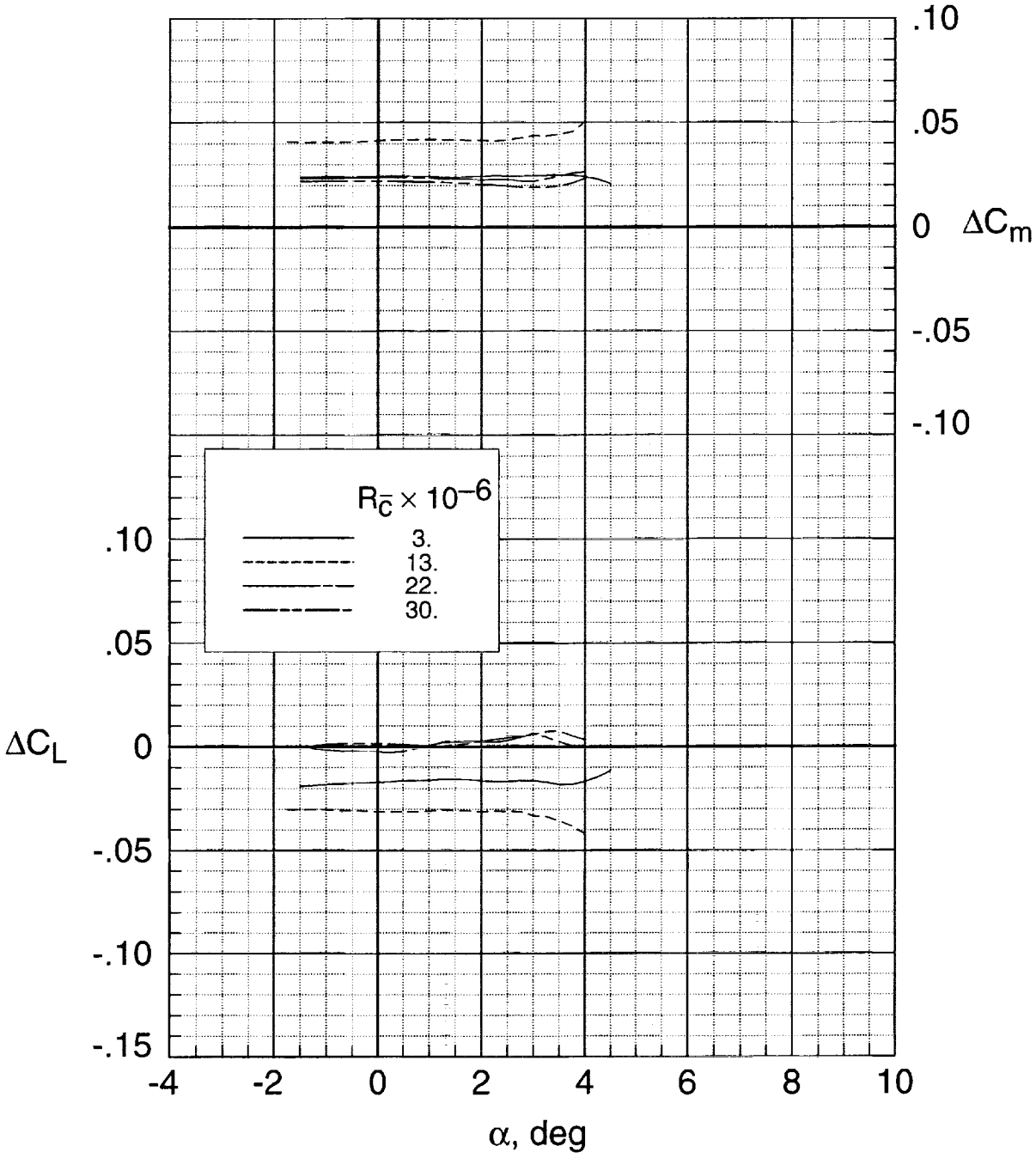

(c) Concluded.

Figure 14. Continued.

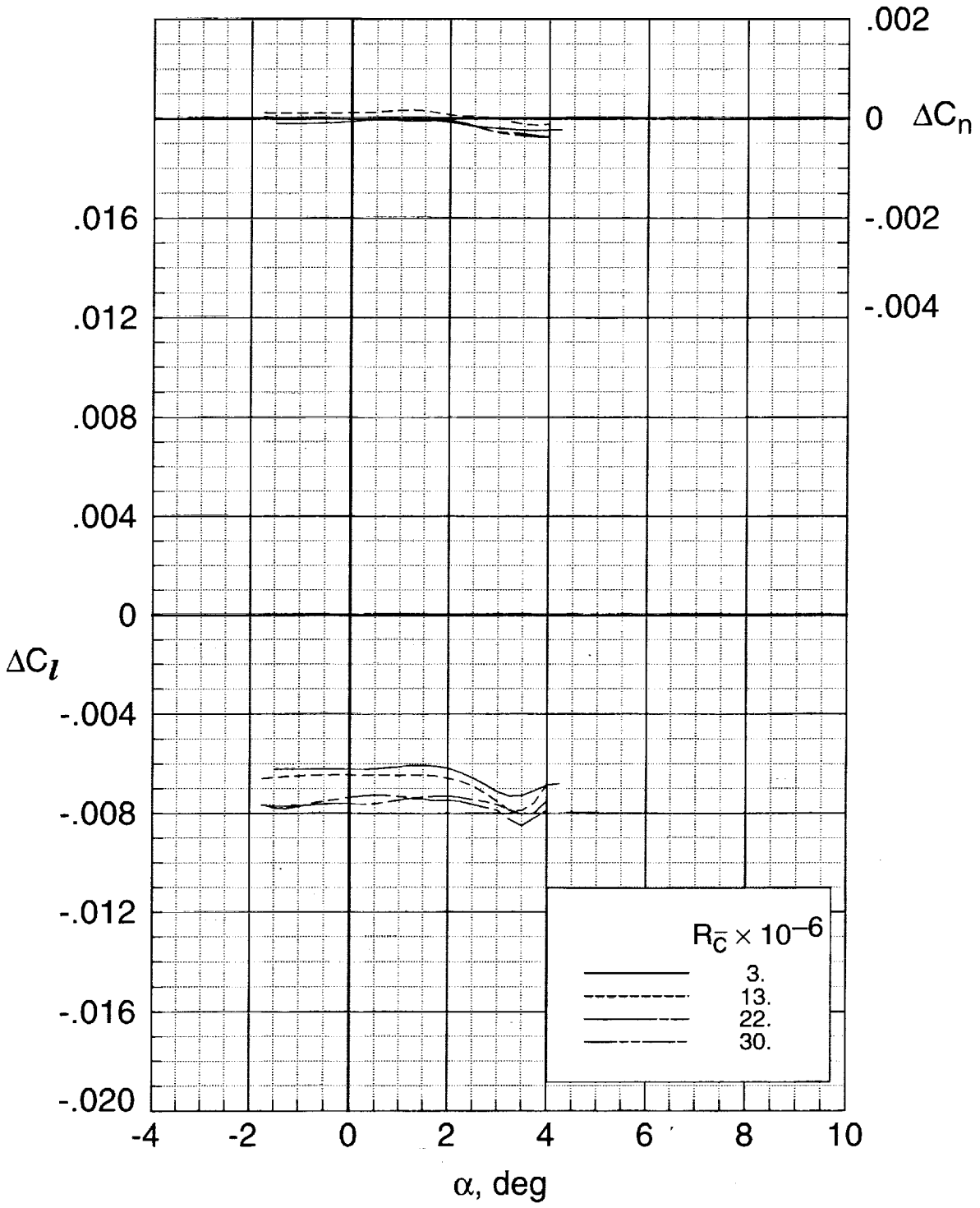

(d) $M_\infty = 0.82$.

Figure 14. Continued.

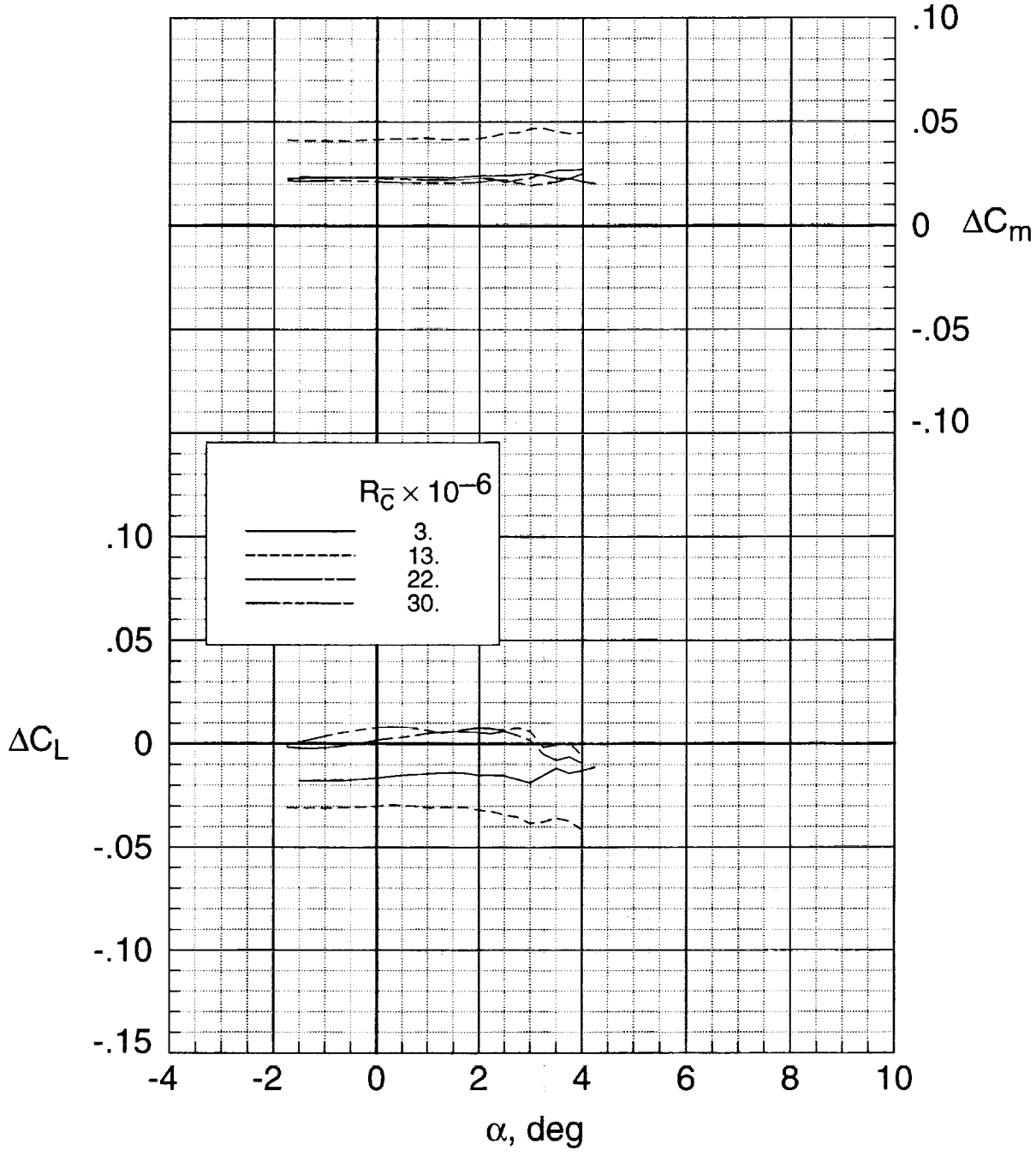

(d) Concluded.

Figure 14. Continued.

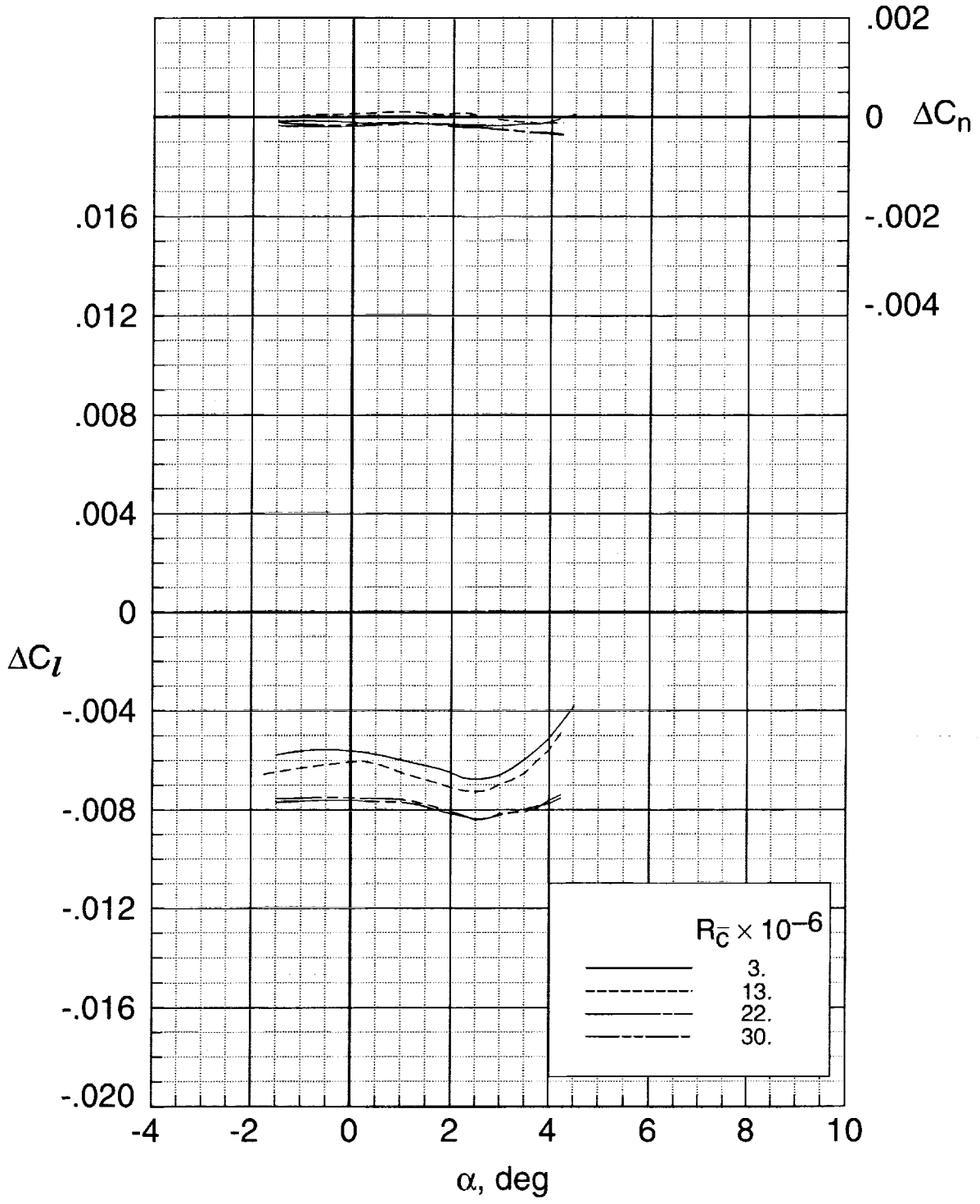

(e) $M_\infty = 0.85$.

Figure 14. Continued.

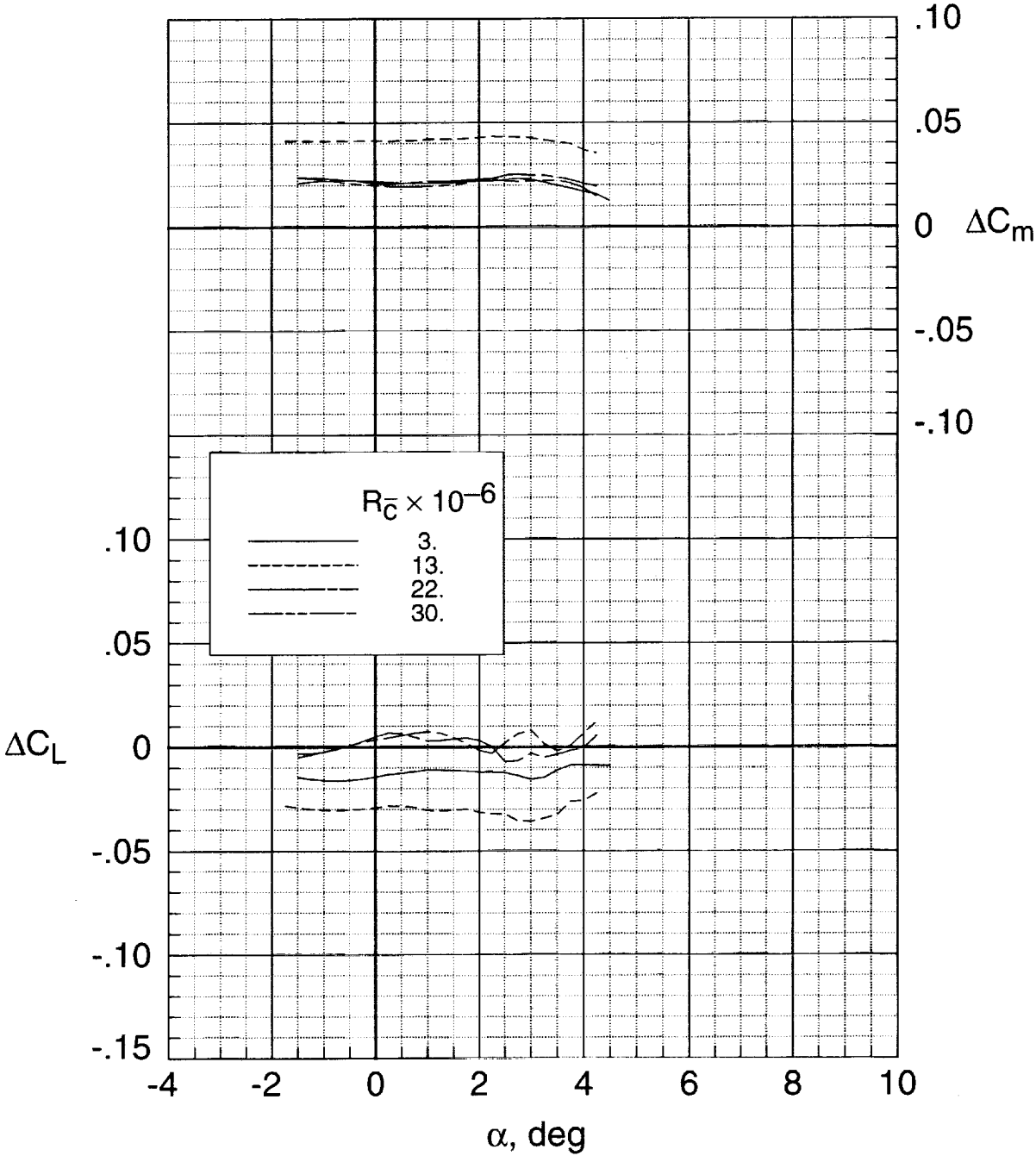

(e) Concluded.

Figure 14. Continued.

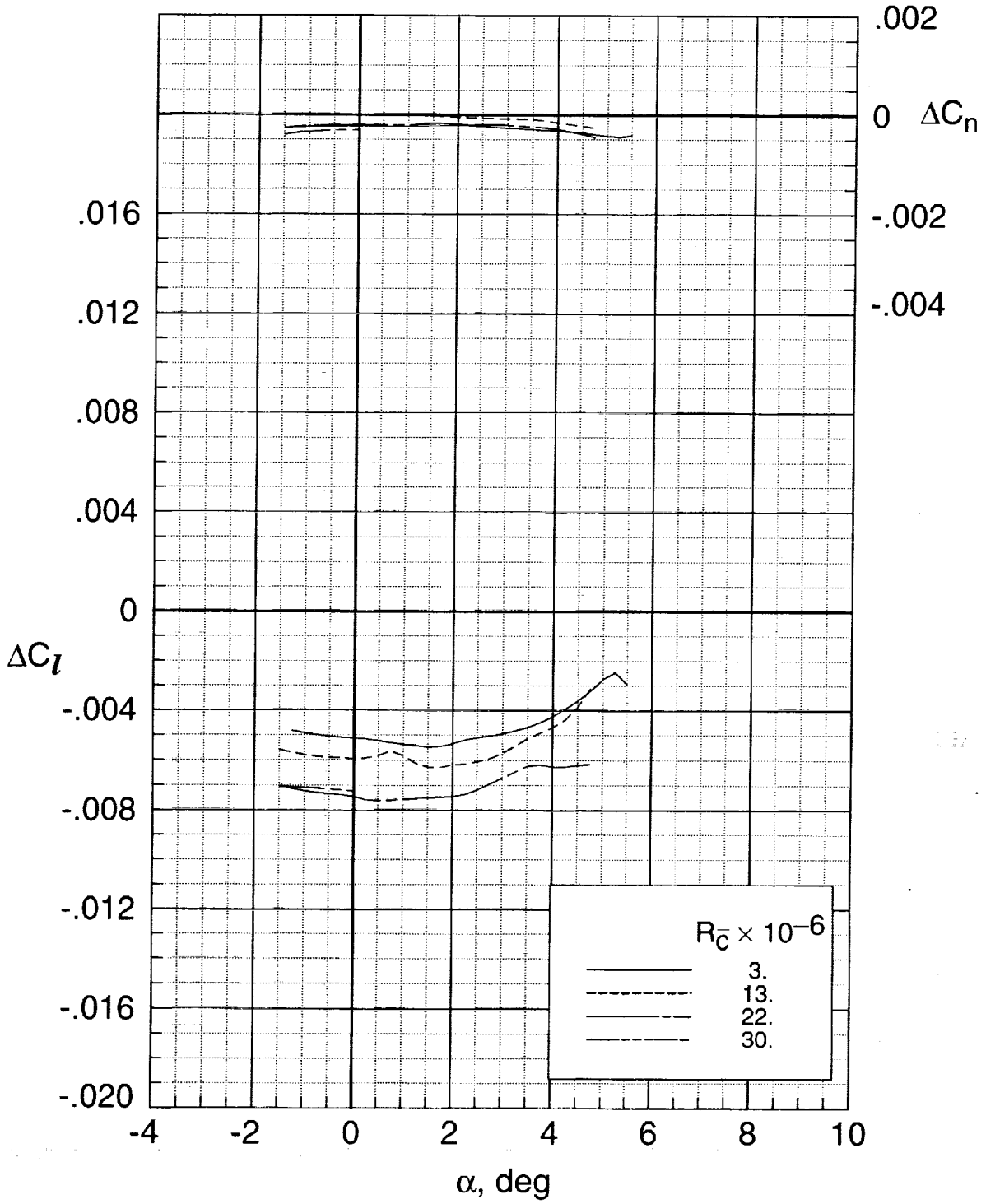

(f) $M_\infty = 0.88$.

Figure 14. Continued.

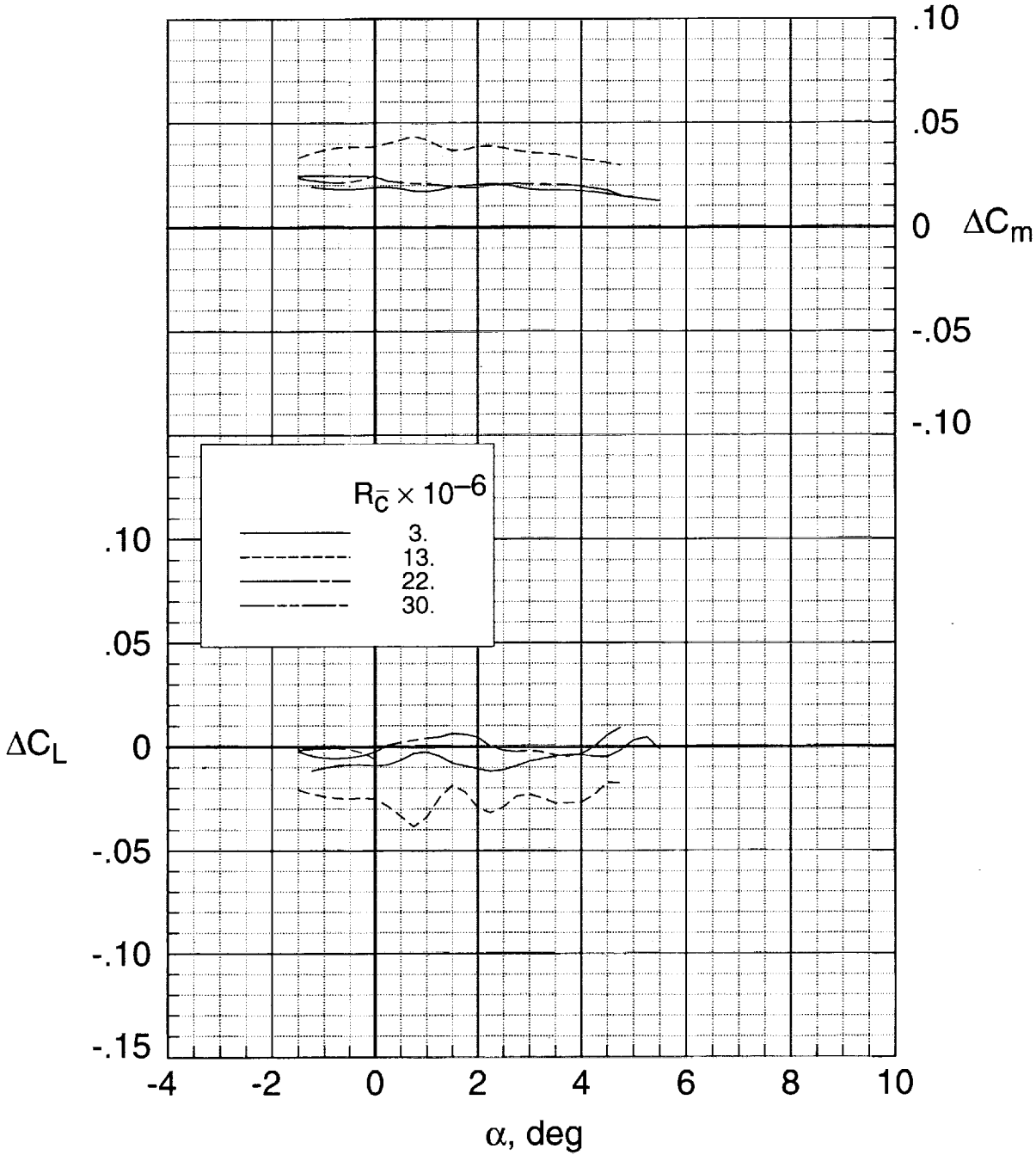

(f) Concluded.

Figure 14. Continued.

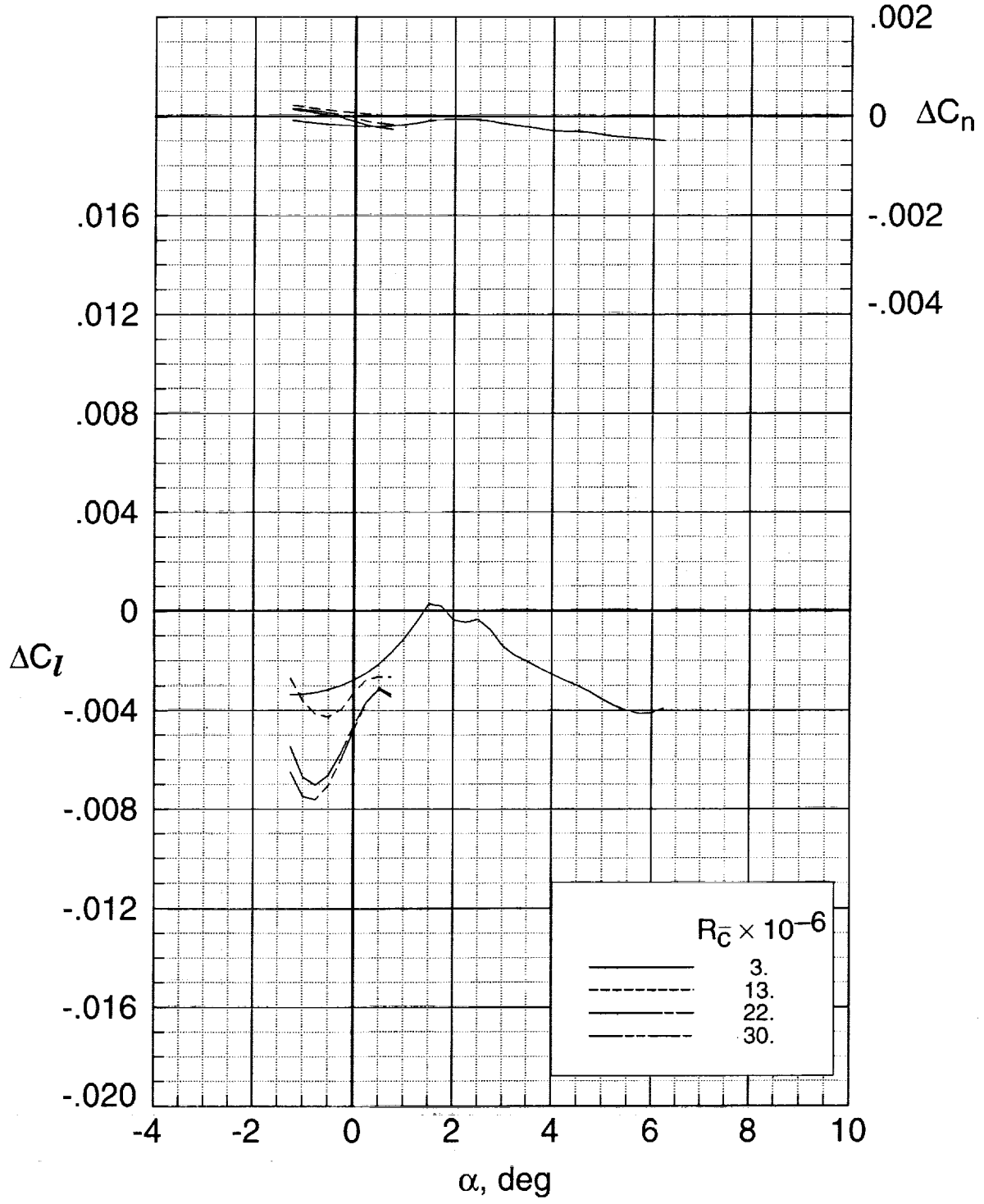

(g) $M_\infty = 0.91$.

Figure 14. Continued.

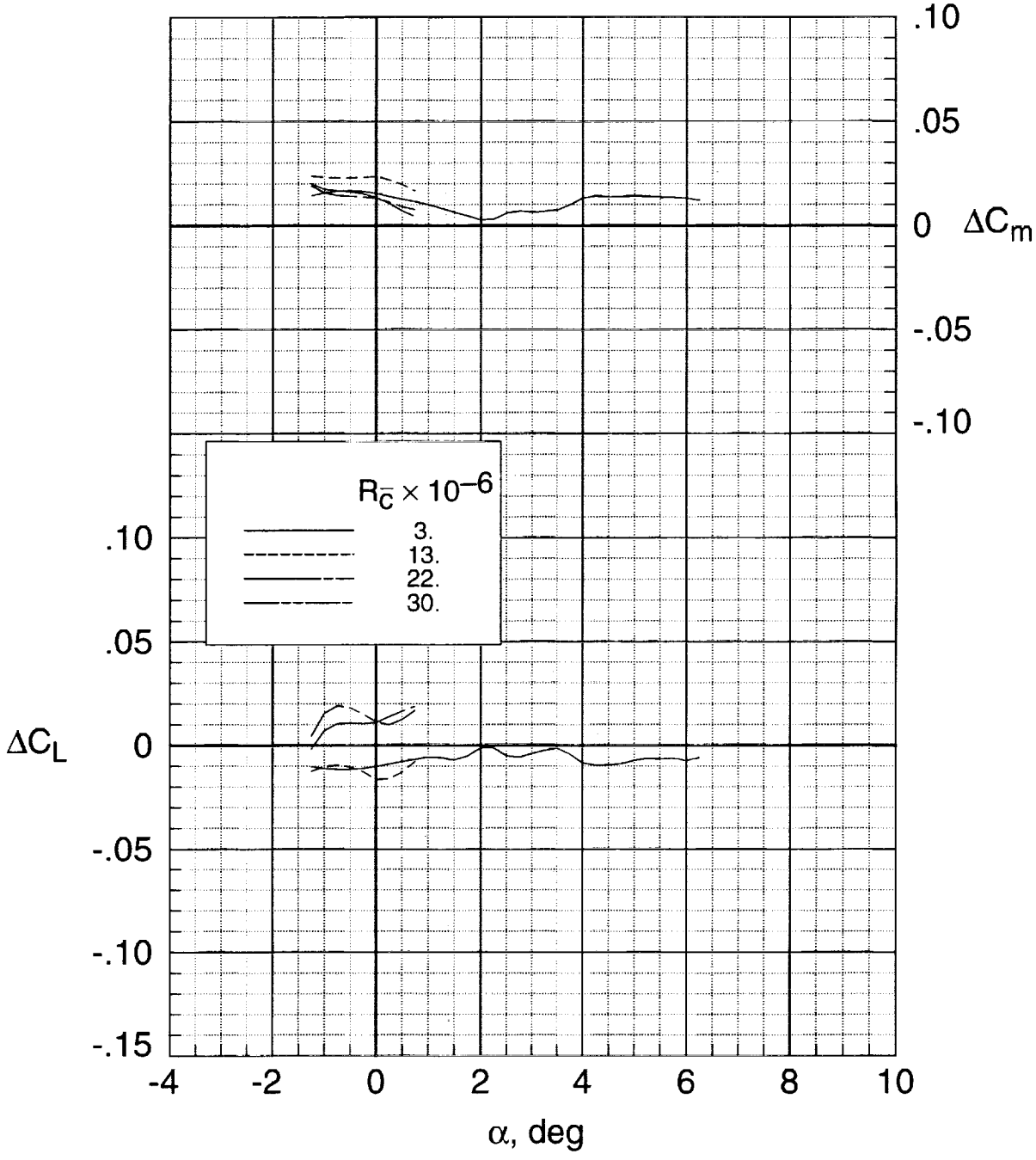

(g) Concluded.

Figure 14. Continued.

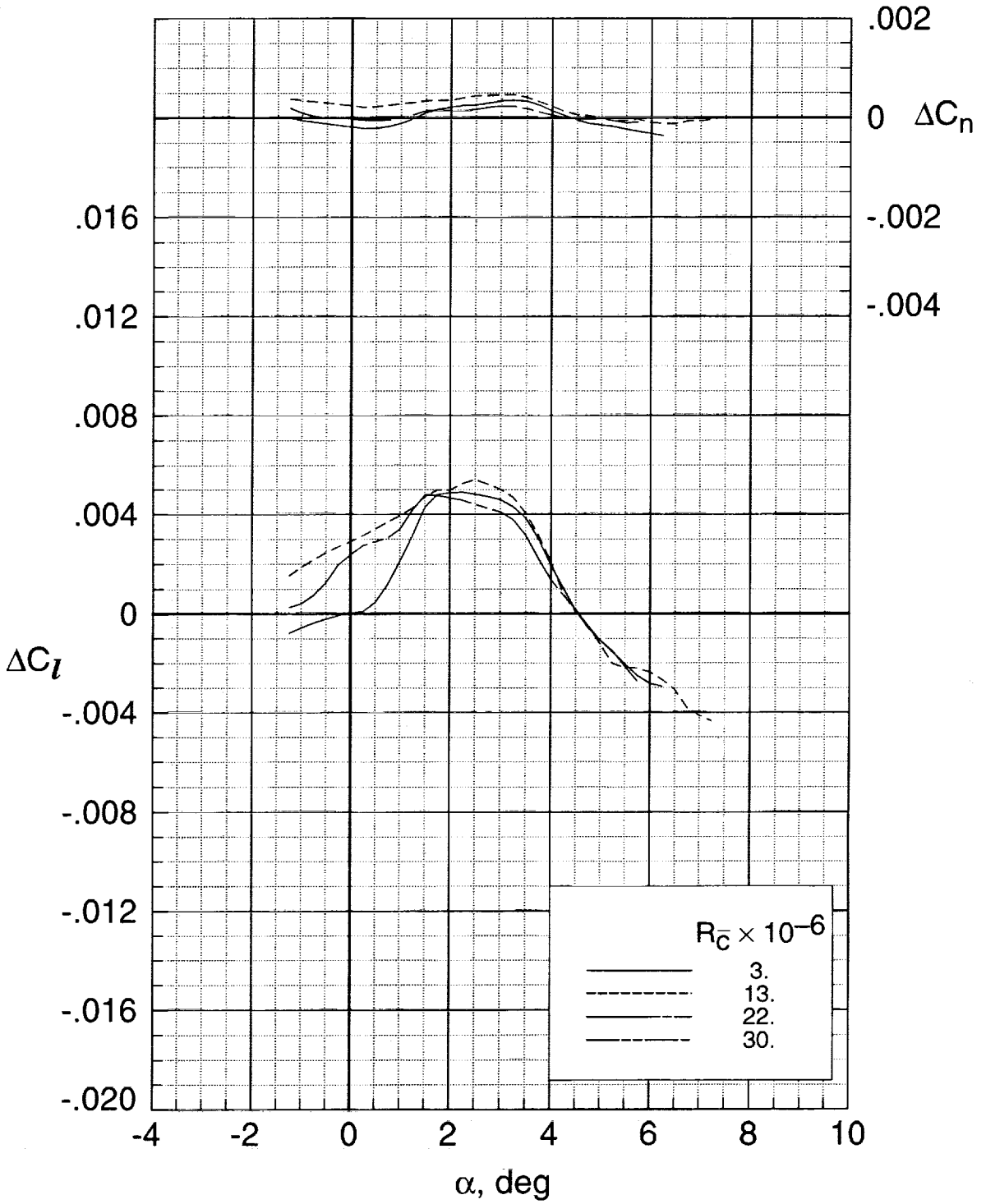

(h) $M_\infty = 0.94$.

Figure 14. Continued.

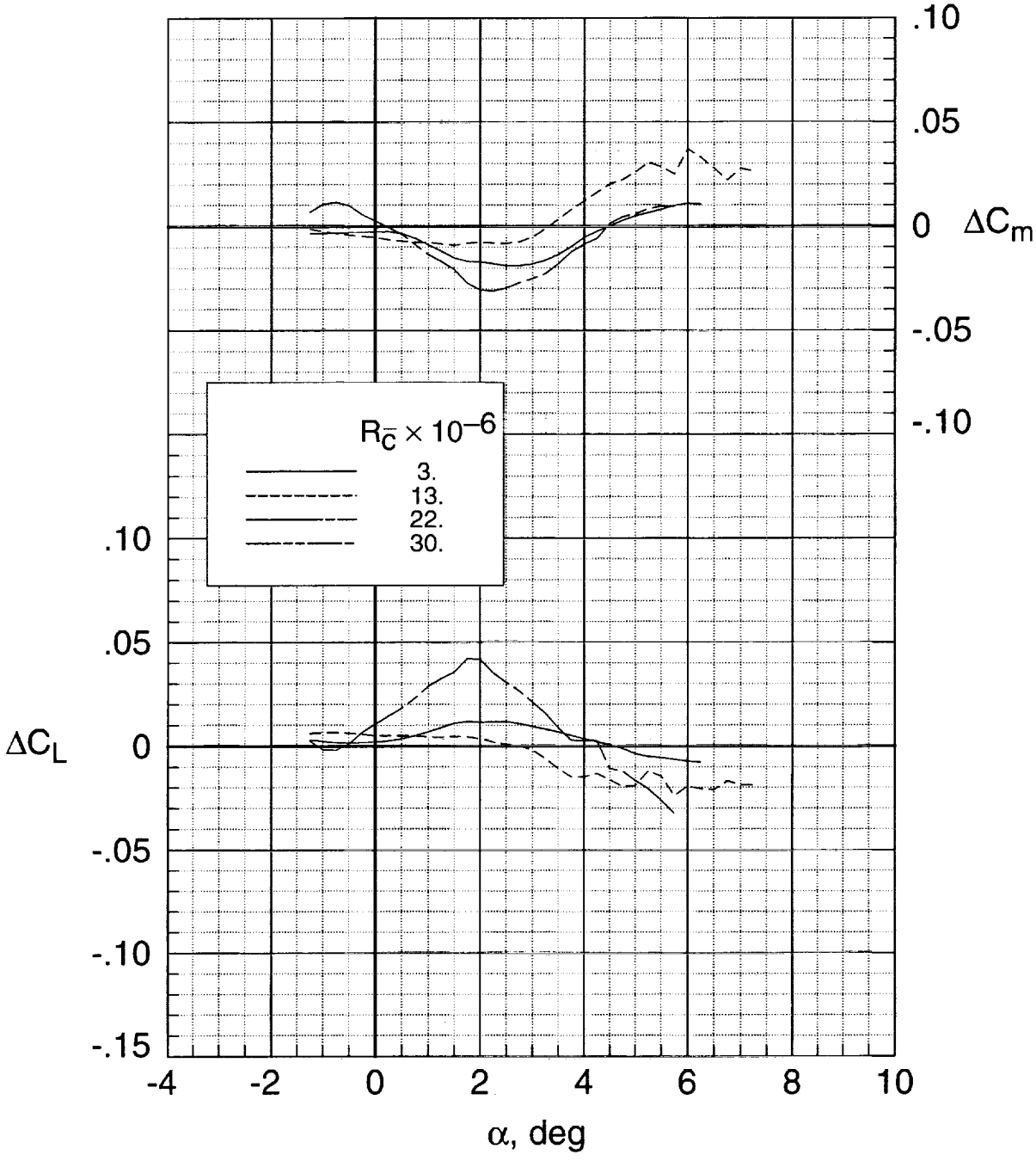

(h) Concluded.

Figure 14. Concluded.

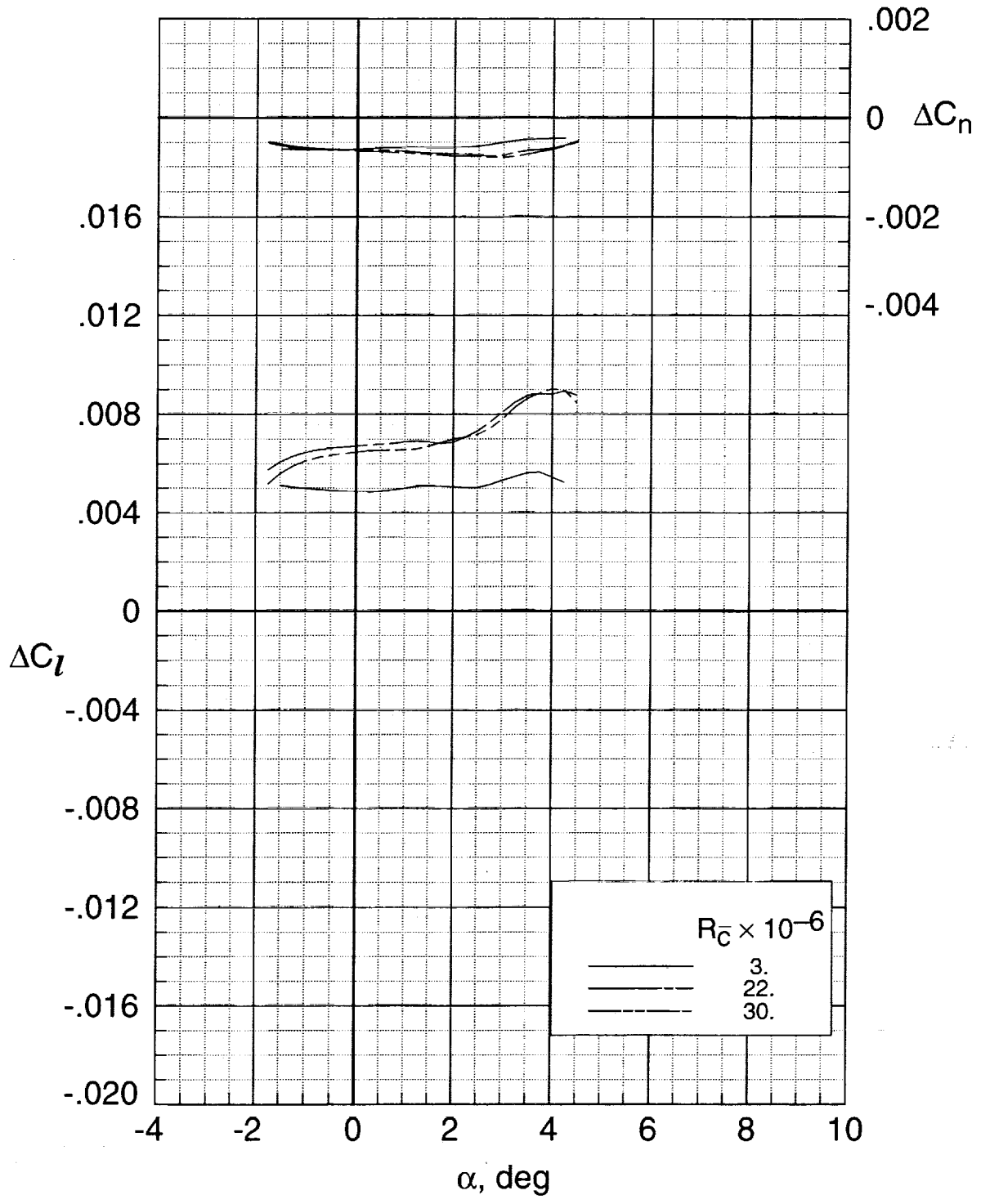

(a) $M_\infty = 0.82$.

Figure 15. Effect of Reynolds number on the aerodynamic characteristics with the outboard ailerons for $\delta_a = 10°$.

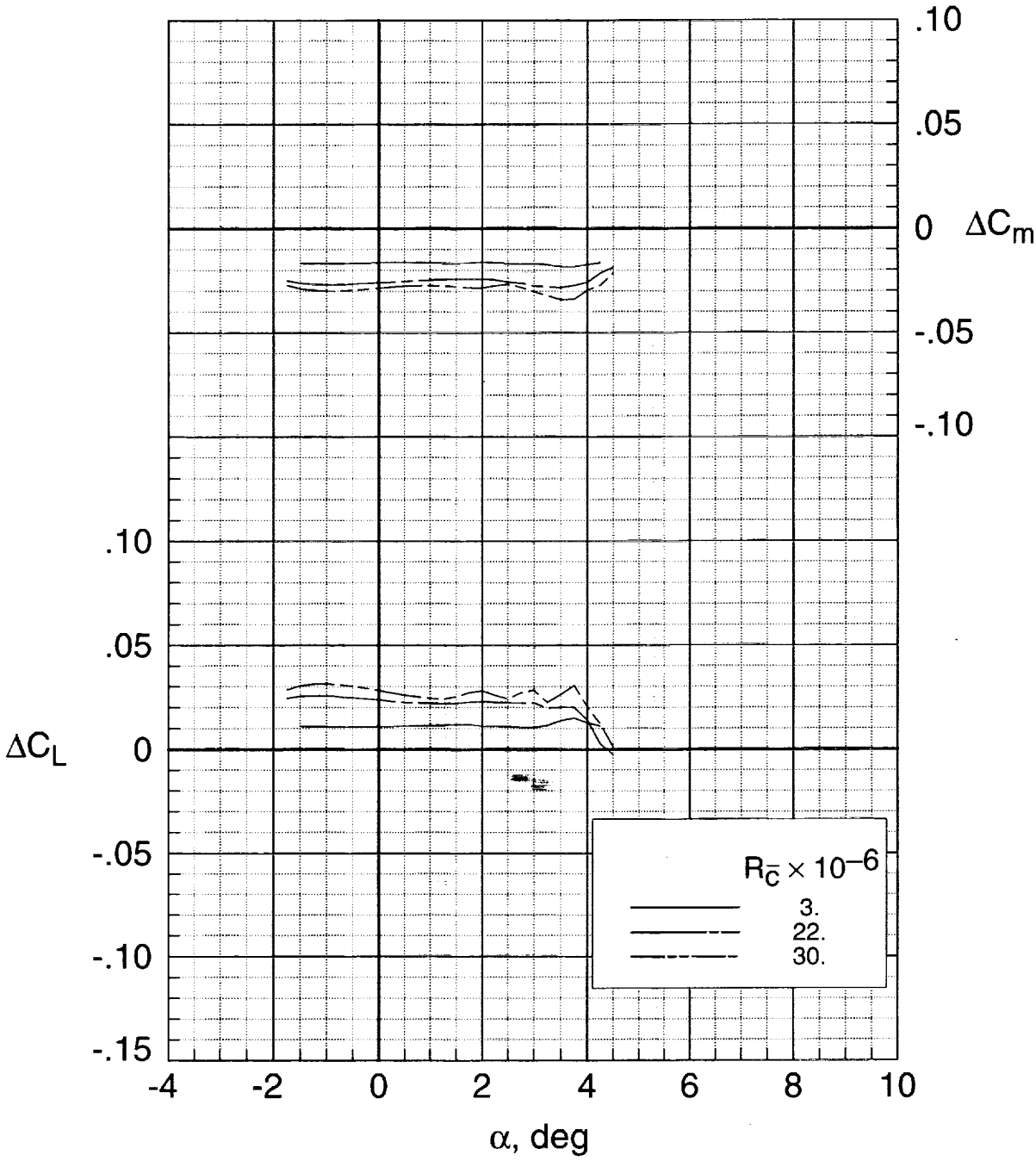

(a) Concluded.

Figure 15. Continued.

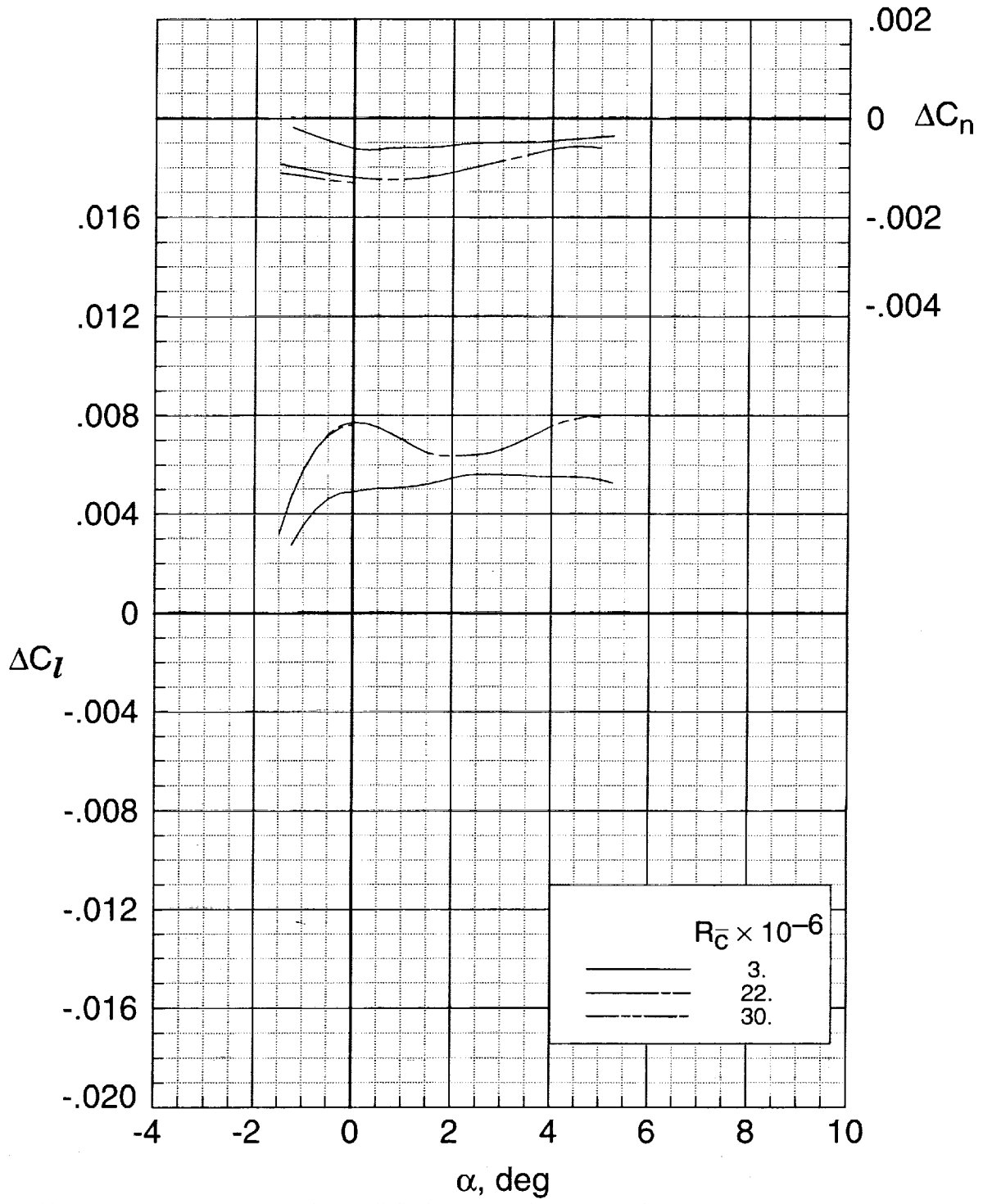

(b) $M_\infty = 0.88$.

Figure 15. Continued.

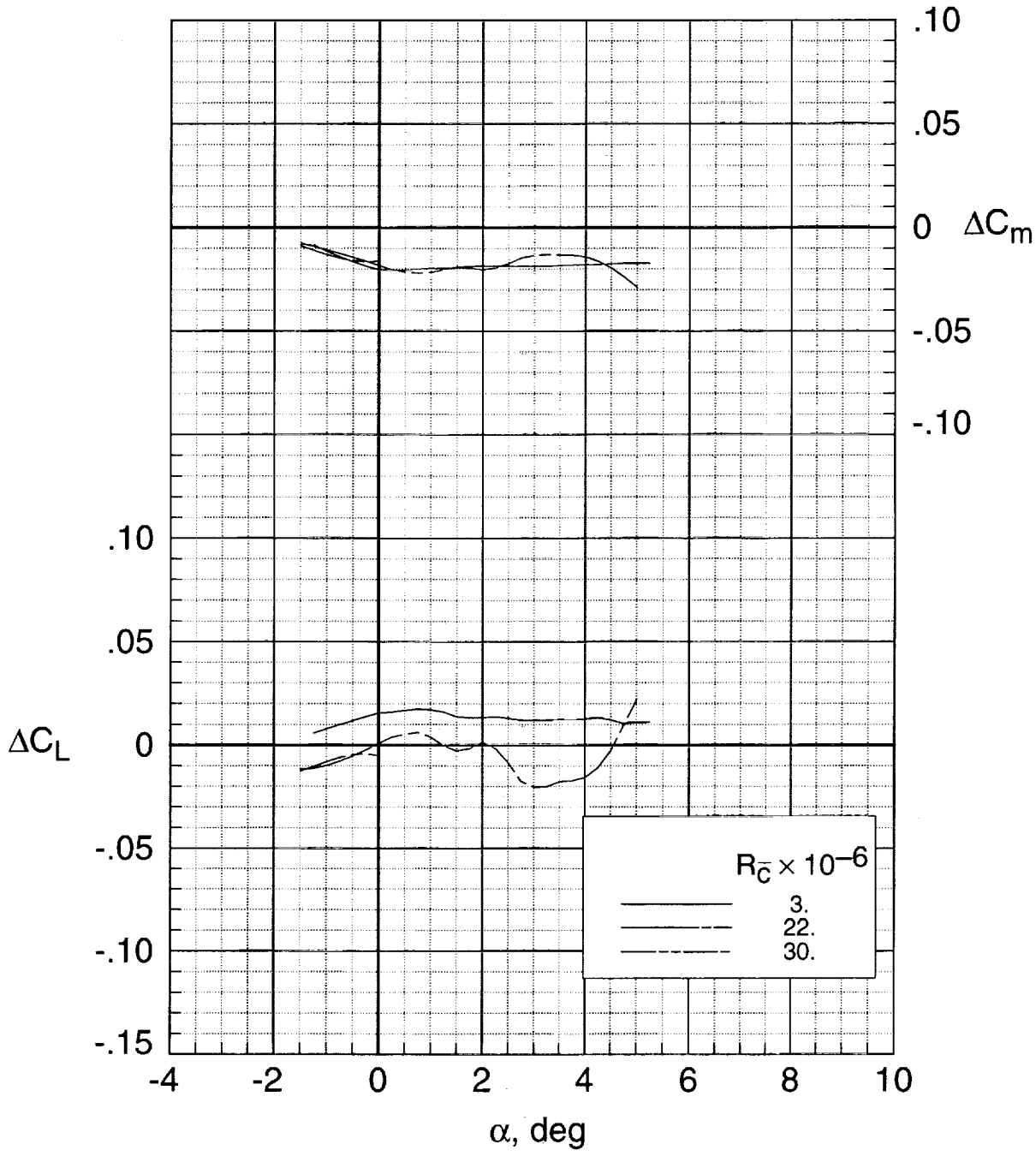

(b) Concluded.

Figure 15. Concluded.

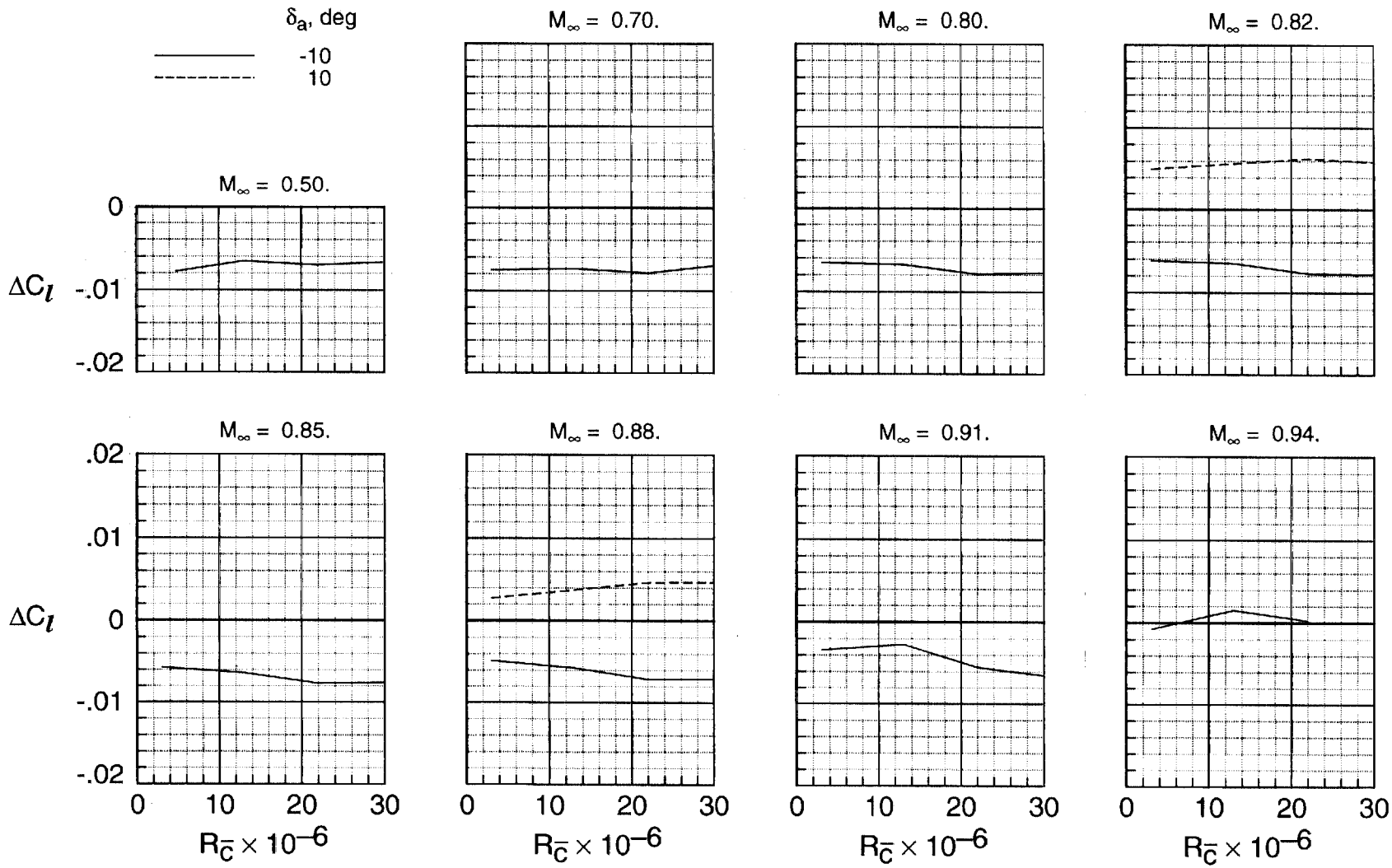

(a) $\alpha = -1.25°$.

Figure 16. Effect of aileron deflection on the rolling moment coefficient increment.

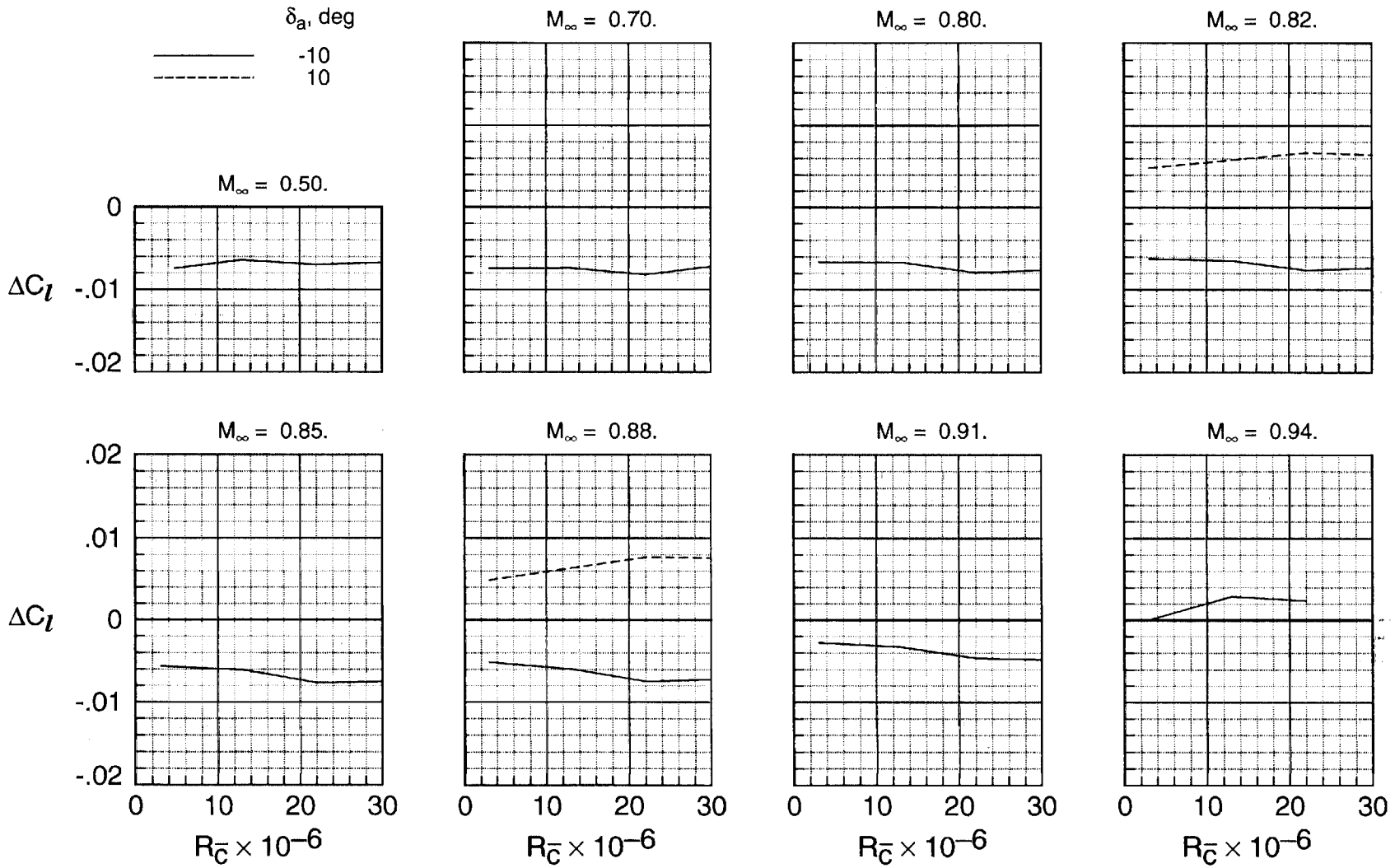

(b) $\alpha = 0.00°$.

Figure 16. Continued.

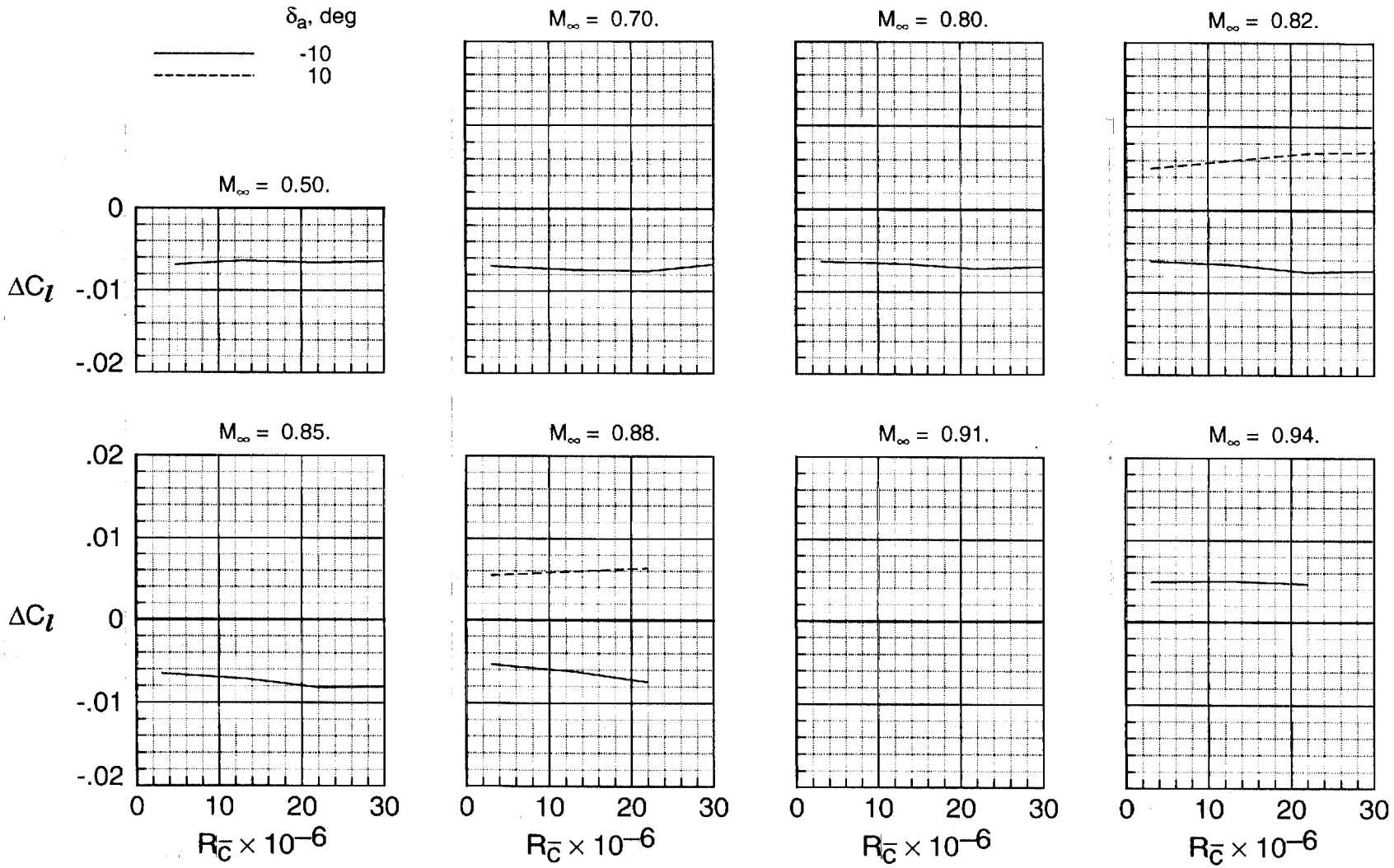

(c) $\alpha = 2.00°$.

Figure 16. Concluded.

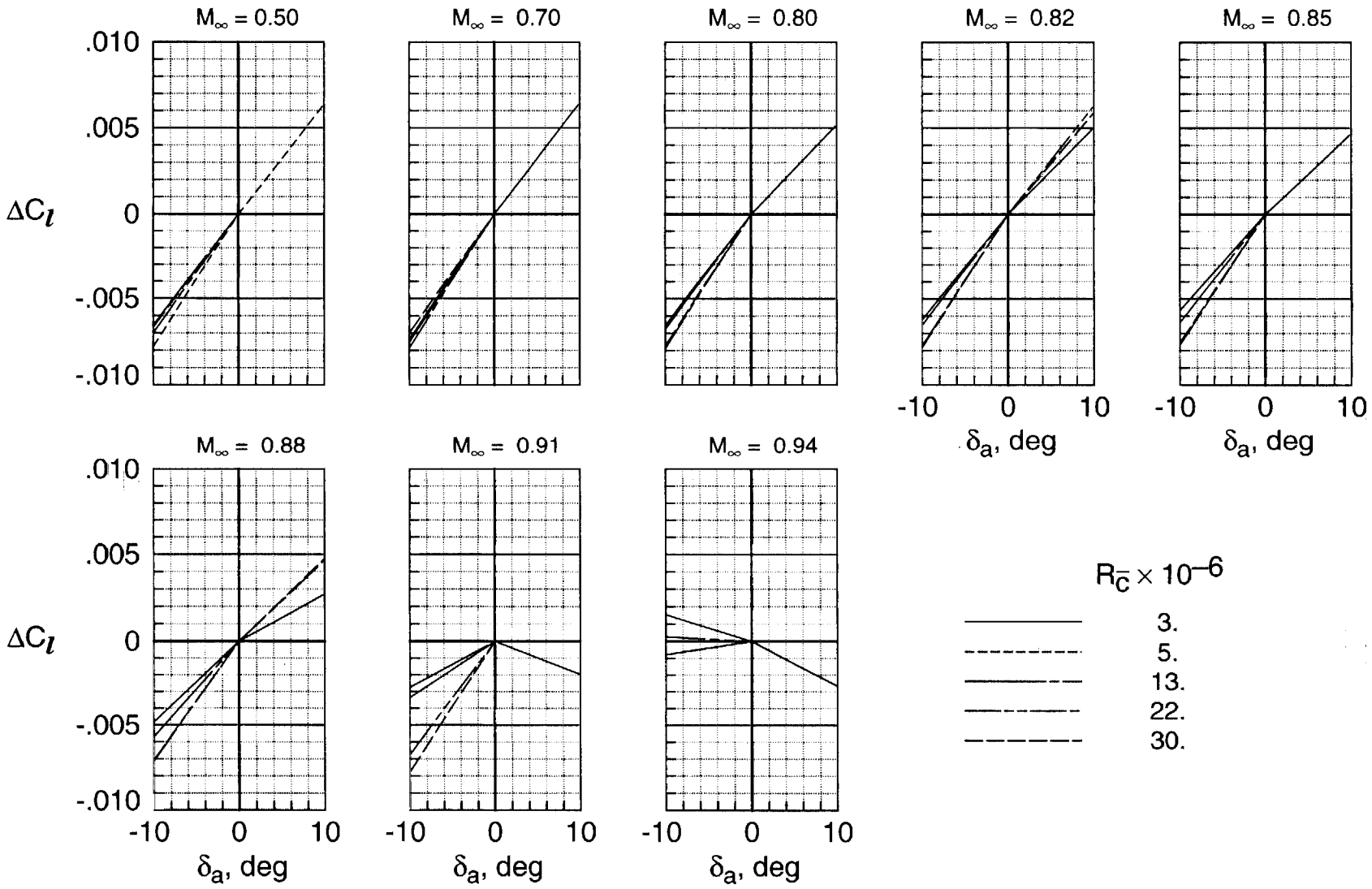

(a) $\alpha = -1.25°$.

Figure 17. Effect of Reynolds number on the aileron control power.

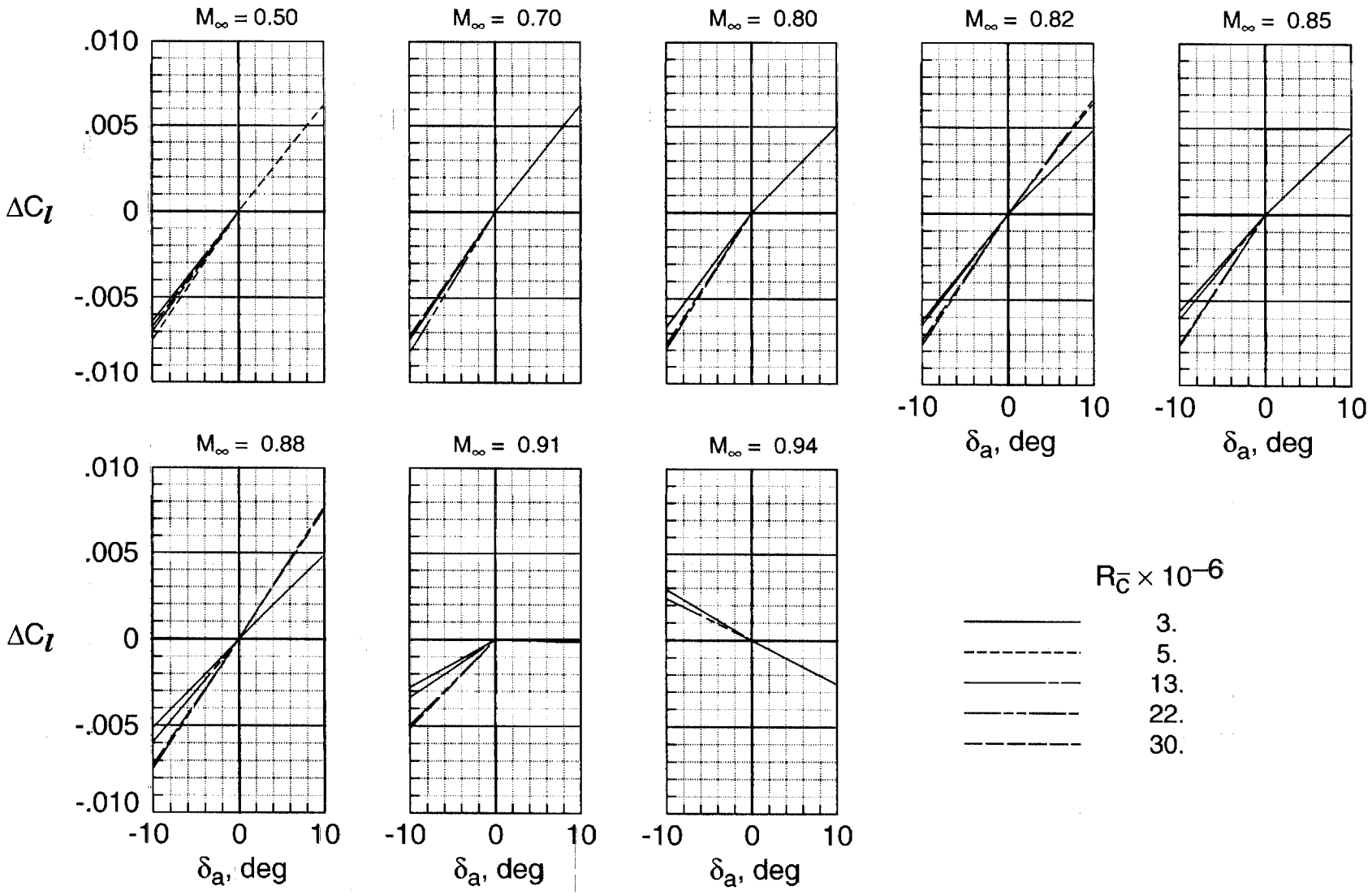

(b) $\alpha = 0.00°$.

Figure 17. Continued.

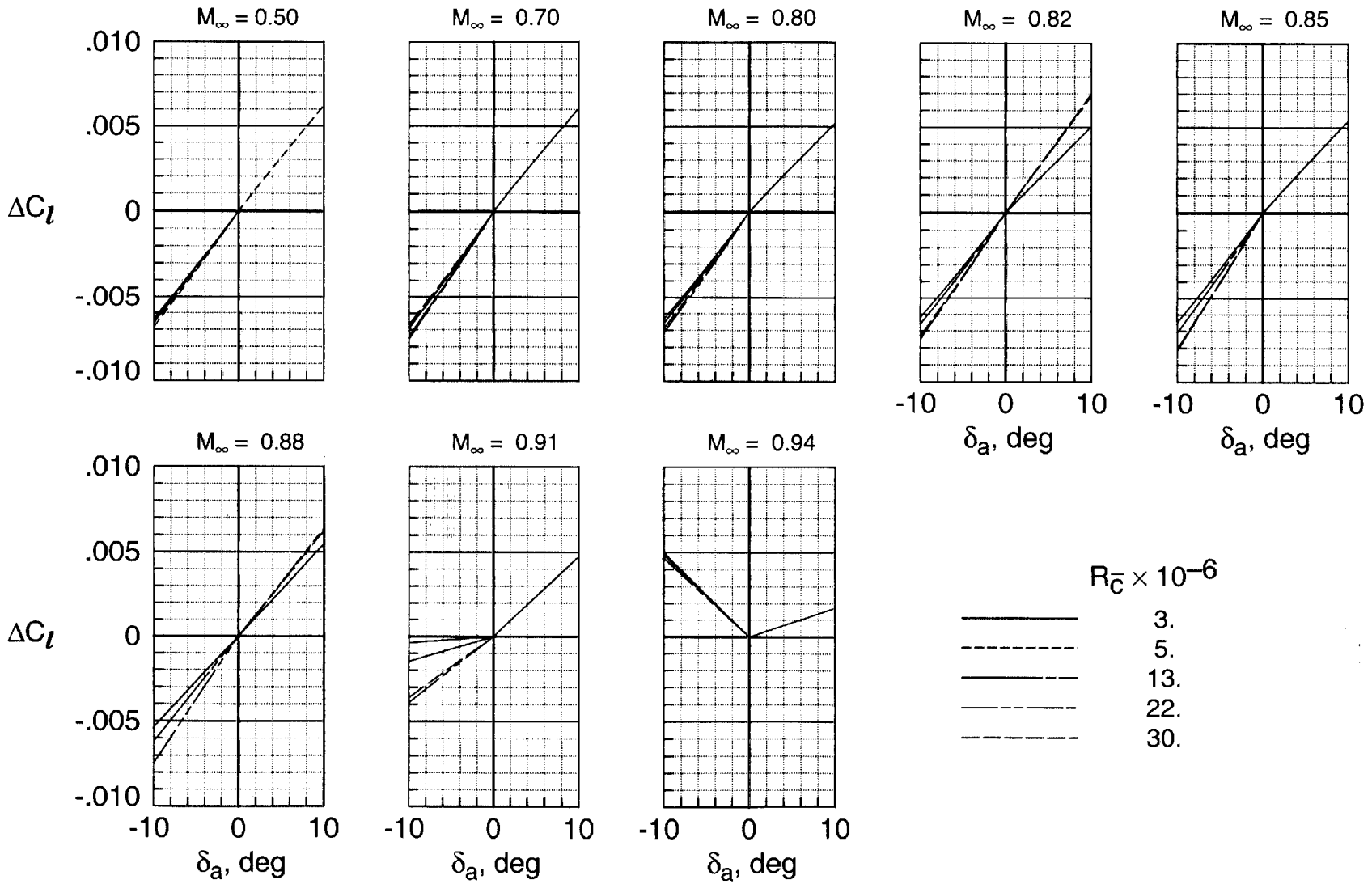

(c) $\alpha = 2.00°$.

Figure 17. Concluded.

REPORT DOCUMENTATION PAGE

Form Approved
OMB No. 0704-0188

1. AGENCY USE ONLY *(Leave blank)*	2. REPORT DATE	3. REPORT TYPE AND DATES COVERED
	October 2000	Technical Memorandum

4. TITLE AND SUBTITLE
Reynolds Number Effects on the Performance of Lateral Control Devices

5. FUNDING NUMBERS
WU 992-20-08-21

6. AUTHOR(S)
Raymond E. Mineck

7. PERFORMING ORGANIZATION NAME(S) AND ADDRESS(ES)
NASA Langley Research Center
Hampton, VA 23681-2199

8. PERFORMING ORGANIZATION REPORT NUMBER
L-18038

9. SPONSORING/MONITORING AGENCY NAME(S) AND ADDRESS(ES)
National Aeronautics and Space Administration
Washington, DC 20546-0001

10. SPONSORING/MONITORING AGENCY REPORT NUMBER
NASA/TM-2000-210541

11. SUPPLEMENTARY NOTES

12a. DISTRIBUTION/AVAILABILITY STATEMENT
Unclassified–Unlimited
Subject Category 02 Distribution: Standard
Availability: NASA CASI (301) 621-0390

12b. DISTRIBUTION CODE

13. ABSTRACT *(Maximum 200 words)*

The influence of Reynolds number on the performance of outboard spoilers and ailerons was investigated on a generic subsonic transport configuration in the National Transonic Facility over a chord Reynolds number range from 3×10^6 to 30×10^6 and a Mach number range from 0.50 to 0.94. Spoiler deflection angles of 0°, 10°, 15°, and 20° and aileron deflection angles of -10°, 0°, and 10° were tested. Aeroelastic effects were minimized by testing at constant normalized dynamic pressure conditions over intermediate Reynolds number ranges. Results indicated that the increment in rolling moment due to spoiler deflection generally becomes more negative as the Reynolds number increases from 3×10^6 to 22×10^6 with only small changes between Reynolds numbers of 22×10^6 and 30×10^6. The change in the increment in rolling moment coefficient with Reynolds number for the aileron deflected configuration is generally small with a general trend of increasing magnitude with increasing Reynolds number.

14. SUBJECT TERMS
Reynolds number effects; Ailerons; Spoilers; Pathfinder I

15. NUMBER OF PAGES
144

16. PRICE CODE
A07

17. SECURITY CLASSIFICATION OF REPORT	18. SECURITY CLASSIFICATION OF THIS PAGE	19. SECURITY CLASSIFICATION OF ABSTRACT	20. LIMITATION OF ABSTRACT
Unclassified	Unclassified	Unclassified	UL